Bio-Inspired Aryldiazonium Carbohydrate Coatings; Synthesis, Surface Modification and Applications in Biofilm Control

A thesis presented to the University of Dublin, Trinity College for the degree of Doctor of Philosophy in Chemistry

Adam Thomas Myles

Prof. Paula E. Colavita & Prof. Eoin M. Scanlan,
School of Chemistry,
University of Dublin, Trinity College
2019

Declaration

I declare that the work thesis has not been submitted as an exercise for a degree at this or any other university and it is entirely my own work.

I agree to deposit this thesis in the University's open access institutional repository or allow the library to do so on my behalf, subject to Irish Copyright Legislation and Trinity College Library conditions of use and acknowledgement.

Adam T. Myles 2019

Acknowledgements

Foremost, I wish to thank my PhD supervisors Paula E. Colavita and Eoin M. Scanlan, for their much appreciated support during this project. Without their assistance, encouragement and friendship this work would not have been possible. For all of the help and advice given these past four years, thank you!

This thesis emanated from research conducted with the financial support of Science Foundation Ireland (SFI) Grants 12/RC/2278 and 12/RC/2302, 12/IP/1273 and 13/CDA/2213. I also wish to acknowledge the School of Chemistry for funding my placement.

I would like to thank our collaborator Prof. Frédéric Barriere for hosting me in his laboratory for one month and his student Thomas Filinos for training me in MFC set-up and analysis. Thanks also to our other collaborators Dr. Thomas Doyle and his student Damian Haberlin for their excellent contribution during our marine field studies. Their expertise was instrumental in the success of these experiments. Additionally, Dr. Doyle's students Aidan and Jasmine have my gratitude for their assistance on the days in set-up and sampling. I'm also grateful to T. McDermott, D. Jackson and F. Kane of the Marine Institute Ireland for access to boating equipment used in the aforementioned field studies.

The past four years have been some of the best years of my life in no small part due to the many friends I have made in Trinity. I wish to thank my group members past and present with thanks to all the Post Doc's, fellow PhD students, undergrads and visiting academics in both the Colavita group and Scanlan Groups, for their assistance and patience through the years. I would be remiss not to mention and give thanks to those of whom I have worked alongside. So in no particular order; Daniela, Carlota, Leticia, Alessandro, Suoyuan, Tomás, Serban, James C, Rita, Michelle, Federico, Joana, Guido, Helen, Danielle, Lauran, Elena, Ruraí, Katie, Joshua and Dylan, thank you for making my time in Trinity a genuinely enjoyable experience.

A special mention is reserved for my colleague, collaborator and good friend, James A. Behan. I have relied on him throughout my PhD and I will continue to depend on his friendship going forward into the future. He has provided a great deal of support throughout my studies and I know I could not have produced this work without him.

I must also acknowledge Robert Baker and his group for providing excellent office banter, specifically I must thank Harrison and Stefano for the ceaseless amusement and interesting conversations they provided. Moreover, I'd like to thank Mr. Sam Edwards for his friendship this past year and I wish him luck in his ongoing studies.

Next, I would like to thank the exceptional staff of Trinity College Dublin whose tireless work makes the research we do possible. Teresa, Maura, Fred, Anne

Marie, Patsy, Mark, & Peter thank you for you kind support. Dr. John O'Brian and Dr. Manuel Ruther have my sincere gratitude for their assistance with NMR analysis. Thanks to Dr. Brendan Twamley for X-Ray analysis, to Dr, Martain Feeney and Dr. Gary Hessman for mass spectroscopy analysis, and to Gavin McManus for assistance with fluorescence microscopy.

To my friends, for your patience and support throughout this project I am eternally grateful. Thanks are especially owed to Jonathan, Laura, and Neil for always being around when I needed them, for always looking out for me, and for injecting some much needed madness into my life. They are the best friends anyone could ask for.

When it comes to family I can't begin to express how important they have been in encouraging me. For my older sister Lauren, and older brother Paul, their respective families, and my younger brother Jordan, thank you for always being there for and encouraging me.

Finally to my parents, Sean and Sharon Myles who have always provided me with love and support, for standing with me throughout every step of this work, I thank you from the bottom of my heart. Without your advice and assistance I wouldn't have made it this far.

Summary

Carbohydrates are a complex class of biomolecules, with many structural conformations and roles in nature. The production of carbohydrate coated surfaces has found application in fields of study including immunology, biochemistry and organic synthesis. Though abundant synthetic methods and applications exist for carbohydrate chemistry, there are many challenges involved in the development of surface glycosylation methods including surface specificity and/or poor morphological control at the surface. One method of surface modification that shows promise in addressing these concerns involves the production of saccharide conjugated aryldiazonium salts with subsequent grafting to the surface. This project investigates the characteristics of lactoside terminated surfaces formed by aryldiazonium grafting under different conditions by use of a range of techniques. In addition to this the glycosylation of surfaces possesses several desired physical properties, notabily hydrophilicity, which may be useful in the production of biofilm resistant surfaces. Biofouling presents as a significant detriment to a range of industries and public health and as such carbohydrate modification of surfaces was investigated as potential biofouling mitigation strategies.

Chapter I provides an overview on glycosylated surfaces, including a literature review on glycoarray production and other surface modification techniques. Concurrently, a brief overview on the methods of surface modification by use aryldiazonium salts is provided. The stages of biofouling propagation is discussed with particular focus on the effects it has on medical devices and in a marine environment. Finally the available methods of biofilm mitigation are discussed and a brief review is provided of previous literature involving surfaces modified with aryldiazonium saccharide coating for antifouling purposes.

A brief overview of carbohydrate modification and details for the synthesis of para-aminophenol conjugated lactoside precursors is provided in Chapter II. Also discussed is the synthetic protocol for the production of a primary face modified para-aminophenol β-cyclodextrin diazonium precursor compound.

Chapter III presents the modification of carbon surfaces with lactose *via* aryldiazonium grafting by two methods, spontaneous nucleophilic surface attack and electrochemical reduction. The resulting surface films are characterised by spectroscopic methods, lectin binding studies, surface wettability studies and non-specific protein retention studies. Significant differences were observed between the two functionalisation methods with electrografted materials possessing properties indicative of more complete coatings with multilayer morphology when compared to suspected monolayer coverage of spontaneously modified surfaces. Concurrently, these surfaces modifications were investigated for potential use as passive antifouling coatings for electrode surfaces in the production of an electrochemical sensor for caffeine post immersion in coffee solution.

Chapter IV describes the process of spontaneous aryldiazonium grafting of lactosides onto non-conductive polymer (PES and Nylon-6) and metal alloy (stainless steel 316) surfaces. Details are provided on surface pre-treatment conditions and subsequent surface characterisation *via* the methods discussed for carbon surfaces above.

A field study involving the immersion of lactose modified polymer and stainless steel coupons in a heavy fouling marine environment is described in Chapter V. Comparative fouling studies were performed against unmodified controls for coupons of each material by various microscopic and spectroscopic techniques. ATP determination in addition to the aforementioned results found no significant difference in degrees of fouling between modified and unmodified materials as sampled, however following a light rinsing protocol all modified samples displayed reduced biomass retention indicative of a good fouling release material.

Aminophenol tailed cyclodextrins were observed to form supramolecular self-assemblies *via* head to tail cavity inclusion with neighbouring molecules. This behaviour was found to render the aminophenol tail unreactive under standard aqueous aryldiazonium salt forming conditions. In Chapter VI, the behaviour of the resulting crystals formed by self-assembly were characterised by X-Ray crystallography, dynamic light scattering and NMR titration experiments. Disaggregation conditions were identified through NMR studies and spontaneous aryldiazonium modification of carbon, nylon and stainless steel surfaces with cyclodextrin moieties was achieved. Modified surfaces were characterised by spectroscopic and protein rejection studies. It was determined by AFM that coatings produced were monolayer in thickness and the effect of cavity binding was investigated by use of a ferrocene redox probe. It was thus concluded that surfaces modified by aryldiazonium grafting retained cavity binding capabilities implying potential applications in active sensing of cyclodextrin binding analytes.

Chapter VII contains the preliminary results of ongoing projects. Initially discussed is the application of lactoside coatings on fouling of complex 3D sturctures in a marine environment. The field study results for lactose modified nylon netting sampes immersed in a marine environment are discussed. Secondly, the initial results of microbial fuel cell start up behaviour from anaerobic wastewater are presented following graphite anode modification *via* mannoside and lactoside arydiazonium grafting. It is observed that mannoside modifiaction may increase fuel cell performance by improved geobacter anodic adhesion however results are preliminary. Finally the initial synthesis of an open chain maltoheptasaccharide from β-cyclodextrin starting materials is discussed.

List of Terms

AFM	Atomic force microscopy
ATP	Adenosine triphosphate
βCD	β-cyclodextrin
BSA	Bovine serum albumin
CON-A	Concanavalin A
CV	Cyclic voltammetry/ Cyclic voltammogram
DCM	Dichloromethane
Egraft	Electrografted
EPS	Extracellular polymeric substances
ESI	Electrospray ionization
FITC	Fluorescein isothiocyanate
FRA	Frequency response analyser
Gal	Galactose
GC	Glassy carbon
Glc	Glucose
IR	Infrared Spectroscopy
IRRAS	Infrared reflectance-absorption spectroscopy
Lac	Lactose
MALDI-TOF	Matrix Assisted Laser Desorption/Ionization-Time of Flight
MS	Mass Spectroscopy
Man	Mannose
N-6	Nylon 6
NMR	Nuclear magnetic resonance
NOE	Nuclear Overhauser Effect
PBS	Phosphate buffered saline
PDMS	Polydimethylsiloxane
PEG	Polyethylene glycol
PES	Polyethersulfone
PNA	peanut agglutinin
PNP/4NP	Para nitrophenol
PTFE	Polytetrafluoroethylene
RMS	Root Mean Squared
RT	Room temperature
SAM	Self-Assembled Monolayer
Spont	Spontaneously modified
SEM	Scanning electron microscopy/micrograph
SS	Stainless Steel
TBT	Tributyltin
UV	Ultra Violet
WCA	Water contact angles
XPS	X-ray photoelectron spectroscopy

Table of Contents

List of Figures

Chapter I

Chapter II

Chapter III

Chapter IV

Chapter V

Chapter VI

Chapter VII

List of Tables

List of Communications

2018 CARBON World Conference on Carbon, Madrid, Spain **(Oral)**

2018 RSC organic Division Ireland Regional Meeting, Belfast **(Poster)**

2017 ISE Student Meeting, Cork, Ireland **(Oral)**

2017 RSC Carbohydrate Section Meeting, Trinity College Dublin **(Poster)**

2017 European Materials Research Society Spring Meeting, France **(Poster)**

List of Publications

2018:

Spontaneous Aryldiazonium Grafting for the Preparation of Functional Cyclodextrin Modified Materials
Adam Myles, James. A. Behan, Brendan Twamley, Paula E. Colavita, & Eoin M. Scanlan
ACS Appl. Bio Mater., **2018**, *1* (3), pp 825–832

2017:

Bioinspired Aryldiazonium Carbohydrate Coatings: Reduced Adhesion of Foulants at Polymer and Stainless Steel Surfaces in a Marine Environment

A. Myles, D. Haberlin, L. Esteban-Tejeda, M. D. Angione, M. P. Browne, T. K. Doyle, E. M. Scanlan & P. E. Colavita.

ACS Sustainable Chem. Eng., 2018, *6* (1), 1141–1151.

2016:

Stable hydrophilic poly (dimethylsiloxane) via glycan surface functionalization."

L. Esteban-Tejeda, T. Duff, G. Ciapetti, M. D. Angione, A. Myles, J. M. Vasconcelos, E. M. Scanlan, P. E. Colavita, *Polymer*, 2016, 106, 1-7.

Chapter I

Introduction

Carbohydrates are a class of biomolecules essential to many biological processes, with roles in energy supply, enzymatic recognition and structural applications. Glycosylated surfaces are abundant in nature essential to cell recognition, lectin adhesion and cell-cell communication. The study of carbohydrates has led to advances in fields such as immunology, protein and nucleic acid chemistry, antibiotics and organic synthesis. In addition to this the glycosylation of surfaces may yet serve a variety applications of industrial, academic and economical interest such as in the production of biofilm resistant surfaces. Biofilms are a prevalent problem in nature, industry and medicine as they lead to enhanced wear of equipment, require expensive cleaning processes and can lead to infection and thrombosis in implantable materials. Herein, the roles of glycosylated surfaces are discussed along with several examples of state of the art surface glycosylation techniques used today. Specifically the process of surface modification through diazonium grafting is discussed with regards to its potential use in the production of biofilm resistant surfaces. The stages of biofilm propagation and potential mediation points are discussed with specific focus on biofilm propagation in-vivo and in marine environments. We review various biofilm control strategies including biocidal and anti-adhesion strategies with the aim of understanding the properties required for good biofilm rejection. Finally, we discuss previously reported carbohydrate surfaces prepared by aryldiazonium chemistry and their ability to minimise adhered protein fouling on carbon and polymer surfaces.

1 Glycosylated surfaces

1.1 Carbohydrates in nature

Carbohydrates comprise one of the largest groups of compounds found in nature. They are essential to life, with key roles in energy production (glucose) and storage (starch/glycogen), they are major structural constituents in the forms of insect shells (chitin) and supporting tissue for plants (cellulose), they form compounds with proteins and lipids in processes essential to many biological reactions[1-4] and are major components of the surfaces of bacterial and animal cells.[5] The saccharide decoration of cell surfaces is termed the glycocalax and is unique for each type of cell; as such it is crucial in the mediation of specific protein-cell interactions.[5] These surface-terminated carbohydrate interactions are of huge interest to carbohydrate chemists and biologists due to their importance in a wide array of biological processes including cell communication,[4, 6] immune responses,[7] bacterial and viral infection[8] enzyme recognition[9] and cellular adhesion[10-11]. It is important to note that many diseases are now recognised to be related to abnormal cell glycosylation[12-13] including cancers[14], diabetes[15] and neurodegenerative diseases.[16-17] As such, the study of carbohydrates, and carbohydrate containing biomolecules at biological surfaces and interfaces is of great importance in the understanding of these processes and is fundamental in the development of technologies for rapid diagnostics and medicines. [18]

1.2 Uses of Surface Bound Saccharides

Due to the complex nature of the structure of glycocalaxes and of carbohydrates in general it is necessary to produce simplified model surfaces in order to study specific carbohydrate-lectin interactions[19]. To achieve this, a simple assay method is generally employed whereby synthetically pure carbohydrates are attached to a test surface to produce a glycosurface or “glycoarray”.[4, 19-20] Glycoarrays allow for rapid screening of biomaterials which bind to the surface and through incorporation into sensor technologies it is possible to rapidly detect and/ or quantify carbohydrate interaction. **Figure 1.1** illustrates several examples of the applications of glycoarrays in the generation of biochemical data.[19]

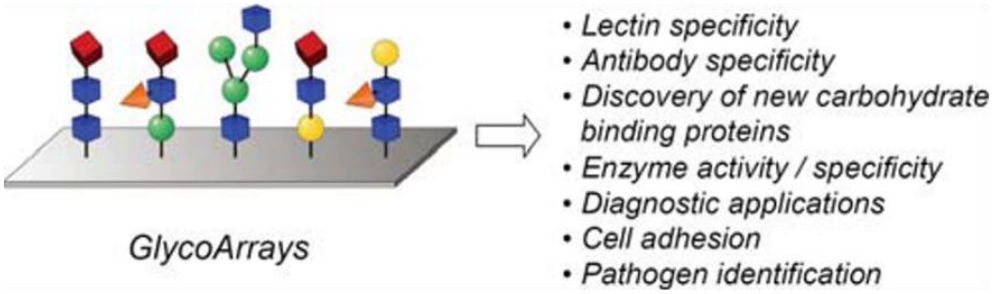

Figure 1.1. Current applications for glycoarrays. Reproduced with permission[19]

The choice of sensor employed for glycoarrays is heavily dependent upon the application in question. Specific lectin and bacterial binding have been investigated through fluorescence studies,[21-22] MALDI-TOF mass spectroscopy[23], and surface plasmon resonance imaging[24].

Further applications for surface glycosylation can be found in the field of medicine. Due to the lectin specificity of cell membranes, research into the production of glycosylated carriers for targeted drug delivery within the cell is steadily progressing.[25] Carbohydrates are also currently under investigation as controlled triggers for immune responses,[26] to combat abnormal cell glycosylation, and to produce novel anti-cancer therapeutics.[27] However these technologies are still in their infancy. It is possible to produce surfaces tailored for specific biofilm cultivation and conversely carbohydrate coated surfaces have been observed to displayed seemingly “biocidal tendencies” with reduction in surfaces adhered biomass observed on many glycosylated surfaces, this property shall be discussed further in subsequent sections.[28]

1.2.1 **Cyclodextrin modified surfaces**

Cyclodextrins are a special class of carbohydrates consisting of a series of glucose monomers joined through a series of (1-4) α-linkages. They are usually denoted based on the number of glucose units comprising the ring, (α=6, β=7, or γ=8). They form a torus structure with hydrophilic exteriors and a hydrophobic interior capable of forming host guest interactions with a wide variety of small organic compounds[29] (**Figure 1.2**).

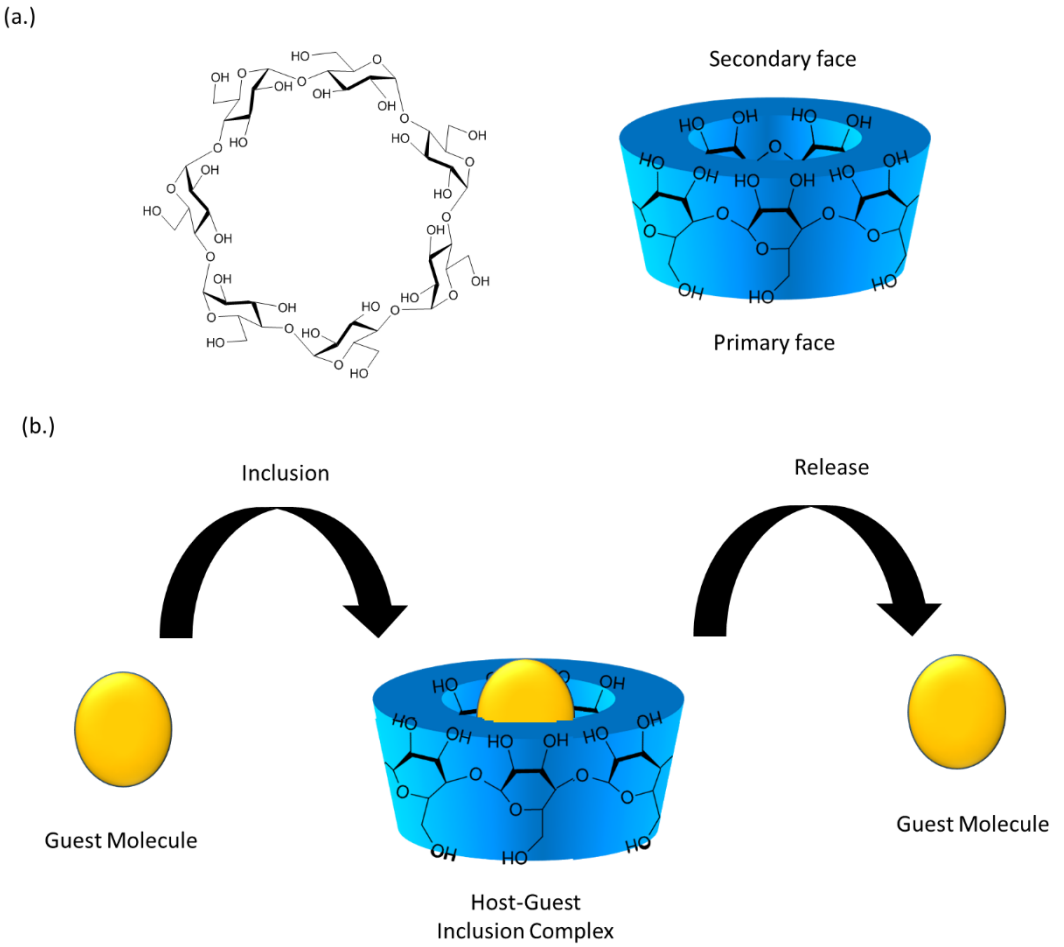

Figure 1.2. **(a.)** Chemical structure of β- Cyclodextrin with schematic representation highlighting Primary and secondary faces**. (b.)** Schematic representation of guest molecule inclusion into and release from the cyclodextrin host's cavity.

Cyclodextrins have long been used in separation science due to their ability to separate positional isomers, functional groups, homologues and enantiomers based on cavity affinity.[30] In addition to this, cyclodextrin modified surfaces have found applications in environmental remediation as organic pollutant scavengers, and in sensor technologies by encapsulating analytes for analysis or with displacement of host-guest fluoremetric/ colourimetric molecules as markers cavity binding.[31-33] Additionally, due to their cavity binding properties, cyclodextrin modified nanoparticles are being studied with regards to potential drug delivery applications with controlled release of the target compound for more efficient therapeutics.[34-35] The uses of cyclodextrin surfaces are further discussed in **Chapter VI**.

1.3 Techniques for the generation of surface bound saccharides

Due to the abundant applications of saccharide coated surfaces there exists great academic and commercial interest in methods for the controlled glycosylation of surfaces. The field of carbohydrate coatings is vast with a wide variety of methods existing for the production of saccharide-terminated surfaces, through both covalent attachment and physical adsorption.[4] The choice of method employed is usually dependant on a range of factors including the substrate material, required surface orientation, and final applications of coated surfaces. The preparation of glycosurfaces using chemical immobilisation has the advantage of yielding stable modifications due to the covalent nature of the bond used for the immobilization of the carbohydrate.[19] Noncovalent immobilization is generally a quick and easy alternative to express carbohydrates on surfaces, although it usually yields less stable glycosurfaces often in random orientations.[4, 19] Methods of noncovalent modification include ionic interactions, hydrogen bonding and hydrophobic interactions.[36]

The production of orientation-controlled surface arrays is routinely obtained by use of self-assembled monolayers (SAM's) terminated with a specific glycan. One of the earliest examples of this comes from Fritz *et. al.* [37] in 1996 with the covalent immobilisation of thiol-terminated sugars adsorbed on a gold surface. Lectin binding surfaces and glycoarrays of mixed carbohydrate components[38] have since been produced through thiol based SAM's adhered on gold surfaces. Alternatively the attachment of unmodified carbohydrates to a reactive surface is also possible. This is usually achieved through modification of the surface to produce reactive terminal SAM units. Examples of this include hydrozide-terminated surfaces[39] or vinylsulfone-terminated surfaces,[40] each of which upon exposure to ultraviolet light covalently bind to the unmodified anomeric position of the target saccharides. This method comes with the benefit of not requiring lengthy multistep saccharide modification processes to introduce a surface graftable moiety, however it does require significant surface pre-treatment and high energy activation in the form of ultraviolet excitation. As such, it is generally unfeasible for large scale surface modification.

Finally the most extensively developed method of surface glycosylation involves the prior modification of the anomeric position of carbohydrates with surface-

reactive groups, resulting in site specific immobilisation. This type of modification, while often requiring extensive synthetic consideration, can generally produce controlled and efficient surface modification under mild reaction conditions.[41] One common method involves so-called “click” reactions, by copper catalysed azide–alkyne cycloaddition.[42-44]

While many of these methods require extensive surface pre-treatment steps to produce a functionalisable surface, as is the case with ‘click’ coupling, or alternatively are specific to one surface type, there exist few surface non-specific modification techniques which could produce controlled surface saccharide morphology. One surface modification method that shows promise in this regard involves the modification of surfaces through the use of aryldiazonium salts.[45]

1.3.1 **Surface Modification through aryldiazonium grafting**

Diazonium surface grafting is a powerful covalent surface modification technique enabling the production of a wide range of surface functionalities on a multitude of material surfaces.[45-47] Aryldiazonium grafting is achieved through the reduction of a salt of general formula ($RArN_2^+$) to generate a reactive aryl radical which subsequently binds to the substrate.[48-50] Diazonium salts however have several drawbacks in their use as surface modifying agents, including difficulty in purification and isolation of the salt compound, intrinsic explosive properties and thermal instability above 4 °C.[50-51] Due to these limitations it is generally preferable to generate the diazonium salt *in-situ* at the substrate surface from the corresponding amine (**Scheme 1.1**). This has been reported for a variety of solvent systems including acidified aqueous environments and aprotic environments such a MeCN.[51] Compounds with various functionalities (generally achieved by tailored choice of a para substituted R-group), have found uses in surface modification by a multitude of diazonium based surface grafting techniques [45] and have produced materials with many applications in sensor technologies[52], energy storage[53] and biofilm mitigation[54] to name a few.

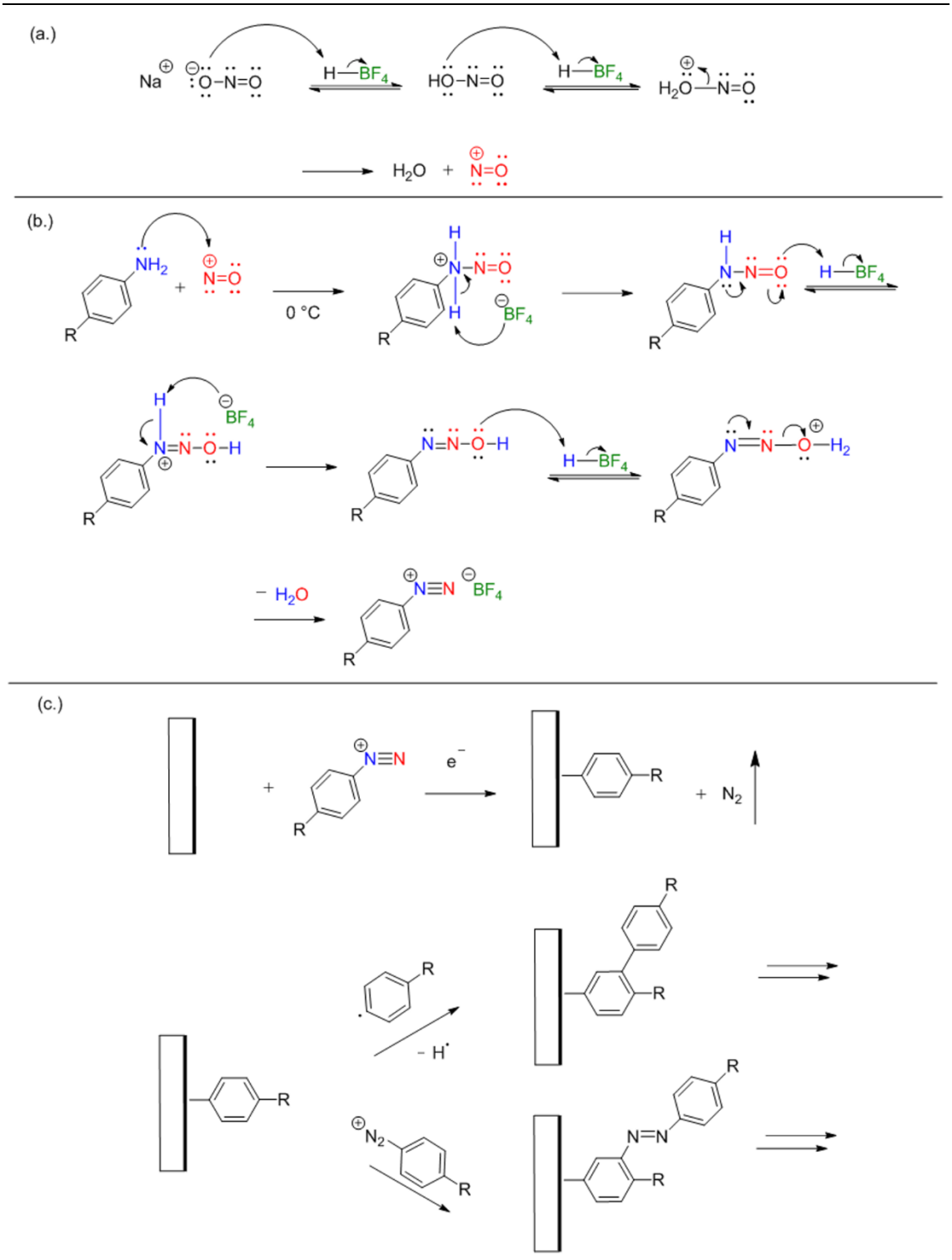

Scheme 1.1. Mechanisms of reactions to produce aryldiazonium salt from its corresponding amine with subsequent surface grafting. **(a.)** An acid (HBF_4) reacts with $NaNO_2$ in solution to form a nitrosonium ion (red). **(b.)** This ion in turn reacts with a para-substituted-arylamine undergoing a dehydration reaction to form the corresponding aryldiazonium salt. **(c.)** Under reductive conditions this salt forms a reactive aryl species by dediazoniation which then produces a covalent bond to a surface in situ, forming mono or multilayers depending on experimental conditions.[49]

Aryldiazonium surface modification has been used to produce several saccharide surface coatings by spontaneous in-situ aryldiazonium salt formation from aminophenol conjugated monosaccharide. Aryldiazonium grafting has received considerable interest in the field of surface modification ever since Delamar *et. al.* [55] first reported on the electroduction of (4-Nitrophenyl) diazonium tetrafluoroborate salts on carbon electrodes. Since then, aryldiazonium grafting has found application on a wide range of substrates including carbon materials (glassy carbon, graphene, amorphous carbon, nanotubes, and diamond),[55-57] additionally metals such as gold[58] and stainless steel[59] as well as semiconductor materials[58] and non-conductive polymer surfaces[45] (PDMS, PES, and PTFE)[45, 60-61] have been modified through various diazonium grafting techniques. The aryldiazonium activation conditions employed in surface grafting are numerous and generally depend on the properties of the underlying substrate. Conductive materials such as gold, graphene and glassy carbon electrodes have historically favoured electrochemical reduction as a means of diazonium activation with examples of these studies dominating modern scientific literature.[49, 53, 62]

However, there exists several other methods of diazonium grafting including spontaneous activation,[63-64] chemical reduction[65], UV assisted modification[66], ultra-sonication,[67] and mechanical modification of surfaces.[68] Of these methods, spontaneous grafting possess significant advantages in the modification of substrates with low conductivity and irregular surface morphology and has successfully been applied to carbon, metal and polymer surfaces in the production of covalently bound mono- and di- saccharide surface coatings.[60, 69-70] Electrografting of aryldiazonium salts has been shown in literature to generally produce “bushy” multilayers on surfaces of varying thickness (1-3 nm or more)[63] with monolayer control being difficult to obtain and generally achieved through choice of a bulky unreactive R group,[71-72] or through addition of a radical scavenger under chemical reduction conditions.[73] The effects of choice of grafting technique on layer formation with disaccharide (lactose) conjugated aryldiazonium salts are further discussed in **Chapter III** with regards to electrografting versus spontaneous modification on carbon surfaces.

2 Surface Biofouling

Biofouling is the process of accumulation of undesired biological materials onto a surface when it is immersed in aqueous media. Biofilms formed through biofouling are often complex, biodiverse and present a persistent problem across many industries due to their detrimental and potentially dangerous effects.[74] Industries affected include pharmaceuticals,[75] food and beverage processing,[76] transport,[77] environmental sensing[78] and agriculture.[79] Progression in biofilm formation is a highly complex, multistep process involving various stages of adhesion, growth and release of fouling species. The stages typically involved in this process are illustrated in **Figure 1.3**. The first steps in biofilm adhesion typically occur within seconds to minutes of initial immersion and typically involve the adhesion of small organic molecules (proteins and glycolipids), producing a conditioned surface to act as a scaffold for larger fouling species such as bacteria to adhere onto. This initial step can be considered as the determining factor in the long-term bioaccumulation of the surface. [80]

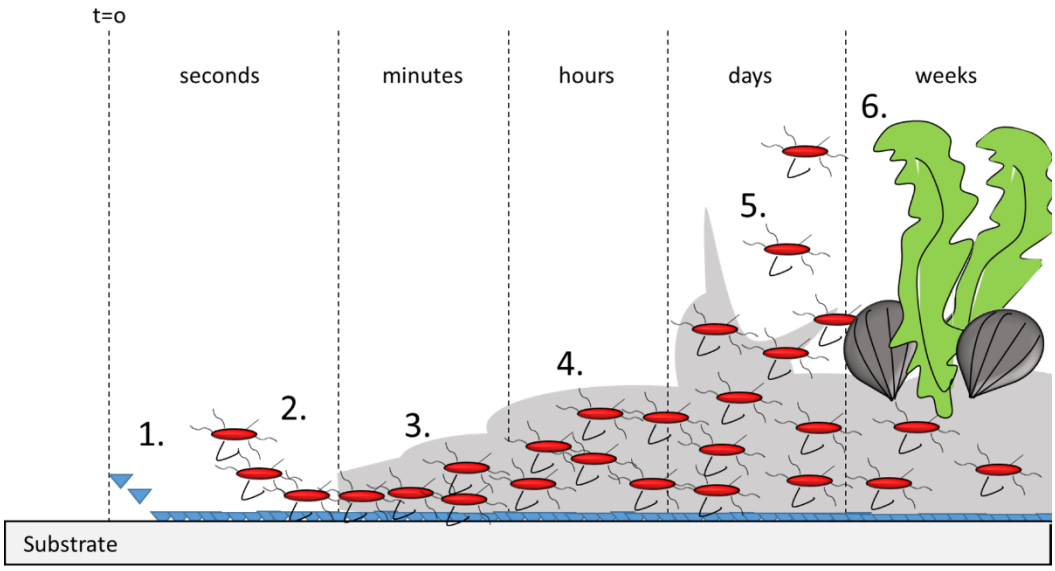

Figure 1.3. Graphic depicting timeline of surface biofouling. (t= 0 corresponds to initial immersion in the fouling media). 1. Within seconds, macromolecules such as proteins, lipids and glycans adhere irreversibly to the surfaces forming a scaffold for further biofilm adhesion. 2. Planktonic microorganisms adhere reversibly to the conditioned surface and then adsorb permanently. 3. The microorganisms produce a protective slime layer from extracellular polymeric substances (EPS). 4. The surface bound microorganisms propagate producing a biofilm. 5. The adhered species release planktonic material back into the matrix for future biofilm formation. 6. Other fouling species and eventually larger macro organisms adhere to the biofilm completing surface fouling.[81-82]

The preconditioned surface allows for planktonic (free moving) bacteria to adhere to the surface reversibly. The bacteria then become irreversibly bound by the secretion of extracellular polymeric substances (EPS) to form an adhesive and protective matrix allowing for further propagation of adhered species on the material surface.[83-84] This so-called "slime" layer protects the forming colony which in turn propagates and spreads planktonic cells back into the solution to begin further colonisation.[84] Moreover if the aqueous matrix contains multiple species the initial adherent film may serve as a pioneering members for further accumulation of other fouling species (bacteria/algae/animals) leading to more complex biofilm formation, which in natural waters tends to facilitate adhesion of larger organisms such as algae and molluscs.[79-81]

The effects of biofilm formation can be seen in cleaning costs, equipment downtime, mechanical erosion of parts, and contamination of products. The types of biofilms and fouling surfaces observed are heavily dependent on the species present within the fouling environment and as such it is difficult to discuss biofilm formation in great detail due to their extensive biodiversity. For the purposes of this study, the discussion will be limited to biofouling progression in implantable materials and marine bioaccumulation.

2.1 Biofouling of Medical Implants

When solid surfaces are interfaced with a biological environment the surfaces are prone to biofouling by adhesion of bacterial or thrombotic agents. This process occurs routinely with medical devices such as implants, stents and needles.[85] In-vivo biofilm formation generally follows the succession of protinatious material adhesion to a surface (fibrous or globular),[86] followed by bacterial attachment and growth (infection) and mammalian cell attachment (thrombosis).[87] Biofouling is a prevalent problem in the field of medicine due to the increased risks of infection, localised toxin production from biofilm metabolism, loss of function of medical bio devices, and potentially dangerous remediation processes,[86] generally requiring surgery for the removal and replacement of befouled implants.[88]

Another important concern from a public health perspective is the role biofilms play in antimicrobial drug resistance.[89] Bacteria within biofilms are more resistant to antimicrobial agents when compared to planktonic cells due to lower mass

transport of antimicrobial molecules within the biofilm to affected cells and potentially because surface adhered cells have different physical characteristics to planktonic cells.[90] Antimicrobial concentrations sufficient for planktonic species are generally insufficient for biofilm populations, [91] with those deep within the biofilm least affected and potentially selecting for resistant subpopulations. This selection for antimicrobial resistant subpopulations may have implications for treatments that use controlled release of antimicrobial agents to prevent biofilm growth on indwelling devices.[92] Bacteria can also transfer extrachromosomal genetic elements within biofilms potentially leading to selection of antimicrobial resistant biofilms.[93-94]

Due to the excessive concerns inherent in medical device fouling discussed above, there is a large push for the development of non-invasive antifouling technologies. A suitable method for medical biofilm mitigation must also possess several criteria, namely, good biocompatibility,[95] high stability under biological stress,[96] and must not produce toxic degradation products[97]. Given that removal and sterilisation of medical devices is a delicate and highly invasive process, methods of remediation ideally focus on prevention and/or retardation of initial biofilm growth, *i.e.* mediation in the early stages of biofouling. Since this generally involves adhesion of protinatious material within the host organism, antifouling surfaces for biomedical applications should consequently reject nonspecific protein adhesion mechanisms and bacterial adhesion.[88]

2.2 Marine biofouling

Marine biofouling is a vastly different process to the *in-vivo* processes described above. Biofouling succession in a marine environment is a complex process involving many physical, chemical and biological factors and, as such, is currently not well understood.[81] Factors such as location, pH, temperature, conductivity, dissolved oxygen content, organic material content, depth, light, hydrodynamic conditions and surface functionality can all affect biofilm formation.[98] Further complications arise in the study of biofouling processes in the marine environment from the biodiversity of fouling species with over 4000 species of organism having been identified as contributing to biofouling.[99] These organisms can be divided into two classifications based on scale, microorganisms which form biofilms and slimes and macro foulants which adhere

to the surface. **Figure 1.4** provides some examples of marine fouling species by size.

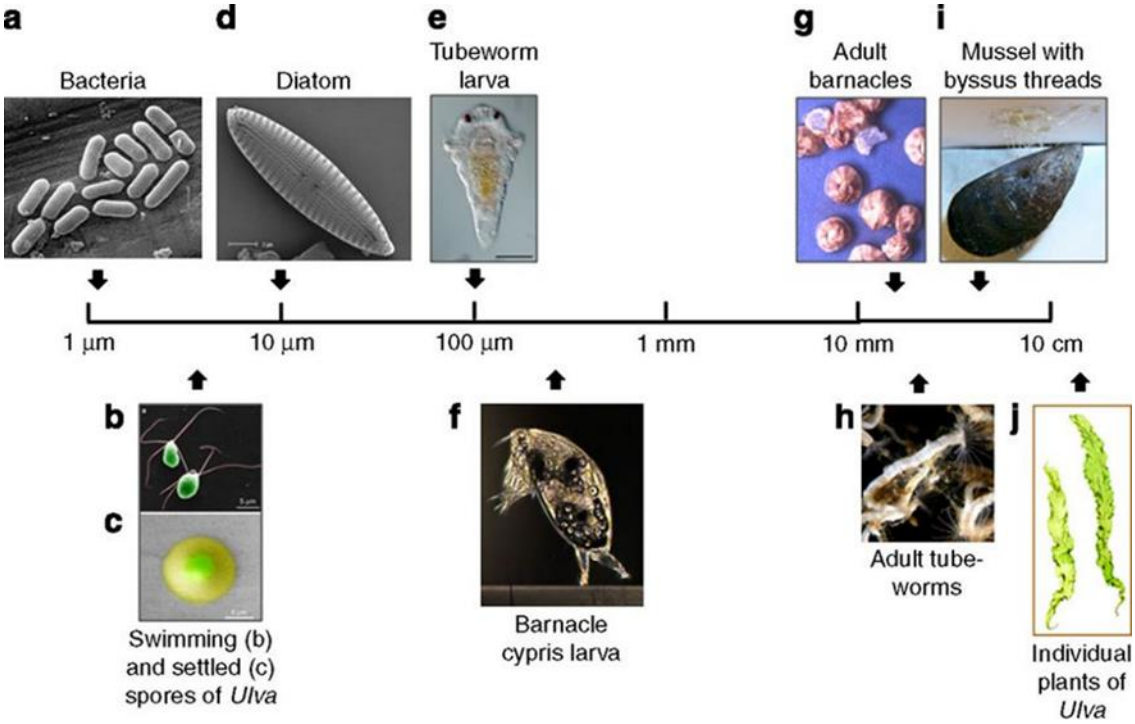

Figure 1.4. **(a.)**Bacteria (scanning electron micrograph (SEM)), **(b)** false-colour SEM of motile spores of the green alga (seaweed) *Ulva*, **(c)** false-colour environmental SEM image of settled spore of *Ulva* showing secreted annulus of swollen adhesive, **(d)** SEM of diatom **(e)** larva of tube worm **(f)** barnacle cypris larva **(g)** adult barnacles, **(h)** adult tubeworms (i) adult mussels showing byssus threads attached to a surface (j) individual plants of the green alga (seaweed) *Ulva.* Reproduced with permission.[100]

Biofouling of marine environments is a problem endemic to all marine industries. It is known to impact on performance of aquatic sensors, compromise the integrity of marine structures, impede flow within subaquatic pipes[101] and greatly increases the cost of fuel for marine transport by increasing weight and drag of biofouled hulls on marine vessels.[102] Additionally biofouling of marine transport has the potential to introduce harmful invasive species to new environments wherein the environmental impact can be devastating.[103] Further impact is seen in aquaculture as biofouling is responsible for increased farmed fish disease and mortality rates.[104]

Biofouling in marine environments is generally considered in 5 steps; Initially adsorption of organic and inorganic macromolecules form a primary film on the surface within seconds of immersion. Secondly, microbial cells attach and immobilise onto the surface. These microbes produce the extracellular polymeric matrix forming a microbial film. A complex multicellular community comprised of

micro-algae, diatoms and sedimentary particles is formed which grows and propagates. Finally, larger marine invertebrates such as barnacles and muscles in addition to algal stalks immobilise and grow on the surface.[105]

Due to the complex nature of marine biofouling, which occurs on a range of surface types, under various conditions with a complex array of organisms with differing fouling methods,[106-107] it is difficult to produce biofilm mitigation processes which prevent fouling completely without resorting to harsh chemical methods or toxic heavy metal coatings. As such methods of biofouling removal are often employed after biofouling reaches a critical mass whereby removal becomes economically and/or environmentally necessary.[108]

2.3 Potential points of remediation

Biofouling mitigation takes several forms. Surfaces which prevent biomass accumulation in the initial stages are known as non-fouling or antifouling materials.[109-110] These may be employed to prevent or slow biofilm formation on the surface of a submerged material, leading to longer active periods between biofilm removal and may potentially provide surfaces from which biological fouling can be more readily detached. Fouling release describes the force required to remove an organism attached to a surface.[109] During the early stages of biofilm adhesion, microbial films can generally be removed with little mechanical force by wiping the surface. In the case of later stage fouling however, much greater mechanical stress is required to produce a pristine surface. Late stage cleaning is generally an expensive and time consuming process, which has the potential to reduce the lifetime of bio-fouled devices.[111]

One method of fouling remediation involves the production of a self-releasing polymeric surface,[112] whereby the fouled surface layer is designed to wear away removing surface adhered biomass. This method has several advantages in that it facilitates easier removal of late stage biomass and can be combined with biocidal materials for controlled release into the media upon exposure of fresh coating under layers.[112]

2.4 Antifouling technologies

2.4.1 Biocidal antifouling

Antifouling surfaces are generally divided into two distinctive categories based on the mechanism of reduction. The first classification concerns 'biocidal surfaces', i.e. surfaces which possess physical or chemical properties which induce necrosis or apoptosis (cell death) of adhered cells.[113] A classic example dating back thousands of years can be found in the historic usage of copper water storage utensils which readily prevented *Staphylococcus aureus* growth by release of toxic copper salts. [114] Other metals such as lead and silver are known to possess similar biocidal properties as heavy metal ions in relatively small concentrations and are known to disrupt normal cell activity through metabolic interference leading to cell death.[115-116] Additionally certain metal oxide materials such as TiO_2 or ZnO possess secondary antimicrobial functionalities in the UV activated catalysis of H_2O and O_2 to produce reactive oxide species which break down cell walls resulting in cell death [117] (**Figure 1.5)**.

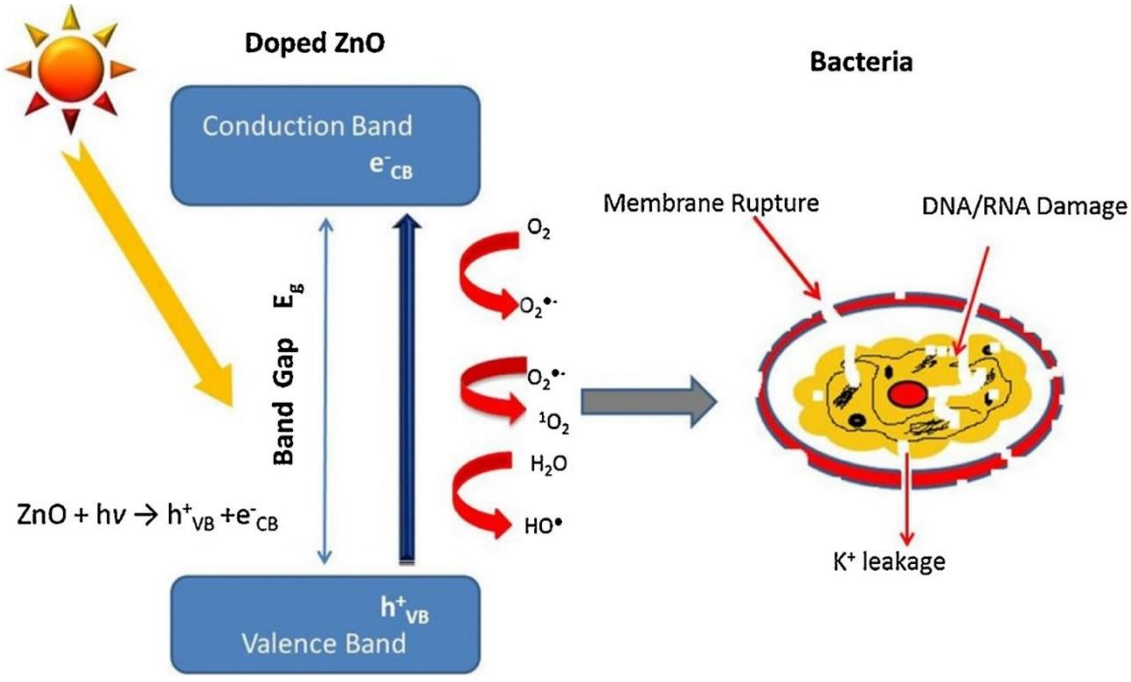

Figure 1.5. The mechanism of photocatalytic antibacterial activity of ZnO. Reproduced with permission.[117]

These cytotoxic antifouling methods however possess several drawbacks in their mechanism of biofilm mitigation, chief of which being their inherent toxicity to humans and other organisms. Due to this property, they are unsuitable for antifouling in the medical implants and additionally due to the bioaccumulation of heavy metal species most leads and organotin antibacterial paints (TBT), historically utilised to prevent fouling of marine vessels are heavily regulated and are now forbidden in maritime use.[118] Due to the limited applications and ecological drawbacks inherent in cytotoxic antifouling technologies, they are generally considered for niche antifouling purposes such as in hospitals as self-sterilising paints[119] or in heavily fouling aquatic environments as organic pollutant scrubbers.[120]

2.4.2 **Anti-adhesion methods**

Antiadhesive methods of biofilm mitigation are generally considered 'green' antifouling technologies as they typically require little in the way of toxic components and generally do not harm the organisms within the fouling media.[121] Similarly, antifouling materials, which address biofouling without killing the bacteria are an effective means of avoiding the development of antimicrobial resistant species.[109] These methods of biofilm rejection are commonly found in nature with several mechanisms employed to achieve the effect. Biomimetic antifouling surfaces are routinely investigated by production of surfaces with one or a combination of the following properties: steric repulsion,[122] micro patterning and controlled nanotopographies;[123] electrostatic repulsion,[121] and controlled surface wettability[124], *i.e.* hydrophobicity or hydrophilicity (**Figure 1.6)**.

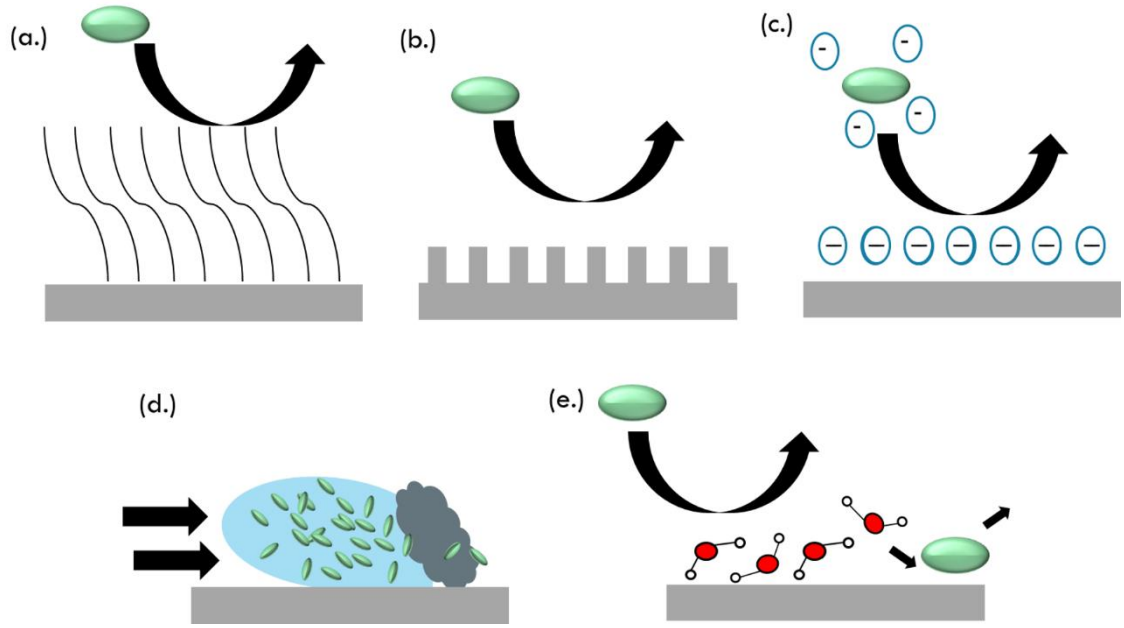

Figure 1.6. Anti-fouling surface material methods of biomass repulsion; **(a.)** Steric repulsion by long polymeric surface chains preventing foulants adhesion. **(b.)** Controlled micro patterned topography provides surfaces with poor adhesive properties for microorganisms. **(c.)** Electrostatic repulsion of charged fouling materials, (amino acids and proteins tend to be negatively charged at neutral pH, above their isoelectric point). **(d.)** Superhydrophobic surfaces, low surface adhesion of hydrophilic fouling material facilitates removal with flow of water. **(e.)** Hydrophilic surfaces, reduce foulant adhesion as species must possess significant energy to displace strongly bound water layer and resist subsequent displacement by water on highly wetting surface.[121]

Steric repulsion methods are a classic example of antifouling surface coating with the most commonly cited example being surface bound polyethylene glycol (PEG) chains. These polymer brushes are the gold standard in antifouling technology as they are known to repel protein adhesion by a combination of steric repulsion and hydrophilicity, although the exact mechanisms for antifouling are still not clearly understood.[109, 125]

Research has demonstrated that micro and nanoscale topographies can significantly reduce bacterial biofouling, for both individual cells and bacterial biofilms.[81, 109, 126] Once again the exact mode of natural antifouling in this case is not well understood however it has been proposed to occur via a range of mechanisms. Firstly, the best known mechanism is the so-called "lotus effect".[127] In this instance a micro patterned surface with enhanced super hydrophobicity causes water to bead up on the surface, and pick up the contaminants as it rolls off. Secondly, the nano-topography may be such that it is unfavourable towards cellular attachment.[128] This can be better illustrated when surface roughness is considered under three conditions. When surface grooves are in close proximity

to one another with gaps smaller than individual bacteria there is minimal cell-substrate interaction. If the grooves approach the size of bacteria they are capable of entering the groove and attaching strongly to the substrate. Finally when grooves greatly exceed the dimensions of the bacteria the surface functions effectively as a flat surface from the bacterial point of view.[128]Thirdly, micro patterning as seen in aquatic animals, (*e.g*. the dermal denticles on shark skin), allows for enhanced drag and the efficient flow of water to slough organisms off of the surface.[129]

In many instances surface wettability is found to play a key role in antifouling processes, however due to the complex nature of biofouling the mechanisms by which it acts are still poorly understood.[54, 109-110] The Baier curve (**Figure 1.7**)[130] seeks to explain the correlation between surface energy and protein adhesion. The critical component of the Baier curve shows that fouling reduction is achieved at a surface tension of 22-24 mN/m, approximately equal to the dispersive component for water.[109] Thus for surfaces submerged in aqueous environments, when materials possess surface free energy of *ca.* 22 mN/m, the thermodynamic cost of surface rewetting is minimised.[130] These surfaces tend to wet easily and are termed 'hydrophilic materials'.

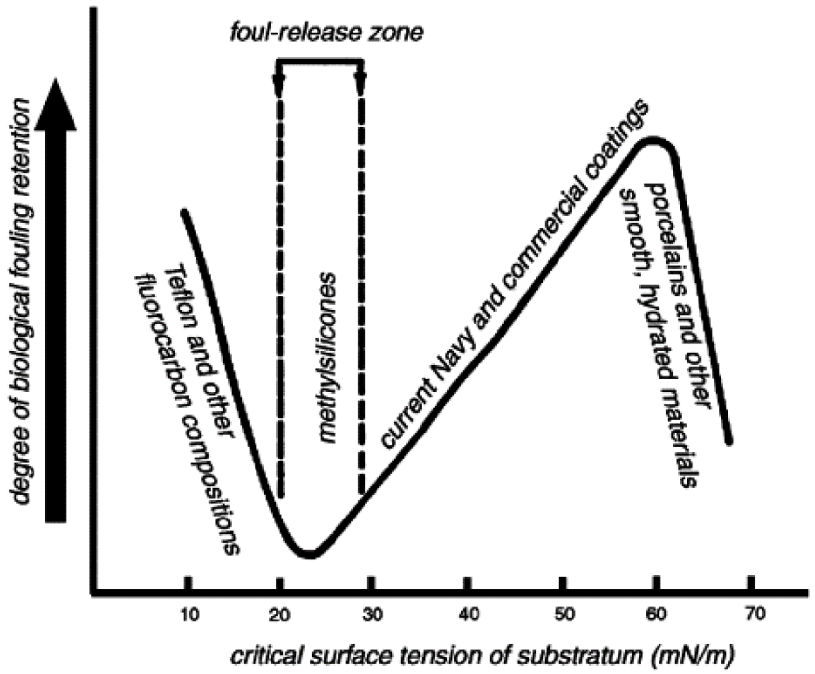

Figure 1.7. The Baier curve correlating the relative degree of biofouling versus critical surface tensions of the substrate. Reproduced with permission.[130]

Hydrophilic surfaces are believed to inhibit fouling by attracting a layer of strongly bound water that cannot be displaced by a protein and thus inhibiting protein adsorption.[131] Proteins however have been observed to physisorb onto hydrophilic surfaces *via* attachment of their coronas to the substratum.[126] Zwitterionic surfaces, (surfaces with both positively and negatively charged groups) are believed to possess antifouling properties by strong attraction of water layers which reject fouling.[132] These materials hold promise as antifouling materials due to their chemical stability and non-cytotoxic fouling resistance.

2.5 Glycosylated surfaces in antifouling technologies

The production of covalently bound saccharide coatings with application of antifouling technologies has been explored previously within the Colavita and Scanlan groups.[60, 69-70, 133] This body of work has previously reported on the modification of carbon and polymeric surfaces with a range of mono- and di-saccharides (**Figure 1.8**), *via* spontaneous aryldiazonium grafting methods.

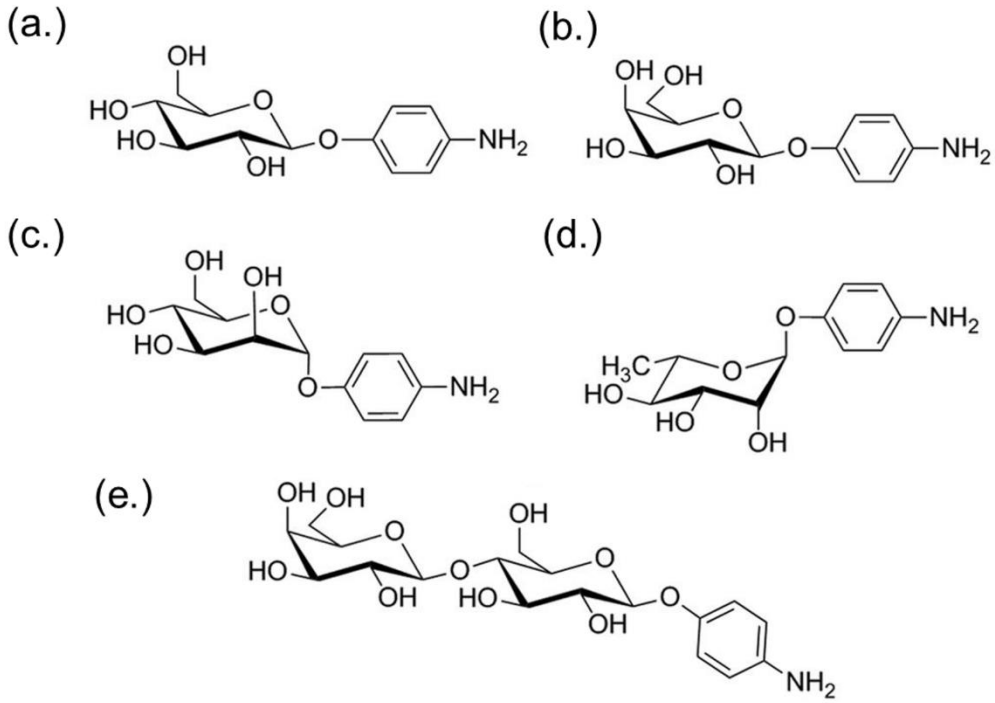

Figure 1.8. 4-aminophenyl glycosides synthesized as precursors for the preparation of carbohydrate layers via aryldiazonium chemistry: **(a.)** 4-aminophenol-β-D-glucopyranose, **(b.)** 4-aminophenol-β-D-galactopyranose, **(c.)** 4-aminophenol-α-D-mannopyranose, **(d.)** 4-aminophenol-α-L-rhamnopyranose and **(e.)** 4-aminophenol-β-D-lactopyranose. Adapted under Creative Commons. Original Article[133]

Due to the high concentration of hydroxyl groups at carbohydrate coated surfaces, it is generally observed that the surface possesses strongly hydrophilic properties and hence acts as hydrophilic anti-adhesive surface.[70, 109, 133-134] These coatings have been found to be stable to sonication,[64] readily increase surface wettability,[133] display specific lectin binding capabilities[60, 69-70] (mannose Con-A binding and galactose PNA specific binding) and readily reject nonspecific protein adhesion (fibrinogen, lysosome and serum albumin) (**Figure 1.9**).

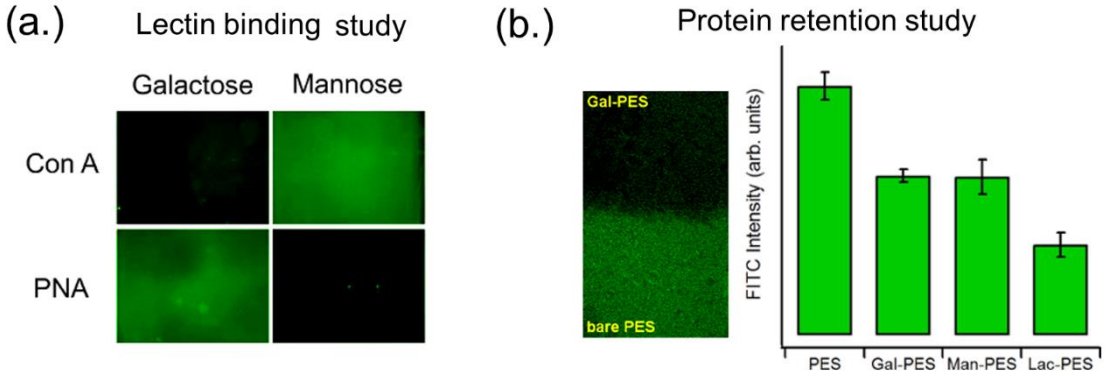

Figure 1.9. (a.) Specific lectin binding Polydimethyl siloxane (PDMS) surfaces functionalised via spontaneous aryldiazonium grafting with galactose and mannose terminations. Fluorescent microscopy of samples immersed in FITC congugated lectins is shown. Fluorescence was observed only upon specific conjugation with a binding lectin i.e. Conclavin-A (Con A) binding is observed on mannose modified surfaces, with Peanut agglutinin (PNA) binding observed only on galactose surfaces. Adapted with permission from [60]). **(b.)** Shows the fluorescent microscopy image of a PES membrane partially coated with galactose by spontaneous aryldiazonium grafting. FITC-BSA retention is observed to be higher unmodified sections. Additionally shown is relative fluoresence intensity proportional to retained proteins charted for bare, galactose, mannose and lactose modified PES samples. (Adapted with permission from *ACS Appl. Mater. Interfaces*, **2015**, *7* (31), pp 17238–17246. Copyright 2015 ACS.[70]

As lectin specificity has been confirmed on surfaces terminated with specific with saccharides formed by aryldiazonium mediated covalent grafting, it is expected that emergent glycoarray technologies could be readily produced by these grafting methods. Additionally due to enhanced nonspecific binding of protinatious materials observed on carbohydrate modified carbon, and polymer surfaces surfaces,[69-70, 133] it is expected that these materials may find potential applications across several industries for biofouling prevention due to their excellent biocompatability and non-toxic degradation products. Further, in work by Angione *et al.*[70] it was observed that lactose functionalities on PES filter membranes when subjected to waste water flow retained lower degrees of biomass when compared to unmodified commercial filters. It was demonstrated

that in the case of complex aqueous environments that are rich in biomass, such as wastewater effluent, carbohydrate surfaces may present useful in biofilm resistant or foulant releasing materials.

3 Aims of this thesis

Surface bound carbohydrates have amassed considerable interest due to their roles in nature and significant potential for useful industrial applications. Because of this there exists a high demand for rapid carbohydrate surface modification techniques with significant control of functionality.

The key aims of this thesis involve the study of aryldiazonium based saccharide coatings to improve our understanding of the surface composition of saccharide modified surfaces with regards to carbohydrate film properties and surface adhered biofilm control. Further applications of this budding technology are to be explored and developed over the course of this study with applications of interest including active sensing technologies, passive fouling control on novel materials of commercial interest and in the development of energy storage devices.

To achieve this, a lactoside based aminophenol aryldiazonium precursor compound will be synthesised by known methods. Using this compound, the effect if any, of choice in diazonium grafting procedure on the resulting saccharide coatings at carbon surfaces will be investigated. Surface properties will be probed by spectroscopic methods, lectin binding capabilities, wettability studies, and protein retention studies. Resulting films will also be investigated for their potential in the application of passive fouling resistant coatings for improvement in electrochemical sensing technologies.

Secondly, protocols will be developed for the spontaneous attachment of aryl-lactoside coatings to nonconductive materials of industrial interest, (namely PES, polyamide, and stainless steel surfaces), with the intent of producing functional materials with enhanced surface biofilm rejection capabilities. The antifouling capabilities of these materials will be further probed under marine fouling conditions by means of immersion in a heavy fouling coastal environment for an extended period of time.

Finally, the synthesis of novel oligosaccharide-based diazonium compounds from β-cyclodextrin will be attempted in the hopes of producing a rapid facile

surface coating protocol to impart the desirable properties of cyclodextrin to a variety of material surfaces for host-guest cavity interactions and antifouling applications.

References

1. Kennedy, J. F.; White, C. A., *Bioactive Carbohydrates in Chemistry, Biochemistry, and Biology*. E. Horwood: **1983**.
2. Dashty, M., A quick look at biochemistry: Carbohydrate metabolism. *Clin Biochem.* **2013,** *46* (15), 1339-1352.
3. Berg, J. M.; Tymoczko, J. L.; Stryer, L., *Biochemistry*. W.H. Freeman: **2002**.
4. Stine, K. J., *Carbohydrate Nanotechnology*. Wiley: **2015**.
5. Martinez-Seara Monne, H.; Danne, R.; Róg, T.; Ilpo, V.; Gurtovenko, A., Structure of Glycocalyx. *Biophys. J.l* **2013,** *104* (2, Supplement 1), 251a.
6. Brandley, B. K.; Schnaar, R. L., Cell-Surface Carbohydrates in Cell Recognition and Response. *J. Leukocyte. Biol.* **1986,** *40* (1), 97-111.
7. Avci, F. Y.; Li, X.; Tsuji, M.; Kasper, D. L., Carbohydrates and T cells: a sweet twosome. *Semin Immunol.* **2013,** *25* (2), 146-151.
8. Kato, K.; Ishiwa, A., The role of carbohydrates in infection strategies of enteric pathogens. *Trop Med Health.* **2015,** *43* (1), 41-52.
9. Busk, P. K.; Lange, L., Function-based classification of carbohydrate-active enzymes by recognition of short, conserved peptide motifs. *App Environ Microb.* **2013,** *79* (11), 3380-3391.
10. Bucior, I.; Scheuring, S.; Engel, A.; Burger, M. M., Carbohydrate-carbohydrate interaction provides adhesion force and specificity for cellular recognition. *J Cell Biol* **2004,** *165* (4), 529-537.
11. Cunto-Amesty, G.; Dam, T. K.; Luo, P.; Monzavi-Karbassi, B.; Brewer, C. F.; Van Cott, T. C.; Kieber-Emmons, T., Directing the Immune Response to Carbohydrate Antigens. *J Biol Chem* **2001,** *276* (32), 30490-30498.
12. Kornfeld, S., Diseases of abnormal protein glycosylation: an emerging area. J *Clin Invest.* **1998,** *101* (7), 1293-1295.
13. Lehle, L.; Strahl, S.; Tanner, W., Protein Glycosylation, Conserved from Yeast to Man: A Model Organism Helps Elucidate Congenital Human Diseases. *Angew Chem Int Ed.* **2006,** *45* (41), 6802-6818.
14. Stowell, S. R.; Ju, T.; Cummings, R. D., Protein glycosylation in cancer. *Annu Rev Path-Mech.* **2015,** *10*, 473-510.
15. King, R. H., The role of glycation in the pathogenesis of diabetic polyneuropathy. *Molecular pathology* **2001,** *54* (6), 400-408.
16. Frenkel-Pinter, M.; Shmueli, M. D.; Raz, C.; Yanku, M.; Zilberzwige, S.; Gazit, E.; Segal, D., Interplay between protein glycosylation pathways in Alzheimer's disease. *Sci Adv.* **2017,** *3* (9).
17. Abou-Abbass, H.; Abou-El-Hassan, H.; Bahmad, H.; Zibara, K.; Zebian, A.; Youssef, R.; Ismail, J.; Zhu, R.; Zhou, S.; Dong, X.; Nasser, M.; Bahmad, M.; Darwish, H.; Mechref, Y.; Kobeissy, F., Glycosylation and other PTMs alterations in neurodegenerative diseases: Current status and future role in neurotrauma. *Electrophoresis* **2016,** *37* (11), 1549-1561.
18. Çelik, E.; Ollis, A. A.; Lasanajak, Y.; Fisher, A. C.; Gür, G.; Smith, D. F.; DeLisa, M. P., Glycoarrays with engineered phages displaying structurally diverse oligosaccharides enable high throughput detection of glycan protein interactions. *Biotechnol J.* **2015,** *10* (1), 199-209.

19. Laurent, N.; Voglmeir, J.; Flitsch, S. L., Glycoarrays—tools for determining protein–carbohydrate interactions and glycoenzyme specificity. *Chem Comm.* **2008,** (37), 4400-4412.
20. Puvirajesinghe, T.; Turnbull, J., Glycoarray Technologies: Deciphering Interactions from Proteins to Live Cell Responses. *Microarrays* **2016,** *5* (1), 3.
21. Kletter, D.; Cao, Z.; Bern, M.; Haab, B., Determining lectin specificity from glycan array data using motif segregation and GlycoSearch software. *Current protocols in chemical biology* **2013,** *5* (2), 157-169.
22. Houseman, B. T.; Mrksich, M., Carbohydrate Arrays for the Evaluation of Protein Binding and Enzymatic Modification. *Chem Biol.* **2002,** *9* (4), 443-454.
23. Zhi, Z.-L.; Laurent, N.; Powell, A. K.; Karamanska , R.; Fais , M.; Voglmeir, J.; Wright, A.; Blackburn, J. M.; Crocker, P. R.; Russell, D. A.; Flitsch, S.; Field , R. A.; Turnbull, J. E., A Versatile Gold Surface Approach for Fabrication and Interrogation of Glycoarrays. *ChemBioChem* **2008,** *9* (10), 1568-1575.
24. Fais, M.; Karamanska, R.; Allman, S.; Fairhurst, S. A.; Innocenti, P.; Fairbanks, A. J.; Donohoe, T. J.; Davis, B. G.; Russell, D. A.; Field, R. A., Surface plasmon resonance imaging of glycoarrays identifies novel and unnatural carbohydrate-based ligands for potential ricin sensor development. *Chem Sci.* **2011,** *2* (10), 1952-1959.
25. Jain, K.; Kesharwani, P.; Gupta, U.; Jain, N. K., A review of glycosylated carriers for drug delivery. *Biomaterials* **2012,** *33* (16), 4166-4186.
26. Lin, K.; Kasko, A. M., Carbohydrate-Based Polymers for Immune Modulation. *ACS Macro Lett.* **2014,** *3* (7), 652-657.
27. Kieber-Emmons, T.; Monzavi-Karbassi, B.; Hutchins, L. F.; Pennisi, A.; Makhoul, I., Harnessing benefit from targeting tumor associated carbohydrate antigens. *Hum Vacc Immunother.* **2016,** *13* (2), 323-331.
28. Valotteau, C.; Calers, C.; Casale, S.; Berton, J.; Stevens, C. V.; Babonneau, F.; Pradier, C.-M.; Humblot, V.; Baccile, N., Biocidal Properties of a Glycosylated Surface: Sophorolipids on Au(111). *ACS Appl Mater Inter.* **2015,** *7* (32), 18086-18095.
29. Bender, M. L.; Komiyama, M., *Cyclodextrin Chemistry*. Springer Berlin Heidelberg: **2012**.
30. Schneiderman, E.; Stalcup, A., *Cyclodextrins: A Versatile Tool in Separation Science*. J. Chromatogr B Sci Appl. **2000**; Vol. 745, p 83-102.
31. Oprea, S.; Potolinca, V. O., Synthesis and Characterisation of Linear and Cross-Linked Cyclodextrin Polyurethane Elastomers. *Polymer-Plas Technol* **2013,** *52* (15), 1550-1556.
32. Mamba, B.; Krause, R.; J. Malefetse, T.; Nxumalo, E., Monofunctionalized cyclodextrin polymers for the removal of organic pollutants from water. Environ Chem Lett. **2007**; Vol. 5, p 79-84.
33. Sadrerafi, K.; Moore, E. E.; Lee, M. W., Association constant of β-cyclodextrin with carboranes, adamantane, and their derivatives using displacement binding technique. *J Incl Phenom Macro.* **2015,** *83* (1), 159-166.
34. Loftsson, T.; Jarho, P.; Másson, M.; Järvinen, T., Cyclodextrins in drug delivery. *Expert Opin Drug Del.* **2005,** *2* (2), 335-351.
35. Otero-Espinar, F. J.; Torres-Labandeira, J. J.; Alvarez-Lorenzo, C.; Blanco-Méndez, J., Cyclodextrins in drug delivery systems. *J Drug Del Sci Tech.* **2010,** *20* (4), 289-301.
36. Willats, W. G. T.; Rasmussen, S. E.; Kristensen, T.; Mikkelsen, J. D.; Knox, J. P., Sugar-coated microarrays: A novel slide surface for the high-throughput analysis of glycans. *Proteomics* **2002,** *2* (12), 1666-1671.
37. Fritz, M. C.; Hähner, G.; Spencer, N. D.; Bürli, R.; Vasella, A., Self-Assembled Hexasaccharides: Surface Characterisation of Thiol-Terminated Sugars Adsorbed on a Gold Surface. *Langmuir* **1996,** *12* (25), 6074-6082.
38. Houseman, B. T.; Mrksich, M., The Role of Ligand Density in the Enzymatic Glycosylation of Carbohydrates Presented on Self-Assembled Monolayers of Alkanethiolates on Gold. *Angew Chem Int Ed.* **1999,** *38* (6), 782-785.

39. Zhi, Z.-l.; Powell, A. K.; Turnbull, J. E., Fabrication of Carbohydrate Microarrays on Gold Surfaces: Direct Attachment of Nonderivatized Oligosaccharides to Hydrazide-Modified Self-Assembled Monolayers. *Anal Chem.* **2006,** *78* (14), 4786-4793.
40. Cheng, F.; Shang, J.; Ratner, D. M., A Versatile Method for Functionalizing Surfaces with Bioactive Glycans. *Bioconjugate Chem.* **2011,** *22* (1), 50-57.
41. Park, S.; Gildersleeve, J. C.; Blixt, O.; Shin, I., Carbohydrate microarrays. *Chem. Soc. Rev.* **2013,** *42* (10), 4310-4326.
42. Meldal, M.; Tornøe, C. W., Cu-Catalyzed Azide−Alkyne Cycloaddition. *Chem. Rev.* **2008,** *108* (8), 2952-3015.
43. Nebhani, L.; Barner-Kowollik, C., Orthogonal Transformations on Solid Substrates: Efficient Avenues to Surface Modification. *Adv. Mater.* **2009,** *21* (34), 3442-3468.
44. Xi, W.; Scott, T. F.; Kloxin, C. J.; Bowman, C. N., Click Chemistry in Materials Science. *Adv. Funct. Mater.* **2014,** *24* (18), 2572-2590.
45. Chehimi, M. M., Aryl Diazonium Salts: New Coupling Agents in Polymer and Surface Science. Wiley: **2012**.
46. Picot, M.; Rodulfo, R.; Nicolas, I.; Szymczyk, A.; Barrière, F.; Rabiller-Baudry, M., A versatile route to modify polyethersulfone membranes by chemical reduction of aryldiazonium salts. J. Membrane Sci. **2012**; Vol. s 417–418, p 131–136.
47. Matrab, T.; Chehimi, M. M.; Boudou, J. P.; Benedic, F.; Wang, J.; Naguib, N. N.; Carlisle, J. A., Surface functionalisation of ultrananocrystalline diamond using atom transfer radical polymerisation (ATRP) initiated by electro-grafted aryldiazonium salts. *Diam. Relat. Mater.* **2006,** *15* (4), 639-644.
48. Mesnage, A.; Lefèvre, X.; Jégou, P.; Deniau, G.; Palacin, S., Spontaneous Grafting of Diazonium Salts: Chemical Mechanism on Metallic Surfaces. *Langmuir* **2012,** *28* (32), 11767-11778.
49. Menanteau, T.; Dias, M.; Levillain, E.; Downard, A. J.; Breton, T., Electrografting via Diazonium Chemistry: The Key Role of the Aryl Substituent in the Layer Growth Mechanism. *J. Phys. Chem. C.* **2016,** *120* (8), 4423-4429.
50. Cao, C.; Zhang, Y.; Jiang, C.; Qi, M.; Liu, G., Advances on Aryldiazonium Salt Chemistry Based Interfacial Fabrication for Sensing Applications. *ACS Appl. Mater. Inter.* **2017,** *9* (6), 5031-5049.
51. Mahouche-Chergui, S.; Gam-Derouich, S.; Mangeney, C.; Chehimi, M. M., Aryl diazonium salts: a new class of coupling agents for bonding polymers, biomacromolecules and nanoparticles to surfaces. *Chem. Soc. Rev.* **2011,** *40* (7), 4143-4166.
52. Hicks, J. M.; Wong, Z. Y.; Scurr, D. J.; Silman, N.; Jackson, S. K.; Mendes, P. M.; Aylott, J. W.; Rawson, F. J., Tailoring the Electrochemical Properties of Carbon Nanotube Modified Indium Tin Oxide via in Situ Grafting of Aryl Diazonium. *Langmuir* **2017,** *33* (20), 4924-4933.
53. Assresahegn, B. D.; Brousse, T.; Bélanger, D., Advances on the use of diazonium chemistry for functionalisation of materials used in energy storage systems. Carbon **2015**; Vol. 92.
54. Gam-Derouich, S.; Gosecka, M.; Lepinay, S.; Turmine, M.; Carbonnier, B.; Basinska, T.; Slomkowski, S.; Millot, M.-C.; Othmane, A.; Ben Hassen-Chehimi, D.; Chehimi, M. M., Highly Hydrophilic Surfaces from Polyglycidol Grafts with Dual Antifouling and Specific Protein Recognition Properties. *Langmuir* **2011,** *27* (15), 9285-9294.
55. Delamar, M.; Hitmi, R.; Pinson, J.; Saveant, J. M., Covalent modification of carbon surfaces by grafting of functionalized aryl radicals produced from electrochemical reduction of diazonium salts. *J. Am. Chem. Soc.* **1992,** *114* (14), 5883-5884.
56. Greenwood, J.; Phan, T. H.; Fujita, Y.; Li, Z.; Ivasenko, O.; Vanderlinden, W.; Van Gorp, H.; Frederickx, W.; Lu, G.; Tahara, K.; Tobe, Y.; Uji-i, H.; Mertens, S. F. L.; De Feyter, S., Covalent Modification of Graphene and Graphite Using Diazonium Chemistry: Tunable Grafting and Nanomanipulation. *ACS Nano* **2015,** *9* (5), 5520-5535.

57. A. Golosova, A.; M. Papadakis, C.; Jordan, R., *Chemical functionalisation of carbon nanotubes with aryl diazonium salts*. *MRS Proceedings* **2011**; Vol. 1362, p qq03-01.
58. Paulik, M. G.; Brooksby, P. A.; Abell, A. D.; Downard, A. J., Grafting Aryl Diazonium Cations to Polycrystalline Gold: Insights into Film Structure Using Gold Oxide Reduction, Redox Probe Electrochemistry, and Contact Angle Behavior. *J. Phys. Chem. C* **2007,** *111* (21), 7808-7815.
59. Le, X. T.; Zeb, G.; Jégou, P.; Berthelot, T., Electrografting of stainless steel by the diazonium salt of 4-aminobenzylphosphonic acid. *Electrochim. Acta* **2012,** *71*, 66-72.
60. Esteban-Tejeda, L.; Duff, T.; Ciapetti, G.; Daniela Angione, M.; Myles, A.; Vasconcelos, J. M.; Scanlan, E. M.; Colavita, P. E., Stable hydrophilic poly(dimethylsiloxane) via glycan surface functionalisation. *Polymer* **2016,** *106*, 1-7.
61. Combellas, C.; Kanoufi, F.; Nunige, S., Surface Modification of Halogenated Polymers. Redox Catalysis Induction of the Polymerisation of Vinylic Monomers. Application to the Localized Graft Copolymerisation of Poly(tetrafluoroethylene) Surfaces by Vinylic Monomers. *Chem. Mate.* **2007,** *19* (15), 3830-3839.
62. Anariba, F.; DuVall, S. H.; McCreery, R. L., Mono- and Multilayer Formation by Diazonium Reduction on Carbon Surfaces Monitored with Atomic Force Microscopy "Scratching". *Anal. Chem.* **2003,** *75* (15), 3837-3844.
63. Barrière, F.; Downard, A. J., Covalent modification of graphitic carbon substrates by non-electrochemical methods. *J. Solid State Electrochem.* **2008,** *12* (10), 1231-1244.
64. Jayasundara, D. R.; Cullen, R. J.; Colavita, P. E., In Situ and Real Time Characterisation of Spontaneous Grafting of Aryldiazonium Salts at Carbon Surfaces. *Chem. Mater.* **2013,** *25* (7), 1144-1152.
65. Mesnage, A.; Abdel Magied, M.; Simon, P.; Herlin-Boime, N.; Jégou, P.; Deniau, G.; Palacin, S., Grafting polymers to titania nanoparticles by radical polymerisation initiated by diazonium salt. *J. Mater. Sci.* **2011,** *46* (19), 6332-6338.
66. Bouriga, M.; Chehimi, M. M.; Combellas, C.; Decorse, P.; Kanoufi, F.; Deronzier, A.; Pinson, J., Sensitized Photografting of Diazonium Salts by Visible Light. *Chem. Mater.* **2013,** *25* (1), 90-97.
67. Dahoumane, S. A.; Nguyen, M. N.; Thorel, A.; Boudou, J.-P.; Chehimi, M. M.; Mangeney, C., Protein-Functionalized Hairy Diamond Nanoparticles. *Langmuir* **2009,** *25* (17), 9633-9638.
68. Pandurangappa, M.; Ramakrishnappa, T.; Compton, R. G., Functionalisation of glassy carbon spheres by ball milling of aryl diazonium salts. *Carbon* **2009,** *47* (9), 2186-2193.
69. Jayasundara, D. R.; Duff, T.; Angione, M. D.; Bourke, J.; Murphy, D. M.; Scanlan, E. M.; Colavita, P. E., Carbohydrate Coatings via Aryldiazonium Chemistry for Surface Biomimicry. *Chem. Mater.* **2013,** *25* (20), 4122-4128.
70. Angione, M. D.; Duff, T.; Bell, A. P.; Stamatin, S. N.; Fay, C.; Diamond, D.; Scanlan, E. M.; Colavita, P. E., Enhanced Antifouling Properties of Carbohydrate Coated Poly(ether sulfone) Membranes. *ACS Appl. Mater. Inter.* **2015,** *7* (31), 17238-17246.
71. Leroux, Y. R.; Hapiot, P., Nanostructured Monolayers on Carbon Substrates Prepared by Electrografting of Protected Aryldiazonium Salts. *Chem. Mater.* **2013,** *25* (3), 489-495.
72. Combellas, C.; Kanoufi, F.; Pinson, J.; Podvorica, F. I., Sterically Hindered Diazonium Salts for the Grafting of a Monolayer on Metals. *J. Am. Chem. Soci.* **2008,** *130* (27), 8576-8577.
73. Breton, T.; Levillain, E.; Thibaud, M.; J. Downard, A., Evidence of monolayer formation via diazonium grafting with a radical scavenger: Electrochemical, AFM and XPS monitoring. Phys. Chem. Chem. Phys. **2015**; Vol. 17.
74. Franklin, M. J.; Chang, C.; Akiyama, T.; Bothner, B., New Technologies for Studying Biofilms. *Microbiol. spectr.* **2015,** *3* (4),

75. Botton, S.; Verliefde, A. R. D.; Quach, N. T.; Cornelissen, E. R., Influence of biofouling on pharmaceuticals rejection in NF membrane filtration. *Water Res.* **2012,** *46* (18), 5848-5860.
76. Chmielewski, R. A. N.; Frank, J. F., Biofilm Formation and Control in Food Processing Facilities. *Compr. Rev. Food Sci. Food Saf.* **2003,** *2* (1), 22-32.
77. Chan, F. T.; MacIsaac, H. J.; Bailey, S. A., Survival of ship biofouling assemblages during and after voyages to the Canadian Arctic. *Mar. bio.* **2016,** *163* (12), 250-250.
78. Venkatesan, R.; Senthilkumar, P.; Vedachalam, N.; Murugesh, P., Biofouling and its effects in sensor mounted moored observatory system in Northern Indian Ocean. *Int. Biodeterior. Biodegradation* **2017,** *116*, 198-204.
79. De Nys, R.; Guenther, J., The impact and control of biofouling in marine finfish aquaculture. In *Advances in Marine Antifouling Coatings and Technologies*, Hellio, C.; Yebra, D., Eds. Woodhead Publishing: **2009**, pp 177-221.
80. Dürr, S.; Thomason, J., *Biofouling*. Wiley: **2009**.
81. Railkin, A. I., Marine Biofouling: Colonisation Processes and Defenses. CRC Press: **2003**.
82. Videla, H. A.; Characklis, W. G., Biofouling and microbially influenced corrosion. *Int. Biodeterior. Biodegradation* **1992,** *29* (3), 195-212.
83. Rabin, N.; Zheng, Y.; Opoku-Temeng, C.; Du, Y.; Bonsu, E.; Sintim, H. O., Biofilm formation mechanisms and targets for developing antibiofilm agents. *Future Med. Chem.* **2015,** *7* (4), 493-512.
84. Kashef, N.; Huang, Y.-Y.; Hamblin, M., Advances in antimicrobial photodynamic inactivation at the nanoscale. *Nanophotonics* **2017**; Vol. 6.
85. Harding, J. L.; Reynolds, M. M., Combating medical device fouling. *Trends Biotechnol.* **2014,** *32* (3), 140-146.
86. Bixler, G. D.; Bhushan, B., Biofouling: lessons from nature. *Philos. Trans. Royal Soc. A* **2012,** 370 (1967), 2381-2417.
87. Wallace, A.; Albadawi, H.; Patel, N.; Khademhosseini, A.; Zhang, Y. S.; Naidu, S.; Knuttinen, G.; Oklu, R., Anti-fouling strategies for central venous catheters. *Cardiovas. Diagn. Ther.* **2017,** *7* (Suppl 3), S246-S257.
88. Gallo, J.; Holinka, M.; Moucha, C. S., Antibacterial surface treatment for orthopaedic implants. *Int. J. Mol. Sci.* **2014,** *15* (8), 13849-13880.
89. Chen, L.; Wen, Y.-m., The role of bacterial biofilm in persistent infections and control strategies. *Int. J. Oral Sci.* **2011,** *3* (2), 66-73.
90. Suci, P. A.; Mittelman, M. W.; Yu, F. P.; Geesey, G. G., Investigation of ciprofloxacin penetration into Pseudomonas aeruginosa biofilms. *Antimicrob. Agents chemother.* **1994,** *38* (9), 2125-2133.
91. Donlan, R. M., Biofilms and device-associated infections. *Emerg. Infect. Diseases* **2001,** *7* (2), 277-281.
92. Cloutier, M.; Mantovani, D.; Rosei, F., Antibacterial Coatings: Challenges, Perspectives, and Opportunities. *Trends Biotechnol.* **2015,** *33* (11), 637-652.
93. Roberts, A. P.; Pratten, J.; Wilson, M.; Mullany, P., Transfer of a conjugative transposon, Tn5397 in a model oral biofilm. *FEMS Microbiol Lett* **1999,** *177* (1), 63-66.
94. Hausner, M.; Wuertz, S., High rates of conjugation in bacterial biofilms as determined by quantitative in situ analysis. *Appl. Environ. Microbiol.* **1999,** *65* (8), 3710-3713.
95. Williams, D. F., On the mechanisms of biocompatibility. *Biomaterials* **2008,** *29* (20), 2941-2953.
96. Lau, E. W., Leads and Electrodes for Cardiac Implantable Electronic Devices. In *Clinical Cardiac Pacing, Defibrillation and Resynchronisation Therapy (Fifth Edition)*, Ellenbogen, K. A.; Wilkoff, B. L.; Kay, G. N.; Lau, C.-P.; Auricchio, A., Eds. Elsevier: **2017**, pp 313-351.e29.
97. ISO 10993-1:2018 Biological evaluation of medical devices — Part 1: Evaluation and testing within a risk management process. **2018**.

98. Lehaitre, M.; Delauney, L.; Compere, C., *Biofouling and underwater measurements*. **2008**; p 463-493.
99. E Callow, M.; E Callow, J., Marine biofouling: A sticky problem. *Biologist (London)* **2002**; Vol. 49, p 10-4.
100. Callow, J. A.; Callow, M. E., Trends in the development of environmentally friendly fouling-resistant marine coatings. *Nature Comm.* **2011,** *2*, 244.
101. Alexander, B. E.; Mueller, B.; Vermeij, M. J. A.; van der Geest, H. H. G.; de Goeij, J. M., Biofouling of inlet pipes affects water quality in running seawater aquaria and compromises sponge cell proliferation. *PeerJ* **2015,** *3*, e1430-e1430.
102. Demirel, Y. K.; Uzun, D.; Zhang, Y.; Fang, H.-C.; Day, A. H.; Turan, O., Effect of barnacle fouling on ship resistance and powering. *Biofouling* **2017,** *33* (10), 819-834.
103. Bax, N.; Williamson, A.; Aguero, M.; Gonzalez, E.; Geeves, W., Marine invasive alien species: a threat to global biodiversity. *Mar. Policy* **2003,** *27* (4), 313-323.
104. Braithwaite, R. A.; McEvoy, L., Marine Biofouling on Fish Farms and Its Remediation. *Adv. Mar. Biol.* **2005**; Vol. 47, p 215-52.
105. Di Donato, P.; Poli, A.; Taurisano, V.; Abbamondi, G.; Nicolaus, B.; Tommonaro, G., Recent Advances in the Study of Marine Microbial Biofilm: From the Involvement of Quorum Sensing in Its Production up to Biotechnological Application of the Polysaccharide Fractions. *J. Mar. Sci. Eng.* **2016,** *4* (2), 34.
106. Kamino, K., Mini-review: Barnacle adhesives and adhesion. *Biofouling* **2013,** *29* (6), 735-749.
107. S., K.; Raghavan, V., Isolation and characterisation of marine biofilm forming bacteria from a ship's hull. *Front. Biol.* **2018,** *13* (3), 208-214.
108. Hopkins, G. A.; Forrest, B. M., Management options for vessel hull fouling: an overview of risks posed by in-water cleaning. *ICES J. Mar. Sci.* **2008,** *65* (5), 811-815.
109. Magin, C. M.; Cooper, S. P.; Brennan, A. B., Non-toxic antifouling strategies. *Mater. Today* **2010,** *13* (4), 36-44.
110. Lejars, M.; Margaillan, A.; Bressy, C., Fouling Release Coatings: A Nontoxic Alternative to Biocidal Antifouling Coatings. *Chem. Rev.* **2012,** *112* (8), 4347-4390.
111. Hua, J.; Chiu, Y.-S.; Tsai, C.-Y., En-route operated hydroblasting system for counteracting biofouling on ship hull. *Ocean Engi.* **2018,** *152*, 249-256.
112. Nurioglu, A. G.; Esteves, A. C. C.; de With, G., Non-toxic, non-biocide-release antifouling coatings based on molecular structure design for marine applications. *J. Mater. Chem. B* **2015,** *3* (32), 6547-6570.
113. Maillard, J.-Y., Antimicrobial biocides in the healthcare environment: efficacy, usage, policies, and perceived problems. *Ther. Clin. Risk. Manag.* **2005,** *1* (4), 307-320.
114. Sudha, V. B. P.; Ganesan, S.; Pazhani, G. P.; Ramamurthy, T.; Nair, G. B.; Venkatasubramanian, P., Storing drinking-water in copper pots kills contaminating diarrhoeagenic bacteria. *J. Health. Popul. Nutr.* **2012,** *30* (1), 17-21.
115. Sondi, I.; Salopek-Sondi, B., Silver nanoparticles as antimicrobial agent: a case study on E. coli as a model for Gram-negative bacteria. *J. Colloid Interf. Sci.* **2004,** *275* (1), 177-182.
116. Tchounwou, P. B.; Yedjou, C. G.; Patlolla, A. K.; Sutton, D. J., Heavy Metal Toxicity and the Environment. In *Molecular, Clinical and Environmental Toxicology: Volume 3: Environmental Toxicology*, Luch, A., Ed. Springer Basel: Basel, **2012**, pp 133-164.
117. Podporska-Carroll, J.; Myles, A.; Quilty, B.; McCormack, D. E.; Fagan, R.; Hinder, S. J.; Dionysiou, D. D.; Pillai, S. C., Antibacterial properties of F-doped ZnO visible light photocatalyst. *J. Hazard. Mater.* **2017,** *324*, 39-47.
118. Nehring, S., After the TBT era: Alternative anti-fouling paints and their ecological risks. *Senck. marit.* **2001,** *31* (2), 341.
119. Shakeri, A.; Yip, D.; Badv, M.; Imani, S. M.; Sanjari, M.; Didar, T. F., Self-Cleaning Ceramic Tiles Produced via Stable Coating of TiO_2 Nanoparticles. *Materials (Basel, Switzerland)* **2018,** *11* (6), 1003.

120. Lee, S.-Y.; Park, S.-J., TiO2 photocatalyst for water treatment applications. *J. Ind. Eng. Chem.* **2013,** *19* (6), 1761-1769.
121. Choudhury, R. R.; Gohil, J. M.; Mohanty, S.; Nayak, S. K., Antifouling, fouling release and antimicrobial materials for surface modification of reverse osmosis and nanofiltration membranes. *J. Mater. Chem. A* **2018,** *6* (2), 313-333.
122. Shahkaramipour, N.; Tran, T. N.; Ramanan, S.; Lin, H., Membranes with Surface-Enhanced Antifouling Properties for Water Purification. *Membranes* **2017,** *7* (1), 13.
123. Myan, F. W. Y.; Walker, J.; Paramor, O., The interaction of marine fouling organisms with topography of varied scale and geometry: a review. *Biointerphases* **2013,** *8* (1), 30.
124. Lu, X.; Peng, Y.; Qiu, H.; Liu, X.; Ge, L., Anti-fouling membranes by manipulating surface wettability and their anti-fouling mechanism. *Desalination* **2017,** *413*, 127-135.
125. Dalsin, J. L.; Messersmith, P. B., Bioinspired antifouling polymers. *Mater. Today* **2005,** *8* (9), 38-46.
126. Genzer, J.; Efimenko, K., Recent developments in superhydrophobic surfaces and their relevance to marine fouling: a review. *Biofouling* **2006,** *22* (5), 339-360.
127. Vanithakumari, S. C.; Yadavalli, P.; George, R. P.; Mudali, U. M. K., Lotus effect-based coatings on marine steels to inhibit biofouling. *Surf. Innov.* **2015,** *3* (2), 115-126.
128. Graham, M.; Cady, N., Nano and Microscale Topographies for the Prevention of Bacterial Surface Fouling. *Coatings* **2014,** *4* (1), 37.
129. Damodaran, V. B.; Murthy, N. S., Bio-inspired strategies for designing antifouling biomaterials. *Biomater. Res.* **2016,** *20* (1), 18.
130. Baier, R. E., Surface behaviour of biomaterials: The theta surface for biocompatibility. *J. Materi. Sci-Mater. M.* **2006,** *17* (11), 1057.
131. Kobayashi, M.; Terayama, Y.; Yamaguchi, H.; Terada, M.; Murakami, D.; Ishihara, K.; Takahara, A., Wettability and Antifouling Behavior on the Surfaces of Superhydrophilic Polymer Brushes. *Langmuir* **2012,** *28* (18), 7212-7222.
132. He, M.; Gao, K.; Zhou, L.; Jiao, Z.; Wu, M.; Cao, J.; You, X.; Cai, Z.; Su, Y.; Jiang, Z., Zwitterionic materials for antifouling membrane surface construction. *Acta Biomaterialia* **2016,** *40*, 142-152.
133. Zen, F.; Angione, M. D.; Behan, J. A.; Cullen, R. J.; Duff, T.; Vasconcelos, J. M.; Scanlan, E. M.; Colavita, P. E., Modulation of Protein Fouling and Interfacial Properties at Carbon Surfaces via Immobilisation of Glycans Using Aryldiazonium Chemistry. *Sci. Rep.* **2016,** *6*, 24840.
134. Banerjee, I.; Pangule, R. C.; Kane, R. S., Antifouling Coatings: Recent Developments in the Design of Surfaces That Prevent Fouling by Proteins, Bacteria, and Marine Organisms. *Adv. Mater.* **2011,** *23* (6), 690-718.

Chapter II

Saccharide Coating Precursor Synthesis

The study of carbohydrates is a challenging endeavour, popularised due to the vast array of biological and industrial processes and functions they are involved in. Carbohydrate synthesis is an ever expanding field with novel saccharides and conjugates produced regularly. In this chapter the design, synthesis and characterisation of Lactoside and Cyclodextrin based Diazonium precursors for surface modification are discussed.

The data Presented in this chapter is reproduced in part from the following publications:

Bioinspired Aryldiazonium Carbohydrate Coatings: Reduced Adhesion of Foulants at Polymer and Stainless Steel Surfaces in a Marine Environment
Adam Myles, Damien Haberlin, Leticia Esteban-Tejeda, M. Daniela Angione, Michelle P. Browne, Thomas K. Doyle, Eoin M. Scanlan , and Paula E. Colavita
ACS *Sustainable Chem. Eng*., **2018**, *6* (1), pp 1141–1151

&

Spontaneous Aryldiazonium Grafting for the Preparation of Functional Cyclodextrin Modified Materials
Adam Myles, James. A. Behan, Brendan Twamley, Paula E. Colavita, & Eoin M. Scanlan
ACS Appl. Bio Mater., **2018**, *1* (3), pp 825–832

1 Introduction

In this chapter we discuss the synthesis of aryldiazonium precursors through the conjugation of carbohydrates to aminophenol moieties. The term carbohydrate is deceptively simple term for a family of organic molecules found abundantly in nature. This class of compounds is essential to life and carbohydrates are involved in myriad biological processes including energy storage, cellular composition, specific lectin recognition and cellular responses. Simple saccharides exist in a cyclic structure with six membered rings (pyranoses) or 5 membered rings (furanoses) with smaller chains unlikely due to the steric strain on the structure. The variability in saccharide units arises due to the fact that each carbon in the chain acts as a stereo-centre with variability in orientation at each site leading to different behaviours.[1-3]

This category of compounds ranges from simple sugars consisting of a single unit, two units or three units covalently attached together (mono-, di-, and tri-saccharides) to larger oligosaccharides (4-10 units) and polysaccharides which can possess thousands of monosaccharide units. Prior work in the Colavita and Scanlan groups has yielded synthetic methods for the production of aminophenol conjugated to a variety of monosaccharides (galactose, glucose, mannose, and rhamnose)[3-5] and the disaccharide (lactose) for use in surface modification.[3, 5-7]

1.1 Lactose Modification

One of the synthetic challenges associated with saccharides comes from the number of reactive hydroxyl sites each molecule possesses. These can render production of a single homogeneous product difficult and in order to modify a particular site on the sugar ring the use of protecting groups is often necessary.[8] In the case of lactose for example, acetyl groups are used to protect the hydroxyl groups preventing unwanted side reactions. Acetyl protection is known to increase solubility of saccharides in organic solvents such as chloroform and DCM leading to easier synthetic processing. Acetyl protection at the C-2 position is a widely utilised strategy for regulating stereo control of glycosylation reactions, a process often referred to as ‘neighbouring group participation’. Acetyl protection also possesses the benefit of providing an easily identifiable infrared spectral pattern.[3-4, 6-7]

Further difficulties in preparation of pure glycan products arise from the tendency of sugars to furnish anomeric mixtures during glycosyloation reactions. Anomers are formed when the cyclic structure ring opens at the C-1 position to form an aldehyde (or ketone) which undergoes cyclisation to form the hemiacetal in either an axial or equatorial position to the anomeric reference atom (C-5). Due to hetero nuclear cyclisation these often exist as an impure mixture of α (axial) and β (equatorial) anomers which can be difficult to separate. Through the use of Koenigs–Knorr reaction of bromoacetyl-lactose it is possible to produce a sterically controlled reaction through neighboring group participation which yields anomerically pure β glycosylation product.[9]

1.2 Cyclodextrin modification

Cyclodextrins are oligosaccharides comprised of a series of (1,4) α-linked glucoside units. The nomenclature of cyclodextrins comes from the chain length of the cyclic structure most commonly containing 6 (α), 7 (β), or 8 (γ) units respectively. They possess a torus structure with hydrophilic exterior and a hydrophobic cavity capable of forming host guest complexes with a variety of organic molecules.[10-11] These compounds have a range of uses and as such the ability to modify cyclodextrins has garnered great scientific and commercial interests.[12-13] Since these molecules do not possess a reactive anomeric carbon as is the case with the mono- and di–saccharides discussed above, it is necessary to substitute either a primary or secondary alcohol. The mono-tosylation of the primary faces of cyclodextrin units is widely used to produce a cyclodextrin compound with a suitable leaving group for further modification.[14-15]A three step synthesis to produce 6-*O*-aminophenol-β-Cyclodextrin is discussed herein.[16]

2 Synthesis of aminophenol aryldiazonium precursors

2.1 Lactose Derivatives

Lactose conjugated aminophenol diazonium precursors can be prepared as shown in **scheme 2.1** to yield the desired lactoside ‘coating’ precursor (6) and an acetyl-protected analogue (5), suitable for infrared confirmation of surface grafting. In addition, the synthetic pathway of fluorine containing analogues (8) &

(9) is shown. These fluorinated analogues were utilised for coverage determinations and further confirmation of grafting by elemental spectroscopy. Commercially available D-lactose was per-acetylated upon treatment with sodium acetate and acetic anhydride to give (2).[17] This was converted to the lactosyl bromide[18] (3) upon treatment with HBr in acetic acid. The glycosyl bromide donor was utilised in the silver ion mediated glycosylation of 4-nitrophenol or 2-fluro-4-nitrophenol to produce the anomericaly pure (4) or (7) respectively.[6] Pd catalysed reduction of these compounds yielded the acetyl protected aminophenol products (5) & (8) which were used to form the lactoside aryldiazonium species. The compounds, upon deprotection *via* exposure to catalytic sodium methoxide, furnished the lactoside coating reagents (6) and (9) used as coating agents in this work.[7]

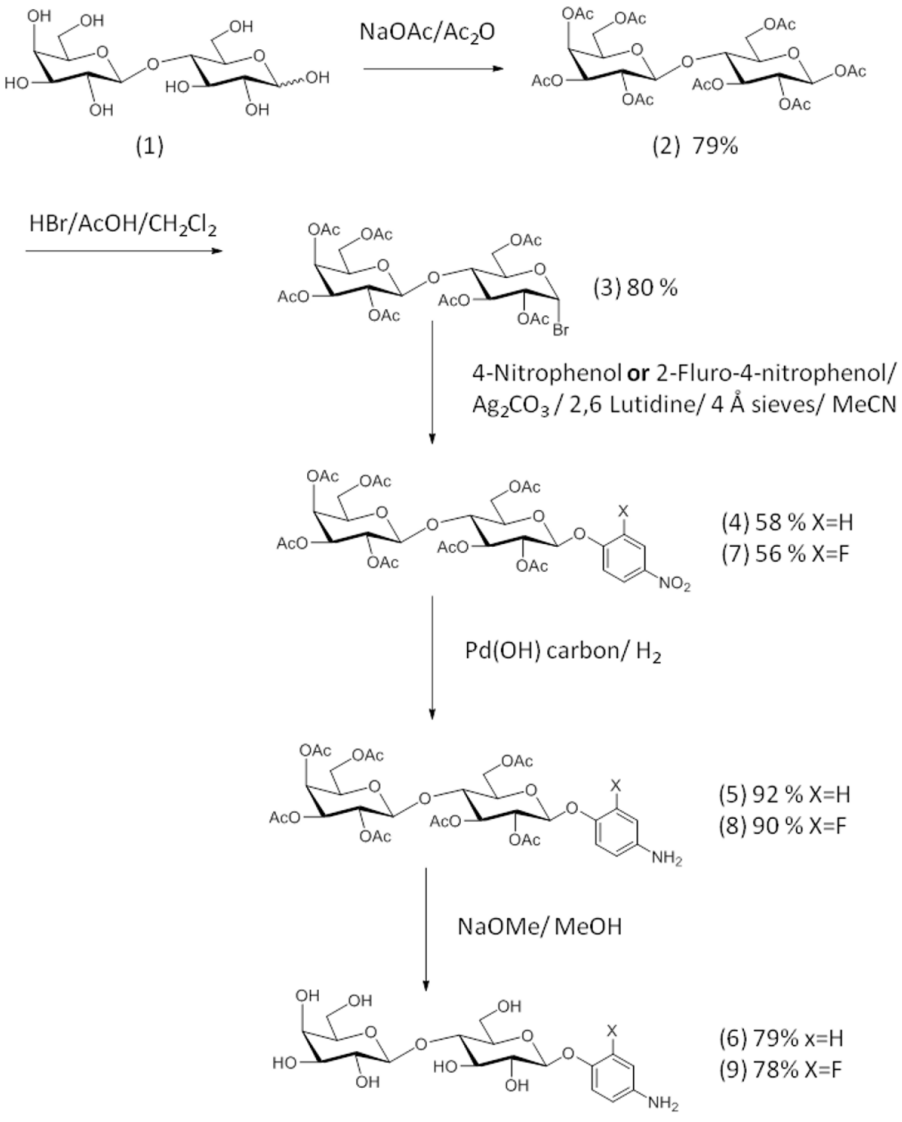

Scheme 2.1. Lactoside diazonium precursor compounds synthesis.

2.2 Cyclodextrin Derivatives

Mono substituted 6-*O*-aminophenol-β-Cyclodextrin (amβCD) was synthesized through a three step protocol outlined below (**Scheme 2.2**). Beta-Cyclodextrin (βCD) (10) was mono-tosylated upon reaction with *p*-toluenesulfonyl chloride in alkaline solution.[14] The reaction mixture was neutralized upon addition of 6 M hydrochloric acid and the resulting precipitate was filtered and repeatedly recrystallized from a 1:1 MeOH/H_2O mixture until a degree of tosylation (DT %) greater than 90% as determined by ^1H NMR was obtained.[15] The monotosyl-βCD (11) was subsequently refluxed at 80 °C in the presence of excess p-nitrophenol in DMF to furnish the nitrophenolic derivative (12).[19] The desired aminophenol derivative (13) was prepared by reduction of (12) in the presence of Pd on charcoal.[6]

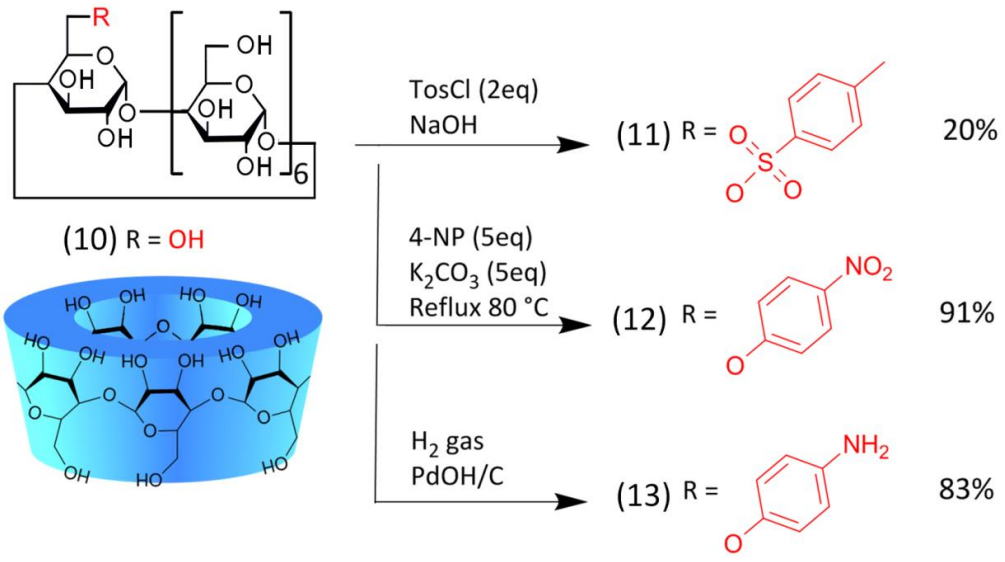

Scheme 2.2. Synthesis of amβCD diazonium precursor. Adapted with permission from *ACS Appl. Bio Mater.*, ***2018**, 1 (3), pp 825–83*. Copyright 2018 American Chemical Society.

3 Synthetic procedures

3.1 Lactoside Diazonium Precursor's Synthesis

Peracetyl-lactoside (2)

D-Lactose purchased from Sigma-Aldrich (20.0 g, 58 mmol, 1 eq) was suspended in Acetic anhydride (100 mL) and heated to 120 °C. Sodium acetate (1 eq) was added slowly to this solution with stirring until all of the solid was dissolved. The solution was stirred for 30 min. Acetic anhydride was removed by pouring the hot solution onto ice water with stirring for 16 h. The resulting white powder was extracted into chloroform. This organic layer was subsequently washed three times with DI water and with saturated sodium bicarbonate solution. The organic layer was evaporated to oil by rotary evaporation and the solid product was precipitated in hexane. (Yield 31.5 g, 79%) IR cm^{-1} 1747 (C=O), 1431 (C=C), 1368 (CH_3), 1209 (C-O acetyl), 1024 (C-O saccharide); ^{1}H-NMR (600 MHz, $CDCl_3$), δ 5.70 (1H, d, $J_{1,2}$ = 8.43 Hz, H-1), 5.37 (1H, s, H-3), 5.26 (1H, t, *J* = 9.08 Hz, H-4), 5.13 (1H, m, H-2), 5.06-4.98 (3H, m, H-2, H-3, H-5), 4.50 (1H, d, *J* = 7.92 Hz, H-1), 4.47 (1H, d, *J* = 11.50 Hz, H-6), 4.19-4.00 (3H, m, 3x H-6), 3.91 (1H, m, H-5) 3.80-3.76 (1H, m, H-4) 2.16, 2.09, 2.07, 2.07, 2.07, 2.06, 2.06, 1.97 (24H, 8 x C(CO)CH3); HRMS (ESI, m/z) [M+Na] calculated for $C_{28}H_{38}O_{19}Na$ 701.1905. Found 701.1904.

Bromo-heptaacetyl-D-lactoside (3)

HBr in AcOH (33 mL, 1 eq) was added drop wise to a solution of **2** (25.0 g, 36.9 mmol, 1 eq) with AC_2O (5 mL) in DCM cooled to 0°C. After 30 min stirring at 0 °C for the solution was allowed to reach RT and stirred for a further 3 h. The resulting solution was washed three times with DI water and saturated sodium bicarbonate solution. The organic layer was evaporated to an oil by rotary evaporation and solid product was recrystallised in petroleum ether or hexane depending on availability. After confirmation of product formation by MS and ^{1}H NMR. (Yield 20.9 g, 80%) ^{1}H-NMR (600 MHz, $CDCl_3$), δ ppm. 6.50 (1H, d, *J* = 3.9 Hz), 5.54 (1H, t, *J* = 9.7 Hz), 5.34 (1H, d, *J* = 3.4 Hz), 5.11 (1H, m), 4.94 (1H, dd), 4.74 (1H, dd), 4.49 (2H, m), 4.24-4.04 (4H, m), 3.90-3.80 (2H, m) 2.14, 2.11, 2.08, 2.07, 2.05, 2.04, 2.04, 1.95 (21H, 7 x C(CO)CH_3); HRMS (ESI, m/z) [M+Na] calculated for $C_{26}H_{35}O_{17}NaBr$ = 721.0955. Found 721.0953.

4-nitrophenyl-heptaacetate-β-D-lactoside (4)

In flame dried vessels under an N_2 environment, **3** (15.0 g, 21.5 mmol), para-nitrophenol (6.0 g, 43.0 mmol) and silver carbonate (11.9 g, 43.0 mmol) were suspended in dry acetonitrile (100 mL) with 4 Å molecular sieves. Aluminium foil was placed around the vessel to minimise light exposure. 2,6-lutodine (5.25 mL, 60.3 mmol) was added and the reaction stirred at RT for 24 h. Following filtration through celite to remove any solids the filtrate was extracted into DCM. This organic layer was subsequently washed three times with DI water and three times with saturated sodium bicarbonate solution. The organic layer was evaporated to an oil by rotary evaporation and a solid product was precipitated in hexane. The resulting solid was then stirred overnight in methanol to remove unreacted PNP. The purified solid product was recovered *via* vacuum filtration (Yield 9.1 g, 58%) IR cm^{-1} 1742 (C=O), 1595 (N-O) 1501 (C=C), 1368 (CH3), 1213 (C-O acetyl), 1053 (C-O saccharide); ^{1}H-NMR (400 MHz, $CDCl_3$), δ 8.18 (2H, d, *J* = 9.2 Hz, Ar-H), 7.03 (2H, d, *J* = 9.2 Hz, Ar-H), 5.35 (1H, d, $J_{1,2}$ = 2.8 Hz, H-1), 5.28 (1H, m, H-4), 5.21-5.08 (3H, m, H-2, H-3), 4.95 (1H, m Hz, H-2), 4.52-4.47 (2H, m, H-4,H-5), 4.16-4.43 (3H, m, H-5, 2 x H-6), 3.92-3.80 (3H, m, H-4, 2 x H-6), 2.14, 2.06, 2.05, 2.05, 2.04, 2.04, 1.95 (21H, m, 7 x C(CO)CH_3)

4-aminophenyl-heptaacetate-β-D-lactoside (5)

Compound **4** (1.0 g, 1.3 mmol) was dissolved in MeOH. To this Pd(OH) on activated carbon (5 mg) was added with stirring. H_2 gas was bubbled through the solution at atmospheric pressure to produce the peracetylated aminophenol derivative **5**. The sample was filtered through celite to remove the solid catalyst and the filtrate was dried under rotary evaporation to yield an off white powder. (Yield 0.90 g, 92%) ^{1}H-NMR (600 MHz, $CDCl_3$), δ 7.27 (2H, d, *J* = 9.0 Hz, Ar-H), 7.05 (2H, d, *J* = 9.0 Hz, Ar-H), 5.39 (1H, d, *J* = 7.7 Hz, H-1), 5.32 (1H, d, *J* = 3.4 Hz, H-4), 5.24 (1H, t, *J* = 9.0 Hz, H-3), 5.12 (1H, d, *J* = 8.6 Hz, H-2), 5.07 (1H, dd, *J* = 3.2 Hz, *J* = 10.5 Hz, H-3), 4.93 (1H, t, *J* = 8.0 Hz, H-2), 4.72 (1H, d, *J* = 8.8 Hz, H-1), 4.40 (1H, d, *J* = 11.9 Hz, H-6), 4.15-4.06 (5H, m, H-4, H-5, 3 x H-6), 4.0 (1H, m, H-5), 2.09, 2.05, 2.0, 2.0, 2.0, 2.0, 1.90 (21H, m, C(CO)CH3); ^{13}C-NMR (125 MHz, $CDCl_3$); δ 173.4, 173.3, 173.1, 172.8, 172.6, 172.6, 172.5 (7 x C=O), 156.0, 125.5 (2 x qC), 124.4, 118.0 (2 x Ar CH), 100.2 (C-1), 97.9 (C-1),

75.6 (C-5), 73.2 (C-3), 72.5 (C-5), 71.4 (C-2), 71.2 (C-3), 70.3 (C-4), 69.7 (C-2), 67.7 (C-4), 62.2 (C-6), 61.6 (C-6), 20.6, 20.5, 20.4, 20.4, 20.3, 20.3, 20.3 (7 x CH3 OAc): HRMS (ESI, m/z): [M-HCl+Na]+ calculated for $C_{32}H_{41}NO_{18}Na$ = 750.2221. Found 750.2242.

4-Aminophenyl-β-D-lactoside (6)

To **5** (0.80 g, 1.8 mmol) suspended in MeOH, a catalytic amount of NaOMe is added with stirring for 2 h at RT. The suspension was neutralised with HCl (6 M) and filtered to obtain the solid white deprotection product **6.** (Yield 370 mg, 79%) ^{1}H-NMR (600 MHz, d_6-DMSO), δ 1H-NMR (600 MHz, d^6-DMSO), δ 6.77 (2H, d, *J* = 8.3 Hz, Ar-H), 6.50 (2H, d, *J* = 8.3 Hz, Ar-H), 4.67 (1H, d, *J* = 8.0 Hz, H-1), 5.34 (1H, d, *J* = 5.3 Hz, OH), 5.10 (1H, d, *J* = 4.2 Hz, OH), 4.78 (1H, d, *J* = 4.4 Hz, OH), 4.74 (1H, s, OH), 4.68 (1H, s, OH), 4.67 (1H, d, *J* = 4.2 Hz, H-1), 4.58 (1H, t, *J* = 6.0 Hz, OH), 4.52 (1H, d, *J* = 4.4 Hz, OH), 4.24 (1H, d, *J* = 7.7 Hz, H-1), 3.55-3.52 (2H, m, 2 x H-6), 3.63 (1H, m, H-5), 3.63 (1H, m, H-4), 3.76-3.64 (2H, m,2 x H-6), 3.41 (1H, m, H-3), 3.38 (1H, m, H-5), 3.48 (1H, m, H-4), 3.34 (1H, m, H-2), 3.23 (1H, m, H-2), 3.33 (1H, m, H-3); ^{13}C-NMR (125 MHz, d_6-DMSO); 148.0 (Ar-C), 143.5 (q-C, Ar-C), 117.8 (q-C, Ar-C), 114.6 (Ar-C), 104.0 (C-1), 102.0 (C-1), 75.8 (C-4), 80.4 (C-5), 65.2 (C-5), 74.9 (C-3), 73.3 (C-3), 73.0 (C-2), 70.5 (C-2), 68.1 (C-4), 60.3 (C-6), 60.4 (C-6); HRMS (ESI, m/z): [M+H]+ calculated for $C_{18}H_{28}NO_{11}$ = 434.1660. Found 434.1657.

The above synthetic procedure is consistently reproducible and has been scaled to yield the aminophenol-lactoside precursor on a multi-gram scale.

2-Fluoro-4-nitrophenyl-heptaacetate-β-D-lactoside (7)

In flame dried vessels under an N2 environment, **3** (10.0 g, 15 mmol), 2-Fluoro-4-nitrophenol (4.0 g, 25.5 mmol) and silver carbonate (8 g, 28.0 mmol) were suspended in dry acetonitrile (100 mL) with 4 Å molecular sieves. Aluminium foil was placed around the vessel to minimise light exposure. 2,6-lutodine (4 mL, 45 mmol) was added and the reaction stirred at RT for 24 h. Following filtration through celite to remove any solids the filtrate was extracted into DCM. This organic layer was subsequently washed three times with DI water and three times with saturated sodium bicarbonate solution. The organic layer was

evaporated to oil by rotary evaporation and a solid product was precipitated in hexane. The resulting material was purified by column chromatography. (Yield 6.5g, 56%) ^{1}H-NMR (600 MHz, $CDCl_3$), δ 8.02 (2H, m, *2x* Ar-H), 7.26 (1H, m Ar-H), 5.39 (1H, s br, H-4gal), 5.32 (1H, t, *J* = 8.7 Hz, H-2glu), 5.24 (1H, t, *J* = 7.6 Hz, H-3glu), 5.18 (1H, d, *J* = 6.6 Hz, H-1), 5.14 (1H, dd, *J* = 7.9 Hz, *J* = 10.5 Hz, H-2gal), 4.99 (1H, dd, *J* = 10.1 Hz *J*=3.6 Hz, H-3 gal), 4.53-4.57 (2H, m, H-1gal, H-6glu), 4.08-4.18 (3H, m, H-6gal, H6-gal', H-6glc'), 3.88-3.96 (2H, m, H-5gal, H-4glc), 3.84 (1H, m, H-5glc) 2.17, 2.11, 2.11, 2.09, 2.09, 2.07, 1.99 (21H, m, 7 x C(CO)CH3); ^{13}C-NMR (125 MHz, $CDCl_3$); δ 170.3, 170.1, 170.1, 170.1, 169.7, 169.4, 169.1 (7 x C=O), 152.9, 151.1 149.8, 143.2, 120.4, 118.1(C-ar) 101.2 (C-1), 99.0 (C-1), 75.8, 73.2, 72.4, 71.2, 70.9, 70.8 69.1, 66.6, 61.7, 60.8 (10x C-2 – C-6), 20.8, 20.7, 20.6, 20.6, 20.6, 20.5, 20.5 (7 x CH3 OAc)

2-Fluoro-4-aminophenyl-heptaacetate-β-D-lactoside (8)

Lactosyl derivative **7** (2.0 g, 2.58 mmol) was dissolved in MeOH (50 mL) and the solution was degassed under N_2 for 10 min. Pd(OH) on carbon (50 mg) as added and the mixture was further degassed for an additional 10 min. The flask was evacuated and subsequently saturated with H_2 over a period of 2 h and monitored via TLC until complete consumption of the starting material was observed. The reaction mixture was filtered through a 0.4 micron filter and the solvent removed to give a solid product (1.7 g; 90%). ^{1}H-NMR (400 MHz, $CDCl_3$), δ ppm. 6.97 (1H, t, *J* = 8.6 Hz, H5-ar), 6.42 (1H, dd, *J* = 12.1 Hz, *J*= 2.89 Hz, H6-ar), 6.33 (1H, m, H3-ar), 5.38 (1H, d, *J* = 2.7 Hz, H4-Gal), 5.27 (1H, d, *J* = 8.67 Hz, H3-Glc), 5.13-5.16 (2H, m, H2-glc,H2-gal), 4.49 (1H, m, H3-gal), 4.74 (1H, d, *J* = 7.7 Hz, H1-glc), 4.49 (2H, m, H1-gal, H6-glc), 4.16-4.03 (3H, m, H6'-glc, H6-gal, H6'-gal), 3.90-3.83 (2H, m, H5-gal, H4-glc), 3.65 (1H, m, H5-glc), 2.17, 2.13, 2.11, 2.09, 2.08, 2.06, 1.93 (21H, m, 7 x CH_3, OAc); ^{13}C-NMR (100 MHz, $CDCl_3$), δ ppm. 170.4, 170.3, 170.2, 170.1, 169.8, 169.8, 169.1 (7 x C=O, OAc), 153.2 (C2 aromatic), 144.1 (C4 aromatic), 136.5 (C1 aromatic), 123.0 (C3 aromatic), 110.3 (C6 aromatic), 103.3 (C5 aromatic), 101.8 (C1-glc), 101.0 (C1-gal), 76.4 (C4-glc), 72.8 (C5-glc), 72.6 (C3-glc), 71.5 (C2-glc), 71.0 (C3-gal), 70.8 (C5-gal), 69.1 (C2-gal), 66.6 (C4-gal), 61.8 (C6-glc), 60.9 (C6-gal) 20.8, 20.8, 20.6, 20.6, 20.6, 20.6, 2.05 (7 x CH_3, OAc). ^{19}F-NMR (376.4 MHz, $CDCl_3$), δ ppm.

-139.10 (1F, s, F1-ar); [M+Na]+ calculated for $C_{32}H_{40}FNNaO_{18}$ = 768.2122. Found 768.2117.

2-Fluoro-4-aminophenyl-β-D-lactoside (9)

The ortho fluorinated aminophenyl derivative was prepared by deacetylation of **8** (1g, 1.3 mmol) through addition of NaOMe as outlined for **6** above. The final compound was isolated as a colourless solid. (Yield 500 mg, 78%) ^{1}H-NMR (600 MHz, d_6-DMSO), δ 6.96 (1H, t, *J* = 9.0 Hz, Ar-H), 6.38 (1H, d, *J* = 13.0 Hz, Ar-H), 6.28 (1H, t, *J* = 9.0 Hz, Ar-H), 5.39 (1H, br s, OH), 5.09 (1H, br s, OH), 4.99 (2H, br s NH2), 4.79 (br s, OH), 4.76 (br s, OH), 4.71 (1H, d, *J* = 7.7 Hz, H1- Glc), 4.67 (br s, OH), 4.57 (br s, OH), 4.52 (br s, OH), 4.24 (1H, d, *J* = 6.5 Hz, H1-Gal), 3.74 (1H, m, H6a-Glc), 3.65-3.60 (2H, m, H6b-Glc, H3-Gal), 3.58-3.46 (3H, m, H6a-Gal, H6b-Gal, H5-Gal),3.44-3.38 (3H, m, H3-Gal, H3-Glc, H4-Glc),3.37-3.31 (2H, m, H2-Gal, H5-Glc), 3.25 (1H, m, H2-Glc). ^{13}C-NMR (125 MHz, d6-DMSO), 152.9 (d, 1 *J* 19F-13C =242 Hz, ArC), 144.9 (d, *J* = 10 Hz, Ar-C), 134.9 (d, *J* = 12 Hz, Ar-C), 119.9 (d, *J* = 2.2 Hz, Ar-C), 109.1 (d, *J* = 2.5 Hz, Ar-C), 103.8 (C1-Gal), 102.0 (C1-Gln), 101.5 (2 *J* 19F-13C = 22 Hz, ArC), 80.3 (C4-Glc), 75.5 (C5-Gal), 74.9 (C3-Glc), 74.8 (C3-Gal), 73.2 (C5-Glc), 73.0 (C2- 7 Glc), 70.5 (C2-Gal), 68.1 (C3-Gal), 60.4 (C6-Gal), 60.2 (C6-Glc); HRMS (ESI, m/z): [M-H]+ calculated for $C_{18}H_{25}NO_{11}F$ = 450.1412. Found 450.1416.

3.2 β-Cyclodextrin Precursor Synthesis

6-*O*-(4-toluenesulfonyl)-β-cyclodextrin (11)

β-CD, **10**, purchased from Sigma-Aldrich (25 g, 0.0225 mol, 1 eq) was dissolved in H_2O (500 mL). 4-toluenesulfonyl chloride (2 eq, 7.4 g, 0.0450 mol) was suspended in this solution and NaOH solution. (1 g/10 mL, 50 mL) was added slowly with stirring for 10 min at RT. Excess 4-toluenesulfonyl chloride was removed by filtration through a sintered glass funnel. The filtrate was treated with slow addition of 6M Hydrochloric acid (15 mL). The resulting white precipitate was collected by filtration and purified by recrystallisation in a 1:1 mix of MeOH/H_2O three times to yield a solid white powder. (Yield 5.5 g, 20 %) ^{1}H-NMR δ ppm (600 MHz, d6-DMSO), δ 7.75 (2H, d, *J* = 8.2 Hz, H-ar), 7.43 (2H, d, *J* =

8.2 Hz, H-ar), 5.63–5.88 (14H, m, OH), 4.85 (6H, s, H-1), 4.75 (1H, s, H-1), 4.65–4.10 (7H, m, OH), 2.98–3.74 (42H, m, H-2 - H6 overlapped with H2O), 2.43 (3H, s, CH3). DT % > 94. ^{13}C-NMR (150 MHz, d_6-DMSO), 145.3 (C-Para), 133.1 (C-Ar1), 130.4 (C-Meta), 128.0 (C-Ortho), 102.5 (C-1), 82.0(C-4) 73.5 (C-3), 72.7 (C-2), 72.4(C-5) , 60.4 (C-6), 21.1 (CH3); HRMS (Maldi M/Z+) calculated for $C_{49}H_{76}O_{37}NaS$= 1311.3684. Found 1311.3716.

$$\text{Degree of Tosylation \% (DT\%)} = \frac{\text{Har}}{4}\text{x}\left(\frac{7}{\text{H1}}\right)\text{x100} = \left(\frac{1.91+1.89}{4}\right)\text{x}\left(\frac{7}{7.03}\right)\text{x100} = 95\%$$

6-*O*-(4-nitrophenyl)-β-cyclodextrin (12)

Compound **11** (1.9 g, 0.0015 mol, 1eq) was added to a solution containing potassium carbonate (2.03g, 0.015 mol, 10 eq) with (2.04g, 0.015 mol, 10 eq) p-nitrophenol in dry DMF (20 mL) under an argon environment under reflux at 80 °C. After 12 h the DMF was removed by rotary evaporation. The solid product was dissolved in a minimum of hot H_2O and recrystallised in acetone multiple times until pure a white powder was obtained. (Yield 1.8 g, 91 %) ^{1}H-NMR δ ppm (400 MHz, D_2O), 8.11 (2H, d, *J* = 9.1 Hz, Ar-H), 7.06 (2H, d, *J* = 9.1 Hz, Ar-H), 4.94 (7H, m, H-1), 3.85-3.47 (42H, m, H2-H6); ^{13}C-NMR δ ppm (100 MHz, D_2O) 164.3 (C-Ar1), 142.2 (C-Para), 126.2 (C-Ortho), 115.6 (C-Meta), 102.4 (C-1), 82.0 (C-4), 73.5(C-2), 72.9 (C-3), 72.0 (C-5), 60.5 (C-6); HRMS (ESI, m/z) [M+K] Calculated for $C_{48}H_{73}KNO_{37}$ = 1294.349300. Found 1294.349311.

6-*O*-(4-aminophenyl)–β-cyclodextrin (13)

Compound **12** (600 mg, 0.005 mmol, 1 eq) was dissolved in a mixture of MeOH/H_2O (1:9) (100 mL). To this solution 50mg PdOH on activated carbon was added with stirring. This suspension was degassed under Ar and H_2 gas was passed through the solution at atmospheric pressure for 2 h at RT. The sample was filtered through celite to remove the solid catalyst and the filtrate was dried under rotary evaporation to yield a white powder. (Yield 500 mg, 83 %) ^{1}H-NMR δ ppm (400 MHz, D_2O), 6.74 (2H, d, *J* = 8.30 Hz Ar-H), 6.60 (2H, d, *J* = 8.30 Hz, Ar-H), 4.91 (7, m, H-1), 4.13-3.40 (42H, m, H2-6); ^{13}C-NMR δ ppm (100 MHz, D_2O) 162.8 (C-Ar1), 140.4 (C-Para), 117.3 (C-Ortho), 116.2 (C-Meta), 101.8 (C-

1), 81.1 (C-4), 73.1(C-3), 72.0 (C-2), 71.8 (C-5), 60.2 (C-6); HRMS (ESI, m/z) [M+K] calculated for $C_{48}H_{75}KNO_{35}$ = 1264.375121. Found 1264.379319.

4 Materials & Methods

4.1 Materials

β-cyclodextrin 98%, p-nitrophenol reagent-plus ≥99%, were purchased from Fisher Scientific; Acetic anhydride 98%, p-toluenesulfonyl chloride 99%, D-Lactose, Palladium hydroxide on activated charcoal, sodium hydroxide, potassium carbonate, Hydrogen bromide solution, 33 wt. % in acetic acid, 2-fluoro-4-nitrophenol 99%, Silver carbonate 99%, and N,N-dimethylformamide anhydrous 99.8%, were purchased from Sigma-Aldrich.

4.2 Instrumentation:

NMR analysis was carried out using a Bruker Advance 400 spectrometer, ^{1}H (400.13 MHz) and ^{13}C (100.6 MHz) with a Bruker Ultrashield (600 MHz) spectrometer utilised for ^{1}H (600.13 MHz) and ^{13}C (150.6 MHz) NMR spectra. Resonances δ units are in ppm downfield from an internal reference. A Q-Tof Premier Waters Maldi-quadrupole time-of-flight mass spectrometer equipped with Z–spray electrospray ionisation (ESI) and matrix assisted laser desorption ionisation (MALDI) sources was employed to obtain mass spectra of synthesised compounds. Infrared spectra bulk powder materials were collected using a Perkin Elmer Spectrum 100 FT-IR Spectrometer with a Universal ATR Sampling Accessory.

References

1. Christensen, T.; Toone, E. J., Calorimetric Evaluation of Protein–Carbohydrate Affinities. In *Methods in Enzymology*, Academic Press: **2003**, pp 486-504.
2. Goettig, P., Effects of Glycosylation on the Enzymatic Activity and Mechanisms of Proteases. *Int J Mol Sci* **2016,** *17* (12), 1969.
3. Zen, F.; Angione, M. D.; Behan, J. A.; Cullen, R. J.; Duff, T.; Vasconcelos, J. M.; Scanlan, E. M.; Colavita, P. E., Modulation of Protein Fouling and Interfacial Properties at Carbon Surfaces via Immobilization of Glycans Using Aryldiazonium Chemistry. *Sci. Rep.* **2016,** *6*, 24840.
4. Jayasundara, D. R.; Duff, T.; Angione, M. D.; Bourke, J.; Murphy, D. M.; Scanlan, E. M.; Colavita, P. E., Carbohydrate Coatings via Aryldiazonium Chemistry for Surface Biomimicry. *Chem. Mater.* **2013,** *25* (20), 4122-4128.
5. Esteban-Tejeda, L.; Duff, T.; Ciapetti, G.; Daniela Angione, M.; Myles, A.; Vasconcelos, J. M.; Scanlan, E. M.; Colavita, P. E., Stable hydrophilic poly(dimethylsiloxane) via glycan surface functionalization. *Polymer* **2016,** *106*, 1-7.
6. Angione, M. D.; Duff, T.; Bell, A. P.; Stamatin, S. N.; Fay, C.; Diamond, D.; Scanlan, E. M.; Colavita, P. E., Enhanced Antifouling Properties of Carbohydrate Coated Poly(ether sulfone) Membranes. *ACS Appl. Mater. Interfaces.* **2015,** *7* (31), 17238-17246.
7. Myles, A.; Haberlin, D.; Esteban-Tejeda, L.; Angione, M. D.; Browne, M. P.; Hoque, M. K.; Doyle, T. K.; Scanlan, E. M.; Colavita, P. E., Bioinspired Aryldiazonium Carbohydrate Coatings: Reduced Adhesion of Foulants at Polymer and Stainless Steel Surfaces in a Marine Environment. *ACS Sustain. Chem. Eng.* **2018,** *6* (1), 1141-1151.
8. Pétursson, S., Protecting Groups in Carbohydrate Chemistry. *J. Chem. Edu.* **1997,** *74* (11), 1297.
9. Koenigs, W.; Knorr, E., Ueber einige Derivate des Traubenzuckers und der Galactose. *Berichte der deutschen chemischen Gesellschaft* **1901,** *34* (1), 957-981.
10. Gong, T.; Zhou, Y.; Sun, L.; Liang, W.; Yang, J.; Shuang, S.; Dong, C., Effective adsorption of phenolic pollutants from water using β-cyclodextrin polymer functionalized Fe3O4 magnetic nanoparticles. *RSC Adv.* **2016,** *6* (84), 80955-80963.
11. Zhao, F.; Repo, E.; Yin, D.; Meng, Y.; Jafari, S.; Sillanpää, M., EDTA-Cross-Linked β-Cyclodextrin: An Environmentally Friendly Bifunctional Adsorbent for Simultaneous Adsorption of Metals and Cationic Dyes. *Environ. Sci. & Technol.* **2015,** *49* (17), 10570-10580.
12. Del Valle, E. M. M., Cyclodextrins and their uses: a review. *Process Biochem.* **2004,** *39* (9), 1033-1046.
13. Sharma, N.; Baldi, A., Exploring versatile applications of cyclodextrins: an overview. *Drug Delivery* **2016,** *23* (3), 729-747.
14. Tripodo, G.; Wischke, C.; Neffe, A. T.; Lendlein, A., Efficient synthesis of pure monotosylated beta-cyclodextrin and its dimers. *Carbohydr. Res.* **2013,** *381*, 59-63.
15. Tan, T.; Ng, S.-c.; Wang, Y.; Xiao, Y., Synthesis of mono-6-tosyl-β-cyclodextrin, a key intermediate for the functional cyclodextrin derivatives. *Protocol Exchange* **2011**.
16. Myles, A.; Behan, J. A.; Twamley, B.; Colavita, P. E.; Scanlan, E. M., Spontaneous Aryldiazonium Grafting for the Preparation of Functional Cyclodextrin-Modified Materials. *ACS Appl. Bio Mater.* **2018**.
17. Percec, V.; Leowanawat, P.; Sun, H.-J.; Kulikov, O.; Nusbaum, C. D.; Tran, T. M.; Bertin, A.; Wilson, D. A.; Peterca, M.; Zhang, S.; Kamat, N. P.; Vargo, K.; Moock, D.; Johnston, E. D.; Hammer, D. A.; Pochan, D. J.; Chen, Y.; Chabre, Y. M.; Shiao, T. C.; Bergeron-Brlek, M.; André, S.; Roy, R.; Gabius, H.-J.; Heiney, P. A., Modular Synthesis of Amphiphilic Janus Glycodendrimers and Their Self-Assembly into Glycodendrimersomes and Other Complex Architectures with Bioactivity to Biomedically Relevant Lectins. *J. Am. Chem. Soc.* **2013,** *135* (24), 9055-9077.

18. Kopitzki, S.; Jensen, K. J.; Thiem, J., Synthesis of Benzaldehyde-Functionalized Glycans: A Novel Approach Towards Glyco-SAMs as a Tool for Surface Plasmon Resonance Studies. *Chemistry – A European Journal* **2010,** *16* (23), 7017-7029.
19. Liu, Y.; Fan, Z.; Zhang, H.-Y.; Yang, Y.-W.; Ding, F.; Liu, S.-X.; Wu, X.; Wada, T.; Inoue, Y., Supramolecular Self-Assemblies of β-Cyclodextrins with Aromatic Tethers: Factors Governing the Helical Columnar versus Linear Channel Superstructures. *J. Org. Chem.* **2003,** *68* (22), 8345-8352.

Chapter III

Lactose Coatings on Carbon surfaces

Carbon surfaces were modified using aryldiazonium chemistry to produce lactoside terminated surfaces. Two different grafting procedures, in situ spontaneous aryldiazonium grafting and electrochemical grafting were used to produce carbon surface films with varying characteristics. Spontaneous aryldiazonium grafting of lactose was achieved by immersion of glassy carbon electrodes in freshly prepared aqueous lactose aryldiazonium salts solution. Alternatively GC disk electrodes were modified potentiostatically by applying a reductive potential for 300 s in similarly prepared aryldiazonium solutions. Surface films were subsequently characterized using a variety of surface characterisation methods, lectin binding studies, and surface redox probes. The potential application of these surface modification protocols for the prevention of biofouling was probed by protein adsorption experiments; the coatings were also briefly investigated as a fouling resistant modification for caffeine sensors in a complex fouling environment. It was concluded that spontaneous grafting produces an approximation of a sparse monolayer coating whereas electrografting has the capability to produce denser multilayer films of lactosides on the surface.

Results in this chapter were obtained in collaboration with Mr. James A. Behan whose contributions include electrochemical experimentation, X-Ray Photoemission Spectroscopy and input on experiment design and data analysis.

1 Introduction

The reduction of aryldiazonium salts onto conductive surfaces is widely employed to produce functional surface coatings. This is achieved by formation of a salt of general formula ($RArN_2^+$) from addition of $NaNO_2$ to an R-aminophenol analogue in acidic media (**Scheme 1.1**). Upon reduction this diazonium salt can covalently graft onto a conductive surface such as glassy carbon or gold to produce a functional film.[1-3] This method of surface modification is popular due to the stability and robustness of the resulting covalently bound film which resists solvation and are stable with ultra-sonication.[4] Moreover through careful choice of the R group it is possible to create a surface with tailored physico-chemical properties and develop novel smart materials.[1, 5-7] Covalent grafting can be achieved by spontaneous attack of a surface in-situ to the aryldiazonium salt [8-10], by addition of a reducing agent to drive in situ surface modification[11] or can be induced potentiostatically by electrochemical reduction in solutions of aryldiazonium cations which then graft onto the electrode surface.[12]

Surface modification with simple saccharides has been studied previously within our group for production of antifouling surfaces.[13-15] Notably work by Zen et al.[16] contains an initial characterisation of modified amorphous carbon surfaces by spontaneous aryldiazonium grafting of a range of monosaccharide and disaccharide compounds. It was found that carbon surfaces when coated with saccharides possess increased hydrophilicity, a characteristic which is thought/proposed to significantly improve the ability to resist nonspecific protein adsorption.[17-18] This study revealed that glycosylated surfaces provide a significant reduction in surface retention of biological contaminants such as serum albumin and fibrinogen, two proteins commonly found in animal serum and which are known to routinely foul medical implants.[16, 19] It was observed that disaccharides such as lactose possess significantly higher protein rejection capabilities when compared to monosaccharide analogues and as such were chosen as the saccharide utilised in this study.

Aryldiazonium grafting has been lauded for its ability to produce a tailored functional surface, however it possesses a substantial drawback in the limited control of multilayer formation.[20] Various methods of monolayer control have been employed in literature, some examples of which include the use of radical

scavengers to inhibit multilayer growth,[21-22] functionalisation with bulky terminal groups to block reactive aryl sites,[23] and grafting with cleavable moieties to chemically trim the surface layer down to controlled monolayer formation.[24] The aforementioned work by Zen *et al.*[25] also demonstrated that lactosides, when spontaneously grafted to amorphous carbon surfaces, form at most monolayer coatings, which is likely due to the steric hindrance of the saccharide R group in addition to the mild activating conditions of spontaneous surface modification. A similar result was obtained in the case of cyclodextrin derivatives of aryldiazonium cations which are observed to form near monolayer coverage upon spontaneous aryldiazonium grafting (This data is discussed in **Chapter VI** of this thesis) Electrochemical reduction is the most prevalent method of aryldiazonium grafting found in literature due to its rapid reaction times and reliable production of complete surface films.[3, 26] In this chapter, the conditions of modification via covalent grafting with aryldiazonium lactosides on conductive carbon surfaces are discussed and the resulting saccharide films formed by two dediazoniation methods, (the previously studied spontaneous grafting[10] and the historically favoured method of electrochemical reduction)[3] are compared.

2 Results and discussion

2.1 Spontaneous Grafting

Spontaneous grafting carried out following previously established methods of diazonium salt formation and subsequent surface modification was utilised to produce amorphous carbon and glassy carbon materials with lactoside surface termination (**scheme 3.1)**.[13, 16] To prepare the functionalisation solution an aminophenol lactoside precursor (**5, 6** or **9**) compound was dissolved in a 1.5 mM HBF_4 solution in H_2O to produce a 1.25 mM solution of saccharide. This solution was chilled to <4 °C in ice for one hour prior to surface modification. This solution was diluted with a solution of 0.010 M $NaNO_2$ (30 mg in 50 mL H_2O) to a final concentration of 1.0 mM saccharide in solution. This activated diazonium cation solution was immediately brought in contact with the surface and incubated in the dark for 1 h allowing the temperature to rise to RT. Aryl cations are formed with the loss of nitrogen. Nucleophilic attack from the conductive surface forms a covalent linkage. The film is not expected to increase significantly following 1 h as the reactivity of the solution is expected to decrease within this

timeframe. After immersion in the functionalisation solution, all carbon samples were sonicated in semiconductor grade MeOH and ultrapure H_2O for 1 min in each solution to remove any physisorbed saccharide which may be present on the surface and in order to confirm covalent adhesion.

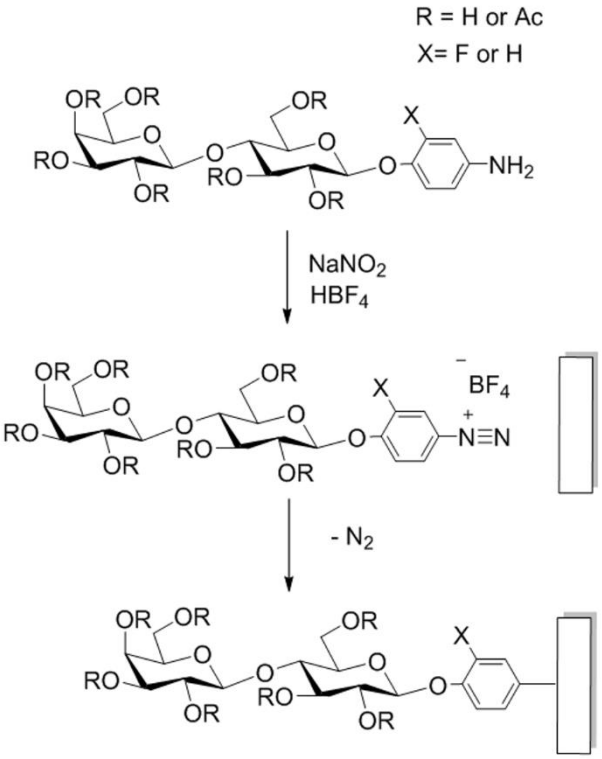

Scheme 3.1. Lactoside aryldiazonium salt formation and in situ surface grafting. Adapted with permission from *ACS Sustainable Chem. Eng.*, **2018**, *6* (1), pp 1141–1151. Copyright 2017 American Chemical Society.

2.2 Electrochemical Modification

Electrochemical modification of glassy carbon electrodes was achieved in diazonium grafting solution by applying a reductive potential in freshly prepared lactoside diazonium solution as described above for spontaneous modification. This process was optimised by James Behan following the previously reported protocols for aryldiazonium electrografting of Brooksby *et al.*[3] The potential applied of -0.5 V vs. Ag/AgCl was chosen -100 mV to the reductive diazonium grafting peak determined to be -0.4 V vs Ag/AgCl by cyclic voltammetry (**Figure 3.1 a**). To produce the electrografted surfaces studied in this chapter freshly polished glassy carbon plates or discs were set up in a three electrode system as the working electrode versus a platinum or graphite counter electrode with an Ag/AgCl reference. Chronoamperometry was performed in a solution of freshly activated diazonium solution at a potential of -0.5 V vs Ag/AgCl for a total time of

300 s following a 30 s resting time with no applied potential. The resulting chronoamperograms (**figure 3.1 b**) reveal a decrease in absolute current.[3] All samples were sonicated for 1 min in each MeOH and H_2O post functionalisation to remove loosely bound materials.

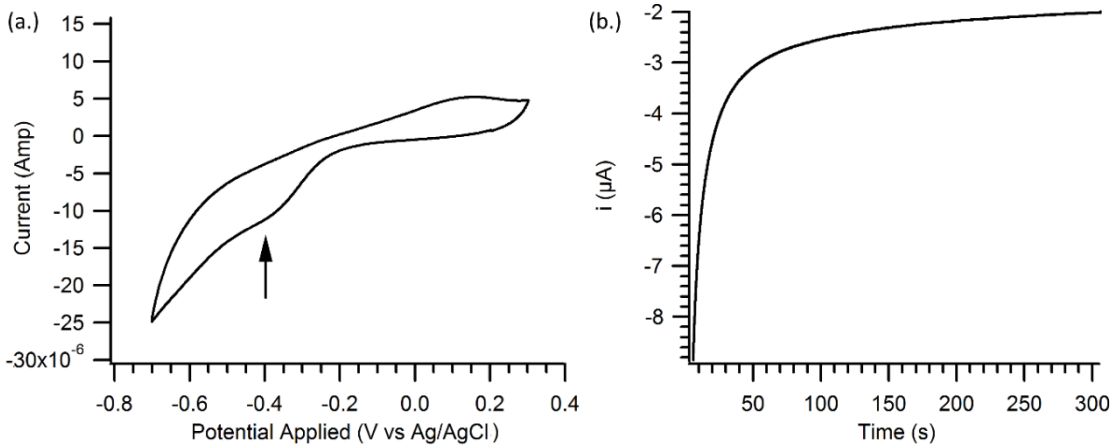

Figure 3.1. (a.) Cyclic voltammogram of glassy carbon disk in 1 mM activated lactoside diazonium solution vs Ag/AgCl at scan rate 200 mVs^{-1}. Peak indicated at -400 mV is reductive diazonium grafting potential. **(b.)** Chronoamperometry of a polished GC electrode at -500 mV for 300 s in 1 mM functionalisation solution.

2.3 Surface Characterisation

Saccharide modification by spontaneous aryldiazonium grafting of amorphous carbon (aC) surfaces was confirmed by the use of the surface infrared technique Infrared Reflectance Absorbance Spectroscopy (IRRAS) using samples prepared by magnetron sputtering of carbon films on a titanium coated silicon substrate[10] and modified using the acetyl protected lactoside precursor **5**. Due to the difficulties associated with thin film infrared characterisation an optically transparent amorphous carbon substrate prepared on a geometrically smooth titanium metal base surface serves to enhance the sensitivity of the IRRAS signal,[10] while the acetyl protecting groups of the surface bound saccharide provide a distinctive infrared spectral pattern which allows for rapid confirmation of saccharide grafting by surface infrared techniques.[13] IRRAS spectra for both acetyl protected lactoside modified surfaces and hydroxylated lactose surfaces prepared using the aryldiazonium precursor **6** are presented in **Figures 3.2.a. & 3.2.b.** respectively, with spectra of the bulk precursor compounds included for comparison. The IRRAS spectrum of amorphous carbon treated with acetyl protected lactosides (**Figure 3.2 a**) displays distinctive peaks at 1747 cm^{-1} (C=O stretching), 1373 cm^{-1} (CH_3 bending) 1260 cm^{-1} (C-O-C asymmetric stretching)

and 1070 cm^{-1} (C-O stretching modes) consistent with peaks expected for acetyl protected glycosides.[10, 14, 27] In the case of surfaces modified using the lactoside precursor **6,** peaks are observed at 1266 cm^{-1} attributed to C-O-C asymmetric stretching within the pentose rings and broad peaks from 1080-1000 cm^{-1} corresponding to C-O stretching modes and O-H deformations of the carbohydrate ring.[27] A peak corresponding to the skeletal C-C stretches of an aromatic ring can also be discerned in the IRRAS spectra at 1500 cm^{-1} and is assigned to the surface linking phenol group.[16, 27]

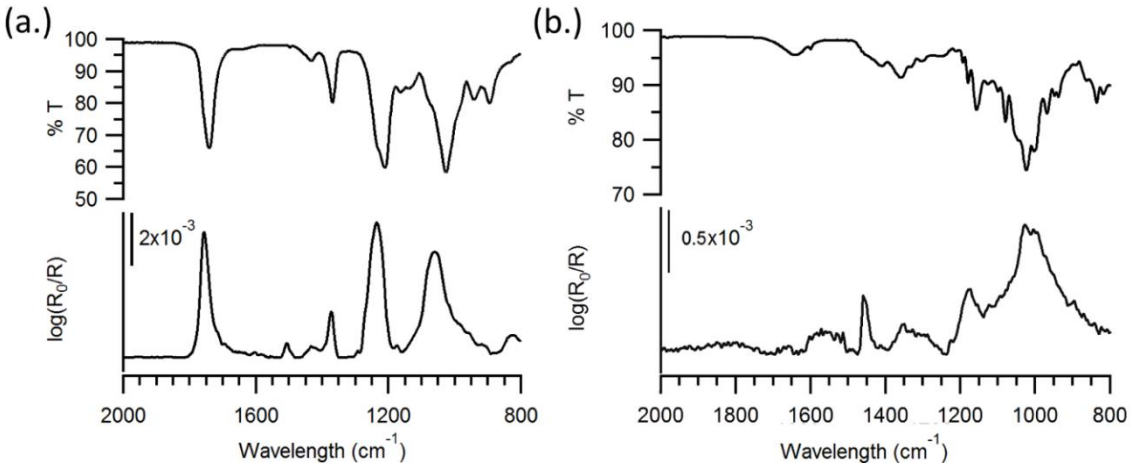

Figure 3.2. FT-IR spectra of **(a.)** amorphous carbon surfaces modified with acetyl protected lactoside 5 (IRRAS, bottom trace) and the bulk aminophenol precursor compound (ATR, top trace) for comparison, and **(b.)** aC surfaces post functionalisation with hydroxylated lactoside 6 (IRRAS, bottom trace) and bulk precursor compound (ATR, top trace). Peak assignments are discussed in the main text.

The presence of these characteristic peaks post sonication is a promising result indicating covalent saccharide anchorage to the surface following the mild spontaneous modification conditions. Any loosely adhered material is not expected to be retained after the strong sonication processes.[4]

IRRAS was deemed unsuitable as a confirmatory technique for saccharide modification on glassy carbon surfaces hence saccharide grafting to these materials was determined instead by lectin binding experiments. Lectins are a type of protein which can bind specifically to certain glycoside groups.[28] Following grafting with lactose compounds the surface is expected to display termination with galactose groups. Peanut agglutinin is a lectin known to bind specifically to galactose[29], thus to confirm the presence of lactoside terminated surfaces on glassy carbon a fluorescein isothiocyanate conjugated peanut agglutinin (PNA-FITC) was used in tandem with fluorescent confocal microscopy

through use of an Olympus BX51 upright microscope equipped with a laser excitation source of 470 nm and a FITC CellSense filter cube emission range 513–556 nm (green).[13-15] Polished glassy carbon discs, unmodified (GC), and lactose-modified (compound **6**) by spontaneous grafting with (Spont) and by electrochemical grafting (Egraft), were immersed in a solution of PNA-FITC 1 mg/mL in PBS in the dark for 1 h. Samples were rinsed lightly with PBS to remove any unbound lectin and immediately studied under fluorescence confocal microscopy. Each sample was prepared in triplicate and the resulting images were analysed by imageJ processing software. The resulting emission intensities are plotted in **Figure 3.3**, and reveal that for modified surfaces (both spontaneous and electrografted) a significantly higher amount of lectin is retained than on freshly polished glassy carbon surfaces.

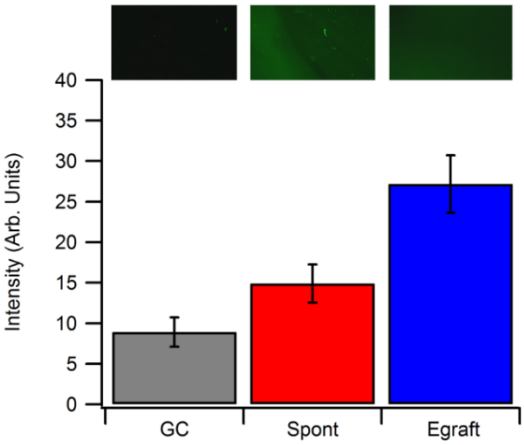

Sample	Intensity (Arb. Unit)
Glassy Carbon	9.8 ± 1.0
Spontaneous	13.6 ± 1.4
Electrografted	27.1 ± 2.1

Figure 3.3. Fluorescence microscopy results for PNA binding to glassy carbon surfaces. Bar plots represent average emission intensities of FITC-PNA conjugated to GC plates following polishing only (GC), spontaneous aryldiazonium grafting with lactose (Spont) and electrochemical grafting with lactose (Egraft). The intensities infer that the emission intensity is higher on lactose-modified surfaces with electrochemical modification producing a higher emission intensity over spontaneous grafting. Variances reported are standard error.

These results are taken as a confirmation that a saccharide terminated surface on glassy carbon substrates can be obtained by both spontaneous and electrochemical modification. Interestingly, the electrochemically modified surfaces display a higher degree of fluorescence over the spontaneously grafted samples which could potentially indicate a higher concentration of surface bound saccharide under electrografting conditions.

To investigate the surface functionality of modified surfaces, XPS analysis was carried out by James A. Behan, using the fluorine containing aminophenol

precursor, **9**, to produce modified glassy carbon surface analogues with a distinctive elemental tag *via* the same methods discussed above. Resulting surveys for bare glassy carbon, and samples subjected to spontaneous and electrochemical modification are shown in **figure 3.4**. The fluorine tag is not expected to significantly impact on functionalisation behaviour and instead simply acts as an elemental label for comparative quantisation of surface saccharide moieties.

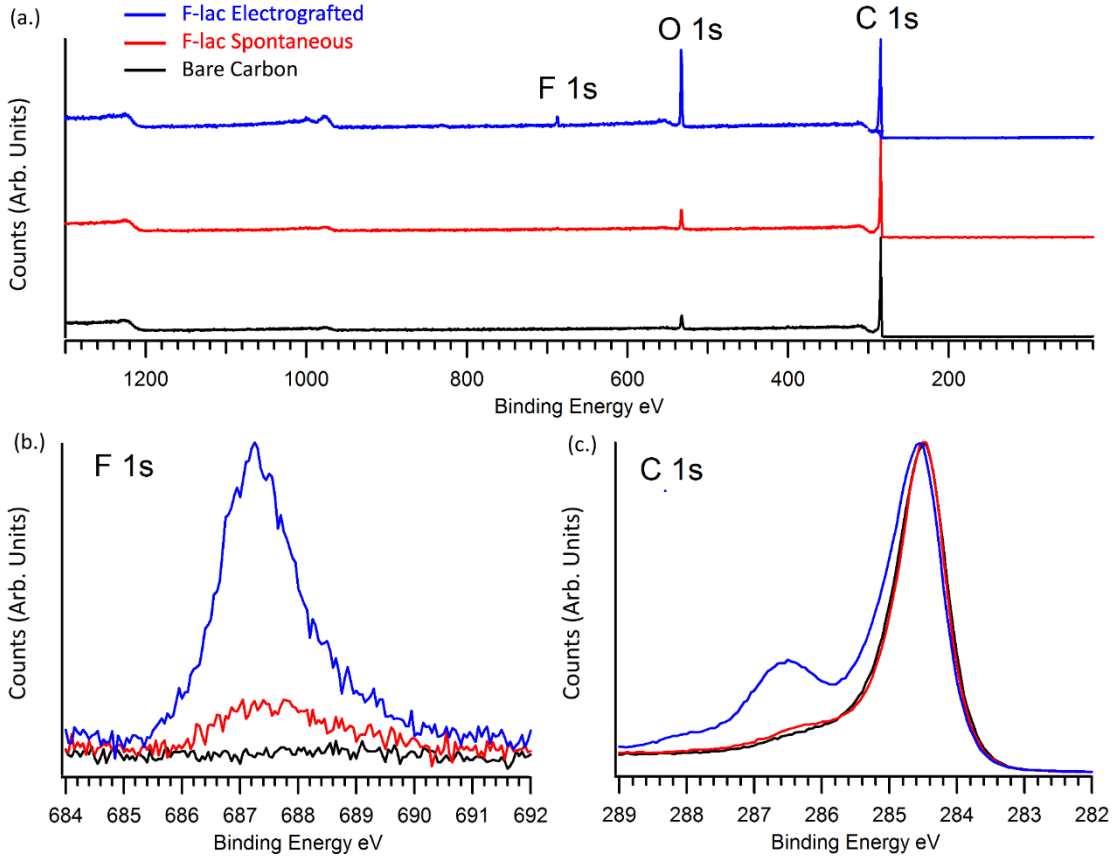

Figure 3.4. (a.) XPS survey spectra of glassy carbon plates after polishing (Bare Carbon) and coated with a fluorinated lactoside derivative (**9**) by spontaneous aryldiazonium grafting (F-Lac spontaneous) and coated b electrochemical grafting (F-Lac Electrografted). **(b.)** the F 1s region for the three surfaces revealing enhanced signal for fluorine in modified samples. **(c.)** the C 1s region showing changes in carbon envelope following surface modification.

Casa XPS software was used to analyse the resulting spectra, the resulting peak contributions and elemental ratios are tabulated (**Table 3.1**). The comparative surveys (**Figure 3.4 a**) show a significant increase in O 1s signal intensity when compared to the relative carbon intensity on surfaces modified with lactose by both methods when compared to pristine glassy carbon surfaces, and most notably on the electrografted surface.

Table 3.1. Relevant Peak assignments and atomic ratios of Polished GC, and fluorinated lactose modified GC samples by Spontaneous grafting, and electrochemical grafting of aryldiazonium salts.

	Polished GC	Spontaneous	Electrografted
C 1s (eV)	**284.5 (71.3 %)**	**284.5 (51.8 %)**	**284.5 (38.5 %)**
	285.2 (16.1 %)	**285.2 (32.2 %)**	**285.2 (33.2 %)**
	286.4 (4.1 %)	**286.4 (4.6 %)**	**286.6 (16.9 %)**
	287.2 (3.2 %)	**287.3 (8.1 %)**	**287.6 (7.8 %)**
F 1s (eV)	**-**	**687.3 (100 %)**	**687.3 (100 %)**
F/C %	**-**	**0.4%**	**2.8 %**
O/C %	**6.2 %**	**10.5 %**	**31.5 %**

The observed apparent increase in O 1s signal is consistent with a largely hydroxylated saccharide surface.[30] Signals appearing at 687.3 eV post functionalisation by spontaneous grafting are attributed to F 1s signals and are found to account for an atomic % ratio of approx 0.4 % to carbon at the modified surface. The appearance of this signal confirms spontaneous modification on glassy carbon substrates as no peaks are observed on pristine samples. A peak in this region centred at 687.3 eV is clearly evident in electrografted species with much higher signal intensity than that observed in spontaneous grafted surfaces (F/C = 2.8 %) indicating that the increase in oxygen signals dose not solely arise by oxidative electrochemical effects and are likely due to the saccharide presence. The factorial increase in the fluorine intensity at electrografted surfaces over spontaneously modified materials is evidence that electrografting produces a denser more complete saccharide coating of either tightly packed monolayer or multilayer films. This is further supported when looking at the C 1s region where we observe a clear shift from a maximum at 284.5 eV typical of sp^2-C centres to 284.5 eV characteristic of sp^3-C surface behaviour after electrografting in line with a change from the XPS spectrum of a graphitised surface to that of a saccharide coated material. This envelope also contains significant C-O contributions from 286.6 eV more indicative of carbohydrates than with that of glassy carbon.[30-31] The significant changes in C 1s envelope for egraft is especially indicative of multilayer since it is on an sp2 rich carbon substrate, the signals of which are expected to normally dominate the C 1s band, however this surface displays predominantly sp3 behaviour consistent with a

more complete surface saccharide coating. This in combination with the PNA binding behaviour data are strong evidence for grafting on glassy carbon by aryldiazonium modification and also provide further evidence to suggest that electrografting produces a significantly higher concentration of surface adhered aryl-saccharides when compared to spontaneous grafting. To study if the higher degree of coating favoured by electrografting methods produces significant morphological changes in nano-topography and roughness of the polished glassy carbon surfaces, atomic force microscopy AFM was utilised to obtain detailed surface images. As the smallest particles size for polishing was 0.5 µm the surfaces are expected to be somewhat rough at this magnification range. The resulting images at 1 μm^2 scale are shown in **Figure 3.5** for comparison. Surfaces features appear to display some differences following spontaneous grafting producing sharp thin peaks sparsely dispersed over the surface when compared to the bare carbon under the saccharide layer. Electrografting also produces a noticeable change in surface morphology with thicker globular features indicative of a bushy multilayer at the surface.

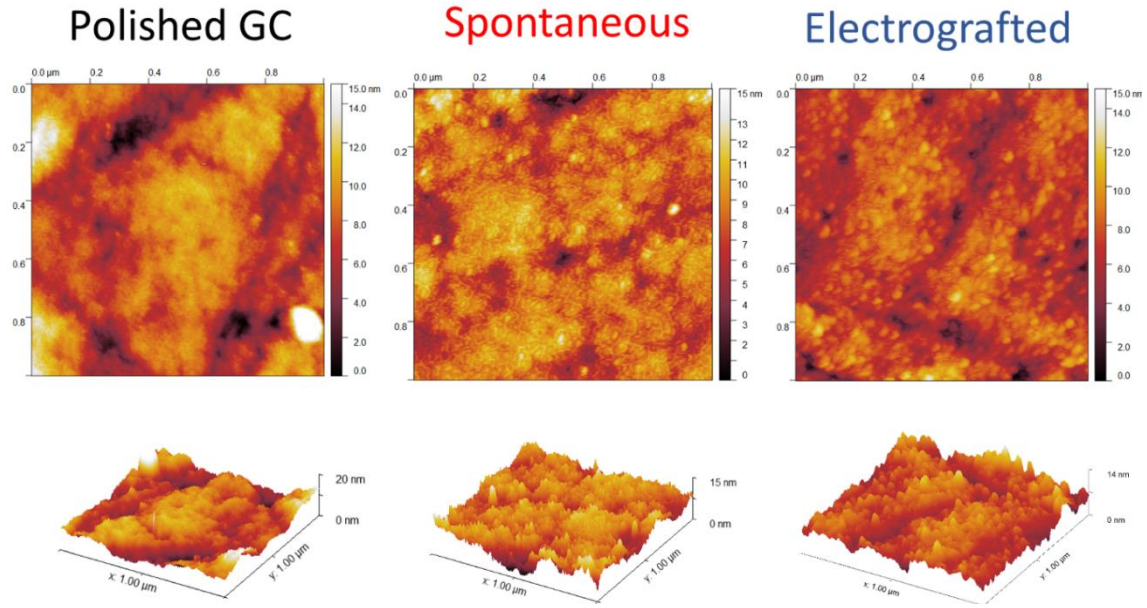

Figure 3.5. Atomic force microscopy of polished glassy carbon plates only (left) and modified with lactose by spontaneous grafting (middle) and through electrochemical grafting (right). All surfaces were measured in a 1 µm x 1 µm window in air tapping mode.

However the Root mean square (R.M.S.) roughness measurements were found to not be significantly different with surfaces possessing a Sq = 1.0 ± 0.2 nm for polished samples, spontaneous surfaces roughness Sq = 1.1 ± 0.1 nm and electrografted surfaces Sq = 0.9 ± 0.1 nm. These results would indicate that

surface roughness is not significantly altered by grafting in these materials and micro topographical features of unmodified surfaces are largely retained post modification. Due to the similarities in surface roughness' it can be assumed that liquid contact angles will behave independently of morphology.[16] To determine to what extent these coatings affect surface properties and behaviour, contact angle (CA) measurements were carried out. Summarised data on wettability is presented below (**Figure 3.6**). Pristine glassy carbon plates (polished and sonicated) have a water CA of ~71 ° in good agreement with results found by Tanner *et al*.[32] for glassy carbon surfaces. Spontaneous modification with lactose leads to a drop in WCA to 47 ° with a further drop to 27 ° observed for electrografted samples. These trends agree well with other saccharide modified materials[15, 33] wherein the increase in hydroxyl surface moieties corresponds to increased hydrophilicity are consistent with what one would expect of a highly glycosylated surface as indicated by PNA binding and XPS analysis, the significantly larger decrease in WCA for egraft samples serves to further indicate an enhanced degree of hydroxylation on the surface consistent with a more dense, (potentially multilayer) saccharide formation on egrafted surfaces.

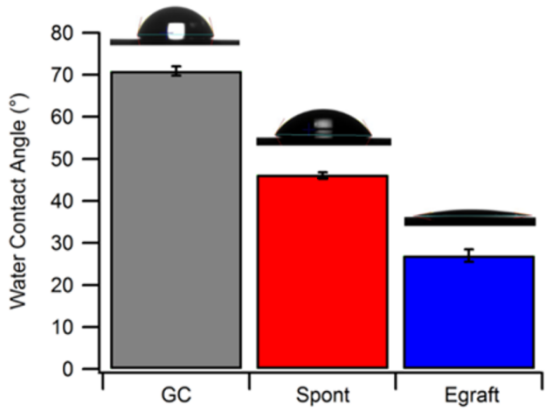

Sample	WCA (°)
Glassy Carbon	70.9 ± 1.1
Spontaneous	46.9 ± 0.6
Electrografted	26.9 ± 1.5

Figure 3.6. Water contact angle values obtained on glassy carbon plates following polishing (GC) with either spontaneous Lactose modification (Spont) or through electrochemical modification (Egraft). Variance reported is standard error.

2.4 Protein Rejection Capabilities

Water CA provides a direct measurement of the wettability of material surfaces. This factor is of significance in biological media and has been identified as an important parameter in biofilm formation.[34] It is widely accepted that increased wettability has significant impact in surfaces which display low biofilm retention however the exact mechanism is not yet known.[18] The capabilities of saccharide

coated surfaces in biofilm rejection is now established in literature.[14, 16] To investigate and compare the protein rejection capabilities of lactose coated surfaces by each modification method and hence determine their viability as a potential biofilm mitigation strategy, glassy carbon samples were immersed in a fluorescently labelled bovine serum albumin solution (0.2 mg / mL) in a phosphate buffered saline (PBS) solution.[14-15] Samples were incubated for 1 h to allow significant time for non-specific adhesion at the surface to occur. Samples were then lightly rinsed under PBS and examined under confocal fluorescent microscopy on an Olympus BX51 upright microscope with laser excitation of 470 nm using a CellSense FITC filter cube. Images were collected for samples in triplicate and fluorescence intensity (green component) was determined by imageJ processing software. **Figure 3.7** compares fluorescence intensities for freshly polished plates, spontaneously modified samples and electrografted samples after BSA-FITC incubation.

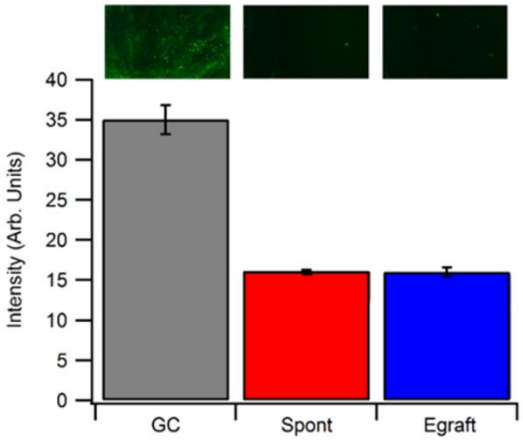

Sample	Intensity (Arb. Unit)
Glassy Carbon	35.5 ± 1.8
Spontaneous	16.1 ± 0.2
Electrografted	16.3 ± 0.6

Figure 3.7. Fluorescence microscopy results for BSA retention on glassy carbon surfaces. Bar plots represent average emission intensities of FITC-BSA adhered to GC plates treated with polishing only (GC), spontaneous aryldiazonium grafting with lactose (Spont) and electrochemical grafting with lactose (Egraft). Lactose coating produces significantly lower BSA retention with no significant differences between spontaneous grafting and electrografting observed. Variances reported are standard error.

In all cases studied unmodified polished glassy carbon displays significant protein retention post immersion in BSA. In contrast both spontaneous and electrografted surfaces display significantly less protein adhesion with no significant differences arising between the two surface modification methods. This result is interesting as it would suggest that a more hydrophilic lactoside multilayer coating is not necessarily beneficial in non-specific protein rejection

and that a sparse monolayer layer may be sufficient in the production of an anti-fouling effect.

2.5 Lactose-coated Electrodes as Redox Probes

To study the effect of lactose coating on glassy carbon electrodes as solution sensitive redox probes cyclic voltammetry was performed by James Behan with two surface sensitive molecular redox molecules, hexaammineruthenium(III) chloride ($Ru(NH_3)_6Cl_3$) and potassium ferricyanide ($K_3Fe(CN)_6$. (**Figure 3.8**).

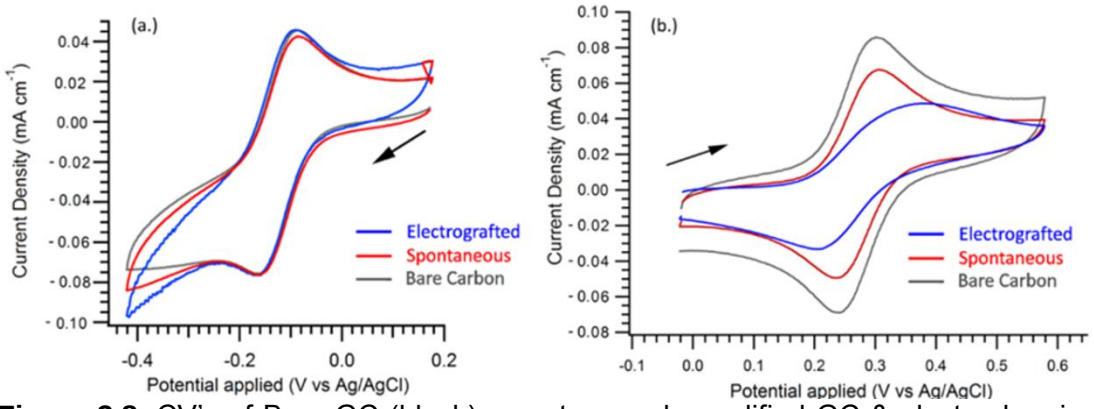

Figure 3.8. CV's of Bare GC (black), spontaneously modified GC & electrochemically modified electrodes in **(a.)** $Ru(NH_3)_6Cl_3$ (1 mM) and **(b.)** $K_3Fe(CN)_6$ (1 mM), with scan rates of 10 mVs^{-1} versus Ag/AgCl in 0.5 M KCl solution.

In the case of the outer sphere ruthenium probe (**Figure 3.8 a**) it was observed that there is no significant change in redox behaviour upon modification with lactoside coatings, even upon modification with a thick electrografted layer. Peak separation was found to be ΔE~60 mV in all cases. This result confirms that these lactoside coatings do not interfere with outer sphere redox processes of ruthenium on glassy carbon and hence may be suitable in the production of a protein resistant electrochemical probe for similarly insensitive analytes. In the case of the more surface sensitive ferricyanide probe it was observed that the sparsely coated spontaneously grafted lactoside layer did not affect redox behaviour greatly when compared to pristine GC electrodes at this concentration and scan rate. The thicker electrografted layer however is observed to deform the peak shape significantly with ΔE increasing from ~60 mV for bare GC and spontaneously grafted GC to a peak separation of ΔE ~ 140 mV consistent with a substantial organic coating at the electrode surface.[35] These results are consistent with the idea of sparse monolayer formation on spontaneously grafted

electrode surfaces and more complete lactoside coating from electrografting giving rise to slower kinetics and greater peak separation in the case of ferricyanide redox probes. It is possible that a sparse lactoside layer formed by spontaneous grafting may be advantageous over electrografting for production of a protein resistant electrochemical probe where surface sensitivity is required.

2.6 Caffeine Sensor Stability

Finally to test the fouling resistance potential of lactose modified surfaces and investigate their potential as electrochemical probes in a complex fouling medium a simple caffeine sensing experiment was performed to determine the efficacy of lactose coating in anti-adhesion of fouling in a commercially available coffee product (Nescafé Dulce Gusto^{TM} Lungo). Coffee is a popular beverage consumed the world over consisting of a complex cocktail of thousands of organic components including aromatic molecules, chlorogenic acids, carbohydrate derivatives, amino acids and proteins *etc.*[36]

Briefly for this study, each electrode type was used to probe a standard sample of caffeine (1.0 mM) at pH 1 in H_2SO_4 (0.1 M) by cyclic voltammetry vs Ag/AgCl with scan rate of 50 mVs^{-1} (**Figure 3.9**). The caffeine oxidation peak was identified at a potential of 1.50 V vs Ag/AgCl for on all electrodes and in good agreement with results obtained by Redivo *et al.*[37] Lactose coating by spontaneous and egrafting did not appear to affect peak position nor the intensity of the peak to a significant extent, with only slight capacitive increase observed for lactoside modified surfaces.

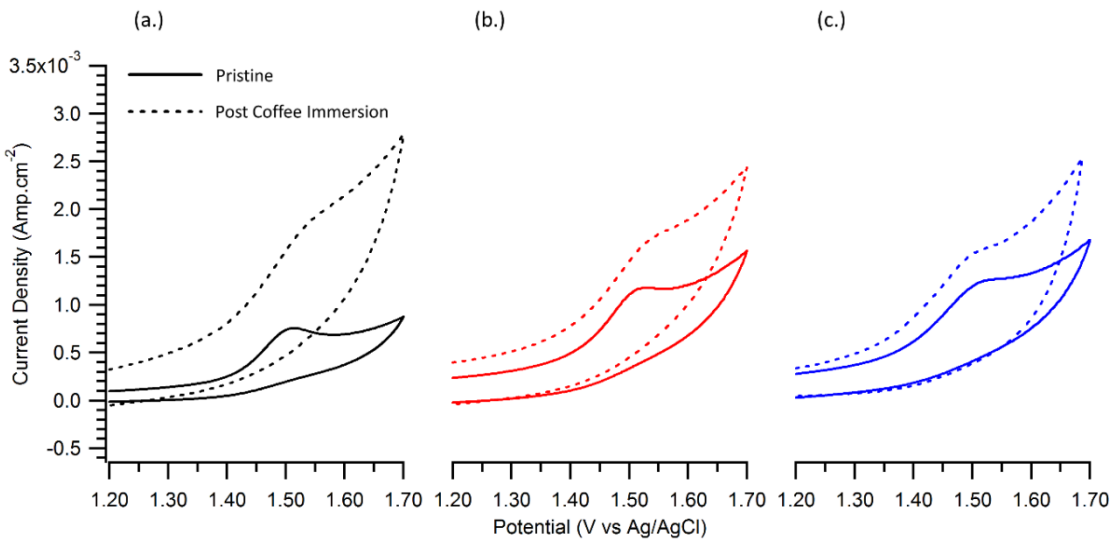

Figure 3.9. Cyclic voltammograms of caffeine (1 mM) in H_2SO_4 (0.1 M) with a scan rate of 50 mVs^{-1} vs Ag/AgCl using **(a.)** Bare GC, **(b.)** Spontaneously modified GC and **(c.)** Electrografted GC electrodes, before and after immersion in coffee for 72 h.

The samples were then immersed over a 72 h period in a commercially available coffee solution prepared fresh using tap water from a soft water region (Dublin 2, Ireland during spring 2018) using a Dolce Gusto™ Delongine coffee maker with a Nescafé Dulce Gusto™ Lungo instant coffee capsule. Following incubation the electrodes were rinsed gently for ten seconds with deionised water under gravity and the caffeine solution was probed again. In all cases background current increased slightly, leading to masking of the oxidative caffeine peak hence lowering sensitivity. Moreover, in the case of bare and sparsely coated samples the peak position shifted slightly to 1.52 V with a loss in peak intensity. The sample which appeared most resistant to change this was the electrochemically modified sample with no apparent change in peak position and the lowest observed capacitive increase. This is likely due to the lower concentration of exposed glassy carbon sites. It was thus concluded that a denser lactoside layer produced by electrografting may provide longer stability in an organic fouling medium such as coffee as a caffeine sensing probe and hence may be more desirable in instances of passive sample probing.

3 Conclusions

Aryldiazonium grafting behaviour on carbon materials was investigated using aminophenol lactoside precursor compounds under two grafting conditions, in situ diazonium salt formation with spontaneous surface grafting over a 1 h incubation period and electrochemical reduction of activated diazonium salt solution by chronoamperometry at potential of –0.5 V for 300 s. Spectroscopic analysis of modified surfaces and lectin binding experiments confirm saccharide surface functionality on both spontaneously grafted and electrografted surfaces with the latter producing significantly higher surface coverage with potential multilayer formation. Each modification was found to significantly increase surface wettability with the electrografted producing far greater reduction in water contact angle. In both instances of saccharide grafting to glassy carbon plates, nonspecific protein retention was found be significantly lower than on that of an unmodified glassy carbon control. This confirms first, that the saccharide based costings possess significant protein rejection capabilities and, second, that a sparse monolayer coating may be sufficient to impart biofilm resistant capabilities onto carbon materials.

4 Materials and Methods

4.1 Chemicals and Materials

Phosphate buffered saline buffer (0.010 M PBS, pH 7.4), sodium nitrite, hydrochloric acid, fluoroboric acid, Peanut agglutinin (PNA) & bovine serum albumin (BSA) conjugates with fluorescein isothiocyanate (FITC) were purchased from Sigma-Aldrich; Sigradur K Glassy carbon plates and Sigradur G Glassy carbon discs were purchased from HTW. Aminophenol-lactoside compounds **5**, **6**, & **9** were synthesised as described in **Chapter II**.

4.2 Substrate surface preparation

Carbon substrates for infrared reflectance absorption spectroscopy experiments (IRRAS) were prepared *via* DC magnetron sputtering (Torr International Inc.) in Ar. Deposition was carried out on an optically thick Ti under layer (Grade 2) on which carbon was subsequently sputtered from a graphite target (99.999%).[10]

Glassy carbon substrates were polished with alumina slurries (Buehler) with decreasing particle size of 1 (on nylon cloth), 0.3 and 0.05 μm (on nylon microcloth); each polishing step was followed by 3 min sonication in each of n-hexane, methanol (semiconductor grade) and ultrapure H_2O.

4.3 Surface characterisation

A Bruker Tensor 27 infrared spectrometer was used to perform Infrared reflectance absorption spectroscopy (IRRAS) characterisation. The spectrometer was equipped with a mercury cadmium telluride detector and a VeeMax II specular reflectance accessory with a wire grid polarizer. All spectra were collected using p-polarised light at an angle of incidence of 80° using an unmodified sample as a background; 100 scans at 4 cm^{-1} were collected for all samples. Water contact angles (WCAs) were determined for all samples using the sessile drop method (FTA1000), using 20 μL droplets. Thickness and surface roughness measurements were carried out via Atomic Force Microscopy (AFM, Oxford Asylum Research) using silicon cantilevers, following previously published procedures at ambient pressure calibrated at 140 kHz.[16]

4.4 Fluorescence microscopy

Sigradur K Glassy carbon plates treated 0.2 mg mL^{-1} solutions of BSA-FITC in PBS at pH 7.4 for 1 h. All samples were washed with PBS solution prior to imaging to remove excess unbound protein. Fluorescence images were acquired using an Olympus BX51 inverted microscope with cellSense digital image processing software. Emission intensities were analysed in triplicate using ImageJ software.

4.5 Electrochemistry

All electrochemical experiments were carried out using a Metrohm Autolab AUT50324 potentiostat using a 3-electrode setup.[25] A static disc holder (Pine Instruments) enclosing the GC disc was used as working electrode, an Ag/AgCl electrode (KCl sat, E = 0.196 V vs SHE) and a graphite rod were used as reference and counter electrodes respectively. The electrochemical cell consisted of a beaker with a custom-made Teflon cap. The temperature was controlled at 25°C using a water bath. All solutions were degassed with Argon

gas prior to measurement. A blanket of Ar was maintained in the headspace over the solution throughout the experiment.

References

1. Delamar, M.; Hitmi, R.; Pinson, J.; Saveant, J. M., Covalent modification of carbon surfaces by grafting of functionalized aryl radicals produced from electrochemical reduction of diazonium salts. *J. Am. Chem. Soc.* **1992,** *114* (14), 5883-5884.
2. Betelu, S.; Tijunelyte, I.; Boubekeur-Lecaque, L.; Ignatiadis, I.; Ibrahim, J.; Gaboreau, S.; Berho, C.; Toury, T.; Guenin, E.; Lidgi-Guigui, N.; Félidj, N.; Rinnert, E.; Chapelle, M. L. d. l., Evidence of the Grafting Mechanisms of Diazonium Salts on Gold Nanostructures. *J. Phys. Chem. C* **2016,** *120* (32), 18158-18166.
3. Brooksby, P. A.; Downard, A. J., Electrochemical and Atomic Force Microscopy Study of Carbon Surface Modification via Diazonium Reduction in Aqueous and Acetonitrile Solutions. *Langmuir* **2004,** *20* (12), 5038-5045.
4. Shewchuk, D. M.; McDermott, M. T., Comparison of Diazonium Salt Derived and Thiol Derived Nitrobenzene Layers on Gold. *Langmuir* **2009,** *25* (8), 4556-4563.
5. Ahmad, R.; Boubekeur-Lecaque, L.; Nguyen, M.; Lau-Truong, S.; Lamouri, A.; Decorse, P.; Galtayries, A.; Pinson, J.; Felidj, N.; Mangeney, C., Tailoring the Surface Chemistry of Gold Nanorods through Au–C/Ag–C Covalent Bonds Using Aryl Diazonium Salts. *J. Phys. Chem C* **2014,** *118* (33), 19098-19105.
6. Sun, Z.; Pint, C. L.; Marcano, D. C.; Zhang, C.; Yao, J.; Ruan, G.; Yan, Z.; Zhu, Y.; Hauge, R. H.; Tour, J. M., Towards hybrid superlattices in graphene. *Nature Comm.* **2011,** *2*, 559.
7. Jiang, C.; Alam, M. T.; Parker, S. G.; Darwish, N.; Gooding, J. J., Strategies To Achieve Control over the Surface Ratio of Two Different Components on Modified Electrodes Using Aryldiazonium Salts. *Langmuir* **2016,** *32* (10), 2509-2517.
8. Mesnage, A.; Lefèvre, X.; Jégou, P.; Deniau, G.; Palacin, S., Spontaneous Grafting of Diazonium Salts: Chemical Mechanism on Metallic Surfaces. *Langmuir* **2012,** *28* (32), 11767-11778.
9. Adenier, A.; Barré, N.; Cabet-Deliry, E.; Chaussé, A.; Griveau, S.; Mercier, F.; Pinson, J.; Vautrin-Ul, C., Study of the spontaneous formation of organic layers on carbon and metal surfaces from diazonium salts. *Surf. Sci.* **2006,** *600* (21), 4801-4812.
10. Cullen, R. J.; Jayasundara, D. R.; Soldi, L.; Cheng, J. J.; Dufaure, G.; Colavita, P. E., Spontaneous Grafting of Nitrophenyl Groups on Amorphous Carbon Thin Films: A Structure–Reactivity Investigation. *Chem. Mater.* **2012,** *24* (6), 1031-1040.
11. Mesnage, A.; Abdel Magied, M.; Simon, P.; Herlin-Boime, N.; Jégou, P.; Deniau, G.; Palacin, S., Grafting polymers to titania nanoparticles by radical polymerisation initiated by diazonium salt. *J. Mater. Sci.* **2011,** *46* (19), 6332-6338.
12. Downard, A. J., Electrochemically Assisted Covalent Modification of Carbon Electrodes. *Electroanalysis* **2000,** *12* (14), 1085-1096.
13. Jayasundara, D. R.; Duff, T.; Angione, M. D.; Bourke, J.; Murphy, D. M.; Scanlan, E. M.; Colavita, P. E., Carbohydrate Coatings via Aryldiazonium Chemistry for Surface Biomimicry. *Chem. Mater.* **2013,** *25* (20), 4122-4128.
14. Angione, M. D.; Duff, T.; Bell, A. P.; Stamatin, S. N.; Fay, C.; Diamond, D.; Scanlan, E. M.; Colavita, P. E., Enhanced Antifouling Properties of Carbohydrate Coated Poly(ether sulfone) Membranes. *ACS Appl. Mater. Interfaces* **2015,** *7* (31), 17238-17246.
15. Esteban-Tejeda, L.; Duff, T.; Ciapetti, G.; Daniela Angione, M.; Myles, A.; Vasconcelos, J. M.; Scanlan, E. M.; Colavita, P. E., Stable hydrophilic poly(dimethylsiloxane) via glycan surface functionalisation. *Polymer* **2016,** *106*, 1-7.
16. Zen, F.; Angione, M. D.; Behan, J. A.; Cullen, R. J.; Duff, T.; Vasconcelos, J. M.; Scanlan, E. M.; Colavita, P. E., Modulation of Protein Fouling and Interfacial Properties

at Carbon Surfaces via Immobilisation of Glycans Using Aryldiazonium Chemistry. *Sci. Rep.* **2016,** *6*, 24840.
17. Lu, X.; Peng, Y.; Qiu, H.; Liu, X.; Ge, L., Anti-fouling membranes by manipulating surface wettability and their anti-fouling mechanism. *Desalination* **2017,** *413*, 127-135.
18. Kobayashi, M.; Terayama, Y.; Yamaguchi, H.; Terada, M.; Murakami, D.; Ishihara, K.; Takahara, A., Wettability and Antifouling Behavior on the Surfaces of Superhydrophilic Polymer Brushes. *Langmuir* **2012,** *28* (18), 7212-7222.
19. Hlady, V.; Buijs, J., Protein adsorption on solid surfaces. *Current Opin. Biotechnol.* **1996,** *7* (1), 72-77.
20. Breton, T.; Downard, A. J., Controlling Grafting from Aryldiazonium Salts: A Review of Methods for the Preparation of Monolayers. *Aust. J. Chem.* **2017,** *70* (9), 960-972.
21. Menanteau, T.; Dabos-Seignon, S.; Levillain, E.; Breton, T., Impact of the Diazonium Grafting Control on the Interfacial Reactivity: Monolayer versus Multilayer. *ChemElectroChem* **2017,** *4* (2), 278-282.
22. Menanteau, T.; Levillain, E.; Downard, A. J.; Breton, T., Evidence of monolayer formation via diazonium grafting with a radical scavenger: electrochemical, AFM and XPS monitoring. *Phys.Chem. Chem. Phys.* **2015,** *17* (19), 13137-13142.
23. Combellas, C.; Kanoufi, F.; Pinson, J.; Podvorica, F. I., Sterically Hindered Diazonium Salts for the Grafting of a Monolayer on Metals. *J. Am. Chem. Soc.* **2008,** *130* (27), 8576-8577.
24. Lee, L.; Leroux, Y. R.; Hapiot, P.; Downard, A. J., Amine-Terminated Monolayers on Carbon: Preparation, Characterisation, and Coupling Reactions. *Langmuir* **2015,** *31* (18), 5071-5077.
25. Behan, J. A.; Stamatin, S. N.; Hoque, M. K.; Ciapetti, G.; Zen, F.; Esteban-Tejeda, L.; Colavita, P. E., Combined Optoelectronic and Electrochemical Study of Nitrogenated Carbon Electrodes. *J. Phys. Chem. C* **2017,** *121* (12), 6596-6604.
26. Bélanger, D.; Pinson, J., Electrografting: a powerful method for surface modification. *Chem. Soc. Rev.* **2011,** *40* (7), 3995-4048.
27. Socrates, G., *Infrared and Raman Characteristic Group Frequencies: Tables and Charts*. Wiley: **2004**.
28. Gutiérrez Gallego, R.; Haseley, S. R.; van Miegem, V. F. L.; Vliegenthart, J. F. G.; Kamerling, J. P., Identification of carbohydrates binding to lectins by using surface plasmon resonance in combination with HPLC profiling. *Glycobiology* **2004,** *14* (5), 373-386.
29. Neurohr, K. J.; Young, N. M.; Mantsch, H. H., Determination of the carbohydrate-binding properties of peanut agglutinin by ultraviolet difference spectroscopy. *J. Bio. Chem.* **1980,** *255* (19), 9205-9209.
30. Dhayal, M.; Ratner, D. M., XPS and SPR Analysis of Glycoarray Surface Density. *Langmuir* **2009,** *25* (4), 2181-2187.
31. Ilangovan, G.; Chandrasekara Pillai, K., Electrochemical and XPS Characterisation of Glassy Carbon Electrode Surface Effects on the Preparation of a Monomeric Molybdate(VI)-Modified Electrode. *Langmuir* **1997,** *13* (3), 566-575.
32. Taner, B.; Deveci, P.; Üstündağ, Z.; Keskin, S.; Özcan, E.; Osman Solak, A., Modification of glassy carbon electrode by the electrochemical oxidation of 3-aminophenylcalix[4]pyrrole in nonaqueous media. *Surf. Interface Anal.* **2012,** *44* (2), 185-191.
33. Myles, A.; Haberlin, D.; Esteban-Tejeda, L.; Angione, M. D.; Browne, M. P.; Hoque, M. K.; Doyle, T. K.; Scanlan, E. M.; Colavita, P. E., Bioinspired Aryldiazonium Carbohydrate Coatings: Reduced Adhesion of Foulants at Polymer and Stainless Steel Surfaces in a Marine Environment. *ACS Sust. Chem. Eng.* **2018,** *6* (1), 1141-1151.
34. Huggett, M. J.; Nedved, B. T.; Hadfield, M. G., Effects of initial surface wettability on biofilm formation and subsequent settlement of Hydroides elegans. *Biofouling* **2009,** *25* (5), 387-399.

35. Menegazzo, N.; Zou, Q.; Booksh, K. S., Characterisation of electrografted 4-aminophenylalanine layers for low non-specific binding of proteins. *New J.Chem.* **2012,** *36* (4), 963-970.
36. Clarke, R. J., *Coffee: Volume 1: Chemistry*. Springer Netherlands: **2012**.
37. Redivo, L.; Stredanský, M.; De Angelis, E.; Navarini, L.; Resmini, M.; Švorc, Ĺ., Bare carbon electrodes as simple and efficient sensors for the quantification of caffeine in commercial beverages. *R.Soc. Open Sci.* **2018,** *5* (5).

Chapter IV

Spontaneous modification on Non-Conductive Surfaces

Polymeric and passivated metal alloy surfaces possess important and numerous applications. Discussed in this chapter is the development of a surface grafting technique using aryldiazonium-lactoside applicable to PES, polyamide and stainless steel surfaces in order to produce a non-specific protein resistant coating. The resulting materials were characterised by water contact angle, infrared and x-ray spectroscopies and protein adsorption/binding experiments.

The data Presented in this chapter is reproduced in part from the following publication:

Bioinspired Aryldiazonium Carbohydrate Coatings: Reduced Adhesion of Foulants at Polymer and Stainless Steel Surfaces in a Marine Environment
Adam Myles, Damien Haberlin, Leticia Esteban-Tejeda, M. Daniela Angione, Michelle P. Browne, Md. Khairul Hoque, Thomas K. Doyle, Eoin M. Scanlan , and Paula E. Colavita.
ACS Sustainable Chem. Eng., **2018**, *6* (1), pp 1141–1151

Contributions are as follows:
Surface Pre-modification protocols were initially developed by M. D. Angione. (polyamides) and L. Esteban-Tejeda (Stainless Steel) for the purposes of aryldiazonium grafting with mono and di-saccharides. XPS data was obtained primarily by S.N. Stamatin and interpretation of XPS data was performed by P.E. Colavita.

1 Introduction

1.1 Aryldiazonium cations for modification of non-conductive surfaces

Metal alloys and polymeric materials are prevalent in industry as filters,[1] storage and reaction vessels,[2] flow transport tubing for foods/drinks and pharmaceutical products,[3] in medical devices[4] in submersible structures and in aquatic transportation, all of which are routinely subject to biofouling.[5] This process affects the lifetime, quality, and the safety of materials produced thus requiring continual costly maintenance, cleaning and replacement of parts. It is due to the resulting commercial interest that the development of improved biofilm resistant technologies is paramount. To this end, techniques for lactoside aryldiazonium grafting were developed for coupons consisting of three representative non-conductive materials of differing physicochemical properties (2 polymeric, and one metal alloy) for production of biofilm resistant materials.

Electro-reduction of aryldiazonium salts in the grafting of metal and polymeric materials is generally possible only on conductive (or semiconductive) surfaces such as polypyrrols[6], which can be biased at reducing potentials. This represents a limitation of this method that makes it challenging for applications in an industrial setting or at large scales. In stark contrast to this, spontaneous grafting provides a simple, readily scalable alternative to electrografting; spontaneous reactions allow for modifications via drop casting, spin coating or surface immersion to produce covalently modified materials, even in cases where making an electric contact is unwieldly or impossible.[7]

It is well established in literature that aryldiazonium compounds readily react with nucleophilic molecules such that upon the loss of nitrogen a nucleophile substituted aryl ring is produced.[8] The reactivity of these diazonium groups was recently exploited by Esteban-Tejeda *et al.*[9] in the production of a lactose and mannose modified polydimethylsiloxane (PDMS) through spontaneous aryldiazonium grafting; it was proposed that hydroxyl moieties found on the polymer surface, post oxidative treatment with caustic bleach solution or by ultraviolet activation, enabled nucleophilic substitution.

Spontaneous aryldiazonium grafting on non-conductive surfaces is readily achieved on polymers such as polyethersulphone (PES) which possess reactive functionality in the form of phenyl components within the polymer structure.[10] On

materials which possess no graftable functionality it is possible to induce surface functionality through pre-treatments such as the carbonisation of Teflon surfaces as performed by Combellas *et al*.[11] or through the use of a commercial surface pre-treatment such as the GraftFast™ polymer, to produce a reactive aryl surface scaffold for further diazonium grafting.[12] Aryldiazonium modification of unmodified polymeric surfaces such as polypropaline[13] and Poly(methyl methacrylate)[14] have also been reported following chemical reduction of corresponding aryldiazonium salts. Spontaneous grafting onto stainless steel has been achieved by Small *et al.,*[15] reporting on the spontaneous attachment of fluorinated aryldiazonium salts on stainless steel from solution, achieved by polishing samples immediately prior to grafting. Mechanical polishing breaks down the steel passive oxide, exposing the iron-rich under layer which can act as an effective spontaneous reductant in aryldiazonium grafting, in agreement with findings on various oxide-free metals.[16]

In this study it was found that Nylon-6 and marine grade Stainless Steel 316 (SS316) coupon samples, when subjected to oxidative surface pre-treatments, possess nucleophilic functional groups which also allows for spontaneous diazonium grafting to occur. To our knowledge this was the first reported use of aryldiazonium modification of a polyamide surface. It should be noted that foregoing pre-treatment steps for nylon and stainless steel samples prior to immersion in activated diazonium solution yields no observable functionalisation behaviour. Wettability studies on modified PES, nylon-6 and stainless steel samples was performed by sessile drop water contact angle. Functionalisation of stainless steel was confirmed by a combination of X-ray photoelectron spectroscopy (XPS) and Infrared reflectance analysis (IRRAS). Nylon-6 functionalisation was probed by fluorescence imaging of lectin-saccharide binding. Saccharide immobilisation was found to increase surface hydrophilicity of all materials tested, such that the saccharide coating results in reduced protein adsorption in the absence of specific protein-saccharide interactions.

2 Results and Discussion

2.1 Polymer and Stainless Steel Modification

Prior work by Angione *et al.*[10] has demonstrated that PES undergoes functionalisation by spontaneous reaction after immersion of pristine substrates in aryl-lactoside cation solutions and this family of materials has previously been characterised. A proposed reaction mechanism with the aryl cation formed from spontaneous diazonium decomposition is shown in **Scheme 1a**. Nylon 6 surfaces were pre-treated by immersion of samples in formaldehyde solutions with hypophosphorus acid. This treatment is known to activate the amide groups of polyamides *via* formation of N-methylol groups onto which grafting can occur.[17-19] For SS316, surfaces were pre-activated prior to functionalisation in caustic hypochlorite (bleach) solutions. This treatment is known to have cleaning and oxidising effects on SS316 surfaces[20-21] and yields a homogeneous hydrophilic passive oxide which cannot directly reduce the aryldiazonium cation. This oxide surface however offers functional M-OH and/or M-OOH sites[15, 22] that are available to chemical reaction. There are few reports of spontaneous aryldiazonium reactions on oxides,[23-24] however the spontaneous formation of M-O-Ar bonds has been demonstrated experimentally.[23]

To ensure no adventitious interaction between the pre-conditiong solutions and the reactive grafting solution, these surfaces were rinsed thoroughly with ultrapure water and dried under inert gas flow, prior to immersion in freshly activated lactose coating solution. Based on our results, spontaneous grafting can take place on passivated stainless steel surfaces *via* aryl group cross-linking. It is likely that, as in the case of reactions with primary alcohols, functionalisation proceeds *via* nucleophilic substitution involving oxide hydroxyl groups (**Scheme 4.1 b**).

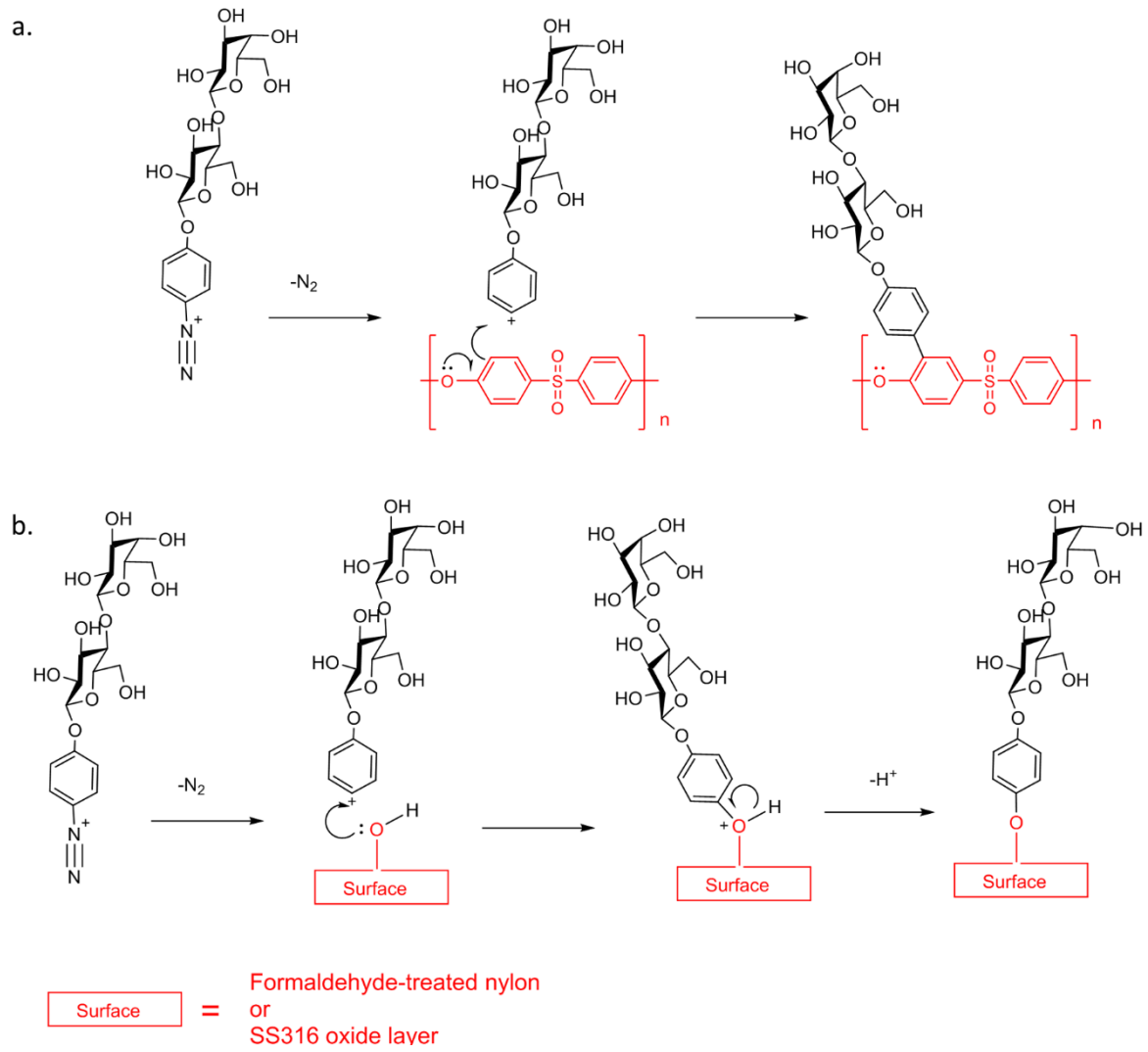

Scheme 4.1. (a.) Potential reaction pathways for reaction of PES with aryl diazonium species. **(b.)**Proposed SN1 mechanism for the reaction of aryldiazonium salts with –OH groups at surfaces, based on the well understood hydrolysis reaction in solution. Both nylon 6 and SS316 display –OH groups after the pre-treatment process described. Adapted with permission from; *ACS Sustainable Chem. Eng.*, **2018**, *6* (1), pp 1141–1151. Copyright 2017 American Chemical Society & *ACS Appl. Mater. Interfaces*, **2015**, *7* (31), pp 17238–17246. Copyright 2015 American Chemical Society.

2.2 Surface Characterisation

2.2.1 Surface Wettability Studies

The effects of modification protocols on material surfaces was investigated by means of water contact angle (WCA) measurements. Pre-functionalisation treatments on N-6 and SS316 were found to increase surface hydrophilicity as evident from a marked change in water contact angle (**Figure 4.1**). The WCA of SS316 decreases from 69.8° to 44.5° following oxidative cleaning, indicating the removal of adhered organics and exposure of a hydrophilic oxide film. The WCA

of nylon decreases from a value of 80.8° to 71.7°. This behaviour is consistent with an increase in the surface density of hydroxyl groups resulting from formaldehyde treatment. We also observe that following immobilisation of hydrophilic saccharide groups the WCA of all three coupon surfaces decreases as expected in agreement with previous reports on the effect of lactoside immobilisation.[25]

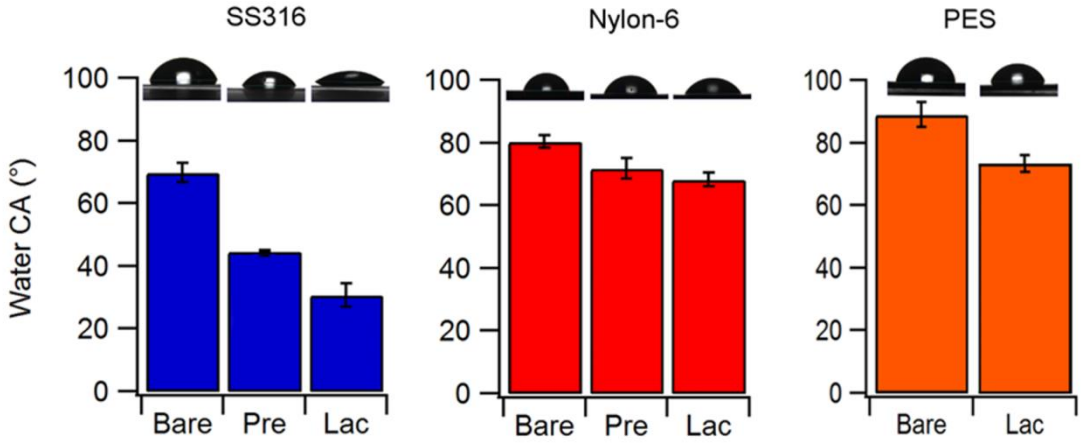

Figure 4.1. Water contact angle values obtained on bare, pre-treated (except for PES) and Lactose-modified (Lac) surfaces of SS316, Nylon-6 and PES. Samples were pre-activated in caustic bleach and formaldehyde solutions in the case of SS316 and nylon-6, respectively. Adapted with permission from *ACS Sustainable Chem. Eng.*, **2018**, *6* (1), pp 1141–1151. Copyright 2017 American Chemical Society.

In order to confirm that the change in surface functionality comes from grafting of our saccharide to the surface and is not a result of pitting of our surfaces by the acidic functionalisation medium, nor caused by physical adhesion of lactose to the surface, an additional study was performed on new coupons subjected to the same pre-treatment conditions as reported above. Pretreated samples were immersed for 1 hour in Deionised water as a control(Pre), a solution containing the lac-aminophenol precursor (compound **6**) in acidic media without any $NaNO_2$ (Phys) and in a solution containing activated lactoside cations with $NaNO_2$ (Lac) (**Figure 4.2**).

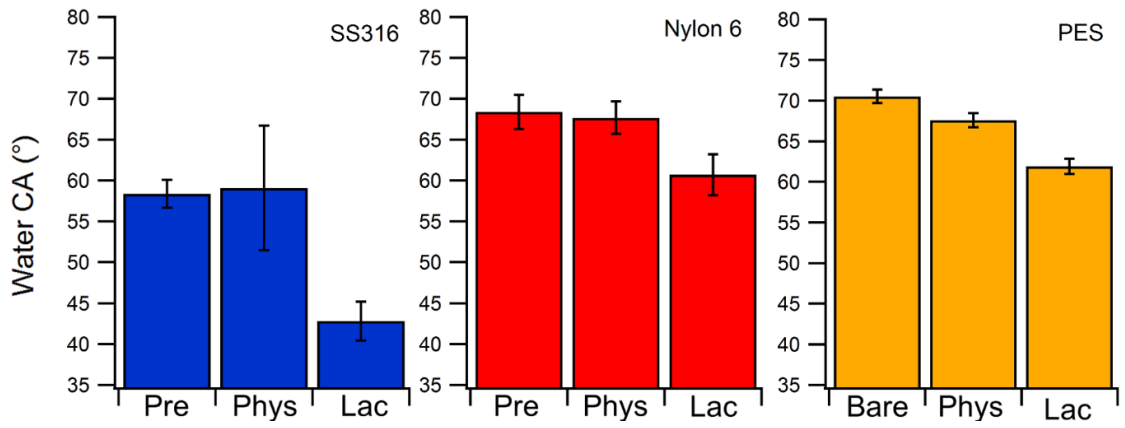

Figure 4.2. Water contact angle of pre-treated surfaces (Pre), surfaces after physisorption tests using aminophenol lactoside precursors in acid (Phys), and after functionalisation using the in situ aryldiazonium generation reaction (Lac). PES samples were only rinsed with MeOH (Bare), as these surfaces do not require pre-conditioning prior to functionalisation. All samples were treated under identical conditions.

It is observed that in all cases the WCA is similar for pre-treated and physisorption controls, while it is significantly reduced after diazotisation, thus confirming the immobilisation of a hydrophilic saccharide layer. As lactose modified PES has previously been characterised this water contact angle study was deemed sufficient to confirm lactoside surface functionality on this material type.[10]

2.2.2 Spectroscopic Characterisation of Stainless Steel surfaces

Functionalisation of SS316 surfaces was further investigated using a peracetylated analogue of the aminophenol lactoside precursor (compound **5**). This precursor compound is chosen since acetyl moieties, due to their intense infrared absorbance, provide distinctive and readily identified infrared labels. **Figure 4.3**. shows the IRRAS spectrum of the functionalised surface with the ATR of bulk precursor saccharide compound for comparison.

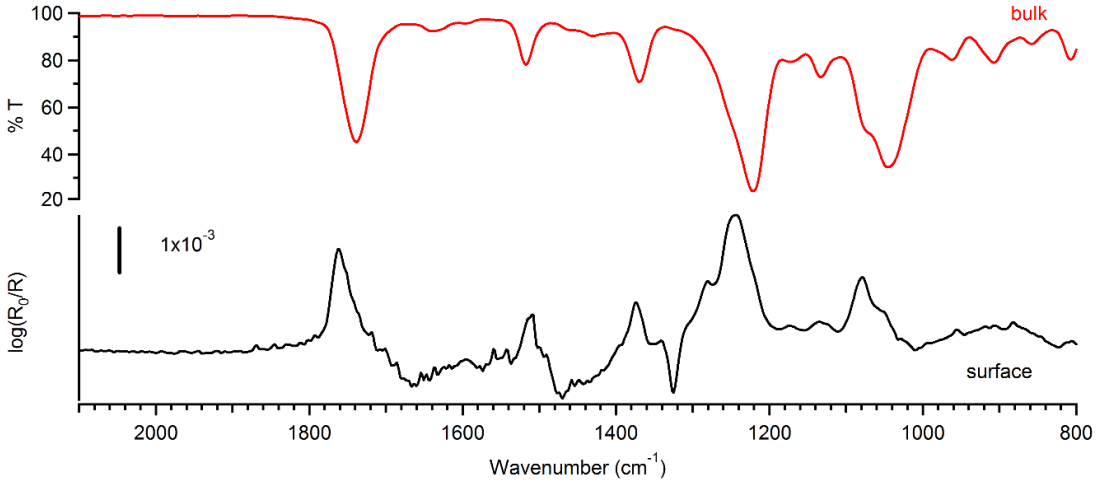

Figure 4.3. IRRAS spectrum of a SS316 sample surface after functionalisation (surface, bottom trace), compared to the transmittance spectrum of the peracetylated phenyl-glycoside precursor compound (bulk, top trace). Adapted with permission from *ACS Sustainable Chem. Eng.*, **2018**, *6* (1), pp 1141–1151. Copyright 2017 American Chemical Society.

Characteristic peaks of acetyl groups can been seen in the IRRAS spectrum in good agreement with those of the bulk precursor compound and previously reported acetyl saccharide grafted surfaces.[25] Peaks are assigned as follows: 1760 cm^{-1} (C=O stretching), 1373 cm^{-1} (CH_3 bending) and 1246 cm^{-1} (C-O-C asymmetric stretching).[10, 26] The peak centred at 1080 cm^{-1} is associated with C−O stretching modes of the carbohydrate ring, while the peak at 1510 cm^{-1} arises from C−C skeletal vibrations of phenyl rings.[10, 26]

To confirm that the peaks on SS surface do not arise simply from physisorbed acetylated-lactoside, the functionalised sample was rinsed in methanol, acetonitrile and ultrapure water immediately after incubation in the functionalisation solution and dried under inert gas. This sample was characterised by IRRAS then subjected to sonication for 1 min in each of the aforementioned solvents and characterised again (**Figure 4.4**).

There is a noticeable drop in intensity post sonication showing that, for acetylated surfaces, sonication is necessary to remove unbound precursor material. Additionally there is a significant retention of peracetyl lactoside groups at the SS316 surface, providing indirect evidence that attachment is likely to occur through covalent bonding as physisorbed material is removed under these conditions.[27]

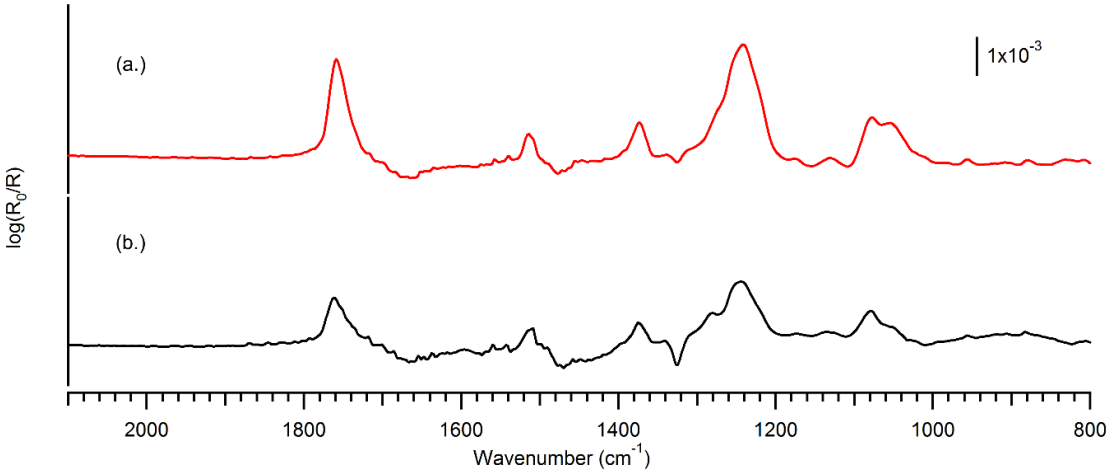

Figure 4.4. IRRAS spectra of organic layers obtained on SS316 surfaces using a peracetylated aminophenol lactoside precursor. **(a.)** layer obtained after functionalisation followed by rinsing in acetonitrile, methanol and water; **(b.)** spectrum obtained after sonication in acetonitrile and methanol. The scale is identical in both traces.

Functionalisation was also confirmed by X-ray Photoemission Spectroscopy (XPS), by use of a fluoro-substituted derivative of the lactoside precursor (see **Chapter II**, compound **9**). This precursor was chosen due to its inclusion of a fluorine atomic tag which provides good elemental contrast between the functional layer and the bare substrate which lacks any significant fluorine contribution. Survey spectra of pre-treated and modified SS316 in **Figure 4.5** show characteristic peaks of stainless steel associated with Fe 2p, Ni LMM, Cr 2p, O 1s, and C 1s lines, while **Figures 4.5.b and 4.5.c** show the spectra of pre-treated and modified SS316, in the F 1s and C 1s regions, respectively.[28-29]

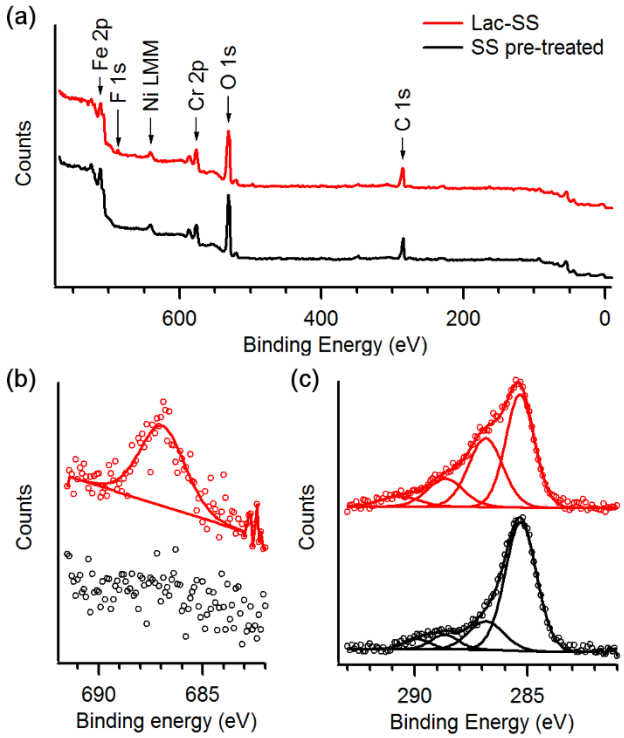

Figure 4.5. (a.) Survey XPS spectra of SS316 after pre-treatment (black) and after modification with F-substituted aryl-lactoside (red). **(b.)** F 1s and **(c.)** C 1s high resolution spectra; these spectra show that upon reaction with aryldiazonium lactosides there appear peak contributions at 687 eV and at 286-289 eV that can be attributed to F-atoms and C—O groups, respectively. Reproduced with permission from *ACS Sustainable Chem. Eng.*, **2018**, *6* (1), pp 1141–1151. Copyright 2017 American Chemical Society.

Peak area ratios were analysed and a fitting of the C 1s line yielded results summarised in **Table 4.1**. The pre-treated SS316 surface shows C/Cr and Cr/Fe atomic ratios that are consistent with those observed by Williams et al.[29] for plasma cleaned SS316. The surface was found to be C- and Cr-rich with respect to the bulk composition, in agreement with previous compositional studies.[30] Deconvolution of the C 1s line shows the presence of four main peaks at 285.3 eV (C—C and C—H), at 286.8 and 288.7 eV (C—O), and at 289.9 eV (C=O), in agreement with previous reports for stainless steel surfaces.[31] Functionalisation results in the appearance of a peak at 687.0 eV which is consistent with the F 1s binding energy in fluorinated organics, where F atoms are in a low F/C content environment.[32-33] This result suggests that after functionalisation the aryl group is bound to the SS316 surface, which is further supported by an increase of the C 1s peak intensity relative to the Cr 2p signal arising from the substrate alloy.

Table 4.1. Summary of results from XPS analysis of spectra in **Figure 4.5**. Values in parentheses indicate %-contribution to the total peak intensity; elemental ratios are

calculated as atomic ratios. Reproduced with permission from *ACS Sustainable Chem. Eng.*, **2018**, *6* (1), pp 1141–1151. Copyright 2017 American Chemical Society.

	SS pre-treated	**Lac-SS**
C 1s (eV)	285.3 (70%)	285.1 (46%)
	286.8 (18%)	286.7 (33%)
	288.7 (7%)	288.4 (15%)
	289.9 (5%)	290.5 (6%)
F 1s (eV)	-	687.0
C/Cr at.	6.9	7.6
F/Cr at.	-	0.30
Cr/Fe at.	0.67	0.68

The fit of the C 1s line of Lac-SS (**Figure 4.5 c**) reveals the appearance of a contribution at 290.5 eV, consistent with the binding energy expected for a C—F group,[32, 34-35] and also shows increased emission in the region 286-289 eV consistent with greater surface density of C—O containing groups from the presence of surface bound glycosides.

The relative sensitivity factor (RSF) corrected peak area ratio (A286+A288):A687 = 12.2 is in good agreement with the 12:1 ratio of C—O to C—F expected from the molecular stoichiometry of the fluorinated precursor, thus confirming the assignment of peaks in the region 286-289 eV to, predominantly, C—O groups from the lactoside, with likely minor contributions from substrate carbon. These results therefore indicate that the functionalisation protocol resulted in surface modification of SS316 with aryl-lactosides.

An estimate of the molecular density can be obtained by assuming that the SS316 substrate surface consists of Cr_2O_3/Fe_2O_3 with 40% Cr_2O_3 content (Cr/Fe = 0.67), as calculated from XPS and in agreement with Williams et al.[29] Considering that both Cr_2O_3 and Fe_2O_3 have a density of 5.2 g cm^{-3}, the photoelectron attenuation depth of Cr 2p photoelectrons can be predicted to be λ = 1.5 nm using Gries' G-1 predictive formula.[36] Under the assumption that no photoelectrons escape from depths >3λ, the average experimental F/Cr 0.17 ± 0.10 atomic ratio measured over 5 samples yields an estimated mean density of 1.9×10^{-9} mol cm^{-2}.[37] For a perfectly smooth surface, this coverage is equivalent to <5 monolayers of lactosides.[38-39]Given that the microscopic roughness factor

of unpolished SS316 is >1, the estimated coverage value suggests the presence of a relatively sparse lactoside layer, as expected from a spontaneous reaction of the oxide surface with these bulky aryldiazonium cations and consistent with thin molecular layers formed on carbon substrates via similar protocols.[25]

2.2.3 **Protein Binding Studies on Nylon and Stainless Steel surfaces**

Lactoside immobilisation was confirmed on nylon through binding studies using PNA lectin. PNA displays binding affinity towards galactose (the terminal sugar in our lactoside coating) and can be used to confirm the presence of surface-bound lactosides which express an available galactose unit at the solid-liquid interface.[40] Lac-SS and Lac-N6 coupons were incubated for 1 h in a solution of fluorescently labelled PNA and rinsed with PBS prior to imaging to remove unconjugated lectin from the surface. Fluorescence microscopy images of pre-treated and Lac-modified surfaces following PNA incubation show comparisons of their average emission intensities, **Figure 4.6**. The stronger emission observed for surfaces after reaction with aryldiazonium cations indicates preferential specific binding to PNA with respect the corresponding bare pre-treated surface and is therefore supporting of functionalisation.

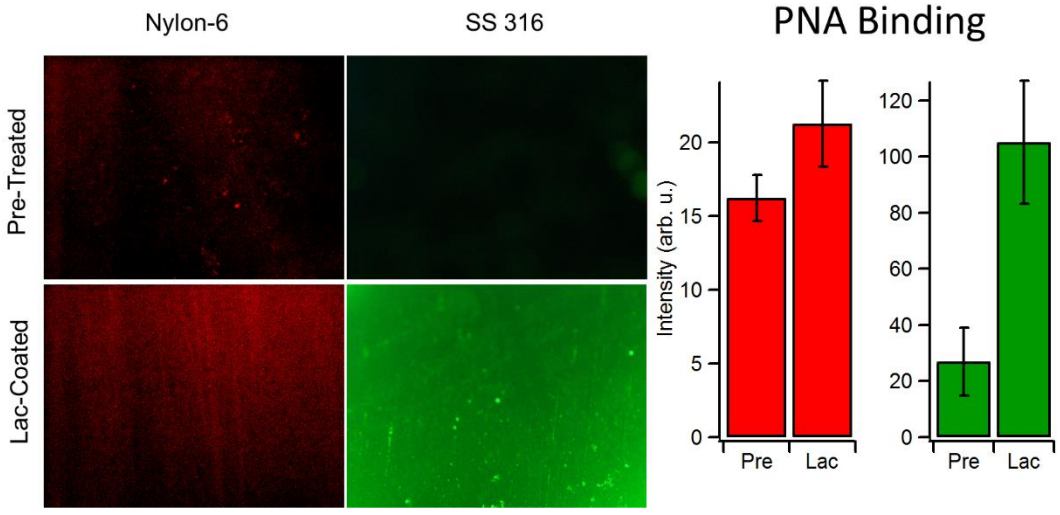

Figure 4.6. Fluorescence images obtained after lectin binding experiments using dye-conjugated PNA on Nylon-6 and SS316 after pre-treatment and after aryldiazonium modification with lactosides (Lac). The images show that the emission intensity is higher

on lactose-modified surfaces. Bar plots represent average emission intensities of Alexa-PNA on Nylon-6 (red bars) and of FITC-PNA on SS316 (green bars) obtained at pre-treated (Pre) and at lactose-modified coupons (Lac). Adapted with permission from *ACS Sustainable Chem. Eng.*, **2018**, *6* (1), pp 1141–1151. Copyright 2017 American Chemical Society.

Additionally samples were immersed in fluorescently labelled BSA solution, a protein that does not display specific binding with glycosides, to determine non-specific protein resistance of the coatings. **Figure 4.7** shows images of pre-treated and Lac-modified SS316 and N6, together with a summary of average emission intensity values obtained using BSA on these coupons. After functionalisation with lactosides a decrease in emission is observed compared to the pre-treated surface, thus indicating that less BSA adsorbs at Lac-SS and Lac-N6 surfaces. This indicates that the increase in fluorescence observed for Lac-SS and Lac-N6 after incubation in PNA solutions is the result of specific galactose PNA interactions and that immobilisation of saccharides to a surface leads to lower retention of unspecific proteins. These results are in agreement with observations on the effect of glycoside coatings on carbon and other polymer surfaces.[9-10, 25, 38]

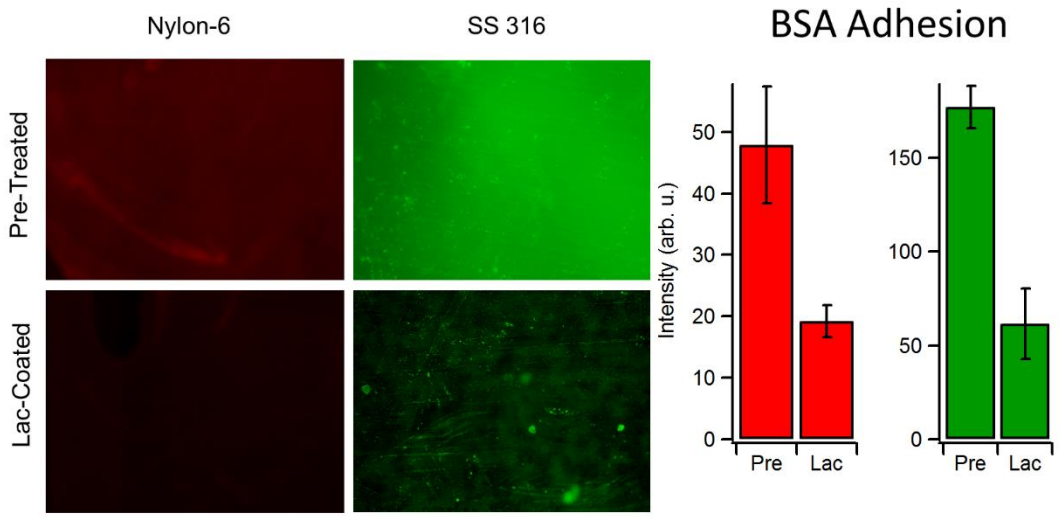

Figure 4.7. Fluorescence images obtained after protein adsorption experiments using dye-conjugated BSA on Nylon-6 and SS316 after pre-treatment and after aryldiazonium modification with lactosides (Lac). The images show that the emission intensity is lower on lactose-modified surfaces. Bar plots represent average emission intensities of Alexa-BSA on Nylon-6 (red bars) and of FITC-BSA on SS316 (green bars) obtained at pre-treated (Pre) and at lactose-modified coupons (Lac). Adapted with permission from *ACS Sustainable Chem. Eng.*, **2018**, *6* (1), pp 1141–1151. Copyright 2017 American Chemical Society.

3 Conclusions

Non-conductive surfaces of industrial interest were modified using the spontaneous lactoside aryldiazonium grafting method. Stainless steel samples were pre-treated using a bleach and base solution and polyamide samples using a formaldehyde solution to produce surfaces with reactive hydroxyl sites. The introduction of hydroxyl surface functionality was confirmed to allow for the modification by spontaneous diazonium grafting for both polyamide and stainless steel surfaces by reaction with the aryl lactoside cations. PES coupons were also modified as previously reported and all lactoside coated surfaces display increased hydrophilic behaviour. In the absence of covalent surface modification conditions with the saccharide solution a simple rinsing procedure was found to result in negligible change in surface wettability. Fluorescent protein retention experiments confirm that, firstly, the galactose unit is expressed on the surface of both nylon and stainless steel samples, and secondly, that treated surfaces possess improved protein rejection capabilities. Grafting on stainless steel surfaces was confirmed by spectroscopic methods by means of spectroscopically tailored lactoside precursors. It was determined that spontaneous aryldiazonium grafting of lactoside sugars produces at most a space monolayer on the surface of stainless steel. Given that the trend of enhanced non-specific protein rejection that these coatings produce is retained across materials of vastly different physicochemical properties it is feasible that this technique can be utilised on technologies of mixed materials. It is expected that this technique will find wide use across industrial applications.

4 Experimental

4.1 Chemicals and Materials

Polyamide- Nylon 6 (N6) sheets, marine grade stainless steel 316 foil (SS316), and Polyethersulfone sheets (PES) were purchased from Goodfellow; formaldehyde solution for molecular biology ≥36.0% in H_2O, hypophosphorous acid solution 50%wt. in H_2O, sodium hypochlorite (bleach), sodium hydroxide, potassium hydroxide, phosphate buffered saline buffer (0.010 M PBS, pH 7.4), sodium nitrite, hydrochloric acid and fluoroboric acid were purchased from Sigma

Aldrich. Bovine Serum Albumin (BSA) conjugates with Alexa Fluor 647 were purchased from Biosciences. Bovine Serum Albumin (BSA) and peanut agglutinin from Arachis Hypogaea (PNA) conjugates with fluorescein isothiocyanate (FITC) were purchased from Sigma Aldrich. 4-aminophenol-β-D-lactopyranose (**6**) and its fluorinated analogue 2-fluoro-4-aminophenol-β-D-lactopyranose (**9**) were synthesized as previously described in chapter 2. The peracetylated lactoside (**5**) was used for infrared experiments.

4.2 Surface Modification

Prior to modification with aryldiazonium cations, both polyamide and stainless steel surfaces were pre-activated, while PES surfaces did not require pre-activation and were used after light cleaning in methanol only. Nylon-6 (N6) samples were pre-activated by overnight immersion at 30 °C in a 36% aqueous formaldehyde solution with a catalytic amount of hypophosphorous acid. Stainless Steel samples (SS316) were pre-treated with 0.5% NaClO in basic aqueous solution (KOH 1% and NaOH 1%);[9] surfaces were immersed three times in fresh solution for 10 min at room temperature. Samples were rinsed thoroughly with deionized water and functionalized *via* immersion in freshly prepared 1.0 mM solutions of aryldiazonium cations generated *in situ* from the corresponding amine, 4-aminophenol-β-D-lactopyranose, following published protocols.[9-10, 25] 1.25 mM solution of the 4-aminophenol in 0.00150 M HBF_4 was prepared and cooled to 4 °C or less in an ice bath for 1 h. The cold precursor solution was diluted via addition of a 0.010 M $NaNO_2$ to a final concentration of 0.001 M in 4-aminophenol precursor, acid and nitrite. Samples were immersed immediately into the precursor solution and kept in the dark for 1 h, then rinsed with deionized water and kept under wet storage in deionized water prior to further testing. Experiments described in this chapter involved the preparation of 25 mL solutions. Functionalisation using peracetylated precursors followed the same protocol except for the use of acetonitrile as a solvent; samples were rinsed using sonication in acetonitrile/methanol, a protocol that had been shown to be effective at removing physisorbed acetylated aryldiazonium glycosides.

4.3 Surface Characterisation

Water contact angles (WCA) were determined for all samples using the sessile drop method (FTA1000), using 20 µL droplets. Infrared reflectance absorption spectroscopy (IRRAS) characterisation was carried out on a Bruker Tensor 27 infrared spectrometer equipped with a mercury cadmium telluride detector and a VeeMax II specular reflectance accessory with a wire grid polariser. All spectra were collected using p-polarized light; 100 scans at 4 cm^{-1} were collected for all samples and an unmodified sample was used as substrate. X-ray photoelectron spectroscopy (XPS) was carried out on a VG Scientific ESCAlab MK II system with an Al Kα source at 90° takeoff angle. Wide surveys and core level spectra were collected at 50 and 20 eV pass energy, respectively. All spectra were calibrated to the Cr $2p_{3/2}$ peak of Cr_2O_3 present in the stainless steel substrate at 576.7 eV.[30, 41] Fits were carried out using commercial software (CasaXPS version 2.3.18) using Voigt line shapes and background correction; atomic ratios were calculated from peak areas after correction for relative sensitivity factors (RSF_{C1s} = 1; RSF_{F1s} = 4.43; RSF_{Cr2p} = 11.7; RSF_{Fe2p} = 16.4), photoelectron attenuation depth of Cr 2p photoelectrons was predicted by means of Gries' G-1 Predictive formula.[36]

4.4 Affinity Binding and Protein Adsorption Studies

To determine protein rejection ability, samples of N6 and SS316 were incubated in 0.2 mg mL^{-1} solutions of BSA fluorescent conjugates in PBS at pH 7.4 for 1 h; Alexa-647 and FITC were the dyes used for N6 and SS316 respectively. To determine lectin binding affinity, samples of SS316 were incubated for 1 h in a 0.2 mg mL^{-1} solution of PNA-FITC conjugate in pH 7.4 PBS buffer with 0.1 mM $CaCl_2$ and $MgCl_2$. All samples were washed with PBS solution prior to imaging to remove excess unbound protein. Fluorescence images were acquired using an Olympus BX51 inverted microscope with cellSense digital image processing software. Emission intensities were analysed in triplicate using Image J software.

References

1. Mansouri, J.; Harrisson, S.; Chen, V., Strategies for controlling biofouling in membrane filtration systems: challenges and opportunities. *J. Mater.Chem* **2010,** *20* (22), 4567-4586.

2. Awad, T. S.; Asker, D.; Hatton, B. D., Food-Safe Modification of Stainless Steel Food-Processing Surfaces to Reduce Bacterial Biofilms. *ACS Appl. Mater. Interfaces* **2018,** *10* (27), 22902-22912.
3. Colavita, P. E., Scanlan, E. M., Angione, M. D. and Duff, T. Beverage Dispensing Equipment WO2016180729 (A1)
2016.
4. Teo, A. J. T.; Mishra, A.; Park, I.; Kim, Y.-J.; Park, W.-T.; Yoon, Y.-J., Polymeric Biomaterials for Medical Implants and Devices. *ACS Biomater. Sci. Eng.* **2016,** *2* (4), 454-472.
5. Dafforn, K. A.; Lewis, J. A.; Johnston, E. L., Antifouling strategies: History and regulation, ecological impacts and mitigation. *Marine Pollut. Bull.* **2011,** *62* (3), 453-465.
6. Raicopol, M.; Andronescu, C.; Atasiei, R.; Hanganu, A.; Pilan, L., Post-Polymerization Electrochemical Functionalization of a Conducting Polymer: Diazonium Salt Electroreduction at Polypyrrole Electrodes. *J. Electrochem. Soc.* **2014,** *161* (12), G103-G113.
7. Chehimi, M. M., *Aryl Diazonium Salts: New Coupling Agents in Polymer and Surface Science*. Wiley: 2012.
8. Clayden, J.; Greeves, N.; Warren, S., *Organic Chemistry*. OUP Oxford: 2012.
9. Esteban-Tejeda, L.; Duff, T.; Ciapetti, G.; Daniela Angione, M.; Myles, A.; Vasconcelos, J. M.; Scanlan, E. M.; Colavita, P. E., Stable hydrophilic poly(dimethylsiloxane) via glycan surface functionalization. *Polymer* **2016,** *106*, 1-7.
10. Angione, M. D.; Duff, T.; Bell, A. P.; Stamatin, S. N.; Fay, C.; Diamond, D.; Scanlan, E. M.; Colavita, P. E., Enhanced Antifouling Properties of Carbohydrate Coated Poly(ether sulfone) Membranes. *ACS Appl. Mater. Interfaces* **2015,** *7* (31), 17238-17246.
11. Combellas, C.; Kanoufi, F.; Mazouzi, D.; Thiébault, A.; Bertrand, P.; Médard, N., Surface modification of halogenated polymers. 4. Functionalisation of poly(tetrafluoroethylene) surfaces by diazonium salts. *Polymer* **2003,** *44* (1), 19-24.
12. Le, X. T.; Doan, N. D.; Dequivre, T.; Viel, P.; Palacin, S., Covalent Grafting of Chitosan onto Stainless Steel through Aryldiazonium Self-Adhesive Layers. *ACS Appl. Mater. Interfaces* **2014,** *6* (12), 9085-9092.
13. Troian-Gautier, L.; Martínez-Tong, D. E.; Hubert, J.; Reniers, F.; Sferrazza, M.; Mattiuzzi, A.; Lagrost, C.; Jabin, I., Controlled Modification of Polymer Surfaces through Grafting of Calix[4]arene-Tetradiazoate Salts. *The J. Phys. Chem. C* **2016,** *120* (40), 22936-22945.
14. Stojcevski, F.; Randall, J. D.; Henderson, L. C., Using variable interfacial adhesion characteristics within a composite to improve flexural strength and decrease fiber volume. *Comp. Sci. Tech.* **2018,** *165*, 250-258.
15. Small, L. J.; Hibbs, M. R.; Wheeler, D. R., Spontaneous Aryldiazonium Film Formation on 440C Stainless Steel in Nonaqueous Environments. *Langmuir* **2014,** *30* (47), 14212-14218.
16. Adenier, A.; Barré, N.; Cabet-Deliry, E.; Chaussé, A.; Griveau, S.; Mercier, F.; Pinson, J.; Vautrin-Ul, C., Study of the spontaneous formation of organic layers on carbon and metal surfaces from diazonium salts. *Surf. Sci.* **2006,** *600* (21), 4801-4812.

17. Beeskow, T.; Kroner, K. H.; Anspach, F. B., Nylon-Based Affinity Membranes: Impacts of Surface Modification on Protein Adsorption. *J. Colloid Interface Sci.* **1997,** *196* (2), 278-291.
18. Cairns, T. L.; Foster, H. D.; Larchar, A. W.; Schneider, A. K.; Schreiber, R. S., Preparation and Properties of N-Methylol, N-Alkoxymethyl and N-Alkylthiomethyl Polyamides. *J. Am. Chem. Soc.* **1949,** *71* (2), 651-655.
19. Lin, J.; Winkelman, C.; Worley, S. D.; Broughton, R. M.; Williams, J. F., Antimicrobial treatment of nylon. *J. Appl. Polym. Sci.* **2001,** *81* (4), 943-947.
20. Tanane O., A. Y., Aitenneite H., El Bouari A.,, Corrosion inhibition of the 316L stainless steel in sodium hypochlorite media by sodium silicate. *J. Mater. Environ. Sci.* **2016,** *7* (1), 131-138.
21. Pierozynski, B. K., I.,, The Influence of Hypochlorite-Based Disinfectants on the Pitting Corrosion of Welded Joints of 316L Stainless Steel Dairy Reactor. *Int. J. Electrochem. Sci.* **2011,** *6*, 3913-3921.
22. Maurice, V.; Cadot, S.; Marcus, P., Hydroxylation of ultra-thin films of α-Cr2O3(0001) formed on Cr(110). *Surf. Sci.* **2001,** *471* (1), 43-58.
23. Hurley, B. L.; McCreery, R. L., Covalent Bonding of Organic Molecules to Cu and Al Alloy 2024 T3 Surfaces via Diazonium Ion Reduction. *J. Electrochem. Soc.* **2004,** *151* (5), B252-B259.
24. Dechézelles, J.-F.; Griffete, N.; Dietsch, H.; Scheffold, F., A General Method to Label Metal Oxide Particles with Fluorescent Dyes Using Aryldiazonium Salts. *Parti. Part. Syst. Char.* **2013,** *30* (7), 579-583.
25. Zen, F.; Angione, M. D.; Behan, J. A.; Cullen, R. J.; Duff, T.; Vasconcelos, J. M.; Scanlan, E. M.; Colavita, P. E., Modulation of Protein Fouling and Interfacial Properties at Carbon Surfaces via Immobilization of Glycans Using Aryldiazonium Chemistry. *Sci. Rep.* **2016,** *6*, 24840.
26. Socrates, G., *Infrared and Raman Characteristic Group Frequencies: Tables and Charts*. Wiley: 2004.
27. Mesnage, A.; Lefèvre, X.; Jégou, P.; Deniau, G.; Palacin, S., Spontaneous Grafting of Diazonium Salts: Chemical Mechanism on Metallic Surfaces. *Langmuir* **2012,** *28* (32), 11767-11778.
28. Hryniewicz, T.; Rokosz, K.; Rokicki, R., Electrochemical and XPS studies of AISI 316L stainless steel after electropolishing in a magnetic field. *Corrosion Science* **2008,** *50* (9), 2676-2681.
29. Williams, D. F.; Kellar, E. J. C.; Jesson, D. A.; Watts, J. F., Surface analysis of 316 stainless steel treated with cold atmospheric plasma. *Appl. Surf. Sci.* **2017,** *403*, 240-247.
30. Mandrino, D.; Godec, M.; Torkar, M.; Jenko, M., Study of oxide protective layers on stainless steel by AES, EDS and XPS. *Surf. Interface Anal.***2008,** *40* (3-4), 285-289.
31. Saulou, C.; Despax, B.; Raynaud, P.; Zanna, S.; Marcus, P.; Mercier-Bonin, M., Plasma-Mediated Modification of Austenitic Stainless Steel: Application to the Prevention of Yeast Adhesion. *Plasma Process. Polym.* **2009,** *6* (12), 813-824.
32. Dilks, A.; Kay, E., Plasma polymerization of ethylene and the series of fluoroethylenes: plasma effluent mass spectrometry and ESCA studies. *Macromolecules* **1981,** *14* (3), 855-862.
33. Ferraria, A. M.; Lopes da Silva, J. D.; Botelho do Rego, A. M., XPS studies of directly fluorinated HDPE: problems and solutions. *Polymer* **2003,** *44* (23), 7241-7249.

34. Golub, M. A.; Wydeven, T.; Johnson, A. L., Similarity of Plasma-Polymerized Tetrafluoroethylene and Fluoropolymer Films Deposited by rf Sputtering of Poly(tetrafluoroethylene). *Langmuir* **1998,** *14* (8), 2217-2220.
35. Gu, X.; Nemoto, T.; Teramoto, A.; Ito, T.; Ohmi, T., Effect of Additives in Organic Acid Solutions for Post-CMP Cleaning on Polymer Low-k Fluorocarbon. *J. Electrochem. Soc.* **2009,** *156* (6), H409-H415.
36. Powell, C. J.; Jablonski, A., NIST Electron Inelastic-Mean-Free-Path Database, Version 1.2. In *NIST Standard Reference Database*, National Institute of Standards and Technology: Gaithersburgh, MD, 2010; Vol. 71.
37. Nichols, B. M.; Butler, J. E.; Russell, J. N.; Hamers, R. J., Photochemical Functionalization of Hydrogen-Terminated Diamond Surfaces: A Structural and Mechanistic Study. *J. Phys. Chem. B* **2005,** *109* (44), 20938-20947.
38. Jayasundara, D. R.; Duff, T.; Angione, M. D.; Bourke, J.; Murphy, D. M.; Scanlan, E. M.; Colavita, P. E., Carbohydrate Coatings via Aryldiazonium Chemistry for Surface Biomimicry. *Chem. Mater.* **2013,** *25* (20), 4122-4128.
39. Hinz, H. J.; Kuttenreich, H.; Meyer, R.; Renner, M.; Fruend, R.; Koynova, R.; Boyanov, A.; Tenchov, B., Stereochemistry and size of sugar head groups determine structure and phase behavior of glycolipid membranes: densitometric, calorimetric, and x-ray studies. *Biochemistry* **1991,** *30* (21), 5125-5138.
40. Maupin, K. A.; Liden, D.; Haab, B. B., The fine specificity of mannose-binding and galactose-binding lectins revealed using outlier motif analysis of glycan array data. *Glycobiology* **2012,** *22* (1), 160-169.
41. Hassel, M.; Hemmerich, I.; Kuhlenbeck, H.; Freund, H.-J., High Resolution XPS Study of a Thin Cr_2O_3(111) Film Grown on Cr(110). *Surf. Sci. Spectra* **1996,** *4* (3), 246-252.

Chapter V

Investigation of Coating Bio-film Rejection Ability in Highly Fouling Marine Environment

Surface treatments that minimise biofouling in marine environments are of interest for environmental monitoring and aquaculture. We report on the effect of saccharide coatings on biomass accumulation at the surface of materials that find applications in marine settings: stainless steel 316 (SS316), nylon-6 (N-6). In addition we included a material readily used in filtration systems for aquatic media poly(ether sulfone) (PES) in order to test its fouling rejection ability under heavy fouling conditions. The performance of all three materials after modification with aryldiazonium saccharide films was tested in the field via immersion of modified coupons in coastal waters over a 20 day time period. Results from combined infrared spectroscopy, light microscopy, scanning electron and He-ion microscopy, in addition to adenosine-triphosphate content assays reveal significantly lower retained biomass on carbohydrate modified samples with respect to unmodified controls.

The data Presented in this chapter is reproduced in part from the following publication:

Bioinspired Aryldiazonium Carbohydrate Coatings: Reduced Adhesion of Foulants at Polymer and Stainless Steel Surfaces in a Marine Environment
Adam Myles, Damien Haberlin, Leticia Esteban-Tejeda, M. Daniela Angione, Michelle P. Browne, Md. Khairul Hoque, Thomas K. Doyle, Eoin M. Scanlan , and Paula E. Colavita
ACS *Sustainable Chem*. Eng., **2018**, 6 (1), pp 1141–1151

Contributions are as follows:
MP Browne assisted with high magnification microscopy on fouled coupon samples, D Haberlin & TK Doyle assisted in field study setup and sampling in addition to biological species identification.

1 Introduction

Materials which are submerged in a marine environment are generally susceptible to rapid biofouling. Submergible structures are particularly susceptible to a wide range of opportunistic fouling organisms.[1-2] Biofouling and colonisation has a negative impact in a wide range of marine specific fields, from marine transport to environmental monitoring and aquaculture.[3-6] The result of this phenomenon has widespread economic and environmental ramifications, from corrosion and loss of functionality in marine structures and vessels,[7-8] to the spread of invasive species[9] and increased farmed fish mortality.[10-12] There are excessive costs associated with performance loss, cleaning and loss of viable stock, and therefore, great interest can be found for the development of new strategies for preventing and or mitigating biofouling in the marine environment. Particularly of interest are non-toxic strategies that are environmentally sustainable, commercially scalable and which comply with the modern regulatory landscape.[1, 3-4, 13]

1.1 Marine Biofilm Control Strategies

Biofilm mitigation historically involved the use of toxic coatings such as lead-based and organotin paints,[14] which interfere at the micro- and macro-fouling stages by cytotoxic activity. However, due to adverse effects on marine ecosystems (aquatic organisms mortality and infertility)[15] these methods have been phased-out and even use of alternative paints and coatings based on copper release is under regulatory scrutiny. The most promising eco-friendly, non-biocidal strategies for anti-fouling materials rely on modifying the physico-chemical properties of submerged materials to minimise adsorption and adhesion mainly at early fouling stages. It can be noted that the disruption of quorum sensing signals to inhibit/regulate biofilm formation potentially offers a more targeted approach than metal-based biocides; however, this technology is in its infancy and its environmental impact on ecosystems remains to be assessed.[16]

Regulation of surface roughness, electrostatic charge distribution and wetting behaviour have all been investigated as non-biocidal methods.[13, 17] Bioinspired engineered nanotopographies are effective for regulating cell/spore settling; however, complex hierarchical patterns are required to repel settling from

heterogeneous populations,[18] thus posing significant problems for cost-effective scalability. Regulation of wetting and spatial control of hydrophobicity at the nanoscale level have also been explored as antifouling mechanisms. Low surface free energy and hydrophobic materials and coatings have a long history in antifouling technologies and some well-known examples are polysiloxanes, fluoropolymers and superhydrophobic coatings.[1, 6, 13, 19-20] At the other end of the spectrum, hydrophilic coatings, such as those based on polyethylene glycols (PEG)[21] and bioinspired superhydrophilic zwitterionic polymers,[22-23] have similarly demonstrated good performance in laboratory tests.

1.2 Carbohydrates in Marine Biofouling Control

Surface-immobilized carbohydrates have previously been investigated for the fabrication of hydrophilic coatings for biofouling prevention.[24-26] Carbohydrates represent an interesting family of biomolecules for the marine framework as they are environmentally benign and because they are highly stable towards oxidation compared to other chemical species such as ethyleneglycols.[19, 21, 27] Prior studies have shown that monosaccharides and di-saccharides self-assembled monolayers (SAMs) have potential to greatly reduce protein fouling on gold surfaces.[28-31] More recently, Ederth et al.[29] demonstrated that galactose-bearing SAMs were successful at reducing *Ulva linza* spore settling, thus showing promise for marine fouling control. Polysaccharides have also been investigated, however the efficient calcium binding affinity displayed by many of these, e.g. hyaluronic and pectinic acids, has been identified as detrimental for fouling control in the marine environment.[32-33] Nonetheless, relative to other functional coatings, carbohydrates are underexplored in marine applications and results from field tests are rare in the literature.

In this chapter the performance of carbohydrates immobilized via aryldiazonium grafting are studied as fouling resistant coatings in a heavy fouling environment, on coupons of three different materials of interest in aquatic infrastructure: marine grade stainless steel 316 (SS316), nylon-6 (N-6) and poly(ethersulphone) (PES). Polyamide materials and metal alloys are used regularly in the marine environment and are particularly susceptible to marine fouling, while PES is a common membrane material used in aquatic sensors. Lactosides were chosen for immobilisation via spontaneous aryldiazonium grafting, because of their lack

of calcium-binding carboxylic acid residues,[32] and on the basis of previously published comparative tests on the performance of simple glycosides.[24-25, 28] Reported herein are the results of immersion tests in a coastal environment for 20 days over a period of heavily fouling, i.e. the summer period, hydroid spawning season. Results from these field tests indicate that carbohydrate coatings show promise as a sustainable and environmentally benign approach for reducing adhesion and retention of marine foulants.

2 Results and Discussion

2.1 Field Study Set-up

Material coupons of 100 x 100 mm^2 size consisting of marine grade Stainless Steel 316 (SS316), Nylon-6 (N-6) and Poly(ether sulfone) PES, were functionalised using diazonium lactoside coating, as characterised in **chapter III** (**scheme 3.1**). This was achieved by bulk preparation of coating solution (3 L) into which coupons of pre-treated SS316 and N-6 along with methanol rinsed PES were simultaneously immersed for 1 hour. Functionalisation of coupons was confirmed by ex-situ characterisation for each material.

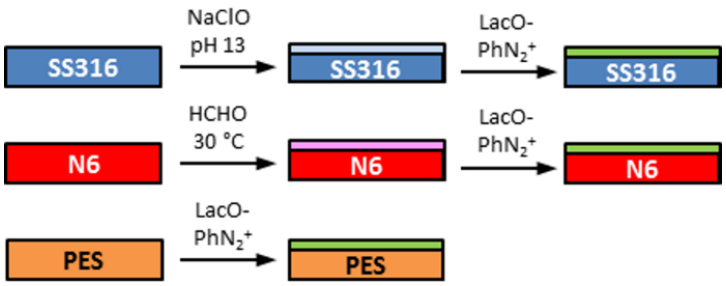

Scheme 5.1. Protocol used for the modification of SS316, N6 and PES. Reproduced with permission from *ACS Sustainable Chem. Eng.*, **2018**, *6* (1), pp 1141–1151. Copyright 2017 American Chemical Society.

Immersion studies were carried out in Bertraghboy Bay, County Galway, at the site of a disused salmon farming platform (Lehanagh pool). Samples were functionalised 24 h prior to immersion on 24th August 2016. They were transported under wet storage to the testing site located 150 m from shore (53.402267°N, 9.820329°W),). Polyethylene frames on which N6, SS316 and PES coupons had been mounted on site and were set up as shown in **Figure 5.1 a**. Frames were transported by power boat to the testing site and suspended

from the edge of the test structure (**Figure 5.1 b**) at a depth of approximately 1 m, considered to be optimal for rapid biofouling.[34]

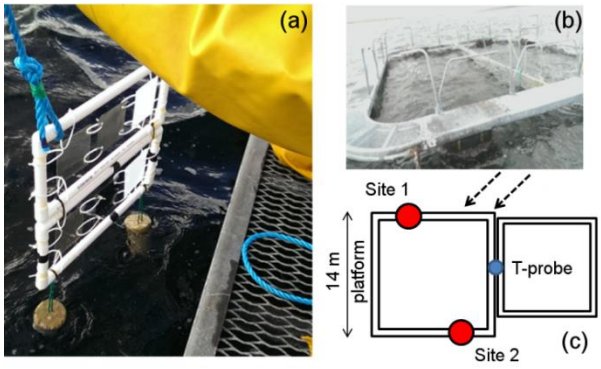

Figure 5.1. (a.) Assembled frame with coupons, arranged from left to right, PES, SS316 and N6, immediately prior to immersion in sea water. **(b.)** Salmon farm platform from which frames with coupons were suspended. **(c.)** Scheme showing two adjacent platforms and the location of frames at Site 1 and Site 2 relative to the tide (dashed arrows); a temperature probe measured surface water temperature at the position indicated in blue. Reproduced with permission from *ACS Sustainable Chem. Eng.*, **2018**, *6* (1), pp 1141–1151 Copyright 2017 American Chemical Society.

The frames were weighted to ensure that all samples would remain in a vertical position throughout the duration of the trial. The trial ran for 20 days over the summer months (Aug 24 – Sept 13). This timeframe was chosen as it was expected to be sufficient time to observe macroscopic biofouling should any occur. The mean water temperature during the 20 day trial was 16.84 ± 0.31 °C (maximum 18.20 °C, minimum 16.23 °C), measured from readings at 1 m depth (StowAway TidbiT). Two positions were chosen for suspending the frames: these are denoted as site 1 and site 2 and are mapped to the platform configuration in **Figure 5.1 c**. Three samples of each control and functionalized coupon were mounted at each site, i.e. a total of 12 coupons, 4 of each material distributed over the two sites. Following the 20 day test, all samples were withdrawn from the water, carefully removed from the frames and transported to the laboratory immersed in freshly sampled seawater. Sections of each coupons were cut prior to rinsing for analysis by microscopy and for ATP determination. Samples were then rinsed under a stream of deionized water delivered by gravity 10 cm above the surface for 30 s on each side. This procedure was used across all samples to remove loosely attached biomass. Samples were then analysed immediately or stored frozen for further characterisation.

2.2 Microscopy of Immersed Coupons

Coupon samples obtained post 20 day immersion displayed minimal differences in fouling among different coupon materials, and between lactose-modified samples and unmodified controls of the same material upon visual inspection (**Figure 5.2**).

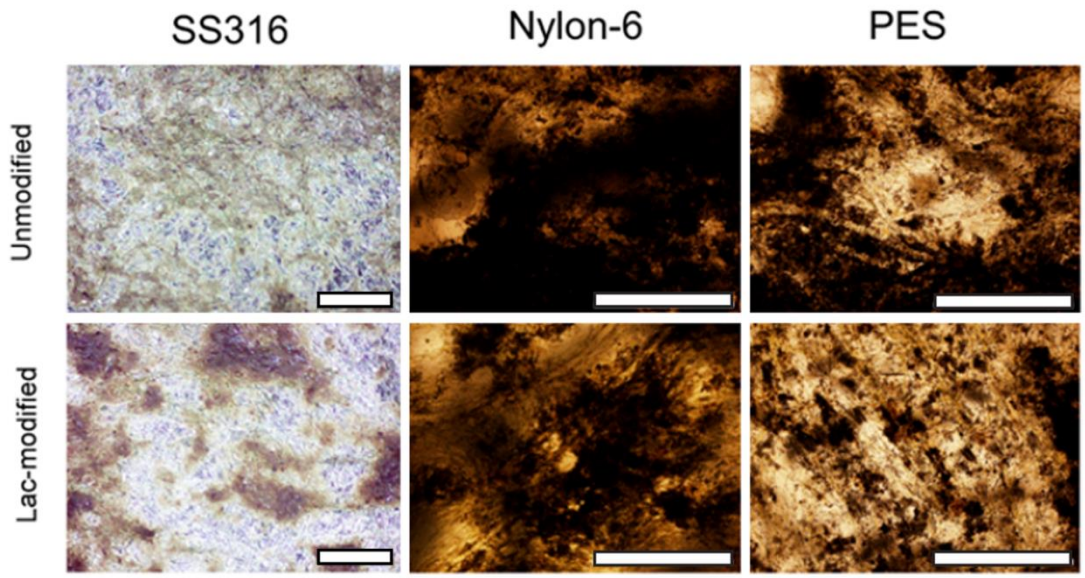

Figure 5.2. Optical microscope images of SS316, nylon-6 and PES coupons extracted after 20 day immersion in coastal waters prior to rinsing; scalebar = 1 mm. Reproduced with permission from *ACS Sustainable Chem. Eng.*, 2018, *6* (1), pp 1141–1151. Copyright 2017 American Chemical Society.

This is likely due to loosely adhered silt and sedimentary materials attached physically to sample surfaces masking underlying surface differences of adhered layers. After controlled light rinsing by ultrapure water under gravity for 10 s each side it was possible to observe clear and significant differences between coated and uncoated samples. **Figure 5.3** shows optical microscopy images representative of SS316, nylon-6 and PES coupons positioned at site 1, together with images of a corresponding pristine surface that had not undergone immersion for comparison. Samples that had been coated with the aryldiazonium layer of lactoside units were found to display a visibly lower density of fouling organisms when compared to unmodified samples. Images of coupons at site 2 reveal a similar trend. Unmodified samples in **Figure 5.3** (top row) show evidence of secondary adhesive structures (algae pads or stalks),[35] which are mostly absent in Lac-modified samples (middle row). These structural features are of importance in the development of microbial slimes.[34]

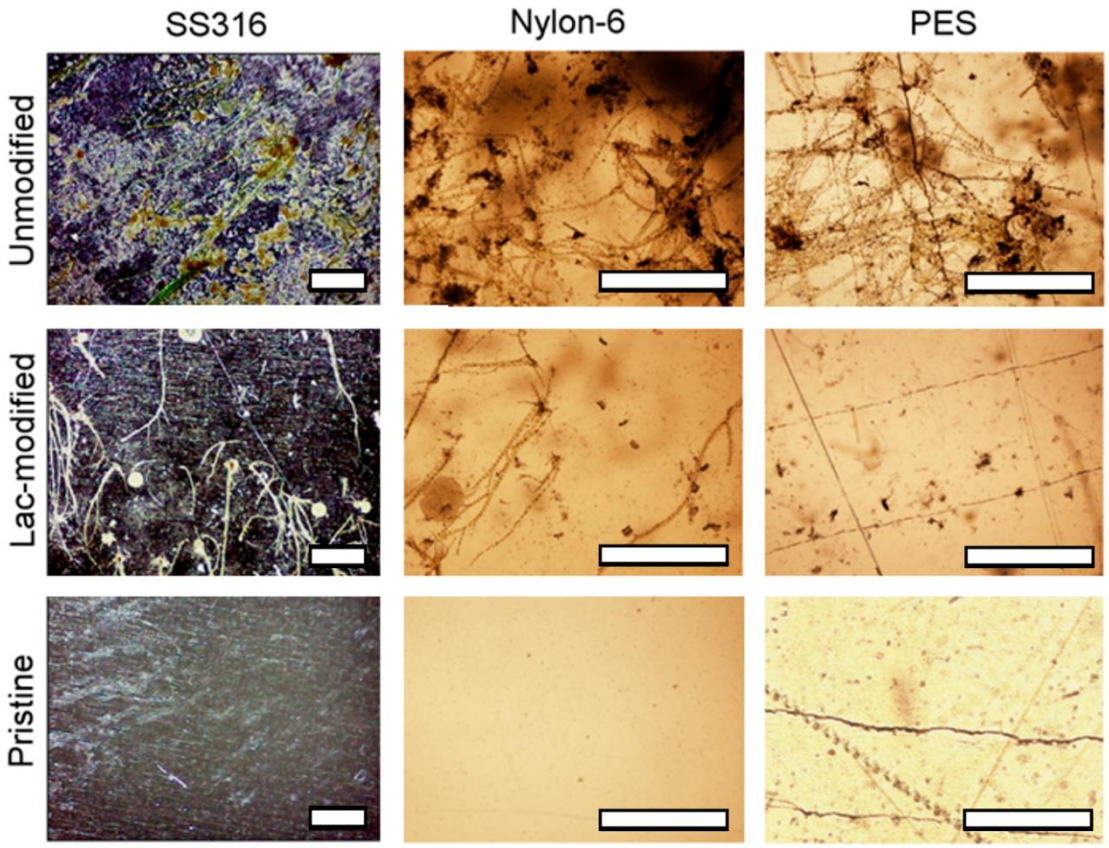

Figure 5.3. Optical microscope images of coupons of SS316, Nylon- and PES (scalebar = 1 mm) extracted after 20 day immersion in coastal waters at site 1 (see Figure 5.1.); samples were rinsed under the identical conditions prior to imaging. The top row shows images of coupons that had not been coated with an aryldiazonium layer of glycosides; the middle row shows coupons that had been coated with a layer of lactosides prior to immersion; the bottom row shows samples as supplied by the vendor, without undergoing any immersion tests. All immersed samples display biomass accumulation however the density of adhered organic matter appears to be higher on unmodified when compared to lactoside-modified samples. Reproduced with permission from *ACS Sustainable Chem. Eng.*, **2018**, *6* (1), pp 1141–1151. Copyright 2017 American Chemical Society.

Higher magnification images obtained by SEM and HIM microscopies on SS316 and polymer coupons, respectively, can be observed in **Figure 5.4**. Interestingly the trend observed for low magnification images of lactose modified surfaces retaining sparser biomass compared to unmodified samples, is retained in the high magnification scanning microscopy images.

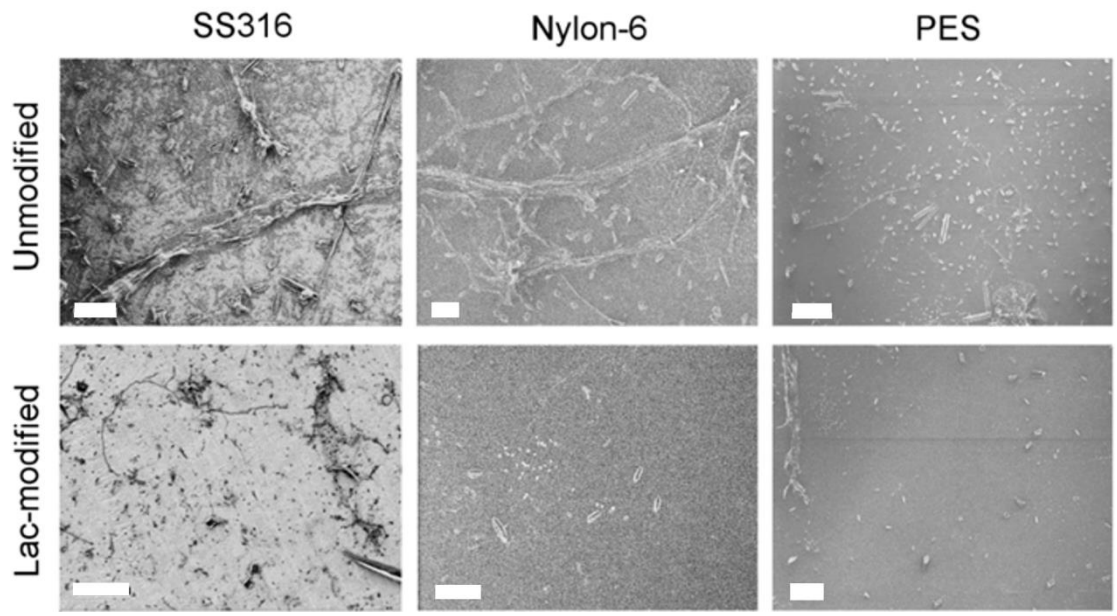

Figure 5.4. Microscopy images of coupons of SS316 (SEM, scalebar = 40 μm), Nylon-6 (HIM, scalebar = 40 μm) and PES (HIM, scalebar = 100 μm). The figures show details of surfaces after 20 day immersion in coastal waters followed by rinsing under identical conditions prior to imaging. The top row shows images of coupons that had not been coated with an aryldiazonium layer of glycosides; the bottom row shows coupons that had been coated with a layer of lactosides prior to immersion. Reproduced with permission from *ACS Sustainable Chem. Eng.*, **2018**, *6* (1), pp 1141–1151. Copyright 2017 American Chemical Society.

It is possible to observe the presence of diatoms and mucilaginous trails; visual inspection suggests that pennate diatoms dominate the retained deposits, in agreement with typical findings in marine fouling experiments.[35] The apparent decrease in diatom populations is encouraging as they are considered important fouling species in the succession of biofilm formation in shallow waters.[34]

3 Adhered Biomass Quantitative Studies

3.1 ATP determination

Total ATP is an indicator of microbial biomass content and can be used to assess biomass accumulation at surfaces.[36] Samples of pre-determined size were cut from coupons and immersed into identical volumes of deionized water, which were sonicated to extract adsorbed biomass into solution. A commercial bioluminescence assay was used in order to compare the ATP content extracted from control and lactose-modified samples. All RLU values were determined in deionized water and dilution factors were chosen which ensured that measurements fell within the linear dynamic range of the assay,[37] as calibrated

against standard samples of ATP in deionised water. This procedure allowed for a conversion of RLU values to ATP concentrations in the extract and subsequent conversion to ATP mass released per unit area. **Figure 5.5.a** shows a summary of ATP determinations obtained for SS316, nylon-6 and PES surfaces after immersion tests and prior to any rinsing. A comparison of ATP values indicates that biofilm accumulation was unaffected by the nature of the substrate material, with similar values obtained for SS316, N6 and PES coupons (P = 0.18). ATP values were found to be similar for control and modified coupons; in the case of SS316, results suggest a beneficial effect from the coating (P = 0.08) at a slightly higher significance level that might be clarified by further studies with a larger sample size. **Figure 5.5 b** shows a comparison of ATP values obtained at the three surfaces after controlled rinsing.

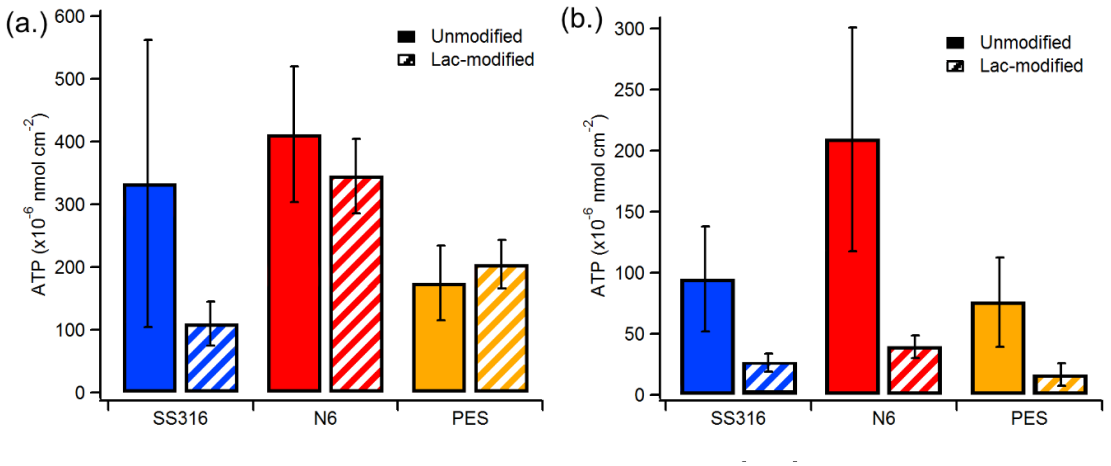

Figure 5.5. Average ATP released per unit area from unmodified (solid) and lactose-modified (striped) SS316, nylon-6 and PES coupons after 20 day immersion tests in coastal waters **(a.)** prior to any rinsing and **(b.)** after controlled rinsing. Error bars indicate 90% C.I. Reproduced with permission from *ACS Sustainable Chem. Eng.*, **2018**, *6* (1), pp 1141–1151. Copyright 2017 American Chemical Society.

The level of ATP measured at unmodified (control) surfaces was found to vary depending on the material, with results indicating that nylon-6 retains the highest levels of biomass. A comparison between control and lactose-modified samples clearly shows that surfaces coated by carbohydrate layers have significantly lower amounts of retained biomass; this was confirmed in the case of SS316 (P = 0.04), N6 (P = 0.03) and PES (P = 0.04). The controlled rinsing process resulted in a reduction of ATP for all samples, however, the effect is noticeably greater in the case of lactose-modified surfaces yielding reductions of 75%, 89% and 92% for SS316, nylon-6 and PES, respectively. These results indicate that

the lactoside layer has a strong impact on the ability of foulants to adhere to the material surface, thus improving resistance to biomass retention; this effect is particularly evident in the case of the two polymers tested.

3.2 IRRAS on Immersed SS316

IRRAS analysis was carried out to compare biomass accumulation at control and modified SS316. This is not possible in the case of N-6 and PES due to the poor reflectance of these substrates. **Figure 5.6** shows representative IRRAS spectra in the amide region of both a control and a lactose-modified SS316 sample after rinsing. The spectra show peaks at 1640 cm^{-1} and 1530 cm^{-1} assigned respectively to the amide I and amide II modes of polypeptides.[38]

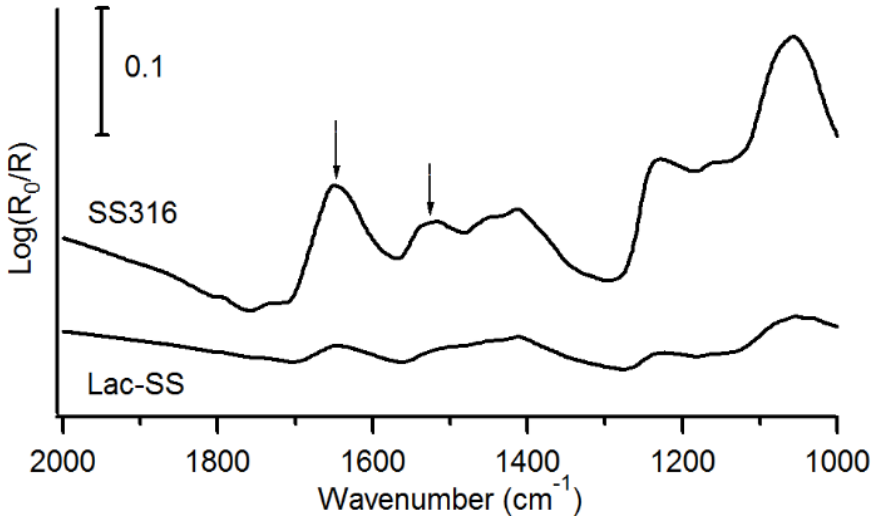

Figure 5.6. IRRAS spectra of SS316 unmodified sample and lactose-modified SS316 after 20 day immersion tests; this specific sample was located at site 2 however in all cases unmodified samples show more intense absorption peaks. Arrows indicate peaks at 1645 cm^{-1} and 1525 cm^{-1} corresponding to amide I and amide II modes, respectively. Reproduced with permission from *ACS Sustainable Chem. Eng.*, **2018**, *6* (1), pp 1141–1151. Copyright 2017 American Chemical Society.

These peaks display higher intensity for unmodified SS316, thus indicating a significantly higher surface density of proteinaceous material accumulated on control surfaces when compared to lactose-modified samples. These results are consistent across both sites and regardless of sample orientation.

3.3 Visible Light Transmittance Measurements

PES coupons used in our studies were optically transparent, therefore, a quantitative assessment of biomass accumulation could also be obtained through measurements of optical depth ($-ln(T)$). **Figure 5.7** shows a comparison of the optical depth at wavelength 600 nm, measured through PES coupons using a pristine PES sample as background.

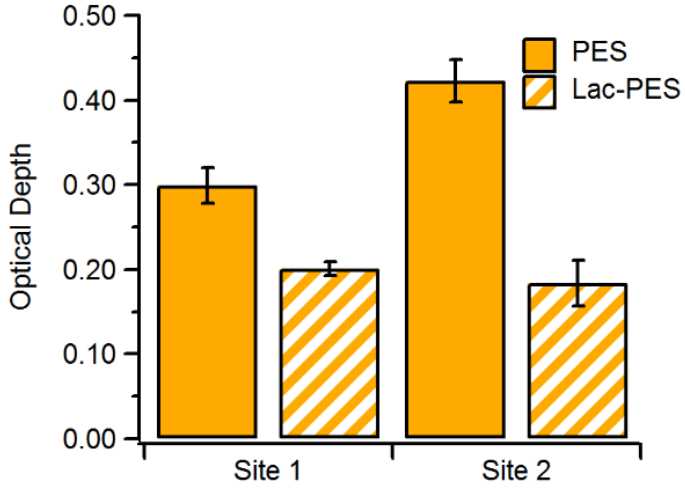

Figure 5.7. Optical depth ($-ln(T)$) of PES coupons at wavelength 600 nm measured after 20 day immersion test followed by controlled rinsing. Lac-modified samples are more transparent than unmodifieid ones. Reproduced with permission from *ACS Sustainable Chem. Eng.*, **2018**, *6* (1), pp 1141–1151. Copyright 2017 American Chemical Society.

Lactose-modified samples were more transparent than unmodified ones, and independently of the site tested, displayed significantly lower depth than that of the corresponding control sample. These results are in agreement with ATP determinations and with microscopy observations.

3.4 Further Discussion

Carbohydrate layers prepared *via* aryldiazonium chemistry are molecular coatings in the 1-2 nm thickness range that preserve the topography of the original substrate,[24, 26] so that their main effect is expected to be on surface chemistry and free energy. Results show that in the absence of rinsing these coatings do not significantly impact on fouling resistance and little difference is observed with controls as loosely bound organic matter is not repelled by our coating. Coupons extracted after the 20 day immersion were significantly fouled by a mixture of organisms and the presence of the coating did not affect marine

biofilm formation. However, the accumulated biomass was dramatically reduced at carbohydrate-modified surfaces after only light rinsing by gravity driven streams. SEM and HIM imaging of samples showed that rinsing leaves a relatively clean surface, indicating effective detachment of the biofilm under very mild treatment. Therefore, these carbohydrate coatings were found to be effective at reducing adhesion of foulants on all three materials tested. Similar findings are reported from field tests carried out by Hibbs et al.[39] with coatings based on zwitterionic polymers. Zwitterionic coatings were found to affect foulant retention after jet rinsing, rather than to lower the amount of biomass accumulated on the coupons over the testing period. The striking agreement with our trends suggests analogies in the mode of action of carbohydrate thin films: these are thought to control fouling by regulating surface hydration, which is a similar mechanism to that proposed for zwitterionic polymers,[1] albeit in the absence of a change in surface electrostatic charge. It has been proposed that the exact distribution of charged regions in zwitterionic coatings might play a role in modulating settlement behaviour;[39] it would be therefore relevant to carry out similar experiments to those by Aldred et al.[23] on settlement behaviour to investigate whether glycoside structure and presentation could be similarly leveraged in carbohydrate coatings. Given the marked differences in physico-chemical properties among SS316 and the two polymers it is encouraging to observe similar trends independent of material, as it suggests potential applicability on a variety of devices, including devices consisting of mixed materials.

4 Conclusions

Functionalisation and field test results suggest that carbohydrate aryldiazonium layers could find applications as fouling resistant coatings. For all materials tested, the density of retained biomass at surfaces was found to be significantly lower on carbohydrate modified samples with respect to unmodified controls. The mode of action of these layers appears to affect biofilm adhesion rather than biofilm formation, operating *via* fouling release rather than *via* antifouling mechanisms. It is recognized that fouling minimisation in natural seawaters is extremely challenging due to the presence of multiple organism populations with

a wide range of adhesion mechanisms. ATP tests suggest that fouling resistance observed for lactoside-aryldiazonium layers is comparable to that observed for more chemically complex coating systems in laboratory assays, which use populations containing a single organism. It is therefore significant that the promising results herein reported were obtained in coastal waters, over prolonged times of exposure and during the summer months, when fouling activity is maximized.

5 Experimental

5.1 Chemicals and Materials

Polyamide- Nylon 6 (N6) sheets, marine grade stainless steel 316 foil (SS316), and Polyethersulfone sheets (PES) were purchased from Goodfellow; formaldehyde solution for molecular biology ≥36.0% in H_2O, hypophosphorous acid solution 50%wt. in H_2O, sodium hypochlorite (bleach), sodium hydroxide, potassium hydroxide, phosphate buffered saline buffer (0.010 M PBS, pH 7.4), sodium nitrite, hydrochloric acid and fluoroboric acid were purchased from Sigma Aldrich. Aquasnap ATP Total Water testing strips were purchased from Water Technology Ltd. 4-aminophenol-β-D-lactopyranose compound x was synthesized as previously described.

5.2 Functionalisation protocol

Pre-treatment and functionalisation solutions were prepared using the same conditions described for laboratory scale experiments in chapter V with the exception of an increase in functionalisation solution to 3 L batches for material modification in field studies in contrast to laboratory experiments which required the preparation of 25 mL solutions. All coupons were cut to uniform size 10 cm x 10 cm where necessary. A 5 mm diameter hole was drilled into each corner for frame mounting and all coupons were cleaned thoroughly by rinsing with semiconductor grade methanol and ultrapure water. Coupons of the same material type were attached together by means of a simple rigging system made by running cable ties through pre-cut holes of diameter approximately 5 mm in the corners of each coupon. The head of the cable tie was used as a spacer ensuring adequate solution contact for pre-treatment and functionalisation. Samples were lowered vertically into the solution and agitated to ensure no

trapped air bubbles were retained on the surface. Following pre-treatment, control samples were removed and all samples for functionalisation were attached together by the same method outlined above. These samples were then immersed in the 3 L freshly prepared functionalisation solution and incubated at room temperature in the dark for 1 hour. Following this they were rinsed thoroughly, separated from their bundles and stored under ultrapure water for transport to the test sight the following day. Functionalisation was confirmed for these materials on an additional coupon of each material from this modification batch.

5.3 Frame design and coupon cutting

Custom sample frames of length 40 mm x 15 mm consisting of polyvinylchloride plumbing pipe (20 mm diameter) and 90° elbow joints connected with water resistant rubber cement (EvoStick) were designed and built to house three coupons each as shown in **Figure 5.8 a** Cable ties were used to fasten coupons to the frame and they we pulled taught. The depth of submersion was controlled by the length of rope used to tie the frames to the floating platform. Two 5 Kg weights were attached to the bottom of each frame to ensure the samples remained submerged and in an upright position for the duration of the trial. For this trial samples were mounted over 4 frames with each frame containing three coupons, one of each material. Lactose coated samples were suspended in frames directly above their respective unmodified counterpart in site 1 and directly below for site 2 to ensure the only variable for each sample site, the difference in depth of approx.. 10 cm, was reversed across both sites; This difference is considered to be negligible as each sample is exposed to the same potential fouling species in the same environmental range (the epipelagic zone, 0 m – 200 m).

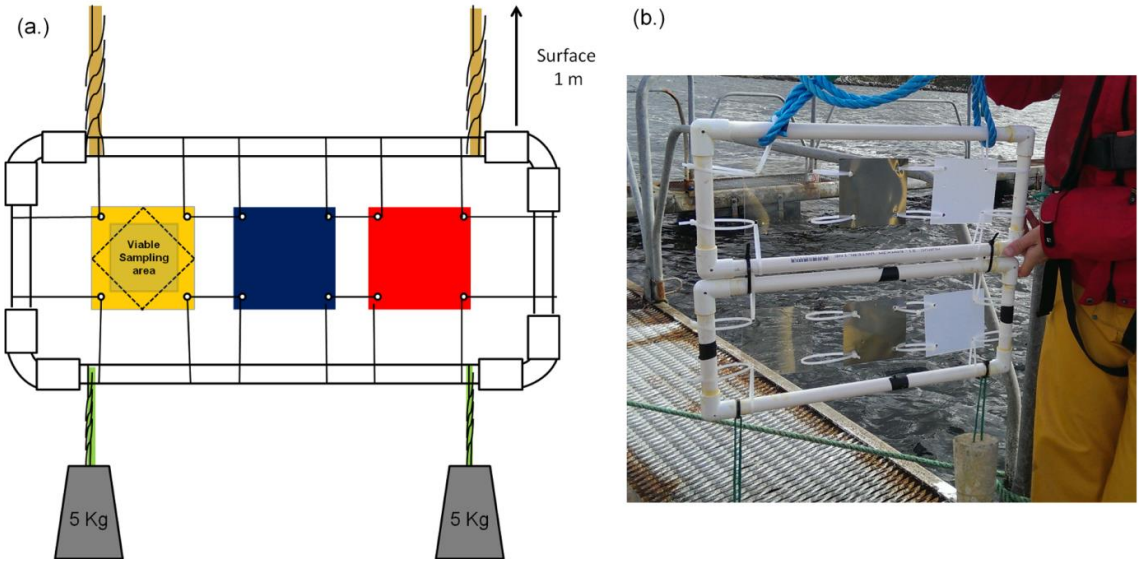

Figure 5.8. (a.) Plans for frames setup with three coupon materials attached to frame and spaced to allow free flow of water around the coupons. Shown is the intended sampling zone for the coupons. Dashed lines indicate where the samples are to be cut to remove any opportunistic fouling at the coupon sides to ensure measurement of 2D foulant accumulation on the faces only. **(b.)** Photograph of final frame setup with paired frames mounted vertically containing unmodified or lactose coated samples. Cable ties were used to secure samples to frames.

The cable ties were found to be a source of anchorage for macro fouling species and as such the coupons were cut indicated in **Figure 5.8 a** shown to remove any opportunistic fouling species with all results obtained coming from samples cut out of the viable sampling zone indicated above. Samples were cut down the middle following the removal of these cuttings to with one half sampled as collected and the other subjected to a light rinsing protocol, water under gravity for 30 s.

5.4 Quantitative measurements

Adenosine triphosphate (ATP) concentrations per square cm of substrate material were determined using the luciferase assay as implemented in a commercial kit (Aquasnap Total Water).[40] The assay was first calibrated using standard solutions and the luminometer (Hygiena) to obtain a conversion from relative luminescence units (RLU) to ATP concentration (in nM range). Samples of approximately 1 cm^2 were cut from each coupon in triplicate; the cutting was suspended in a known volume of deionized water (10 mL or 5 mL, depending on level of fouling) in sterile centrifuge tubes and then sonicated for 10 min. The value of RLU was determined for each water sample and converted to ATP

concentrations; water samples were diluted if needed to bring the ATP concentration within the linear range of the assay. Post sonication, the cuttings were dried under argon and their mass determined; the relative exposed area was estimated from the mass of the cleaned sample cutting and this value was used to surface-normalise ATP determinations on individual cutting. Values were compared using ANOVA at 5% significance level ($\alpha = 0.05$). Infrared reflectance absorption spectroscopy (IRRAS) characterisation was carried out on a Bruker Tensor 27 infrared spectrometer equipped with a mercury cadmium telluride detector and a VeeMax II specular reflectance accessory with a wire grid polariser. All spectra were collected using p-polarized light; 100 scans at 4 cm^{-1} were collected for all samples and an unmodified sample was used as substrate. Optical depths were calculated from UV-Vis transmittance measurements (Lambda 35 Perkin Elmer).

References

1. Callow, J. A.; Callow, M. E., Trends in the development of environmentally friendly fouling-resistant marine coatings. *Nature Comm.* **2011,** *2*, 244.
2. Fitridge, I.; Dempster, T.; Guenther, J.; de Nys, R., The impact and control of biofouling in marine aquaculture: a review. *Biofouling* **2012,** *28* (7), 649-669.
3. Cao, S.; Wang, J.; Chen, H.; Chen, D., Progress of marine biofouling and antifouling technologies. *Chinese Science Bulletin* **2011,** *56* (7), 598-612.
4. Chambers, L. D.; Stokes, K. R.; Walsh, F. C.; Wood, R. J. K., Modern approaches to marine antifouling coatings. *Surf. Coat. Tech.* **2006,** *201* (6), 3642-3652.
5. Yebra, D. M.; Kiil, S.; Dam-Johansen, K., Antifouling technology—past, present and future steps towards efficient and environmentally friendly antifouling coatings. *Prog. Org. Coat.* **2004,** *50* (2), 75-104.
6. Whelan, A.; Regan, F., Antifouling strategies for marine and riverine sensors. *J. Environ. Monitor.* **2006,** *8* (9), 880-886.
7. Videla, H. A.; Characklis, W. G., Biofouling and microbially influenced corrosion. *Int. Biodeterior. Biodegradation* **1992,** *29* (3), 195-212.
8. Schultz, M. P.; Bendick, J. A.; Holm, E. R.; Hertel, W. M., Economic impact of biofouling on a naval surface ship. *Biofouling* **2011,** *27* (1), 87-98.
9. Minchin, D.; Gollasch, S., Fouling and Ships' Hulls: How Changing Circumstances and Spawning Events may Result in the Spread of Exotic Species. *Biofouling* **2003,** *19* (sup1), 111-122.
10. Ruane, N. M.; Rodger, H.; Mitchell, S.; Doyle, T.; Baxter, E.; Fringuelli, E. *GILPAT: An Investigation into Gill Pathologies in Marine Reared Finfish*; Marine Institute: **2013**.
11. Carl, C.; Guenther, J.; Sunde, L. M., Larval release and attachment modes of the hydroid Ectopleura larynx on aquaculture nets in Norway. *Aquacult. Res.* **2011,** *42* (7), 1056-1060.

12. Baxter, E. J.; Sturt, M. M.; Ruane, N. M.; Doyle, T. K.; McAllen, R.; Rodger, H. D., Biofouling of the hydroid Ectopleura larynx on aquaculture nets in Ireland: Implications for finfish health. *Fish Veterinary Journal* **2012,** *13*, 17-29.
13. Magin, C. M.; Cooper, S. P.; Brennan, A. B., Non-toxic antifouling strategies. *Mater. Today* **2010,** *13* (4), 36-44.
14. Senda, T.; Miyata, O.; Kihara, T.; Yamada, Y., Inspection Method for the Identification of TBT-containing Antifouling Paints. *Biofouling* **2003,** *19* (sup1), 231-237.
15. Brüschweiler, B. J.; Würgler, F. E.; Fent, K., Cytotoxicity in vitro of organotin compounds to fish hepatoma cells PLHC-1 (Poeciliopsis lucida). *Aquat. Toxicol.* **1995,** *32* (2), 143-160.
16. Dobretsov, S.; Teplitski, M.; Paul, V., Mini-review: quorum sensing in the marine environment and its relationship to biofouling. *Biofouling* **2009,** *25* (5), 413-427.
17. Bixler, G. D.; Bhushan, B., Biofouling: lessons from nature. Philosophical Transactions of the Royal Society of London, Series A: Physical Sciences and Engineering **2012,** 370 (1967), 2381.
18. Schumacher, J. F.; Aldred, N.; Callow, M. E.; Finlay, J. A.; Callow, J. A.; Clare, A. S.; Brennan, A. B., Species-specific engineered antifouling topographies: correlations between the settlement of algal zoospores and barnacle cyprids. *Biofouling* **2007,** *23* (5), 307-317.
19. Banerjee, I.; Pangule, R. C.; Kane, R. S., Antifouling Coatings: Recent Developments in the Design of Surfaces That Prevent Fouling by Proteins, Bacteria, and Marine Organisms. *Adv. Mater.* **2011,** *23* (6), 690-718.
20. Lejars, M.; Margaillan, A.; Bressy, C., Fouling Release Coatings: A Nontoxic Alternative to Biocidal Antifouling Coatings. *Chem. Rev.* **2012,** *112* (8), 4347-4390.
21. Rosenhahn, A.; Schilp, S.; Kreuzer, H. J.; Grunze, M., The role of "inert" surface chemistry in marine biofouling prevention. *Phys. Chem. Chem. Phys.* **2010,** *12* (17), 4275-4286.
22. Kirschner, C. M.; Brennan, A. B., Bio-Inspired Antifouling Strategies. *Annu. Rev. Mater. Res.* **2012,** *42* (1), 211-229.
23. Aldred, N.; Li, G.; Gao, Y.; Clare, A. S.; Jiang, S., Modulation of barnacle (Balanus amphitrite Darwin) cyprid settlement behavior by sulfobetaine and carboxybetaine methacrylate polymer coatings. *Biofouling* **2010,** *26* (6), 673-683.
24. Angione, M. D.; Duff, T.; Bell, A. P.; Stamatin, S. N.; Fay, C.; Diamond, D.; Scanlan, E. M.; Colavita, P. E., Enhanced Antifouling Properties of Carbohydrate Coated Poly(ether sulfone) Membranes. *ACS Appl. Mater. Interfaces* **2015,** *7* (31), 17238-17246.
25. Esteban-Tejeda, L.; Duff, T.; Ciapetti, G.; Daniela Angione, M.; Myles, A.; Vasconcelos, J. M.; Scanlan, E. M.; Colavita, P. E., Stable hydrophilic poly(dimethylsiloxane) via glycan surface functionalisation. *Polymer* **2016,** *106*, 1-7.
26. Zen, F.; Angione, M. D.; Behan, J. A.; Cullen, R. J.; Duff, T.; Vasconcelos, J. M.; Scanlan, E. M.; Colavita, P. E., Modulation of Protein Fouling and Interfacial Properties at Carbon Surfaces via Immobilisation of Glycans Using Aryldiazonium Chemistry. *Sci. Rep.* **2016,** *6*, 24840.
27. Perrino, C.; Lee, S.; Choi, S. W.; Maruyama, A.; Spencer, N. D., A Biomimetic Alternative to Poly(ethylene glycol) as an Antifouling Coating: Resistance to Nonspecific Protein Adsorption of Poly(l-lysine)-graft-dextran. *Langmuir* **2008,** *24* (16), 8850-8856.
28. Ostuni, E.; Chapman, R. G.; Holmlin, R. E.; Takayama, S.; Whitesides, G. M., A Survey of Structure−Property Relationships of Surfaces that Resist the Adsorption of Protein. *Langmuir* **2001,** *17* (18), 5605-5620.
29. Ederth, T.; Ekblad, T.; Pettitt, M. E.; Conlan, S. L.; Du, C.-X.; Callow, M. E.; Callow, J. A.; Mutton, R.; Clare, A. S.; D'Souza, F.; Donnelly, G.; Bruin, A.; Willemsen, P. R.; Su, X. J.; Wang, S.; Zhao, Q.; Hederos, M.; Konradsson, P.; Liedberg, B., Resistance of Galactoside-Terminated Alkanethiol Self-Assembled Monolayers to Marine Fouling Organisms. *ACS Appl. Mater. Interfaces* **2011,** *3* (10), 3890-3901.

30. Luk, Y.-Y.; Kato, M.; Mrksich, M., Self-Assembled Monolayers of Alkanethiolates Presenting Mannitol Groups Are Inert to Protein Adsorption and Cell Attachment. *Langmuir* **2000,** *16* (24), 9604-9608.
31. Hederos, M.; Konradsson, P.; Liedberg, B., Synthesis and Self-Assembly of Galactose-Terminated Alkanethiols and Their Ability to Resist Proteins. *Langmuir* **2005,** *21* (7), 2971-2980.
32. Cao, X.; Pettit, M. E.; Conlan, S. L.; Wagner, W.; Ho, A. D.; Clare, A. S.; Callow, J. A.; Callow, M. E.; Grunze, M.; Rosenhahn, A., Resistance of Polysaccharide Coatings to Proteins, Hematopoietic Cells, and Marine Organisms. *Biomacromolecules* **2009,** *10* (4), 907-915.
33. Nurioglu, A. G.; Esteves, A. C. C.; de With, G., Non-toxic, non-biocide-release antifouling coatings based on molecular structure design for marine applications. *J.Mater. Chem. B* **2015,** *3* (32), 6547-6570.
34. Railkin, A. I., Marine Biofouling: Colonisation Processes and Defenses. CRC Press: **2003**.
35. Molino, P. J.; Wetherbee, R., The biology of biofouling diatoms and their role in the development of microbial slimes. *Biofouling* **2008,** *24* (5), 365-379.
36. Karl, D. M., Total microbial biomass estimation derived from the measurement of particulate adenosine-5′-triphosphate. In *Handbook of methods in aquatic microbial ecology*, Kemp, P. F.; Cole, J. J.; Sherr, B. F.; Sherr, E. B., Eds. Lewis Publishers: Boca Raton :, **1993**, pp 359-368.
37. Omidbakhsh, N.; Ahmadpour, F.; Kenny, N., How Reliable Are ATP Bioluminescence Meters in Assessing Decontamination of Environmental Surfaces in Healthcare Settings?. *PLoS ONE* **2014,** *9* (6), e99951.
38. Socrates, G., Infrared and Raman Characteristic Group Frequencies: Tables and Charts. John Wiley & Sons: **2001**.
39. Hibbs, M. R.; Hernandez-Sanchez, B. A.; Daniels, J.; Stafslien, S. J., Polysulfone and polyacrylate-based zwitterionic coatings for the prevention and easy removal of marine biofouling. *Biofouling* **2015,** *31* (7), 613-624.
40. Beeskow, T.; Kroner, K. H.; Anspach, F. B., Nylon-Based Affinity Membranes: Impacts of Surface Modification on Protein Adsorption. *J.Colloid Interface Sci.* **1997,** *196* (2), 278-291.

Chapter VI

Preparation of β-Cyclodextrin Based Aryldiazonium Coating for Multifunctional Materials.

A mild and efficient surface modification protocol for the preparation of β-cyclodextrin (βCD) modified surfaces through aryldiazonium mediated grafting is reported. Mono substituted 6-O-aminophenol-β-Cyclodextrin (amβCD) was synthesised through a three-step protocol. This compound was found to form supramolecular aggregates in aqueous solutions at relatively low concentrations via cavity-directed self-assembly. Disruption of these supramolecular structures through judicious choice of solvent was found to be essential for the formation of the reactive aryldiazonium species from the amino-phenolic precursor and for spontaneous surface grafting from aqueous solutions. Cyclodextrin thin films were prepared on both carbon macroscopic substrates and electrodes and were characterised via infrared reflectance absorption spectroscopy (IRRAS), cyclic voltammetry and water contact angle measurements. Protein adsorption studies demonstrated that βCD adlayers reduced non-specific protein adsorption. βCD moieties in adlayers can be used nonetheless for specific host-guest complexation and are grafted at the surface with monolayer coverage (1.2×10^{-10} mol cm^{-2}) as demonstrated via experiments using ferrocene, a redox probe. Finally, cyclodextrin covalent immobilisation was demonstrated on both stainless steel and polyamide samples, two substrates with wide ranging technological applications.

The data Presented in this chapter is reproduced in part from the following publication:

Spontaneous Aryldiazonium Grafting for the Preparation of Functional Cyclodextrin Modified Materials
Adam Myles, James. A. Behan, Brendan Twamley, Paula E. Colavita, & Eoin M. Scanlan
ACS Applied Bio Materials **2018**, *1* (3), pp 825–832

All X-Ray Crystallographic measurements and calculations were performed by B.Twamley., J.A. Behan assisted with electrochemical measurements and coating estimate calculations. P.E. Colavita assisted analysis of NMR titration data.

1 Introduction

Cyclodextrins (CD) are cyclic oligosaccharides most commonly consisting of 6 (α), 7 (β) or 8 (γ) glucose units linked together by a (1, 4) glycosidic bond. They possess a torus structure with a hydrophilic exterior, and a relatively hydrophobic cavity capable of forming host-guest inclusion complexes with a wide range of hydrophobic compounds.[1-2] These unique properties of cyclodextrins, coupled with their relative abundance and low-cost, render them extremely versatile and useful substrates with diverse applications in supramolecular chemistry, drug delivery, separation science, solubility enhancement and sensor technology.[3-5] In order to impart the desirable features of cyclodextrin onto surfaces, there exist a range of surface modification techniques including physisorption, chemisorption and covalent modification approaches. Importantly, several of these approaches maintain the functionality of the cyclodextrin cavity on the surface and enable the design of functional materials with broad application. Surface modification can be achieved *via* physisorption methods such as hydrogen bonding or through host-guest activity with surface expressed binding groups.6 Physisorbed coatings generally display low stability and can typically be removed by physical displacement through sonication. More stable cyclodextrin surfaces can be achieved either by production of a polymeric deposition incorporating cyclodextrins,[1-2, 7-8] or through chemisorption, i.e. specific chemical modification to produce covalently bound cyclodextrins at the surface. Examples of this include grafting to cellulose *via* acid crosslinking,[9] production of gold surfaces modified *via* thiol-ene chemistry,[10] and electrochemical grafting of cyclodextrins onto conductive surfaces.[6, 11] Covalent immobilisation of cyclodextrins has several benefits over physisorption and polymeric layer deposition, including coating stability and potential to retain surface properties and morphology. Spontaneous diazonium grafting is an attractive strategy for the production of a covalently modified cyclodextrin surface as it involves mild conditions, it is easily scalable and it is applicable to a wide variety of materials including carbon, polymer and metal alloy surfaces.[12-17] However, to the best of our knowledge there are no reports on the application of these spontaneous reactions to cyclodextrin immobilisation. We have demonstrated previously that modification of surfaces through aryldiazonium

chemistry with mono- and disaccharides is possible on a wide variety of materials including carbon and polymers.[13-14, 16, 18] The aryl ring is required for formation of a more stabilised diazonium cation, as alkyl diazonium species are typically highly unstable and unsuitable for surface functionalisation. The mono tosylation of the primary face (i.e. the 6' alcohol of the saccharide) opens up many avenues for cyclodextrin modification,[8, 19] including a potential pathway for producing a cyclodextrin diazonium salt-based grafting agent. Modification of the primary face to include an aromatic tail can however result in βCD in aqueous solution to readily form supramolecular host-guest complexes.[20-22] Complex formation can compromise the reactivity of aromatic tail groups *via* inclusion in the cavity of neighboring βCD units and thus potentially prevent further reactions such as those leading to surface covalent grafting.

In this work we report the synthesis and characterisation of a βCD-based aryldiazonium precursor molecule. We demonstrate that prevention of supramolecular host-guest assembly is essential for successful spontaneous surface grafting.[23-25] Disruption was achieved *via* cavity binding of a high affinity substrate such as adamantane or through modulation of the solvent polarity, with the latter method resulting in surfaces that display βCD-sites available for binding of organic substrates. Carbon materials were modified using aryldiazonium salts generated from these CD-glycosides in aqueous solutions and under mild conditions, resulting in glycosylated surfaces that display protein rejection behaviour in the absence of specific host-guest interactions.[13, 16, 26] Cavity binding of surface-bound cyclodextrin was confirmed using a ferrocene/ferrocenium redox probe.[11] The functionalisation method was subsequently applied to two insulating surfaces of industrial interest: a metal alloy, stainless steel 316, and a polyamide, nylon-6, thus expanding the range of applications of this functionalisation methodology.[26]

2 Results and discussion

2.1 Aryldiazonium precursor characterisation

Functionalisation of carbon surfaces was first attempted *via* diazotisation of amβCD under standard activating conditions (1 mM, aqueous $NaNO_2/H^+$), as indicated in **Scheme 6.1.**, which are known to result in covalent grafting onto carbon for lactoside coatings.[16] However, these conditions provided no evidence of surface modification as determined by wettability tests and infrared studies. It was hypothesised that this failure to graft may be due to self-assembly induced inactivation of the amino-phenolic tail, thus preventing diazotisation and/or covalent grafting of aryldiazonium cations.[20-22]

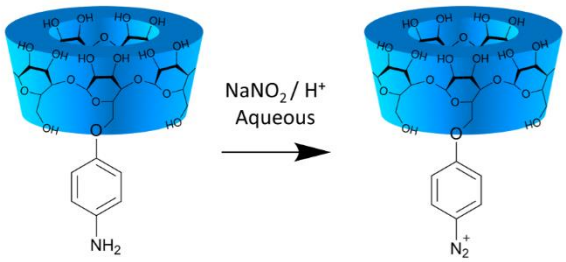

Scheme 6.1. Proposed aryl diazonium salt formation. Reproduced with permission from *ACS Appl. Bio Mater., **2018**, 1 (3), pp 825–832*. Copyright 2018 American Chemical Society.

This process can readily occur if a neighbouring cyclodextrin moiety complexes the amino-phenolic tail within its cavity leading to formation of supramolecular aggregates. In order to confirm that aggregation of amβCD occurs in aqueous conditions at 1.0 mM, a solution of amβCD was prepared in ultrapure water with sonication. This solution was filtered through a 0.45 µm PES membrane filter and analyzed *via* dynamic light scattering (DLS), following a 1 h period of incubation at room temperature. DLS results are shown (**Figure 6.1**) and reveal scattering intensity equivalent to spherical particles with hydrodynamic radius >100 nm for amβCD 1.0 mM.

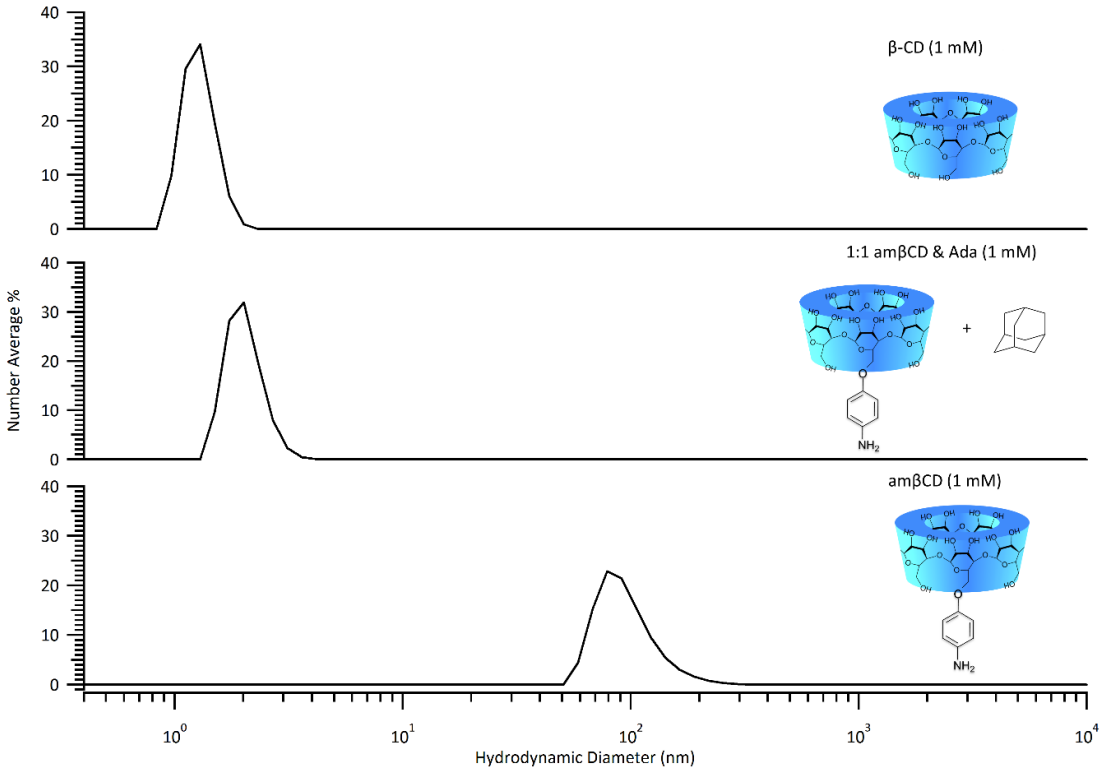

Figure 6.1. DLS results showing particle size distributions in deionised water at 1.0 mM of β-cyclodextrin (top), compound **13** (amβCD) with adamantane 1:1 complex (middle) and compound **13** only (Bottom). Samples were sonicated 1 h at 25 °C, filtered through a 0.45 μm membrane and kept at room temperature for 1 h prior to DLS measurements. Reproduced with permission from *ACS Appl. Bio Mater., **2018**, 1 (3), pp 825–832*. Copyright 2018 American Chemical Society.

This indicates that aggregates of amβCD develop readily over 1 h in aqueous solution at relatively low concentrations under ambient conditions. Identical experiments using unmodified βCD unit do not yield scattering intensity at hydrodynamic sizes >2 nm (**Figure 6.1**), in agreement with prior reports,[27] and strongly indicating that aggregate formation is directly caused by the presence of the amino-phenolic tails in amβCD. DLS experiments carried out under identical conditions but with addition of adamantane (a compound known to strongly bind in 1:1 ratio to the cyclodextrin cavity)[24] to amβCD resulted in nearly identical stability to that of unmodified β-CD. This result strongly indicates that the cavity-binding of the amino-phenolic tail is crucial to aggregate formation.

Further evidence of involvement of amino-phenolic tails in the aggregation process was obtained from the ^{1}H NMR of aromatic protons of freshly prepared solutions of amβCD in D_2O, as shown for 1.2 and 3.0 mM concentrations in **Figure 6.2 a**. ^{1}H NMR spectra show a clear change in chemical shift indicating differences in the local environment of these protons at the two concentrations. This confirms that cavity directed self-assembly *via* host-guest interactions of the phenyl rings is important for the aggregation process.

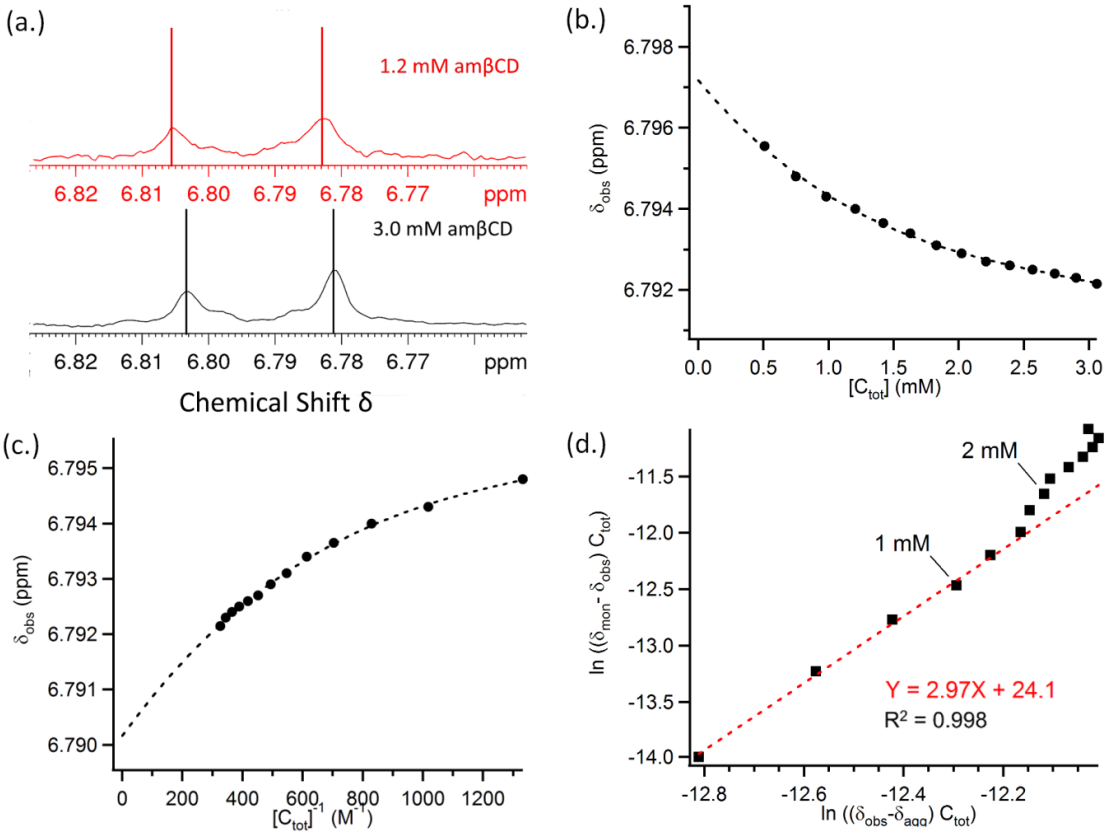

Figure 6.2. (a.) ^{1}H NMR (400 MHz) of amβCD in D_2O at 1.2 and 3.0 mM showing differing observed chemical shift of aromatic doublet, due to host-guest interactions. **(b.)** Plot of observed chemical shift versus $[C_{tot}]$ amβCD in D_2O with polynomial fit to determine δ_{mon} (6.7972 ppm) & **(c.)** plot of observed chemical shift versus $[C_{tot}]^{-1}$ of amβCD in D_2O with polynomial fit to determine δ_{agg} (6.7902 ppm). Points are experimental data, dashed line is best fit. **(d.)** Plot of concentration components from eq. 5 for determining the aggregation number n from the slope; points represent measured data and the dased line is the best fit trend line. Adapted with permission from *ACS Appl. Bio Mater., **2018**, 1 (3), pp 825–832*. Copyright 2018 American Chemical Society.

NMR titration experiments were performed over the concentration range 0.5-3.0 mM and show a progressive change in the observed chemical shift (δobs) of aromatic protons. The δobs can be expressed as a function of the total concentration (Ctot), the relative chemical shift of the aromatic protons in

monomeric βCD (δmon) and that of aromatic protons in the cavity of host-guest aggregates (δagg).This equilibrium is derived as follows;

Monomer- aggregate equilibrium in aqueous solution:

$$n\,[\text{Monomer}] \overset{K_a}{\rightleftharpoons} [\text{Aggregate}]$$

Where C_{mon} , C_{agg} and C_{tot} are monomer, aggregate and total concentration, respectively,

K_a is the association constant for the monomer-aggregate equilibrium and *n* is aggregation number:

$$C_{tot} = C_{mon} + n\,C_{agg}$$

$$\frac{C_{mon}}{C_{tot}} + n\,\frac{C_{agg}}{C_{tot}} = 1 \qquad (1)$$

The observed chemical shift (δ_{obs}) can be expressed as the weighted average of monomer and aggregate chemical shifts, δ_{mon} and δ_{agg} respectively, as shown below:

$$\delta_{obs} = \frac{C_{mon}}{C_{tot}}\delta_{mon} + n\frac{C_{agg}}{C_{tot}}\,\delta_{agg} \qquad (2)$$

By substitution of (1) into (2) we obtain:

$$\delta_{obs} = \left(1 - n\frac{C_{agg}}{C_{tot}}\right)\delta_{mon} + n\frac{C_{agg}}{C_{tot}}\,\delta_{agg}$$

$$\delta_{obs} = \delta_{mon} + n\frac{C_{agg}}{C_{tot}}\left(\delta_{agg} - \delta_{mon}\right)$$

$$\delta_{obs} - \delta_{mon} = n\frac{C_{agg}}{C_{tot}}\left(\delta_{agg} - \delta_{mon}\right)$$

$$C_{agg} = \frac{\delta_{obs} - \delta_{mon}}{\delta_{agg} - \delta_{mon}}\frac{C_{tot}}{n} \qquad (3)$$

The constant for the monomer-aggregate equilibrium K_a can be expressed as:

$$K_a = \frac{C_{agg}}{\left(C_{tot} - nC_{agg}\right)^n}$$

$$\Rightarrow \ln K_a = \ln C_{agg} - n\ln\left(C_{tot} - nC_{agg}\right) \qquad (4)$$

From (3) and (4):

$$\ln K_a = \ln\left(\frac{\delta_{obs} - \delta_{mon}}{\delta_{agg} - \delta_{mon}}\frac{C_{tot}}{n}\right) - n\ln\left(C_{tot} - n\frac{\delta_{obs} - \delta_{mon}}{\delta_{agg} - \delta_{mon}}\frac{C_{tot}}{n}\right)$$

$$\ln K_a = \ln\left(\frac{\delta_{obs} - \delta_{mon}}{\delta_{agg} - \delta_{mon}}\frac{C_{tot}}{n}\right) - n\ln\left(\frac{\delta_{agg} - \delta_{obs}}{\delta_{agg} - \delta_{mon}}C_{tot}\right)$$

$$\ln K_a = \ln\left(\frac{\delta_{obs} - \delta_{mon}}{\delta_{agg} - \delta_{mon}}C_{tot}\right) - \ln n - n\ln\left(\frac{\delta_{agg} - \delta_{obs}}{\delta_{agg} - \delta_{mon}}C_{tot}\right)$$

$$\ln K_a + \ln n = \ln\left((\delta_{mon} - \delta_{obs})C_{tot}\right) - \ln\left(\delta_{mon} - \delta_{agg}\right) - n\ln\left(\left(\delta_{obs} - \delta_{agg}\right)C_{tot}\right) + n\ln\left(\delta_{mon} - \delta_{agg}\right)$$

A rearrangement of the equation above yields equation (5) for the monomer-aggregate equilibrium.

$$\ln\left(C_{tot}(\delta_{mon} - \delta_{obs})\right) = n\ln\left(C_{tot}\left(\delta_{obs} - \delta_{agg}\right)\right) + \ln n - (n-1)\ln\left(\delta_{mon} - \delta_{agg}\right) + \ln K_a \qquad (5)$$

This equation reveals the relationship between the association constant for the monomer-aggregate equilibrium of amβCD, Ka, and the aggregation number n. The relative chemical shifts, δ_{mon} and δ_{agg} are determined following the procedure by Lui et al.[13] by extrapolation to the y-axis of a cubic fit of δ_{obs} vs. C_{tot} and of δ_{obs} vs. C_{tot}^{-1} as shown in **Figures 6.2 b & c**, respectively. Values thus obtained were δ_{mon} = 6.7972 ppm and δ_{agg} = 6.7902. A linear fit of the concentration expressions from equation 5 (**Figure 6.2 d**) yields the aggregation number n = 2.97, confirming that this species forms trimeric structures at concentrations <1.5 mM.

At higher concentrations it is possible to observe a second regime that suggests formation of larger aggregates (n>3). These findings are consistent with reports that show that dimerisation results in further host-guest self-assembly in other phenyl-modified βCD species.[20-22] From the intercept of the best fit to equation (1), a pKtri = -5.66 is obtained for the trimer equilibrium constant. Assuming a non-cooperative self-assembly process (pKn = (n-1) pK2, n ≥ 2), the dimer formation constant is estimated at pKdim = 2.83, or Kdim ≈ 680, in excellent agreement with phenyl-CD host-guest Ka values reported by Liu et al.[21]

Cyclodextrins displaying modifications with aromatic groups have been reported to form crystals *via* one of three pathways, cavity-tail self-inclusion, packed layers and one dimensional self-assembly.[20-22] Crystals of amβCD were grown from solutions in both D_2O and H_2O over 15 days at >3 mM concentration.

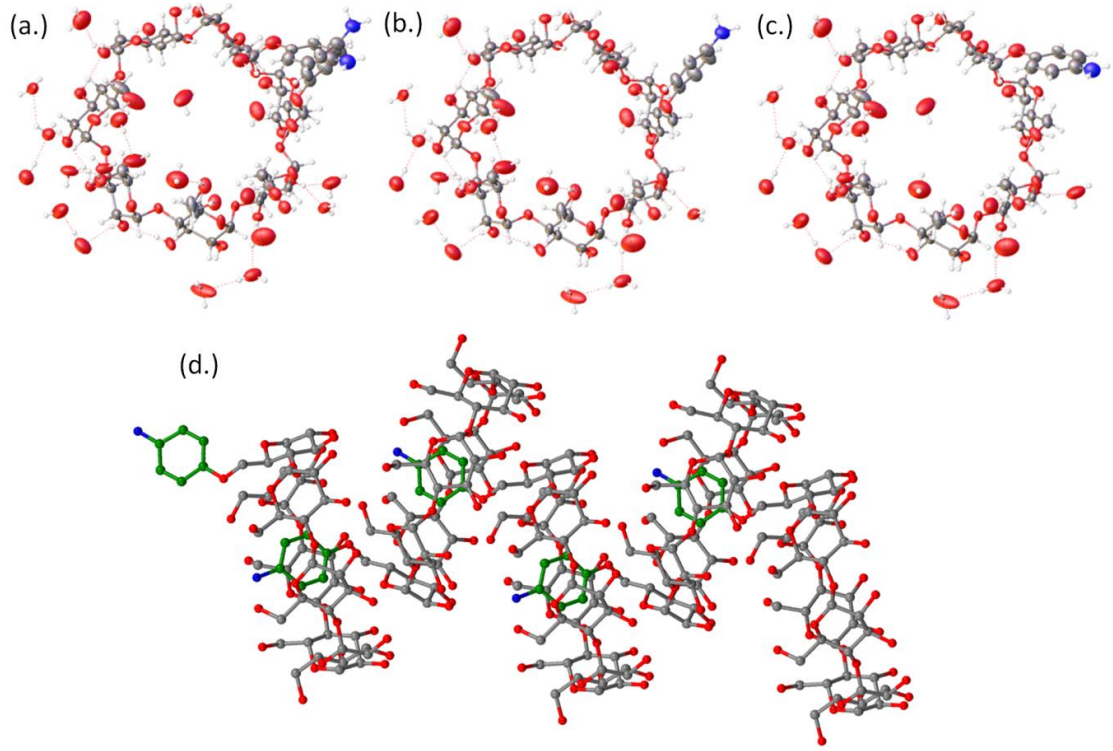

Figure 6.3. Molecular structure of amβCD shown with **(a.)** disordered moieties, **(b.)** with major occupancy for the aminophenol group (72%) and ethoxy groups (75 and 79%), and **(c.)** minor occupancy (28% and 25, 21% respectively). Dotted lines indicate hydrogen bonding patterns. Atomic displacement is shown at 50% occupancy. **(d.)** Shown is an illustration of the one-dimensional head to tail helical self-assembly of amβCD determined by X-ray crystallography. Aromatic carbons have been highlighted (green); water of crystallisation and hydrogen atoms have been omitted for clarity. Adapted with permission from *ACS Appl. Bio Mater., **2018**, 1 (3), pp 825–832*. Copyright 2018 American Chemical Society.

X-ray crystallographic data analysis reveals that the amino phenolic tailed compound crystallizes by aromatic tail penetration into the cyclodextrin cavity

along a screw axis to form a linear head-to-tail supramolecular structure (**Figure 6.3 d.**).[21] These data confirm that self-assembly occurs *via* the insertion of the amino-phenol tail into the βCD cavity and would account for the inactivity of this precursor compound. Results indicate that aggregate disruption is essential for the amino-phenolic tails to be available for further reactions. As shown by DLS, it is possible to achieve this *via* cavity-blocking with a high-affinity substrate such as adamantane. However, binding of such substrates effectively blocks the cavity, while it is more advantageous for further applications to achieve disruption by modulating solvent conditions while retaining an empty cavity. Nuclear Overhauser Effect (NOE) NMR spectroscopy was used to investigate the role solvent plays in supramolecular assembly.

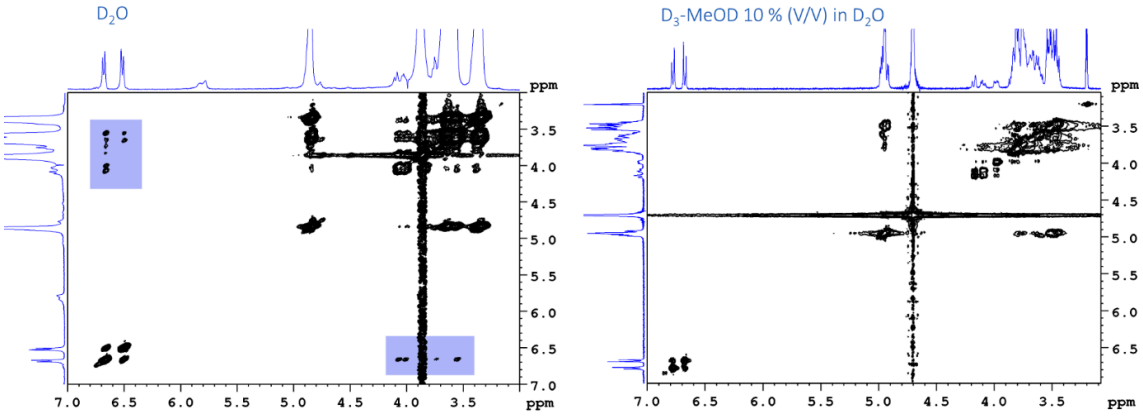

Figure 6.4. ^{1}H-^{1}H NOESY Spectrum of amβCD in D_2O; through space interactions between aromatic (tail) and saccharide (cavity) protons are highlighted in blue. (Left) ^{1}H-^{1}H NOESY Spectrum of amβCD in D_3-MeOD 10% v/v in D_2O. (Right) No interaction peaks are observed between aromatic (tail) and saccharide (cavity) implying negligible host-guest interaction under these conditions. Adapted with permission from *ACS Appl. Bio Mater., **2018**, 1 (3), pp 825–832*. Copyright 2018 American Chemical Society.

^{1}H-^{1}H NOESY was performed on amβCD under various conditions to determine effective disaggregation conditions. In D_2O (**Figure 6.4**) strong interactions were seen between the aromatic protons at 6.8 and 6.6 ppm and the saccharide protons of the cavity, particularly the glycan H-5 and H-3 protons at peak positions 3.6 and 3.7 ppm, thus confirming host-guest interactions.[21] These peaks disappear upon when exposing the supramolecular assembly to a solvent system which contains a significant organic component, *i.e.* 10% v/v MeOH in water. It was thus concluded that self-assembly behaviour of compound **13** can be minimised either through pre-emptive host-guest binding or through careful modulation of solvent conditions.[23-24]

2.2 Carbon functionalisation with βCD moieties

Surface functionalisation was carried out under conditions that promote disaggregation of **13** in solution while retaining a free cavity available for binding. Diazotisation and surface grafting reactions were therefore carried out in 10% MeOH in aqueous solutions (**Scheme 6.2**): a 1.25 mM solution of amβCD was prepared in 1.25 mM HBF_4. This solution was then chilled to < 4 °C for 1 h, and subsequently diluted by addition of 0.010 M $NaNO_2$ to a final concentration of 1.0 mM βCD. Immediately after diazotisation, the aryldiazonium cation solution was placed in contact with the substrate material, by either immersion or drop casting; the surface was kept in the dark for 1 h and subsequently rinsed and sonicated in methanol and water prior to characterisation.[13-14, 18, 26]

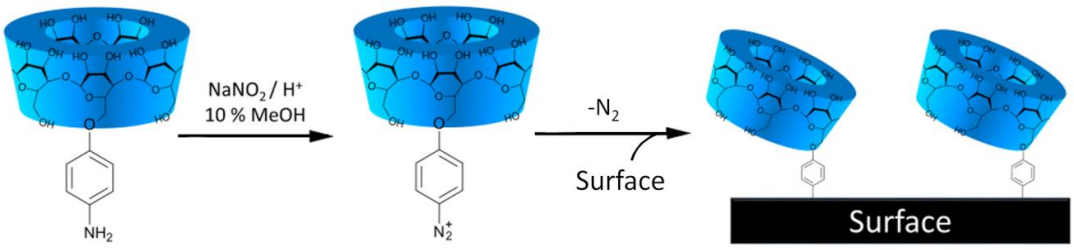

Scheme 6.2. Surface modification with cyclodextrin by spontaneous aryldiazonium grafting. Adapted with permission from *ACS Appl. Bio Mater., **2018**, 1 (3), pp 825–832*. Copyright 2018 American Chemical Society.

Confirmation of spontaneous βCD grafting onto amorphous carbon was obtained by ex-situ infrared reflectance absorption spectroscopy (IRRAS). **Figure 6.5.a.** shows the IRRAS of a carbon surface[28] modified *via* the process above. The transmittance spectrum of amβCD precursor compound in bulk form is also shown for comparison. Both spectra display characteristic peaks at 1145 cm^{-1}, 1080 cm^{-1}, 1024 cm^{-1} and 993 cm^{-1} corresponding to C-O stretching modes and O-H deformations of the carbohydrate rings.[29] The presence of these peaks is diagnostic of the presence of carbohydrate moieties at the carbon surface and is consistent with formation of a βCD adlayer. These peaks were not observed in the IRRAS of samples which had been immersed in a 10% MeOH solution of amβCD alone, without $NaNO_2$. Importantly, the peaks were also absent from

samples immersed in an aqueous solution of amβCD and $NaNO_2/H^+$, but prepared without addition of 10% MeOH. The above control experiments indicate that both diazotisation conditions and disruption of host-guest complex aggregates are essential to observe evidence of surface functionalisation. Furthermore, they strongly indicate that βCD immobilisation occurs *via* covalent bond formation by the reaction of the aryldiazonium cation with the carbon substrate.[13, 18, 26, 28]

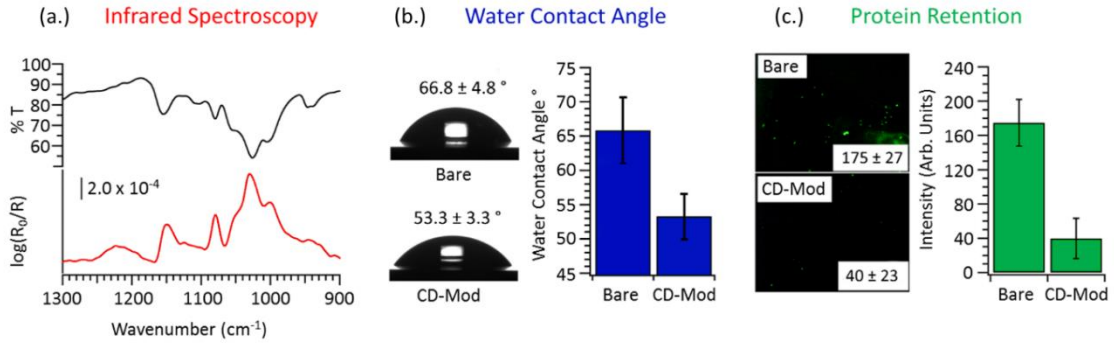

Figure 6.5. (a.) Infrared spectra showing transmittance spectrum of bulk amβCD diazonium precursor (top trace, black) and an IRRAS spectrum of a carbon surface after spontaneous grafting with βCD (bottom trace, red). **(b.)** Water contact angle (WCA) results for polished glassy carbon plates before (bare) and after (CD-Mod) functionalisation with βCD; a significant decrease in WCA is observed after modification reactions. **(c.)** Protein adsorption studies on polished glassy carbon (bare) and on βCD-functionalised carbon (CD-Mod) using FITC-BSA; values are average emission intensity after incubation in FITC-BSA solutions, while error bars represent 95 % C. Adapted with permission from *ACS Appl. Bio Mater., **2018**, 1 (3), pp 825–832*. Copyright 2018 American Chemical Society.

Reaction of carbon with aryldiazonium cations of amβCD was also found to result in a significant change in surface wetting properties, consistent with the presence of a saccharide adlayer. **Figure 6.5 b**. shows the water contact angle (WCA) of glassy carbon (GC) before and after functionalisation. Results indicate that there is a significant decrease in WCA from (65.8 ± 4.8) ° (95 %CI) to (53.3 ± 3.3) ° (95 %CI). The increased hydrophilicity is attributed to increased surface density of hydroxyl groups resulting from grafting of βCD, and it is in agreement with reported changes after modification with simpler mono- and di-saccharide moieties.[13-14, 18, 26] To investigate whether changes in wetting properties also affect interfacial interactions with biomolecules such as proteins,[13, 18, 26, 30-31] GC plates were incubated in buffered solutions of fluorescently labelled bovine serum albumin (BSA-FITC) at room temperature for 2 h. GC plates were rinsed

and subsequently examined under microscopy with fluorescence excitation at 470 nm. The βCD-modified GC displayed lower FITC emission, thus indicating reduced protein retention when compared to unmodified samples (**Figure 6.5.c.**). These findings correlate well with WCA data and are consistent with previous findings on saccharide-modified surfaces.[13-14]

2.3 Surface functionality and coverage estimates

βCD is known to form 1:1 inclusion complexes with ferrocene in solution,[11,32] therefore ferrocene was used as a redox probe to confirm availability of the surface-bound cavity to host-guest complexation. Glassy carbon electrodes subjected to different treatments including CD functionalisation conditions (**Figure 6.6 a & b**) simple polishing conditions (**Figure 6.6 c**) and physisorption conditions (**Figure 6.6 d**) were immersed in a 5.0 mM solution of ferrocene in MeOH, rinsed with deionised water and then tested *via* cyclic voltammetry (CV) at 200 mV s^{-1} in 0.5 M KCl aqueous supporting electrolyte.

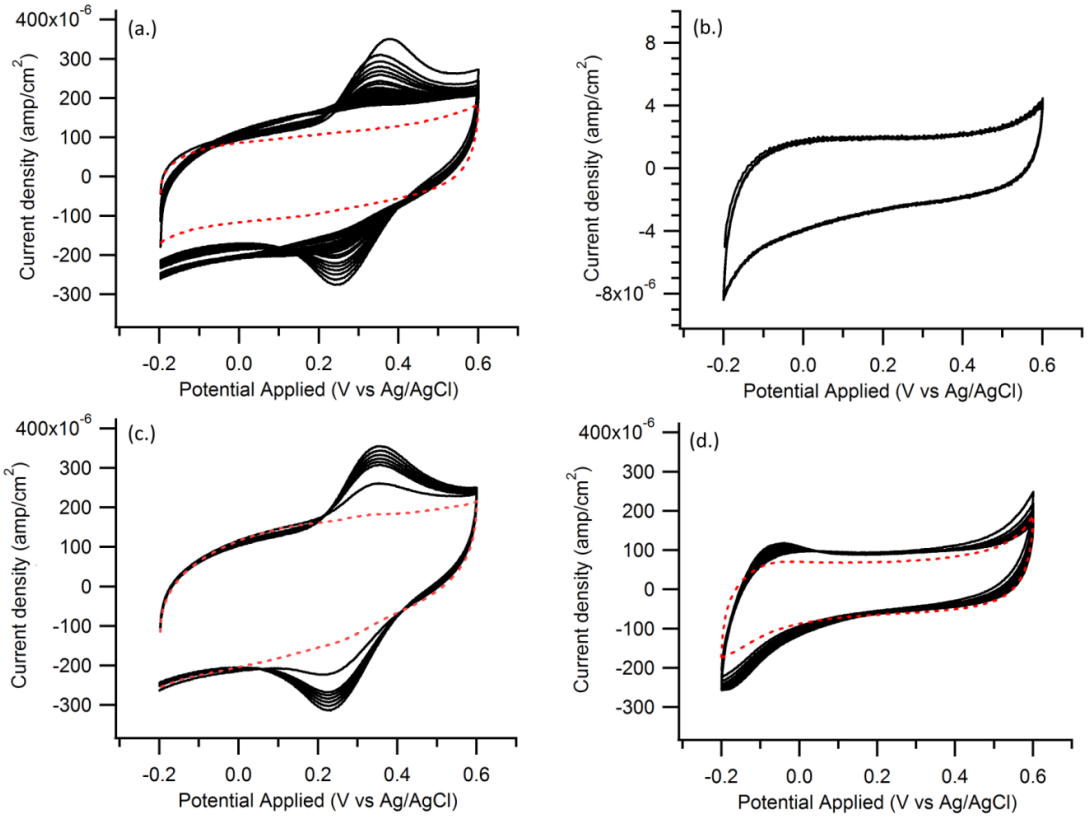

Figure 6.6. (a) Cyclic voltammograms of a cyclodextrin modified GC electrode post Fc immersion with sequential cycling until significant reduction of faradaic peaks was observed (scan 1-40); the dashed red trace is a CV of the CD-coated electrode prior to immersion in Fc solutions. **(b.)** a bare glassy carbon electrode after immersion in ferrocene. **(c.)** CVs obtained after re-immersion of (a.) in a 5 mM Fc solution for 40 min (scan 2-10 & scan 20); the dashed red trace is the same as the final scan obtained from (a) and is reported for comparison. **(d.)** a bare electrode immersed in cyclodextrin precursor solution without activation by NaNO2, (dashed red trace) and post ferrocene immersion (black trace). No Fc/Fc^+ redox peaks are observed in the absence of a covalently bound cyclodextrin surface film. All voltammograms were obtained in 0.5 M KCl solutions at 200 mV s-1. Adapted with permission from *ACS Appl. Bio Mater., **2018**, 1 (3), pp 825–832*. Copyright 2018 American Chemical Society.

GC electrodes modified with βCD (**Figure 6.6 a**) display the characteristic oxidation and reduction peaks of ferrocene/ferrocenium (Fc/Fc^+) with a formal potential at 0.26 V vs. Ag/AgCl.[11] In contrast, in the absence of modification, the bare GC surface (Figure 6b) and an electrode subjected to cyclodextrin physisorption conditions (Figure 6d) shows no evidence of faradaic peaks thus indicating that no significant amounts of ferrocene physisorb at bare GC. This would imply that peaks arise from specific CD-ferrocene binding interactions at the electrode interface. The first anodic sweep in Figure 6a is markedly different from that of subsequent cycles and its greater asymmetry suggests the presence of contributions from non-surface bound redox species. This behaviour is likely

to arise from small amounts of weakly bound Fc^+ that is free to diffuse into solution. Peaks in subsequent cycles display instead symmetric peaks, whose intensity decreases slightly over multiple cycles. This is consistent with progressive partitioning of the more soluble Fc^+ species into the aqueous phase after each anodic sweep.[11] This is further supported by **Figure 6.6 c** which shows the same electrode used to generate CV's in **Figure 6.6 a** following a second immersion in ferrocene solution. Redox peak behaviour recovers significantly implying a highly stable layer of cyclodextrin remains at the surface following repeated scans within this potential window. These CD moieties are then capable of forming further host-guest interactions with analyte molecules following cavity evacuation.

An additional benefit in the use of ferrocene as a surface sensitive redox probe can be seen in the determination of surface density of occupied βCD-sites The total integrated charge associated with the anodic peak of the second cycle (0.2-0.5 V) was used to provide an estimate of surface coverage, Γ, for βCD-Fc complexes. Using equation (6) for a 1-electron transfer (n = 1), a scan rate v = 0.2 V s^{-1} and an experimentally determined electrode geometric area A = 0.196 cm^2 :[33]

$$\Gamma = \frac{Q}{nFA} = \frac{\int_{V_1}^{V_2} idV}{nFAv} \qquad (6)$$

The value of Γ obtained was 1- 2 × 10^{-10} mol.cm^{-2}. To determine an estimate of monolayer coverage (Γ) for cyclodextrin; surface coverage in moles.cm^{-1} was calculated for circles with approximate of amβCD's diameter when orientated towards the surfaces perpendicular to the phenolic ring and was taken as approximately the distance of O28-C63 as seen in **Figure 6.7**.

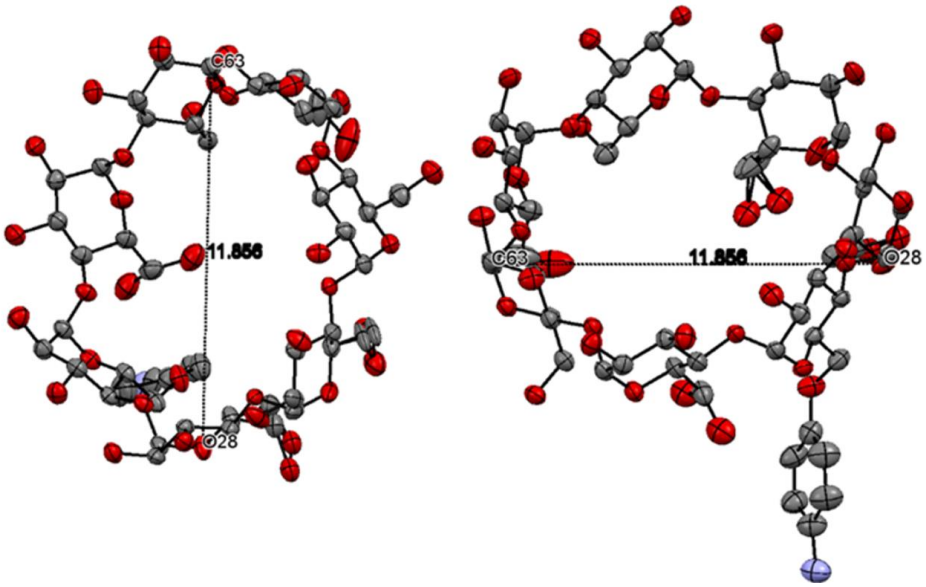

Figure 6.7. Distance of cyclodextrin along planar coordinates when observed down the aromatic ring. C-63 – O-28 = 11.86 Å. Reproduced with permission from *ACS Appl. Bio Mater., **2018**, 1 (3), pp 825–832*. Copyright 2018 American Chemical Society.

Monolayer coverage was estimated as a maximum hexagonal packing density:

$$\eta_h = \frac{\pi\sqrt{3}}{6} = 0.9069$$

Each Cyclodextrin molecule was modelled as a circle of diameter 1.186×10^{-7} cm.

Area covered by each molecule of Cyclodextrin (A_{CD}) is therefore:

$$A_{CD} = \pi r^2 = \pi.(0.593 \times 10^{-7}\ \text{cm})^2 = 1.104 \times 10^{-14}\ \text{cm}^2.\text{molecule}^{-1}$$

Therefore the coverage in a hexagonal close packed system is:

$$\Gamma = \frac{1}{A_{CD}}\ \text{x}\ \frac{\eta_h}{6.022\times10^{23}} \approx 1.4\ \text{x}\ 10^{-10}\ \text{mol.cm}^{-2}$$

This value calculated from crystallographic data for a hexagonal closed-packed layer of amβCD with its phenyl ring oriented normal to the carbon surface is in excellent agreement with the value obtained from the electro reduction of ferrocene as above. This indicates that spontaneous aryldiazonium grafting of amβCD results in monolayer coverage.

Further evidence for monolayer coverage was provided by atomic force microscopy measurements of the thickness of βCD adlayers. (**Figure 6.8**). The step height was found to be 0.84 ± 0.25 nm, which is consistent with the presence of a sparse layer and in agreement with previous determinations of aryldiazonium monolayers.[34] Control experiments using identical conditions on a bare carbon surface did not yield a height step.

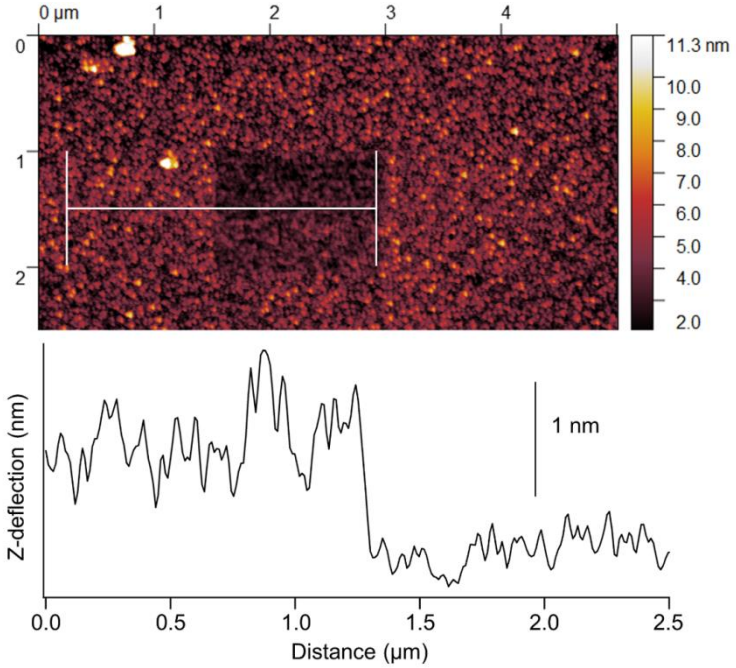

Figure 6.8. AFM topographic image of a βCD layer formed on sputtered amorphous carbon (top) after removal of a portion of the film with the AFM tip. The height profile averaged over 100 scans (bottom) shows a step edge used to estimate the layer thickness. Reproduced with permission from *ACS Appl. Bio Mater., **2018**, 1 (3), pp 825–832*. Copyright 2018 American Chemical Society.

Monolayer control of aryldiazonium functionalisation reactions is notoriously difficult to achieve, due to the tendency of these cations to cross-link yielding multilayers, particularly under electrografting conditions. The steric hindrance of the CD moiety is therefore likely to provide an intrinsic control mechanism for suppressing multilayer formation, as observed in previous studies on applications of bulky substituent's for monolayer control.[18, 35-39]

2.4 Functionalisation of non-conductive surfaces with β-CD

One of the major advantages of spontaneous aryldiazonium reactions is the ability to impart surface functionality onto materials without the requirement of an electrical contact. This makes the spontaneous reaction a versatile method which

was recently extended from the modification of conductors, e.g. carbon, Ni, Fe, Zn, [12] to the modification of polymeric insulators [13-14, 26] and oxide passivated alloy surfaces such as stainless steel.[17, 26] Therefore, we investigated the applicability of spontaneous grafting for the immobilisation of βCD onnylon-6 and stainless steel 316 (SS316), a polymeric and an alloy material of importance for a wide range of applications. Nylon-6 samples were pre-treated *via* formaldehyde activation, while SS316 coupons were subject to an oxidative activation treatment.[26] Samples were subsequently immersed in solutions of the aryldiazonium cation from amβCD, as discussed in Scheme 2.

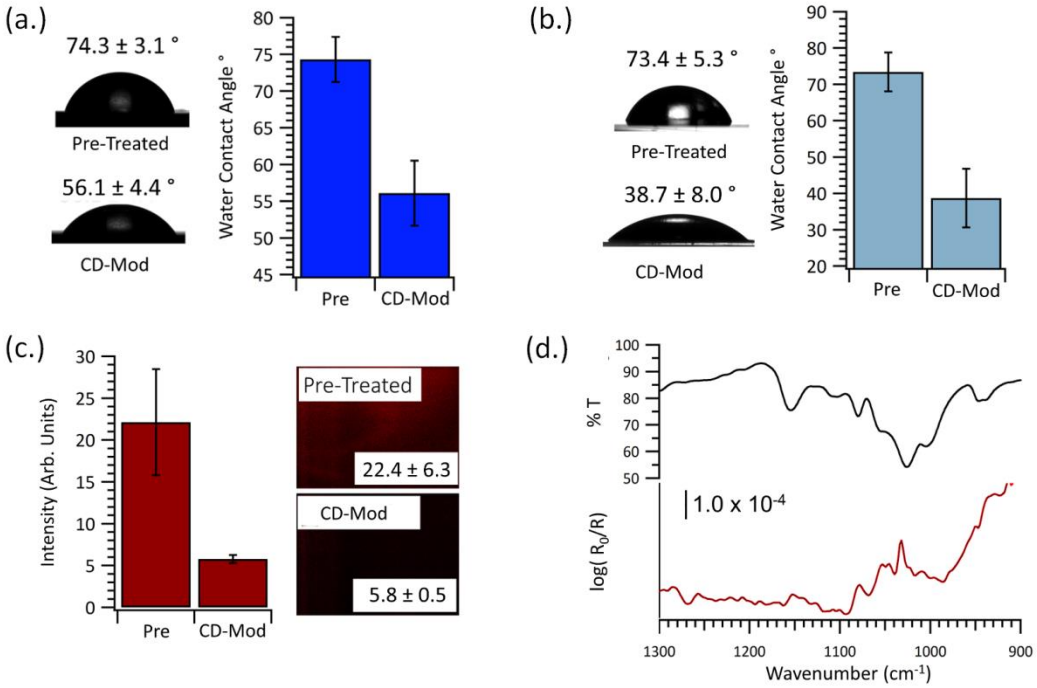

Figure 6.9. Water contact angles for nylon-6 **(a.)** and SS316 **(b.)** before and after spontaneous reactions with aryldiazonium cations from amβCD. **(c.)** Protein adsorption tests on nylon-6 using fluorescently labelled BSA (Alexa-BSA); the bar chart shows average emission intensity measured after incubation in Alex-BSA solutions on surfaces before and after modifications. **(d.)** IRRAS spectrum obtained on SS316 after functionalisation reactions with βCD; the transmittance spectrum of amβCD is shown in the graph for comparison. Reproduced with permission from *ACS Appl. Bio Mater., **2018**, 1 (3), pp 825–832*. Copyright 2018 American Chemical Society.

Figures 6.9 a & b show the resulting WCA values obtained on nylon-6 and SS316 both prior to, and post immersion in the aryldiazonium grafting solution. In all cases, hydrophilicity increased, as expected after modification with βCD adlayers. The effect on protein adsorption resulting from βCD grafting on nylon-6 was also characterised using buffered solutions of BSA labelled with Alexa Fluor-647. After incubation in such solutions the total emission arising from

adsorbed protein is lower in the case of nylon-6 modified with βCD (Figure 9c). The IRRAS spectrum obtained from SS316 surfaces after modification with βCD is shown in Figure 9d. The spectrum compares well with the one obtained in transmittance from the precursor amβCD. These experiments therefore confirm that the spontaneous reaction results in grafting of βCD functional moieties on materials with a wide range of properties.

3 Conclusions

We have demonstrated that a synthetic *p*-nitrophenol cyclodextrin substrate, prepared from native β-cyclodextrin *via* a three step synthesis is suitable for aryldiazonium grafting onto a range of materials. The synthesised CD-derivative aggregates in solution, at relatively low concentrations, *via* cavity directed self-assembly. We demonstrate that disruption of these aggregates is essential for successful functionalisation and that this can be achieved *via* cavity binding with high-affinity substrates or *via* modulation of solvent properties. The latter method was leveraged to achieve spontaneous grafting of βCD groups. The resulting adlayers were found to be hydrophilic and to reduce protein retention, while the binding properties of βCD moieties were preserved once covalently linked to the surface. This suggests that these βCD adlayers can potentially play a dual role in reducing non-specific binding to biomolecules, while presenting a binding cavity available for leveraging specific host-guest interactions. Importantly, the specific route to surface immobilisation reported in this work yielded closed-packed monolayers of βCD, a feature that is important e.g. for effective control of assay sensitivity in βCD sensing applications. It is anticipated that this approach will find widespread application in the preparation of cyclodextrin surfaces as the process is readily scalable, and applicable to a wide range of polymeric, alloy and carbon surfaces.

4 Methods and Materials

4.1 Chemicals and Materials

Adamantane 99+% was purchased from Fisher Scientific; P-toluenesulfonyl chloride 99%, sodium hypochlorite (bleach), sodium hydroxide, potassium hydroxide, phosphate buffered saline buffer (0.010 M PBS, pH 7.4), sodium

nitrite, hydrochloric acid, fluoroboric acid, ferrocene 98% and bovine serum albumin (BSA) conjugates with fluorescein isothiocyanate (FITC) were purchased from Sigma-Aldrich; BSA conjugates with Alexa Fluor 647 were purchased from Biosciences; Marine grade stainless steel 316 foil (SS316), and polyamide sheets Nylon-6 (N-6) were purchased from Goodfellow; Sigradur K Glassy carbon plates and Sigradur G Glassy carbon discs were purchased from HTW.

4.2 Diazonium Precursor Molecule Characterisation

NMR titration experiments were performed on an Agilent 400-MR equipped with a 5mm OneNMR probe for proton and multinuclear detection and an automatic sample changer. Infrared spectra of bulk precursor samples were measured on a PerkinElmir Spectrum100 FTIR with an ATR sampling accessory. Hydrodynamic diameters of modified β-cyclodextrin compounds in solution were determined via dynamic light scattering (DLS) measurements on a Malvern Zeta Sizer Nano ZS; curves are obtained using refractive indices of n = 1.56 and n = 1.33 for the cyclodextrin aggregates and liquid phase, respectively.

4.3 Substrate Surface Preparation

Carbon substrates for infrared reflectance absorption spectroscopy experiments (IRRAS) were prepared *via* DC magnetron sputtering (Torr International Inc.) in Ar; deposition was carried out on an optically thick Ti under layer (Grade 2) on which carbon was subsequently sputtered from a graphite target (99.999%). Glassy carbon substrates were polished with alumina slurries (Buehler) with decreasing particle size of 1 (on nylon cloth), 0.3 and 0.05 μm (on nylon microcloth); each polishing step was followed by 3 min sonication in each of n-hexane, methanol (semiconductor grade) and ultrapure H_2O.

4.4 General Functionalisation Procedure

Initially surfaces were cleaned using semiconductor grade methanol and ultrapure H_2O and were modified with aryldiazonium cyclodextrin cations through spontaneous grafting protocols similar to those reported previously for other diazonium based carbohydrate surface coatings. A 1.5 mM solution of HBF_4 was prepared in a 10 % MeOH: DI H_2O solution which was used to make a solution of 1.25 M amβCD which was subsequently chilled to < 4 °C in ice for 1 h. This solution was then diluted to a final concentration of 0.0010 M using a 0.010 M

solution of $NaNO_2$. The sample surface was then placed in contact with this solution, kept in the dark for 1 h at RT, rinsed with deionised water, sonicated in MeOH, and H_2O for 1 min in each solvent, dried under argon flow and stored under argon prior to analysis. This procedure was followed for all non-polymeric surfaces, which are easily damaged by sonication and which were instead subjected to a light rinsing step. Nylon-6 samples were preactivated by overnight immersion at 30 °C in a 36% aqueous formaldehyde solution with a catalytic amount of hypophosphorous acid. Stainless steel samples (SS316) were pretreated with 0.5% NaClO in basic aqueous solution (KOH 1% and NaOH 1%) for 1 h.

4.5 Surface Characterisation

A Bruker Tensor 27 infrared spectrometer was used to perform Infrared reflectance absorption spectroscopy (IRRAS) characterisation. The spectrometer was equipped with a mercury cadmium telluride detector and a VeeMax II specular reflectance accessory with a wire grid polarizer. All spectra were collected using p-polarised light at an angle of incidence of 80° using an unmodified sample as a background; 100 scans at 4 cm^{-1} were collected for all samples. Water contact angles (WCAs) were determined for all samples using the sessile drop method (FTA1000), using 20 µL droplets. Thickness and surface roughness measurements were carried out via Atomic Force Microscopy (AFM, Asylum Research) using silicon cantilevers, following previously published procedures using silicon cantilevers, at ambient pressure calibrated at 140 kHz.

4.6 Fluorescence Microscopy.

To determine protein rejection ability, Sigradur K Glassy carbon plates treated with the above functionalisation procedure and un-modified control plates were immersed in 0.2 mg mL^{-1} solutions of BSA-FITC or BSA- Alexa Fluor® 647 conjugates in PBS at pH 7.4 for 1 h. All samples were washed with PBS solution prior to imaging to remove excess unbound protein. Fluorescence images were acquired using an Olympus BX51 inverted microscope with cellSense digital image processing software. Emission intensities were analysed in triplicate using ImageJ software.

4.7 Electrochemistry

Cyclic voltammetry were performed in aqueous 0.5 M KCl at a scan rate of 200 mV s^{-1} with a potential window between -0.2 V and 0.6 V. Electrochemical measurements were carried out using a Metrohm Autolab AUT50324 potentiostat using a 3-electrode setup. A static disc holder (Pine Instruments) enclosing the GC disc was used as working electrode, a saturated Ag/AgCl electrode and a graphite rod were used as reference and counter electrodes respectively. The electrochemical cell consisted of a beaker with a custom-made Teflon cap and all solutions were degassed with Argon gas prior to measurement.[33] Ferrocene binding experiments were performed by immersion of GC electrodes in a 5.0 mM solution of ferrocene in MeOH for 45 mins. Samples were rinsed gently with DI water to remove unbound ferrocene prior to cyclic voltammetry measurements.

References

1. Gong, T.; Zhou, Y.; Sun, L.; Liang, W.; Yang, J.; Shuang, S.; Dong, C., Effective adsorption of phenolic pollutants from water using β-cyclodextrin polymer functionalized Fe3O4 magnetic nanoparticles. *RSC Adv.* **2016,** *6* (84), 80955-80963.
2. Zhao, F.; Repo, E.; Yin, D.; Meng, Y.; Jafari, S.; Sillanpää, M., EDTA-Cross-Linked β-Cyclodextrin: An Environmentally Friendly Bifunctional Adsorbent for Simultaneous Adsorption of Metals and Cationic Dyes. *Environ. Sci. Tech.* **2015,** *49* (17), 10570-10580.
3. Aïcha, G.; Vincent, H.; Frédéric, T.; Claire-Marie, P.; Christine, I.; Jean-Marc, B., Elaboration of antibiofilm surfaces functionalized with antifungal-cyclodextrin inclusion complexes. *FEMS Immunol. Med. Microbiol.* **2012,** *65* (2), 257-269.
4. Hu, Q.-D.; Tang, G.-P.; Chu, P. K., Cyclodextrin-Based Host–Guest Supramolecular Nanoparticles for Delivery: From Design to Applications. *Acc. Chem. Res.* **2014,** *47* (7), 2017-2025.
5. Zhang, Y.; Xu, H.; Ma, X.; Shi, Z.; Yin, J.; Jiang, X., Self-Assembly of Amphiphilic Anthracene-Functionalized β-Cyclodextrin (CD-AN) through Multi-Micelle Aggregation. *Macromol. Rapid Commun.* **2016,** *37* (12), 998-1004.
6. Park, I.-K.; von Recum, H. A.; Jiang, S.; Pun, S. H., Supramolecular Assembly of Cyclodextrin-Based Nanoparticles on Solid Surfaces for Gene Delivery. *Langmuir* **2006,** *22* (20), 8478-8484.
7. Li, H.; Meng, B.; Chai, S.-H.; Liu, H.; Dai, S., Hyper-crosslinked β-cyclodextrin porous polymer: an adsorption-facilitated molecular catalyst support for transformation of water-soluble aromatic molecules. *Chem. Sci.* **2016,** *7* (2), 905-909.
8. Raoov, M.; Mohamad, S.; Abas, M. R., Synthesis and Characterisation of β-Cyclodextrin Functionalized Ionic Liquid Polymer as a Macroporous Material for the Removal of Phenols and As(V). *Int. J. Mol. Sci.* **2014,** *15* (1), 100-119.
9. Voncina, B.; Le Marechal, A. M., Grafting of cotton with β-cyclodextrin via poly(carboxylic acid). *J.Appl. Polym. Sci.* **2005,** *96* (4), 1323-1328.

10. Shi, Y.; Goodisman, J.; Dabrowiak, J. C., Cyclodextrin Capped Gold Nanoparticles as a Delivery Vehicle for a Prodrug of Cisplatin. *Inorg. Chem.* **2013,** *52* (16), 9418-9426.
11. Diget, J. S.; Petersen, H. N.; Schaarup-Jensen, H.; Sørensen, A. U.; Nielsen, T. T.; Pedersen, S. U.; Daasbjerg, K.; Larsen, K. L.; Hinge, M., Synthesis of β-Cyclodextrin Diazonium Salts and Electrochemical Immobilisation onto Glassy Carbon and Gold Surfaces. *Langmuir* **2012,** *28* (49), 16828-16833.
12. Adenier, A.; Barré, N.; Cabet-Deliry, E.; Chaussé, A.; Griveau, S.; Mercier, F.; Pinson, J.; Vautrin-Ul, C., Study of the spontaneous formation of organic layers on carbon and metal surfaces from diazonium salts. *Surf. Sci.* **2006,** *600* (21), 4801-4812.
13. Angione, M. D.; Duff, T.; Bell, A. P.; Stamatin, S. N.; Fay, C.; Diamond, D.; Scanlan, E. M.; Colavita, P. E., Enhanced Antifouling Properties of Carbohydrate Coated Poly(ether sulfone) Membranes. *ACS Appl. Mater. Interfaces* **2015,** *7* (31), 17238-17246.
14. Esteban-Tejeda, L.; Duff, T.; Ciapetti, G.; Daniela Angione, M.; Myles, A.; Vasconcelos, J. M.; Scanlan, E. M.; Colavita, P. E., Stable hydrophilic poly(dimethylsiloxane) via glycan surface functionalisation. *Polymer* **2016,** *106*, 1-7.
15. Hicks, J. M.; Wong, Z. Y.; Scurr, D. J.; Silman, N.; Jackson, S. K.; Mendes, P. M.; Aylott, J. W.; Rawson, F. J., Tailoring the Electrochemical Properties of Carbon Nanotube Modified Indium Tin Oxide via in Situ Grafting of Aryl Diazonium. *Langmuir* **2017,** *33* (20), 4924-4933.
16. Jayasundara, D. R.; Cullen, R. J.; Colavita, P. E., In Situ and Real Time Characterisation of Spontaneous Grafting of Aryldiazonium Salts at Carbon Surfaces. *Chem. Mater.* **2013,** *25* (7), 1144-1152.
17. Small, L. J.; Hibbs, M. R.; Wheeler, D. R., Spontaneous Aryldiazonium Film Formation on 440C Stainless Steel in Nonaqueous Environments. *Langmuir* **2014,** *30* (47), 14212-14218.
18. Zen, F.; Angione, M. D.; Behan, J. A.; Cullen, R. J.; Duff, T.; Vasconcelos, J. M.; Scanlan, E. M.; Colavita, P. E., Modulation of Protein Fouling and Interfacial Properties at Carbon Surfaces via Immobilisation of Glycans Using Aryldiazonium Chemistry. *Sci. Rep.* **2016,** *6*, 24840.
19. Tripodo, G.; Wischke, C.; Neffe, A. T.; Lendlein, A., Efficient synthesis of pure monotosylated beta-cyclodextrin and its dimers. *Carbohydr. Res.* **2013,** *381*, 59-63.
20. Liu, Y.; Fan, Z.; Zhang, H.-Y.; Diao, C.-H., Binding Ability and Self-Assembly Behavior of Linear Polymeric Supramolecules Formed by Modified β-Cyclodextrin. *Org. Lett.* **2003,** *5* (3), 251-254.
21. Liu, Y.; Fan, Z.; Zhang, H.-Y.; Yang, Y.-W.; Ding, F.; Liu, S.-X.; Wu, X.; Wada, T.; Inoue, Y., Supramolecular Self-Assemblies of β-Cyclodextrins with Aromatic Tethers: Factors Governing the Helical Columnar versus Linear Channel Superstructures. *J. Org. Chem.* **2003,** *68* (22), 8345-8352.
22. Liu, Y.; You, C.-C.; Zhang, M.; Weng, L.-H.; Wada, T.; Inoue, Y., Molecular Interpenetration within the Columnar Structure of Crystalline Anilino-β-cyclodextrin. *Org. Lett.* **2000,** *2* (18), 2761-2763.
23. Eftink, M. R.; Andy, M. L.; Bystrom, K.; Perlmutter, H. D.; Kristol, D. S., Cyclodextrin inclusion complexes: studies of the variation in the size of alicyclic guests. *J. Am. Chem. Soc.* **1989,** *111* (17), 6765-6772.
24. Harries, D.; Rau, D. C.; Parsegian, V. A., Solutes Probe Hydration in Specific Association of Cyclodextrin and Adamantane. *J. Am. Chem. Soc.* **2005,** *127* (7), 2184-2190.
25. Soto Tellini, V. H.; Jover, A.; García, J. C.; Galantini, L.; Meijide, F.; Tato, J. V., Thermodynamics of Formation of Host−Guest Supramolecular Polymers. *J. Am. Chem. Soc.* **2006,** *128* (17), 5728-5734.
26. Myles, A.; Haberlin, D.; Esteban-Tejeda, L.; Angione, M. D.; Browne, M. P.; Hoque, M. K.; Doyle, T. K.; Scanlan, E. M.; Colavita, P. E., Bioinspired Aryldiazonium Carbohydrate Coatings: Reduced Adhesion of Foulants at Polymer and Stainless Steel

Surfaces in a Marine Environment. *ACS Sustainable Chem. Eng.* **2018,** *6* (1), 1141-1151.
27. Bonini, M.; Rossi, S.; Karlsson, G.; Almgren, M.; Lo Nostro, P.; Baglioni, P., Self-Assembly of β-Cyclodextrin in Water. Part 1: Cryo-TEM and Dynamic and Static Light Scattering. *Langmuir* **2006,** *22* (4), 1478-1484.
28. Cullen, R. J.; Jayasundara, D. R.; Soldi, L.; Cheng, J. J.; Dufaure, G.; Colavita, P. E., Spontaneous Grafting of Nitrophenyl Groups on Amorphous Carbon Thin Films: A Structure–Reactivity Investigation. *Chem.Mater.* **2012,** *24* (6), 1031-1040.
29. Socrates, G., Infrared and Raman Characteristic Group Frequencies: Tables and Charts. John Wiley & Sons: **2001**.
30. Mbuli, B. S.; Nxumalo, E. N.; Mhlanga, S. D.; Krause, R. W.; Pillay, V. L.; Oren, Y.; Linder, C.; Mamba, B. B., Development of antifouling polyamide thin-film composite membranes modified with amino-cyclodextrins and diethylamino-cyclodextrins for water treatment. *J. Appl. Polym. Sci.* **2014,** *131* (8).
31. Yu, Z.; Pan, Y.; He, Y.; Zeng, G.; Shi, H.; Di, H., Preparation of a novel anti-fouling [small beta]-cyclodextrin-PVDF membrane. *RSC Adv.* **2015,** *5* (63), 51364-51370.
32. Nietzold, C.; Dietrich, P.; M; Lippitz, A.; Panne, U.; Unger, W.; E; S, Cyclodextrin & ferrocene host & guest complexes on silicon oxide surfaces. *Surf. Interface Anal.* **2016,** *48* (7), 606-610.
33. Behan, J. A.; Stamatin, S. N.; Hoque, M. K.; Ciapetti, G.; Zen, F.; Esteban-Tejeda, L.; Colavita, P. E., Combined Optoelectronic and Electrochemical Study of Nitrogenated Carbon Electrodes. *J Phys. Chem. C* **2017,** *121* (12), 6596-6604.
34. Zen, F.; Angione, M. D.; Behan, J. A.; Cullen, R. J.; Duff, T.; Vasconcelos, J. M.; Scanlan, E. M.; Colavita, P. E., Modulation of Protein Fouling and Interfacial Properties at Carbon Surfaces via Immobilisation of Glycans Using Aryldiazonium Chemistry. *Sci. Rep.* **2016,** *6*, 24840.
35. Combellas, C.; Jiang, D.-e.; Kanoufi, F.; Pinson, J.; Podvorica, F. I., Steric Effects in the Reaction of Aryl Radicals on Surfaces. *Langmuir* **2009,** *25* (1), 286-293.
36. Combellas, C.; Kanoufi, F.; Pinson, J.; Podvorica, F. I., Sterically Hindered Diazonium Salts for the Grafting of a Monolayer on Metals. *J. Am. Chem. Soc.* **2008,** *130* (27), 8576-8577.
37. Greenwood, J.; Phan, T. H.; Fujita, Y.; Li, Z.; Ivasenko, O.; Vanderlinden, W.; Van Gorp, H.; Frederickx, W.; Lu, G.; Tahara, K.; Tobe, Y.; Uji-i, H.; Mertens, S. F. L.; De Feyter, S., Covalent Modification of Graphene and Graphite Using Diazonium Chemistry: Tunable Grafting and Nanomanipulation. *ACS Nano* **2015,** *9* (5), 5520-5535.
38. Zhao, H.; Li, D.; Dong, G.; Duan, L.; Liu, X.; Wang, L., Volatilize-Controlled Oriented Growth of the Single-Crystal Layer for Organic Field-Effect Transistors. *Langmuir* **2014,** *30* (40), 12082-12088.
39. Chretien, J.-M.; Ghanem, M. A.; Bartlett, P. N.; Kilburn, J. D., Covalent tethering of organic functionality to the surface of glassy carbon electrodes by using electrochemical and solid-phase synthesis methodologies. *Chemi. Eur. J.***2008,** *14* (8), 2548-2556.

Chapter VII

Ongoing Work with Preliminary Results

Included in this chapter are the preliminary results of ongoing projects related to this PhD project :
Discussed are the results of a collaborative project involving lactose coatings on salmon farm netting in a marine biofouling study for complex 3-dimensional structures with regards to biomass accumulation and ease of cleaning. The aim of this study was to investigate the effect of a novel non-toxic antifouling coating applied to nylon netting when deployed in a salmon farm in the southwest of Ireland. This coating had proved effective at reducing protein adsorption at various surfaces and at reducing adhesion of marine foulants on topographically smooth coupons of nylon-6 in our previous studies.
Secondly the preliminary results of biofuel cell start-up in colaboration with Fréderic Barriére of the University of Rennes are discussed. An investigation on geobacter adhesion and growth on anodic graphite rods when modified with Lactosides and mannosides by aryldiazonium grafting is included.
Finally the synthesis of an open chain anomericaly modified aminophenol-maltoheptaose diazonium precursor compound was attempted through the selective acetylation and acetolysis of beta-cyclodextrin. This synthesis proved difficult due to the excessive anomeric cleavage observed with smaller fragments propagated through each modification step. These smaller chain oligosaccharides proved laborious to purify and resulted in low yields. A sample batch was synthesised and used as a proof of concept in grafting studies on amorphous carbon surfaces but due to time constraints repeat synthesis for full characterisation was not attempted.

The data presented in this chapter are in part from ongoing collaborative projects with contributions listed as follows:

The study of lactose coating in marine biofouling mitigation for nylon netting is a part of the larger MaREI project in collaboration with TK Doyle and D Haberlin. Field study setup, material sampling, biological species identification and biomass quantitation in addition to with light microscopy were performed by D Hablerlin.

Microbial fuel cell studies were performed in the host institution of Université de Rennes 1, under the supervision of Prof. Frédéric Barrière and was funded in part by the Ulysses Fellowship. Fuel cells set-up and analysis was assisted with by Mr. Thomas Flinois.

1 Lactose coating for Marine Biofouling

Biofouling on finfish cages is an extensive problem in modern aquaculture.[1-6]. To investigate the potential efficacy of lactose coating on netting as a non-toxic antifouling agent in salmon farming, nylon net samples were functionalised by spontaneous aryldiazonium grafting following a preconditioning surface hydroxylation step in formaldehyde solution as described in chapter VI.[7] Netting panels were set up and an immersion field study was performed over two sites with biofilm growth monitored over a 31 day period.

1.1 Netting Functionalisation and Field Study Setup

The nylon panels were immersed in deionised water and rinsed under agitation approximately 10 times to remove dust and debris prior to coating. The coating process was carried out as previously described,[7] whereby netting panels were incubated in a formaldehyde solution, containing catalytic amounts of hypophosphorous acid, at 30 °C overnight. Panels were rinsed thoroughly with deionised water and functionalised via immersion in freshly prepared 1.0 mM solutions of lactoside-bearing aryldiazonium cations generated *in situ* from the corresponding amine **6**. Samples were incubated in the dark for 1 h in the diazonium salt solution, rinsed in deionised water and then stored wet in sealed polyethylene bags (Ziploc®) until deployment at the salmon farm within 24 h of functionalisation. Coating on nylon-6 with lactoside-bearing aryldiazonium cations has previously been demonstrated to result in an increase in hydrophilicity and similarly functionalisation was confirmed via lectin binding studies as described previously.[7]

Over a 31 day period from August 8th to September 7th, 2015, net panels were deployed at Roancarrig in Bantry Bay (51.657°N, 9.765°W), southwest Ireland. To investigate the effect of the antifouling coating, 24 panels were deployed at the Roancarrig salmon farm in two 12 panel arrays, with 6 treated and 6 untreated panels in each array. A treated and untreated panel was removed from each array after 2, 4, 6, 11, 20 and 31 days of immersion.

Each panel was removed from the array and placed directly into a Ziploc® bag filled with ambient sea water and sealed. The panels were transported back to the lab in a cool box, 2 hours after sampling. To test the effect of treatment of the nets on ease of cleaning, each panel was rinsed using filtered (10 µm and UV

filter) sea water. Each panel was rinsed under a pump feed hose, held 25 cm above the sample for 20 s, at a constant flowrate of 0.25 l/s. The fouling material and organisms rinsed from the net panel was caught in a 180 µm sieve. A small subsample of each net panel was removed, placed in a sterile vial and used for ATP analysis.

1.2 Macrofouling studies

Initial results obtained by D. Haberlin found no significant difference in macro fouling effects between modified and control nylon netting samples post immersion. Mean fouling biomass released from netting panels was observed to not be significantly different between control and modified samples with algae, hydroid and amphipod species present on samples at various stages. The attachment of macroscopic foulants appears to be facilitated by the 3D structure of nylon netting leading to stable scaffolds which provide significant anchorage for adhesion (**Figure 7.1**)

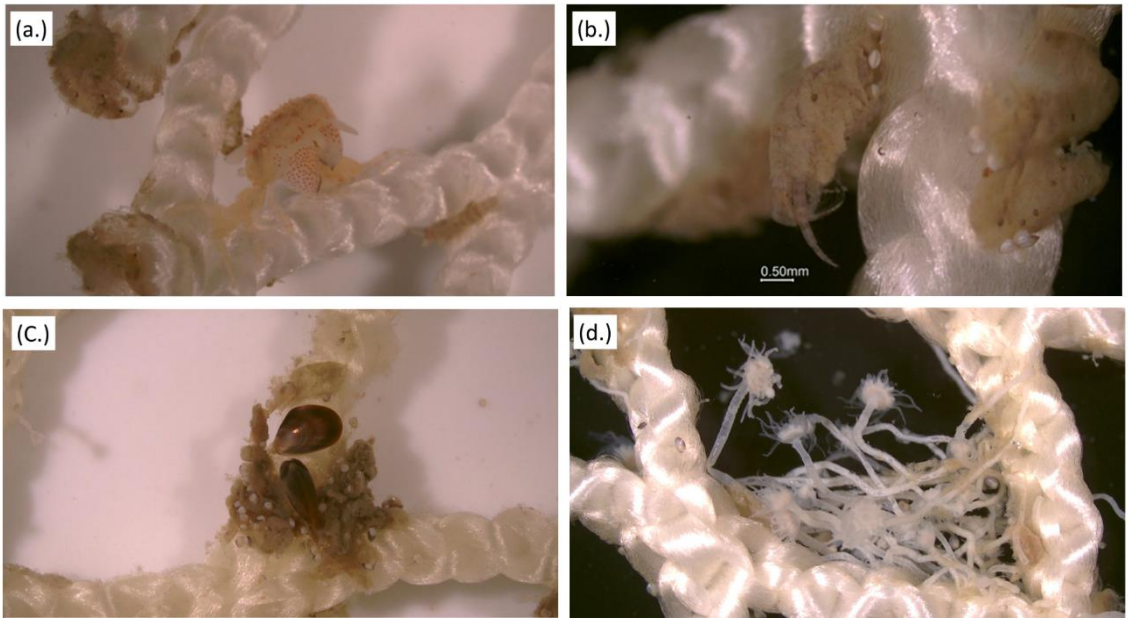

Figure 7.1. Visible light Microscopy of nylon netting following marine immersion studies. **(a.)** Lactose modified nylon samples after 2 days immersion in marine environment. Caprellid amphipods are observed attached to nylon netting at this period. **(b.)** Nylon netting following 6 day immersion with amphipods building structuress from algae and diatoms. **(c.)** Heavily foulied lactose coated nylon fiber junction. Muscles are oserved growing well at these junctions **(d.)** Hydroids growing on modified nylon scallfold. They are observed wrapping around nylon netting for anchorage. Image courtesy of Damien Haberlin.

It was observed that amphipods (ghost shrimp) quickly adhere to solid nylon (**Figure 7.1 a**) netting and quickly enhance fouling by building structures from algae and diatomic materials (**Figure 7.1 b**).[8] It is also seen that macro fouling species such as these are not deterred by lactose coating on materials with high surface area as seen on nylon netting samples which offer good protection from current flow at netting junctions, hence allowing for rapid adhesion of macro fouling species (**Figure 7.1 c**). Ectopleura hydroids, quickly develop through asexual reproduction, growing a root-like system of stolons to adhere to the net (F**igure 7.1 d**).[8] It can be concluded from these results that the modification with aryldiazonium lactoside is not sufficient on its own to deter macrofouling on nylon netting samples in the marine environment.

1.2.1 ATP Determination of Microfouling

The level of microfouling on samples was monitored by measuring the concentration of adenosine triphosphate (ATP) released by the netting samples, as an indicator of the amount of biomass? strongly bound to the surface.[9] A commercial luciferase assay and luminometer were used (Aquasnap Total Water, Hygiena). Approximately 1 cm long sections of netting were cut from three different locations in each netting panel. The cutting was rinsed lightly to remove adhered macro foulants with all samples treated under the same conditions. Rinsed cuttings were suspended in 30 mL of deionised water in sterile centrifuge tubes and then sonicated for 10 min. The value of RLU was determined for each water sample and converted to ATP concentrations. Water samples were diluted where necessary to bring the ATP concentration within the linear range of the assay. Following ATP analysis the cuttings were removed from the solution, dried under argon and their mass determined to normalise ATP determinations on individual cuttings. Results are reported as nmol of ATP released per gram of dry netting (nmol/g_{net}). The levels of ATP increased significantly with immersion time after 11 or more days immersion (**Figure 7.2**). The treatment did not appear to influence ATP levels from 2, 4 or 6 days immersion. For all studies, post 12 day immersion, treated panels display less ATP released by sonication than untreated panels, with significant differences observed after 20 and 31 days immersion.

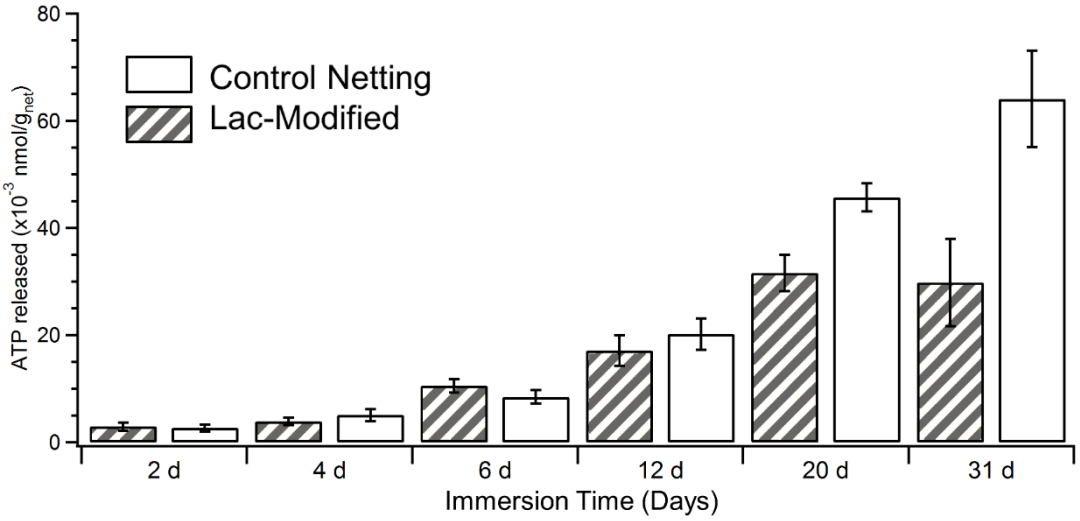

Figure 7.2. Comparison of ATP concentrations combined over two sites for nylon netting samples (both lactose modified and unmodified controls) immersed in a marine environment with samples collected at indicated intervals over a total period of 31 days.

The reduction in ATP content released by netting samples is in good agreement with results obtained at smooth nylon surfaces and suggests a difference in microfoulant retention after rinsing.[7] This result indicates that resistance to biomass retention is retained on fibrous nylon substrates albeit limited to microfoulants.

1.3 Future studies in a marine environment

Future work involves further biological and surface characterisation of modified 3D materials and includes potential combination of surface saccharide modification with other fouling reduction technologies such as surface topographical modification and bubble curtain technologies, in attempts to produce a usable biofouling resistant material for marine technologies. [10-11]

1.4 Materials

Lactose-aminophenol diazonium precursor compound **6** was prepared as described in chapter II. Formaldehyde solution for molecular biology ≥36.0% in H_2O, hypophosphorous acid solution 50%wt. in H_2O were purchased from sigma Aldrich. Aquasnap Total ATP test strips were purchased from Water Technology Ireland. Nylon netting for modification setup frames were provided by D. Haberlin.

2 Microbial Biofuel Cell Start-Up

Microbial fuel cells (MFC's) are devices consisting of bacterial catalysts which convert chemical energy in the form of organic or inorganic matter, to electrical energy through metabolic processes of electrode adhered bacteria. MFC's offer several promising applications in green energy production, however their performances in power generation is considered too modest to be economically viable. Improved interfacial adhesion of biofilms to the electrodes is expected to enhance performance of MFC's.[12-13] Geobacter are a species of anaerobic electroactive gram negative bacteria capable of metabolising acetate to produce electricity.[14] In nature most bacteria attach to and live in close association to surfaces.[15-16] This is generally achieved by gram negative bacteria by fimbrial adhesions to proteinatious membranes or saccharide surfaces.[16] Bacterial adhesion in a complex medium such as anaerobic waste water sludge is expected to follow a progression of adhesion and may involve several pioneering species attaching to an anodic surface prior to the target geobacter film formation.[17] In this study we investigate the effect of mannose and lactose coating of graphitic anodes has on fuel cell start-up.

2.1 Setup graphite modification

Fuel cells were set up as shown in **Figure 7.3 a**, with assistance from T. Flinois. Initially graphite rods of diameter 4.5 mm were cut to a suitable size (10 cm) and polished with micromesh sandpaper (grade 12,000) to remove any adhered contaminants. These electrodes were then sonicated for 5 min in each acetone, absolute ethanol and ultrapure water to remove loosely adhered carbon. One graphite rod was then subjected to chronoamperometry at -0.6 V vs SCE for 35 s in a freshly prepared 1 mM mannoside diazonium solution[18] and another in 1 mM lactoside diazonium solution[7, 11] to produce a mannose modified anode and a lactose modified anode respectively (**Figure 7.3 b & c**). A bare control electrode was prepared by sanding, sonication and immersion in ultrapure water prior to fuel cell set up. The cells consisted of a simple H-type setup with two compartments for each anodic and cathodic solutions separated by a PES membrane which allowed for ion exchange processes. The anodic compartment was equipped with two apertures for easy gas purging and electrochemical analysis. The anodic fuel cell culture was composed of 50 mL phosphate buffered

saline solution (pH 7.4), 150 mL anaerobic waste water sludge (sampled from Rennes waste water treatment plant, 2 Chemin de la Prevalaye, 35000 Rennes, France), 0.5 g of sodium acetate and 50 mL of pure geobacter culture. This solution was degassed with argon for 15 min. The cathode cell contained 250 mL of a 0.1 M sodium ferricyanide solution in PBS and a graphite electrode with surface area in vast excess to that of the anode.

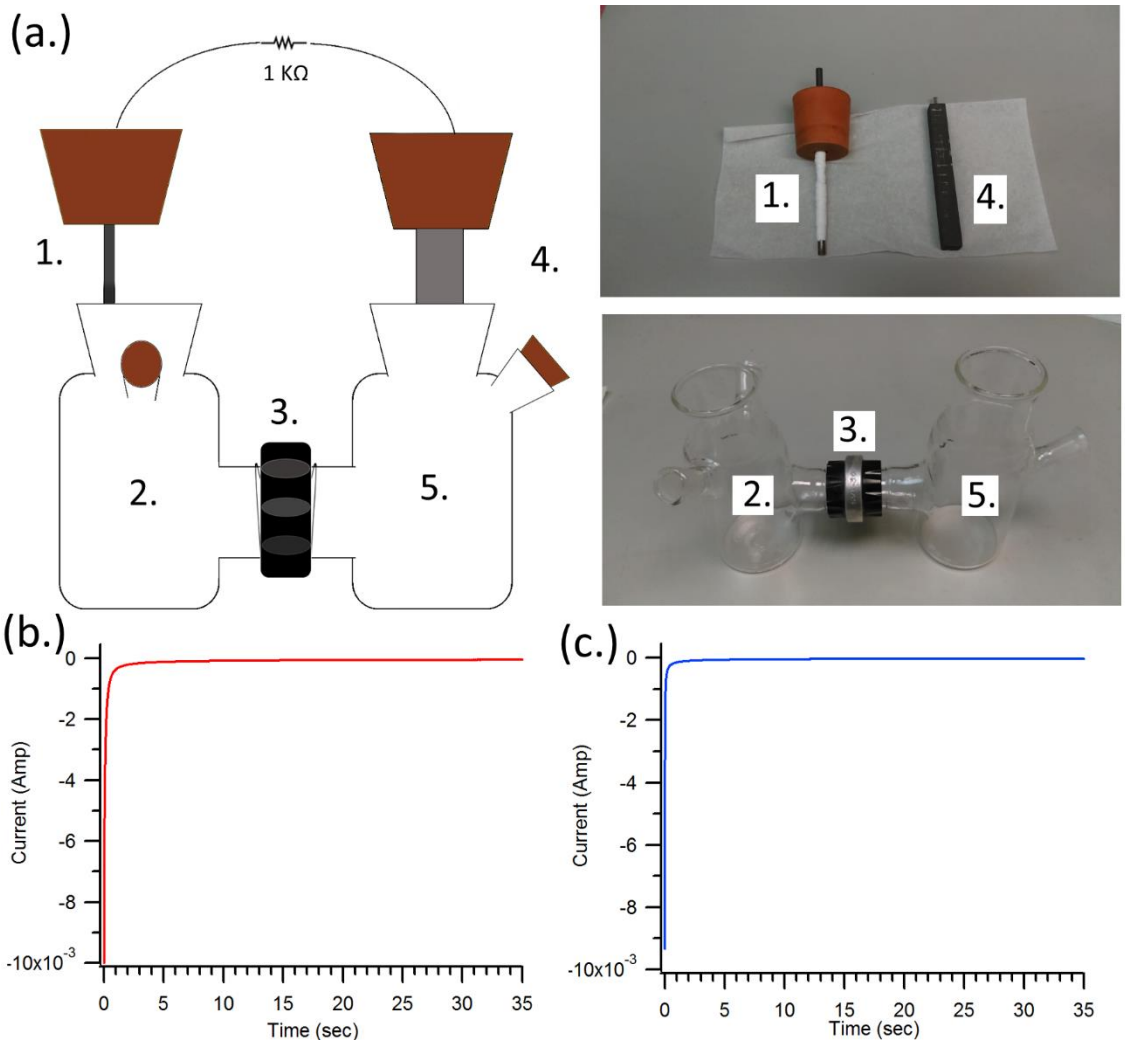

Figure 7.3. (a.) Two chamber H-type fuel cell set-up shopwing individual components: 1. graphite anode (bare control, mannose grafted or lactose grafted); anodes were covered in Teflon to standardise the surface area exposed on each electrode, 2. Anodic cell with apatures for gas sparging/ insertion of reference electrodes (contains geobacter spiked waste water solution with acetate nutriants), 3. Bridging connector with PES ion exchange membrane. 4. Graphite cathode, Large surface area 5. Cathodic cell (containing $Na_4Fe(CN)_6$ 0.1M in PBS solution). The cell is completed by a bridging load consisting of a 1 KΩ resistor. **(b.)** Chronoamperogram of graphite anode in mannoside diazonium solution (-0.6 V vs SCE for 35 s). **(c.)** Chronoamperogram of graphite anode in lactoside diazonium solution (-0.6 V vs SCE for 35 s).

Each cell was sealed with a rubber stopper and the circuit was completed by connecting each electrode *via* conductive wire to a load consisting of a 1 kΩ resistor. The anode was covered in foil to prevent algal growth and the cells were incubated in a water bath at 30 °C.

2.1.1 MFC Start-up Monitoring

The progress of each cell (control, mannose modified lactose modified) was monitored by cyclic voltammetry at various time intervals over a month long period. Shown in **Figure 7.4 a** are cyclic voltammograms of microbial fuel cells vs SCE in the potential window of -0.6 V to 0 V at a scan speed of 0.001 V s^{-1} for each MFC. Measurements were taken after 4, 6, 11, 13, 16, 20, and 26 days after initial set-up. Each cell was "fed" by the addition of a 4 mL of 2.5 M sodium acetate solution at 4, 6, 13, 16, 20, and 26 days from the initial MFC set-up. Measurements were made in the morning for each cell before and after spiking of the anodic solution with sodium acetate to observe the differences between an acetate depleted sample and acetate saturated samples. An exception to this is seen at the 11 day time point where no acetate was added as acetate oxidation peaks were observed suggesting sufficient nutrients were present for fuel cell growth. Acetate was not added so as to not over saturate the MFC's. Control cells showed no significant acetate oxidation behaviour at any point in the test period. This result implies poor geobacter adhesion and/ or growth occurs at an unmodified graphite anode. For the MFC with a mannose terminated anode, little oxidative behaviour is observed in the first 6 days post fuel cell set-up. After 11 days however, two strong peaks appear which are attributed to the oxidation of acetate by electroactive bacterial species at the anode surface. The presence of multiple peaks suggests that there are different metabolic processes for acetate occurring at the anode surface likely arising from two or more competing surface bound species. Peaks observed at -0.1 V are found to decrease over time with a significant loss in intensity at 13 days, when compared to just two days prior on day 11. This is potentially the effect of an electroactive pioneering species at the surface, which is displaced by the longer lived geobacter strain giving rise to the oxidative peak observed at -0.4 V. This late stage oxidative behaviour corresponds well with anodic geobacter based MFC's reported previously by Picot *et al.*[19]

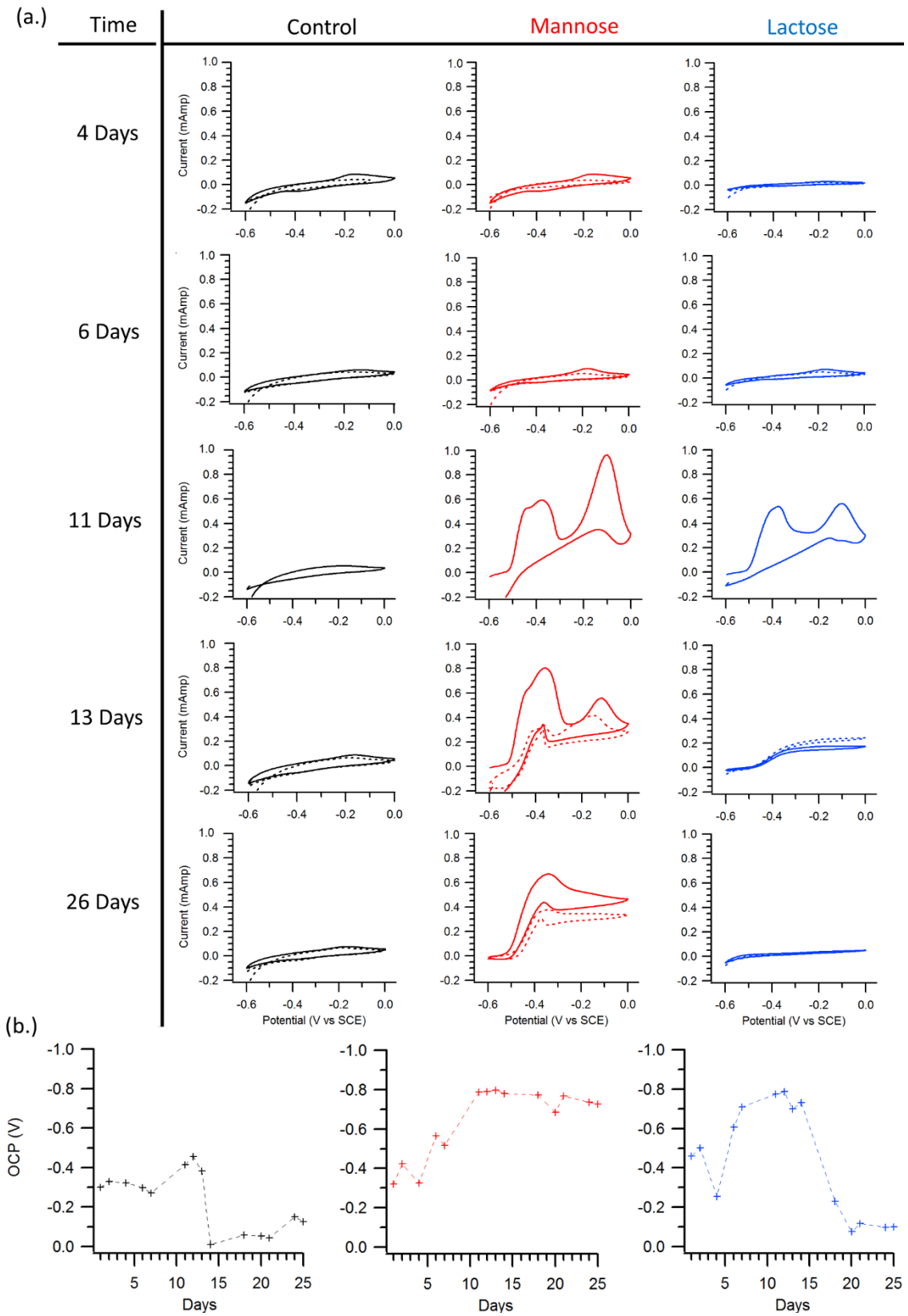

Figure 7.4. (a.) Cyclic voltammograms of fuel cells with graphite anodes (bare control, black; mannose modified, red; lactose modified, blue) in the window -0.6 to 0 V vs SCE at scan rate 1mVs^{-1} at various time intervals (4, 6, 11, 13 and 26 days) to monitor MFC progress. Dashed traces are fuel cells without any acetate addition, solid lines are after saturation by addition of 4 mL sodium acetate (2.5 M). **(b.)** Open circuit potential OCP of control (black), mannose (red) and lactose cells (blue) measured over 25 days.

The presence of this oxidative behaviour is taken as an indicator of successful cultivation of geobacter at the mannose modified anode surface at 26 days.
The same trend of multiple peaks in oxidative processes potentially indicative of multispecies biofilm growth processes is also observed in the start-up stages of the lactoside modified MFC with oxidative behaviour up to 11 days post set-up with significant depletion in oxidation peak behaviour post the 13 day time point leading to total fuel cell failure after 16 days. There are several possible reasons for the sudden failure of this fuel cell including potential biomass collapse with bacterial mass reaching an unsustainable threshold for adhesion to the anode due to weak attachment at the modified surface.
Additionally the open circuit potentials (OCP) of the bacterial fuel cell were taken at various time points in the study (**Figure 7.4 b**). OCP's were measured using a standard multimeter and were taken as the value read at 20 s after connecting the device. In the case of days where acetate was added, OCP was measured prior to addition. All three MFC's initially show an OCP of between -0.3 V and -0.4 V with the mannose and lactose modified MFC's showing rapid increase in absolute potential measured after 6 days. Each cell increased in output up to 10 days whereby the mannose and lactose cells peaked between -0.75 V and -0.80 V. The trends observed by cyclic voltammetry for the mannose and lactose modified MFC are corroborated by this data with significant growth in OCP output observed up to 15 days in each cell. The mannose modified sample retained a high output potential throughout and the lactose modified MFC peaked at 13 days followed by a significant drop off in output potential consistent with the loss of electroactive surface species. The unmodified control cell did not indicate significant geobacter growth at any stage in this experiment. These results are promising indicators that the modification of graphite anodes with terminal saccharide units has the potential to enhance geobacter adhesion/ growth from anaerobic waste water media and hence have the potential to enhance the performance of MFC's, with mannose terminated graphite especially providing a promising support surface for microbial growth.

2.2 Materials and methods

Fuel-cell equipment and chemicals were provided by Prof. Frédéric Barriere at Université de Rennes. All commercially available chemical agents were

purchased from sigma Aldrich. Graphite rods used as anodes were purchased from Morgan Advanced Materials. Lactose-aminophenol aryldiazonium precursor **6** was synthesised as described previously (**Chapter II**)

2.2.1 Aminophenol-mannoside synthesis

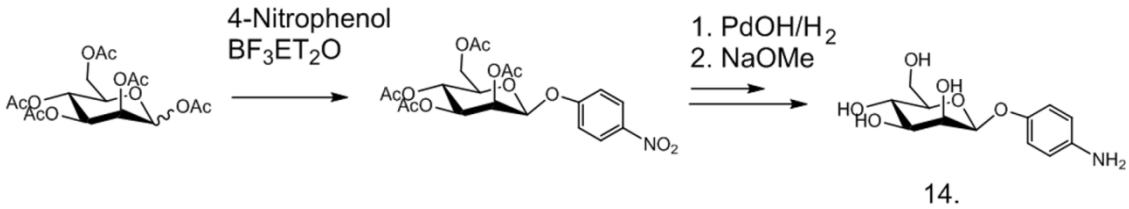

Scheme 7.1. Synthesis of 4-aminophenol-α-mannopyranose aryldiazonium precursor **14**.

Mannose-aminophenol precursor was prepared following previously published methods (**Scheme 7.1**).[18] Briefly 4-nitrophenol is glycosylated directly with peracetylated mannose *via* lewis-acid activation by BF_3Et_2O.[20] The resulting p-nitrophenyl-tetraacetyl-a-mannopyranoside is subsequently reduced by use of a Pd catalyst and deprotected by addition of sodium methoxide in MeOH to yield the aminophenol-mannoside diazonium precursor **14**. [18]

^{1}H-NMR (400 MHz, D_2O): δ ppm: 6.87 (2H, d, *J* = 8.7 Hz, ArH), 6.68 (2H, d, *J* = 8.6 Hz, ArH), 5.28 (1H, d, *J*= 1.6 Hz , H1), 4.00 (1H, dd, *J*= 1.3 Hz, *J*= 3.2 Hz, H2), 3.86 (1H, dd, *J*= 3.2 Hz, *J*= 9.1 Hz, H3), 3.70-3.55 (4H, m,H4, H6, H6', H5)

2.2.2 Electrochemical analysis

Chronoamperometry and cyclic voltammetry was performed on cells a using a Metrohm Autolab AUT50324 potentiostat using a saturated calomel electrode (SCE) as reference electrode. A platinum wire was used as the counter electrode for chronoamperometry. OCP of fuel cells was measured using a multimeter.

2.3 Further studies in MFC development

Due to limited availability of MFC chambers only one MFC modified by each carbohydrate coating (mannose and lactose) and one control cell were set up. To remediate this in future trials a smaller H-type cell was designed (~82.5 mL volume) and 10 cells were produced from transparent plastic (**Figure 7.5**). Replicate MFC's start-up experiments are in progress with studies performed by

Dr. A. Iannaci of the Colavita Group, using saccharide modified graphite anodes. The resulting microbial colonies are to be characterised by high resolution microscopy and DNA sequencing to further characterise MFC growth processes and dominant species.

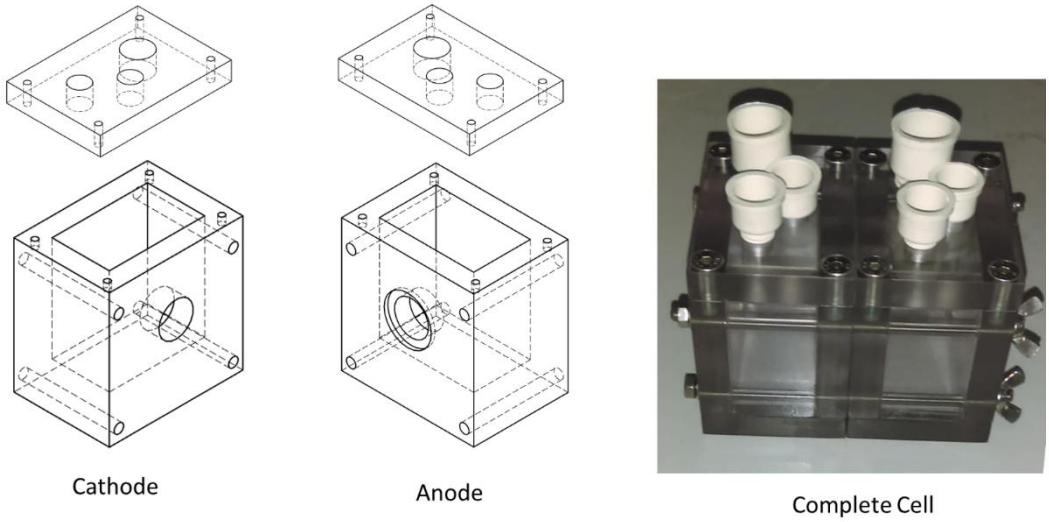

Figure 7.5. Twin cell MFC design for geobacter development on modified graphitic anodes. Cells are connected by threaded rods with a bridging aperature containing PES ion exchange membrane held in place by a nitrile (buna) O-ring. Approximate maximum volume of each cell ~82.5 mL.

3 Maltoheptaose Diazonium Precursor Development

Synthesis of a linear chain maltoheptaose precursor from cyclodextrin was attempted by multistep process (S**cheme 7.2**). Initially peracetylated maltoheptaose was synthesised through a one pot acetylation of β-CD suspended in acetonitrile with a catalytic amount of a Lewis acid (iron trichloride) refluxed at 30 °C for 2 h with subsequent acetolysis achieved by raising the temperature to 70 °C with stirring for an additional 2.5 h. The formation of the heptasaccharide was monitored *via* silica gel TLC with a 20% toluene/ethyl acetate mobile phase. Upon the observation of smaller fragmentation products formation, the reaction was quenched in ice water. From the solid precipitate open chain maltoheptaose was separated from the per-acetylated cyclic compound using silica column with a 20% toluene/ethyl acetate mobile phase. A bromo leaving group was introduced diastereoslectively at the anomeric position through reaction HBr in glacial acetic acid and DCM with stirring at 0 °C 3.5 h. Under anhydrous conditions, this compound was used in the glycosylation of 4-nitrophenol using silver carbonate in pyridine. This product was dried in *vacuo* and purified *via* silica gel column chromatography using 20 % toluene/ethyl acetate as a mobile phase to remove the unreacted 4-nitrophenol in addition to the hemiacetal side product. The major product was found by NMR to be the β-anomer. This product was used to produce a peracetylated aminophenol-maltoheptaose diazonium precursor by reduction of the nitro group to the corresponding amine. This was achieved through the use of a palladium catalyst on activated carbon with a steady stream of H_2 gas bubbled through the oligosaccharide solution in methanol at RT for 3h. The Pd catalyst was removed by filtration through celite and the solid product was extracted from solution by rotary evaporation until dry. To produce the deacetylated aminophenol-maltoheptaose, the peracetylated product was treated under Zemplén conditions.[21]

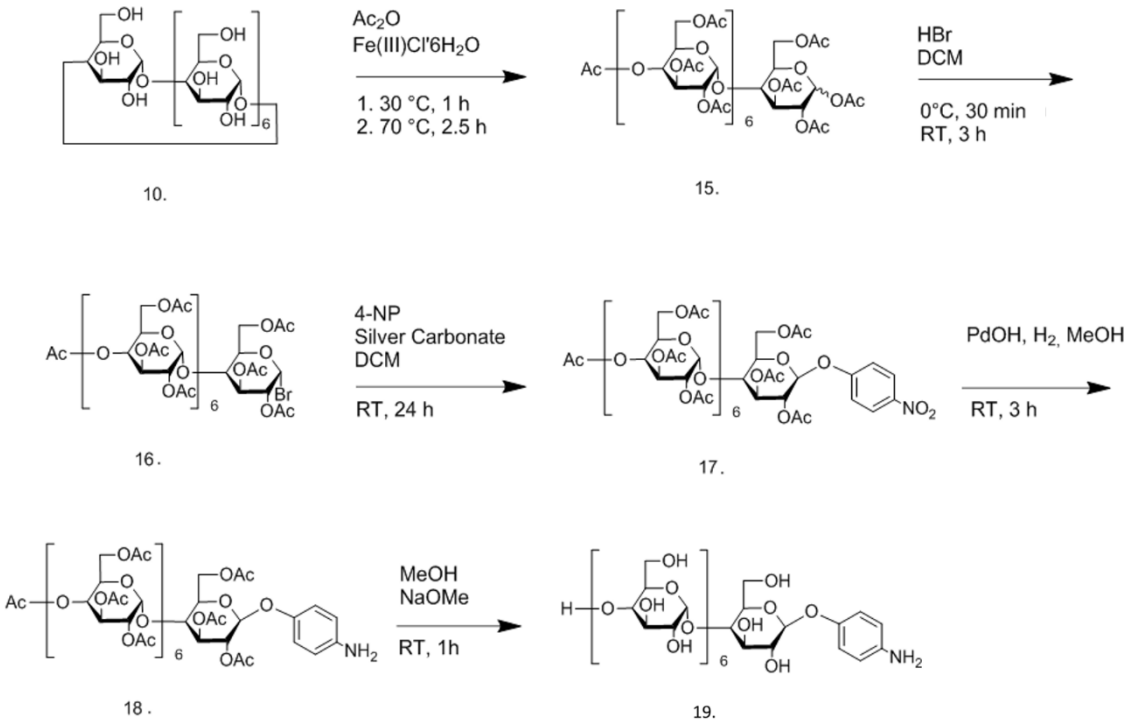

Scheme 7.2. Maltoheptasaccharide-aminophenol precursor synthetic pathway.

3.1 Surface grafting with Maltoheptaose samples

As a proof of concept for oligosaccharide surface modification, significant quantities of both synthesised products, acetyl protected and deprotected heptasaccharide aminophenol, were prepared under spontaneous diazonium conditions (1 mM sugar in HBF_4 with $NaNO_2$). Amorphous carbon sputtered on Ti coated silicon substrates were immersed in the activated solutions, sonicated and IRRAS studies were performed to investigate covalent grafting (**Figure 7.6**)

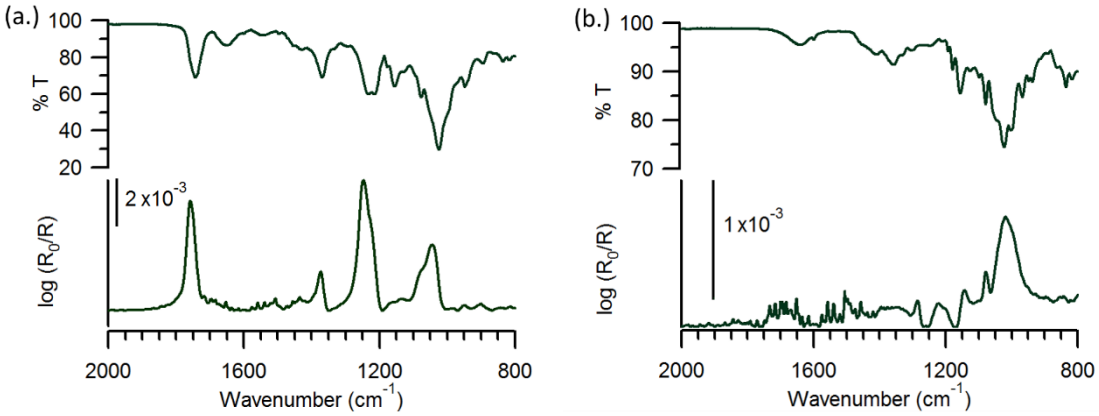

Figure 7.6. FTIR of **(a.)** acetyl protected heptasaccharide and **(b.)** deprotected saccharides, on amorphous carbon subsrtates (IRRAS, bottom trace) with bulk spectra shown for comparison (ATR, Top trace)

From **Figure 7.6 a** we confirm the presence of surface bound acetate and sugar peaks at 1762 cm^{-1}, 1380 cm^{-1}, 1252 cm^{-1} and 1053 cm^{-1}.[22] These peaks agree with similar spectra obtained for smaller acetyl protected disaccharide coatings[7, 18, 22] (see **Chapter III**). We additionally confirm grafting of deprotected sugar species in **Figure 7.6 b.** with peaks observed at 1082 cm^{-1}, 1052 cm^{-1} and 1030 cm^{-1} (corresponding to C-O stretching and O-H vibrations). [22]

3.2 Maltoheptaose Synthesis

2,3,4,6-tetra-*O*-acetyl-α-D-glucopyranosyl-(1,4)-*O*-2,3,6-tri-*O*-acetyl-α-D-glucopyranosyl-(1,4)-*O*-2,3,6-tri-*O*-acetyl-α-D-glucopyranosyl-(1,4)-*O*-2,3,6-tri-*O*-acetyl-α-D-glucopyranosyl-(1,4)-*O*-2,3,6-tri-*O*-acetyl-α-D-glucopyranosyl-(1,4)-*O*-2,3,6-tri-*O*-acetyl-α-D-glucopyranosyl-(1,4)-*O*-1,2,3,6-tetraacetate-D-glucopyranose (15)

β-Cyclodextrin purchased from Sigma-Aldrich (5g, 4.5 mmol) was suspended in Acetic anhydride (50 mL) with Iron (III) Chloride hexahydrate (0.325g) and heated to 30°C with stirring for 2 hours until acetylation was complete. The cyclic saccharide solution was heated to 80 °C to initiate acetolysis and the reaction was monitored by TLC until smaller oligosaccharide side products were seen to form (approx. 1h). Acetic anhydride was removed by pouring the hot solution onto ice water with stirring. The resulting white powder was extracted into DCM which was subsequently washed three times with DI water and with saturated sodium bicarbonate solution. The organic layer was dried with magnesium sulfate and the solid product was recovered in *vacuo* by rotary evaporation. The solid product **15** was purified *via* silica gel column chromatography 20% toluene/EtOAc.. (Yield 4.2g, 45%) **IR** cm^{-1} 1747 (C=O), 1373 (CH_3), 1213 (C-O acetyl), 1019 (C-O saccharide); ^{1}H-NMR (600 MHz, $CDCl_3$), δ 6.25 (1H, d, J_{12}= 3.67 Hz, H-1), 5.37-5.89 (48H, m), 2.29-1.97 (66H, m, 22 x $C(CO)CH_3$), 1.68 (3H, s, $C(CO)CH_3$); HRMS (MALDI, m/z): $[M+Na]^+$ calculated for $C_{88}H_{118}O_{59}Na$ = 2121.6131. Found 2141.6064

2,3,4,6-tetra-*O*-acetyl-α-D-glucopyranosyl-(1,4)-*O*-2,3,6-tri-*O*-acetyl-α-D-glucopyranosyl-(1,4)-*O*-2,3,6-tri-*O*-acetyl-α-D-glucopyranosyl-(1,4)-*O*-2,3,6-tri-*O*-acetyl-α-D-glucopyranosyl-(1,4)-*O*-2,3,6-tri-*O*-acetyl-α-D-glucopyranosyl-(1,4)-*O*-2,3,6-tri-*O*-acetyl-α-D-glucopyranosyl-(1,4)-2,3,6-triacetate–β-D-glucopyranosyl bromide (16)

Under cooling to 0 °C, HBr in AcOH (3 mL) was added drop wise to a solution of **15** (2.0 g, 1 mmol, 1 eq) in DCM (5 mL). After stirring at 0 °C for 3 h the resulting solution was washed three times with iced DI water and saturated sodium bicarbonate solution. The solid product **16** was recrystallised in *vacuo* and the crude product immediately carried over to the next step without further purification. (yield. 1.0 g)

4-nitrophenyl-*O*-2,3,4,6-tetra-*O*-acetyl-α-D-glucopyranosyl-(1,4)-*O*-2,3,6-tri-*O*-acetyl-α-D-glucopyranosyl-(1,4)-*O*-2,3,6-tri-*O*-acetyl-α-D-glucopyranosyl (1,4)-*O*-2,3,6-tri-*O*-acetyl-α-D-glucopyranosyl-(1,4)-*O*-2,3,6-tri-*O*-acetyl-α-D-glucopyranosyl-(1,4)-*O*-2,3,6-tri-*O*-acetyl-α-D-glucopyranosyl-(1,4)-,2,3,6-triacetate-D-glucopyranoside (17)[23]

In flame a dried round bottom flask under N2 **16** (1.0 g crude material) PNP (350 mg, 2.5 mmol) and silver carbonate (700 mg, 2.5 mmol) were suspended in dry pyridine (10 mL). Aluminium foil was placed around the vessel to minimise light exposure. The solution was stirred at RT for 4 h. Following filtration through celite to remove any solids the filtrate was dried under rotary evaporation and extracted into DCM. This organic layer was subsequently washed three times with DI H_2O and three times with saturated sodium bicarbonate solution. The organic layer was evaporated to oil by rotary evaporation and the solid product was precipitated in hexane. The resulting solid was slurried overnight in methanol to remove any remaining PNP. The remaining solid was recovered *via* filtration. The product was purified by silica gel column chromatography, 20% toluene/EtOAc, to produce the β-anomer of **17** (Yield over 2 steps 150 mg) **IR** cm^{-1} 1747 (C=O), 1373 (CH_3), 1213 (C-O acetyl), 1019 (C-O saccharide); ^{1}H-NMR (600 MHz, $CDCl_3$), δ 8.25 (2H, d, *J = 9.52* Hz, Ar-H), 7.10 (2H, d, *J = 9.52* Hz, Ar-H), 5.46-3.90 (49H, m), 2.24-1.27 (66H, m, 22 x C(CO)CH_3); HRMS (MALDI, m/z): $[M+Na]^+$ calculated for $C_{92}H_{119}NO_{60}Na$ = 2220.6189. Found 2220.6294.

4-aminophenyl-*O*-2,3,4,6-tetra-*O*-acetyl-α-D-glucopyranosyl-(1,4)-*O*-2,3,6-tri-*O*-acetyl-α-D-glucopyranosyl-(1,4)-*O*-2,3,6-tri-*O*-acetyl-α-D-glucopyranosyl-(1,4)-*O*-2,3,6-tri-*O*-acetyl-α-D-glucopyranosyl-(1,4)-*O*-2,3,6-tri-*O*-acetyl-α-D-glucopyranosyl-(1,4)-*O*-2,3,6-tri-*O*-acetyl-α-D-glucopyranosyl (1, 4)-,2,3,6-triacetate-D-glucopyranoside (18)

Compound **17** (100 mg, 0.045 mmol) was suspended in methanol (50mL) with PdOH on activated carbon (1mg). H_2 was passed through the suspension under atmospheric pressure for 14 h. The resulting sample was dissolved fully in DCM and filtered through celite to remove the solid catalyst. The sample was concentrated to a solid under rotary evaporation to yield a red solid. (Yield 80 mg, 81%). HRMS (MALDI, m/z): $[M+Na]^+$ calculated for $C_{92}H_{121}NO_{58}Na$= 2190.6447. Found 2190.6516.

This compound was utilised for synthesis of **18** below with 10 mg used in diazonium grafting study to confirm amorphous carbon modification.

4-aminophenyl-*O*-α-D-glucopyranosyl-(1,4)-*O*-α-D-glucopyranosyl-(1,4)-*O*-α-D-glucopyranosyl-(1,4)-*O*-α-D-glucopyranosyl-(1,4)-*O*-α-D-glucopyranosyl-(1,4)-*O*-α-D-glucopyranosyl-(1,4)-D-glucopyranoside (19)

Compound **19** was prepared by deprotection of **18** (70 mg, 0.045 mmol), under Zemplén deprotection conditions (sodium methoxide in methanol). (yield 33 mg, 90%) **IR** cm^{-1} 3823 (H_2O), 1335 (C-C), 1159 (C-H), 1078 (O-H), 1024 (C-O); HRMS (MALDI, m/z) [M+Na] Calculated for $C_{48}H_{72}NO_{37}$ = 1266.4123. Found 126.1485.

30 mg of this compound was used in diazonium grafting studies as a proof of concept. With more time and with appropriate purification strategies, it is expected that this synthetic method can be optimised to produce a viable synthetic strategy for open chain oligosaccharide based diazonium coating strategies.

References

1. Martell, L.; Bracale, R.; Carrion, S. A.; Giangrande, A.; Purcell, J. E.; Lezzi, M.; Gravili, C.; Piraino, S.; Boero, F., Correction: Successional dynamics of marine fouling hydroids (Cnidaria: Hydrozoa) at a finfish aquaculture facility in the Mediterranean Sea. *PLOS ONE* **2018,** *13* (5), e0196883.
2. Fitridge, I.; Dempster, T.; Guenther, J.; de Nys, R., The impact and control of biofouling in marine aquaculture: a review. *Biofouling* **2012,** *28* (7), 649-669.
3. Braithwaite, R.; McEvoy, L., Marine biofouling on fish farms and its remediation. *Adv. Mar. Bio.* **2004,** *47*, 215-252.
4. Hodson, S. L.; Lewis, T. E.; Burkea, C. M., Biofouling of fish-cage netting: efficacy and problems of in situ cleaning. *Aquaculture* **1997,** *152* (1), 77-90.
5. Greene, J. K.; Grizzle, R. E., Successional development of fouling communities on open ocean aquaculture fish cages in the western Gulf of Maine, USA. *Aquaculture* **2007,** *262* (2), 289-301.
6. Kassah, J., Development of biofouling on salmon cage nets and the effects of anti-fouling treatments on the survival of the hydroid (*Ectopleura larynx*)(Ellis & Solander, 1786). **2012**.
7. Myles, A.; Haberlin, D.; Esteban-Tejeda, L.; Angione, M. D.; Browne, M. P.; Hoque, M. K.; Doyle, T. K.; Scanlan, E. M.; Colavita, P. E., Bioinspired Aryldiazonium Carbohydrate Coatings: Reduced Adhesion of Foulants at Polymer and Stainless Steel Surfaces in a Marine Environment. *ACS Sustainable Chem. Eng.* **2018,** *6* (1), 1141-1151.
8. Žutinić, P.; Petrić, I.; Gottstein, S.; Gligora Udovič, M.; Kralj Borojević, K.; Kamberović, J.; Kolda, A.; Plenković-Moraj, A.; Ternjej, I., Microbial mats as shelter microhabitat for amphipods in an intermittent karstic spring. *Knowl. Manag. Aquat. Ecosyst.* **2018,** (419), 7.
9. Muthukumar, T.; Aravinthan, A.; Lakshmi, K.; Venkatesan, R.; Vedaprakash, L.; Doble, M., Fouling and stability of polymers and composites in marine environment. *Int. Biodeterior. Biodegradation* **2011,** *65* (2), 276-284.
10. Scardino, A. J.; Fletcher, L. E.; Lewis, J. A., Fouling control using air bubble curtains: protection for stationary vessels. *J. Mar. Eng Technol.* **2009,** *8* (1), 3-10.
11. Callow, J. A.; Callow, M. E., Trends in the development of environmentally friendly fouling-resistant marine coatings. *Nature Comm.* **2011,** *2*, 244.
12. Choudhury, P.; Prasad Uday, U. S.; Bandyopadhyay, T. K.; Ray, R. N.; Bhunia, B., Performance improvement of microbial fuel cell (MFC) using suitable electrode and Bioengineered organisms: A review. *Bioengineered* **2017,** *8* (5), 471-487.
13. Lapinsonnière, L.; Picot, M.; Poriel, C.; Barrière, F., Phenylboronic Acid Modified Anodes Promote Faster Biofilm Adhesion and Increase Microbial Fuel Cell Performances. *Electroanalysis* **2013,** *25* (3), 601-605.
14. Franks, A. E.; Nevin, K. P., Microbial Fuel Cells, A Current Review. *Energies* **2010,** *3* (5), 899.
15. Garrett, T. R.; Bhakoo, M.; Zhang, Z., Bacterial adhesion and biofilms on surfaces. *Prog.Nat. Sci.* **2008,** *18* (9), 1049-1056.
16. Klemm, P.; Schembri, M. A., Bacterial adhesins: function and structure. *Int. J. Med.Microbiol.* **2000,** *290* (1), 27-35.
17. Ziegler, A. S.; McIlroy, S. J.; Larsen, P.; Albertsen, M.; Hansen, A. A.; Heinen, N.; Nielsen, P. H., Dynamics of the Fouling Layer Microbial Community in a Membrane Bioreactor. *PLoS ONE* **2016,** *11* (7), e0158811.
18. Jayasundara, D. R.; Duff, T.; Angione, M. D.; Bourke, J.; Murphy, D. M.; Scanlan, E. M.; Colavita, P. E., Carbohydrate Coatings via Aryldiazonium Chemistry for Surface Biomimicry. *Chem.Mater.* **2013,** *25* (20), 4122-4128.

19. Picot, M.; Lapinsonnière, L.; Rothballer, M.; Barrière, F., Graphite anode surface modification with controlled reduction of specific aryl diazonium salts for improved microbial fuel cells power output. *Biosens. Bioelectron.* **2011,** *28* (1), 181-188.
20. Das, R.; Mukhopadhyay, B., Chemical O-Glycosylations: An Overview. *ChemistryOpen* **2016,** *5* (5), 401-433.
21. Wang, Z., Zemplén Deacetylation. In *Comprehensive Organic Name Reactions and Reagents*, John Wiley & Sons, Inc.: 2010.
22. Socrates, G., *Infrared and Raman Characteristic Group Frequencies: Tables and Charts*. Wiley: 2004.
23. Farkas, E.; Jánossy, L.; Harangi, J.; Kandra, L.; Lipták, A., Synthesis of chromogenic substrates of α-amylases on a cyclodextrin basis. *Carbohydr. Res.* **1997,** *303* (4), 407-415.

Appendix:

NMR data of synthesised compounds:

^{1}H NMR (400 MHz, $CDCl_3$) of Compound **2.**

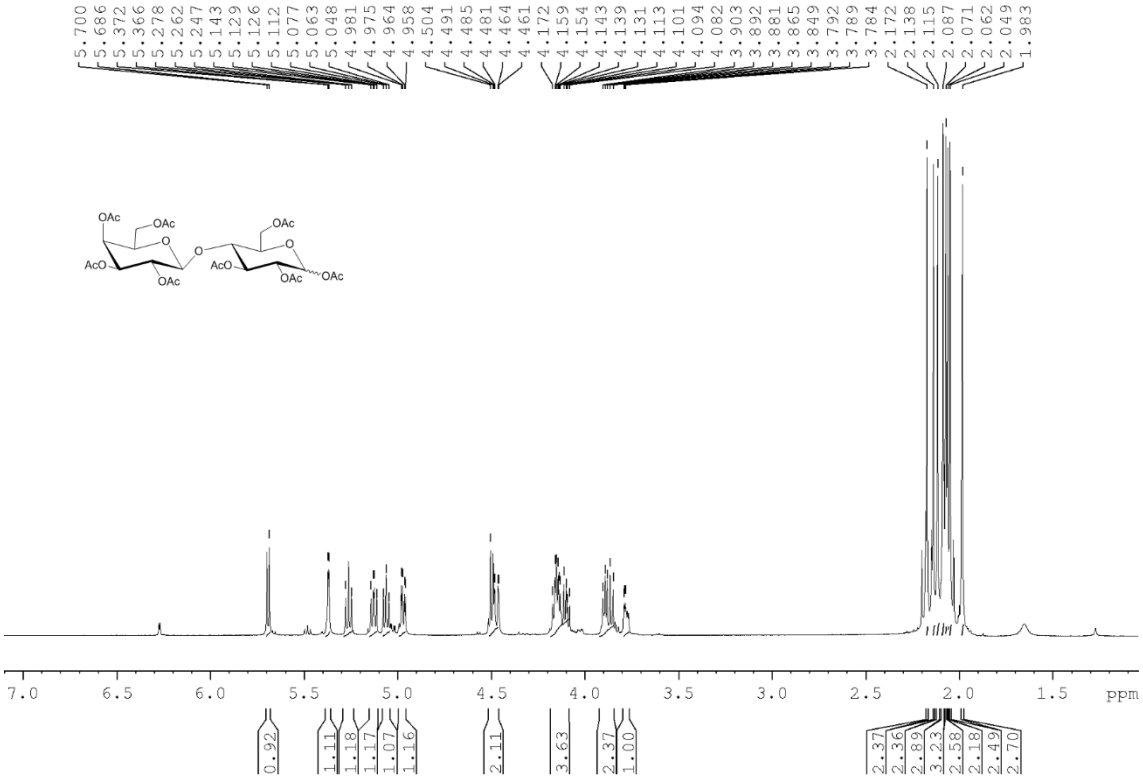

^{1}H NMR (400 MHz, $CDCl_3$) of Compound **3.**

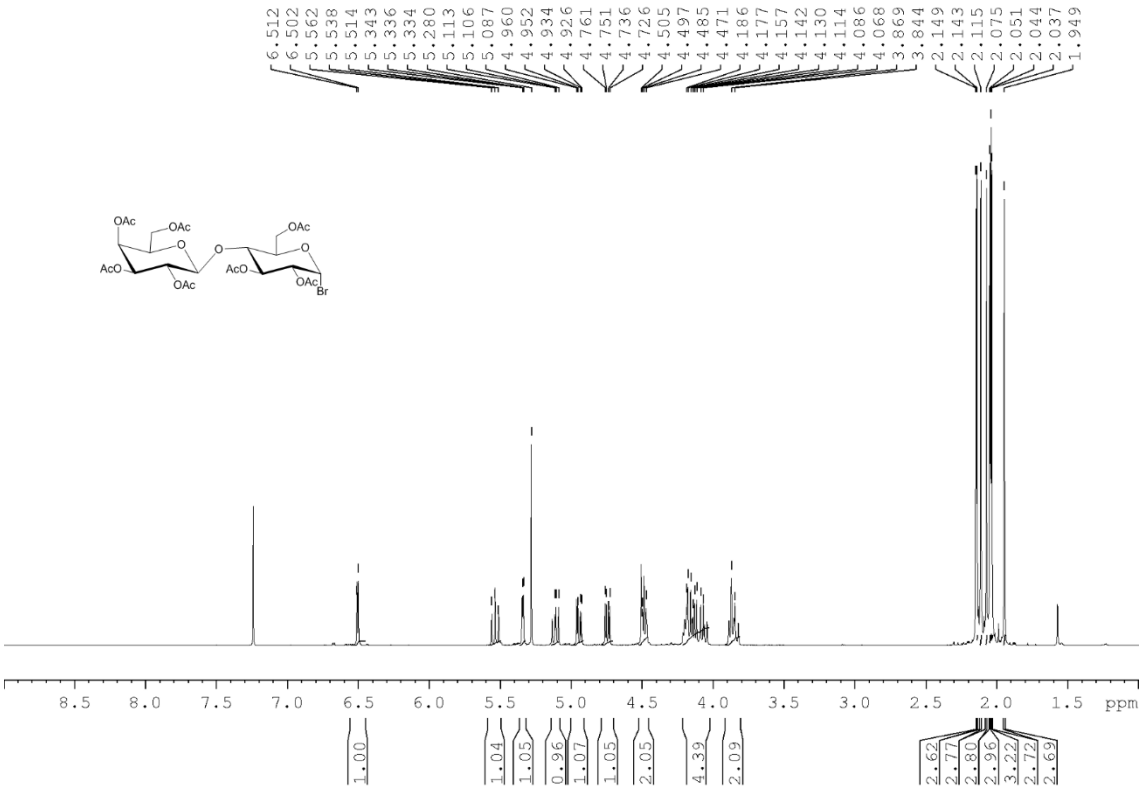

^{1}H NMR (400 MHz, $CDCl_3$) of Compound **4**

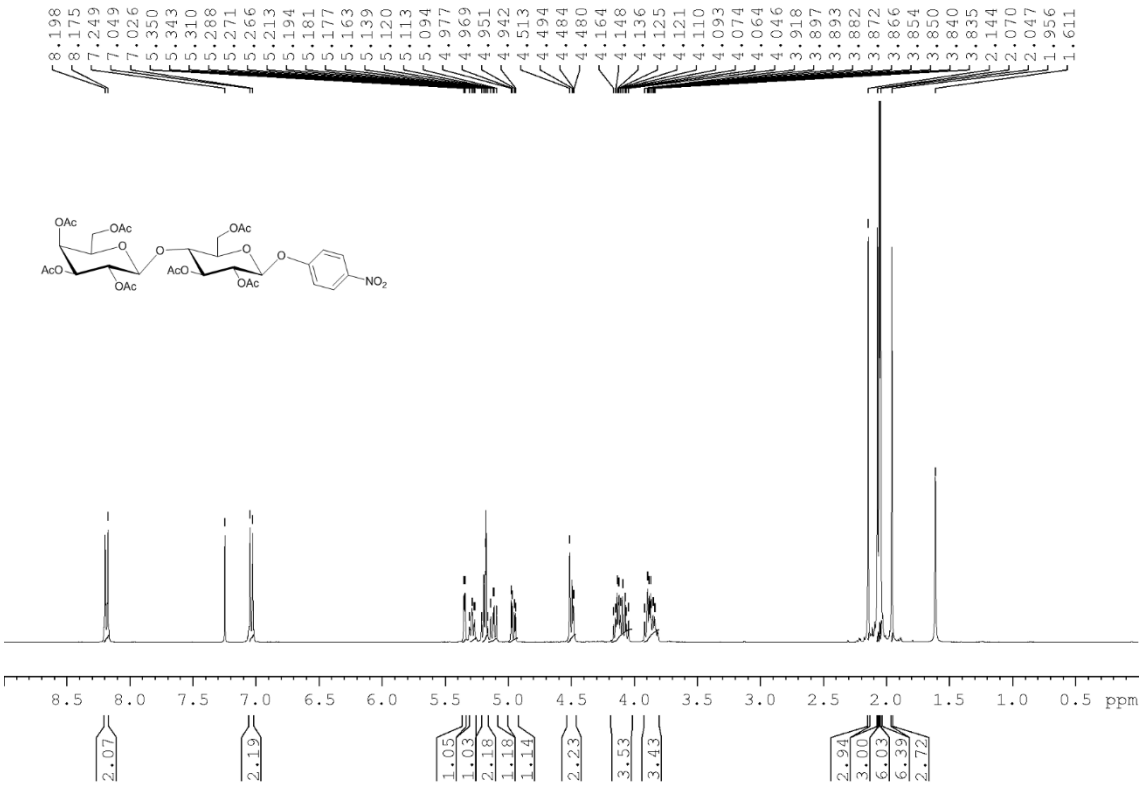

^{13}C NMR (100 MHz, $CDCl_3$) of Compound **4**

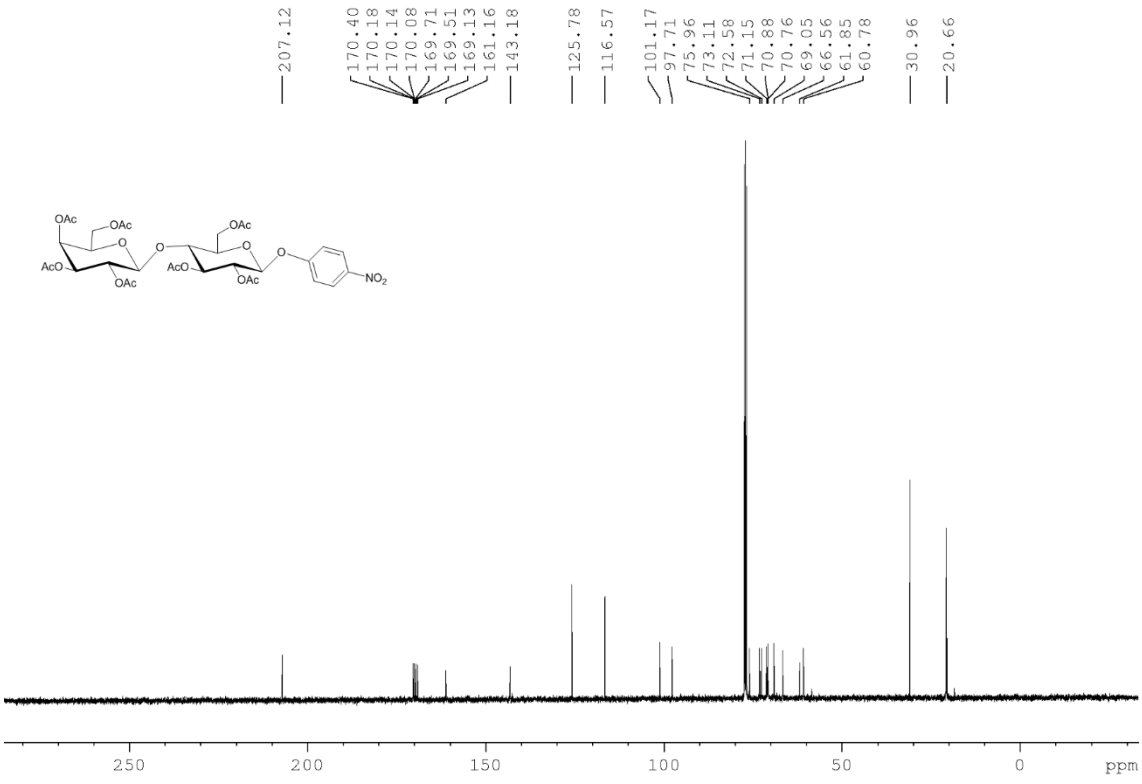

^{1}H NMR (600 MHz, $CDCl_3$) of Compound **5**

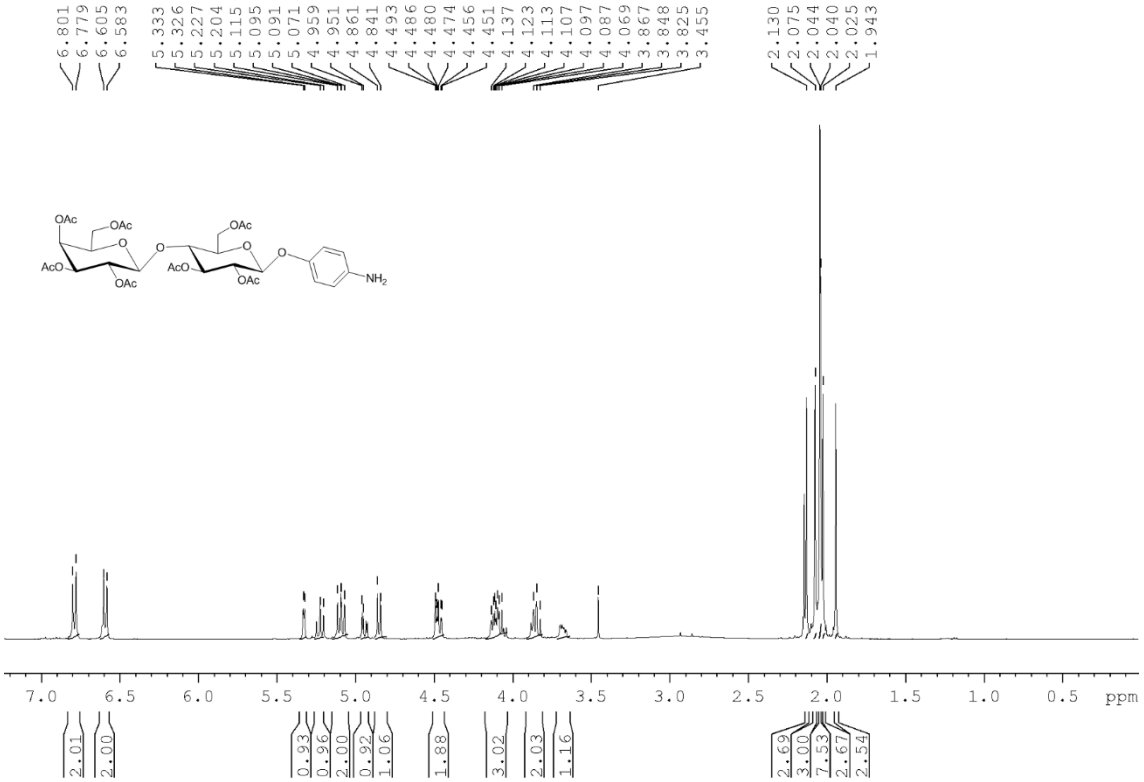

^{13}C NMR (150 MHz, $CDCl_3$) of Compound **5**

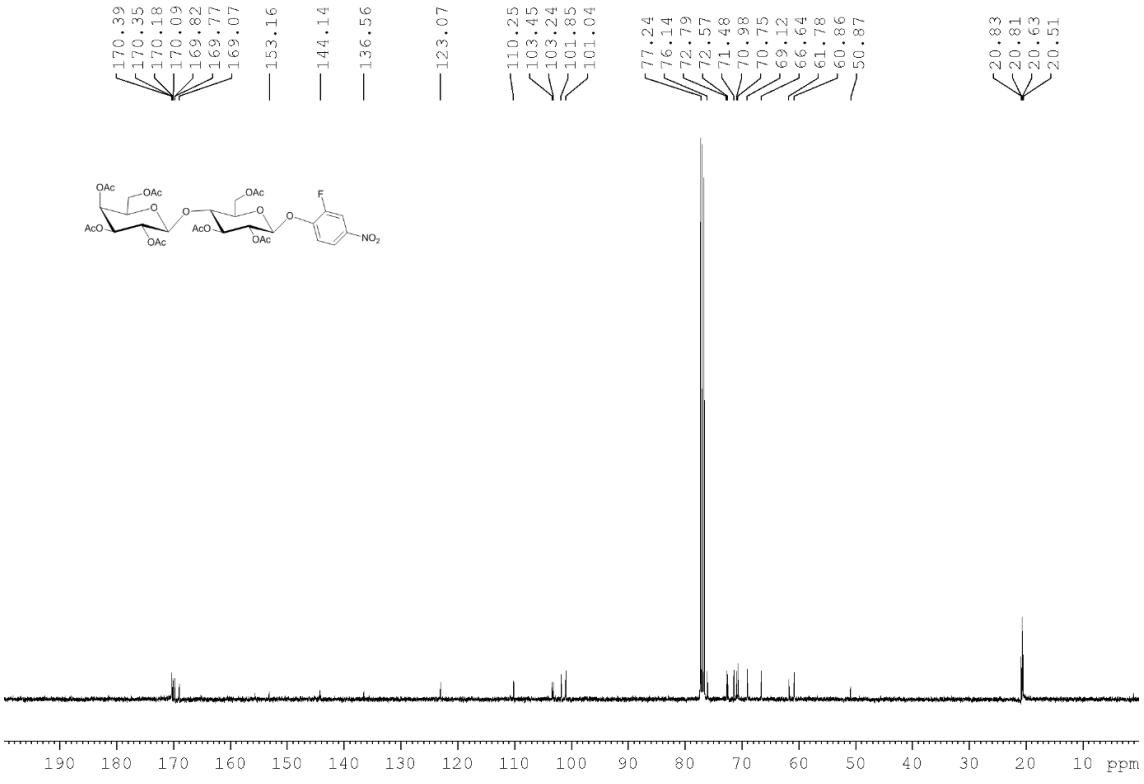

1H NMR (400 MHz, D_2O) of Compound **6**

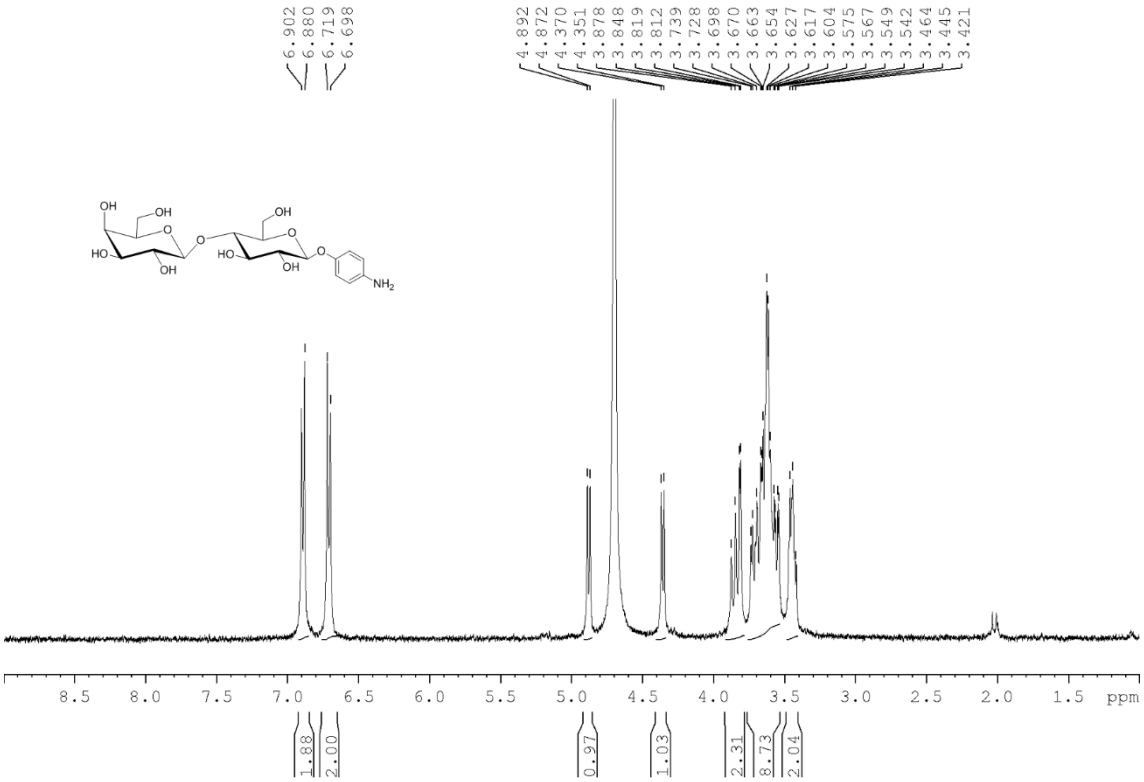

13C NMR (100 MHz, D_2O) of Compound **6**

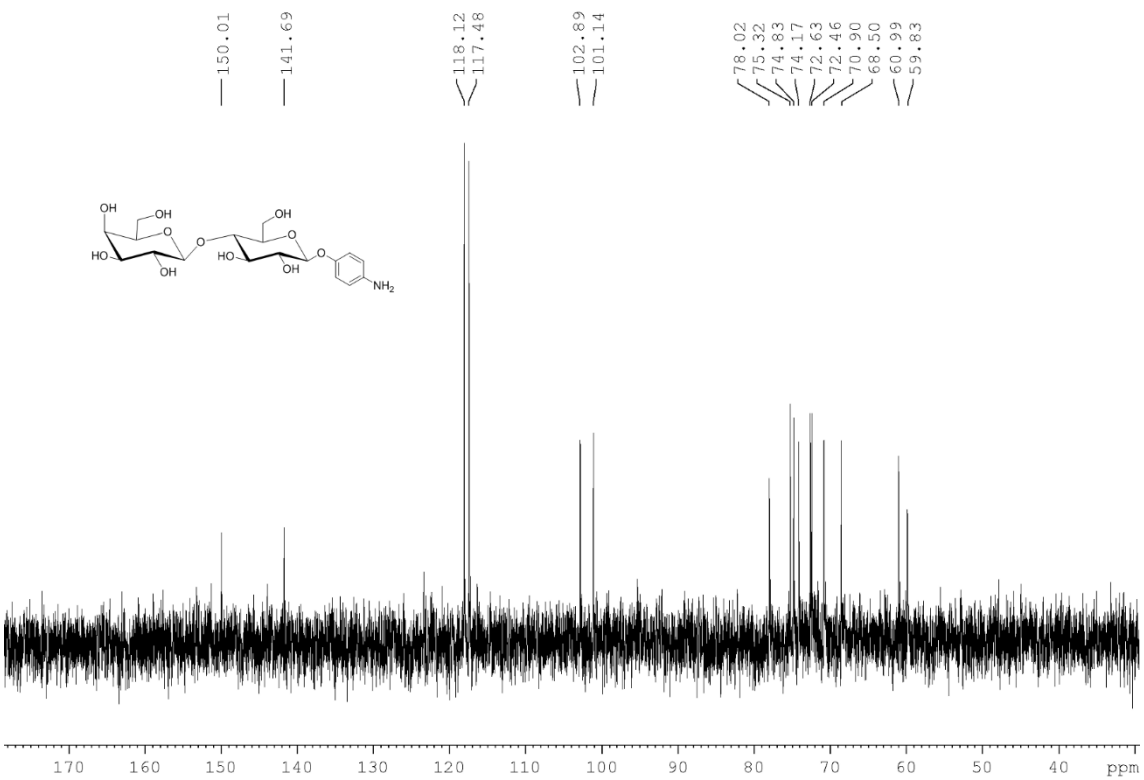

^{1}H NMR (400 MHz, $CDCl_3$) of Compound **7**

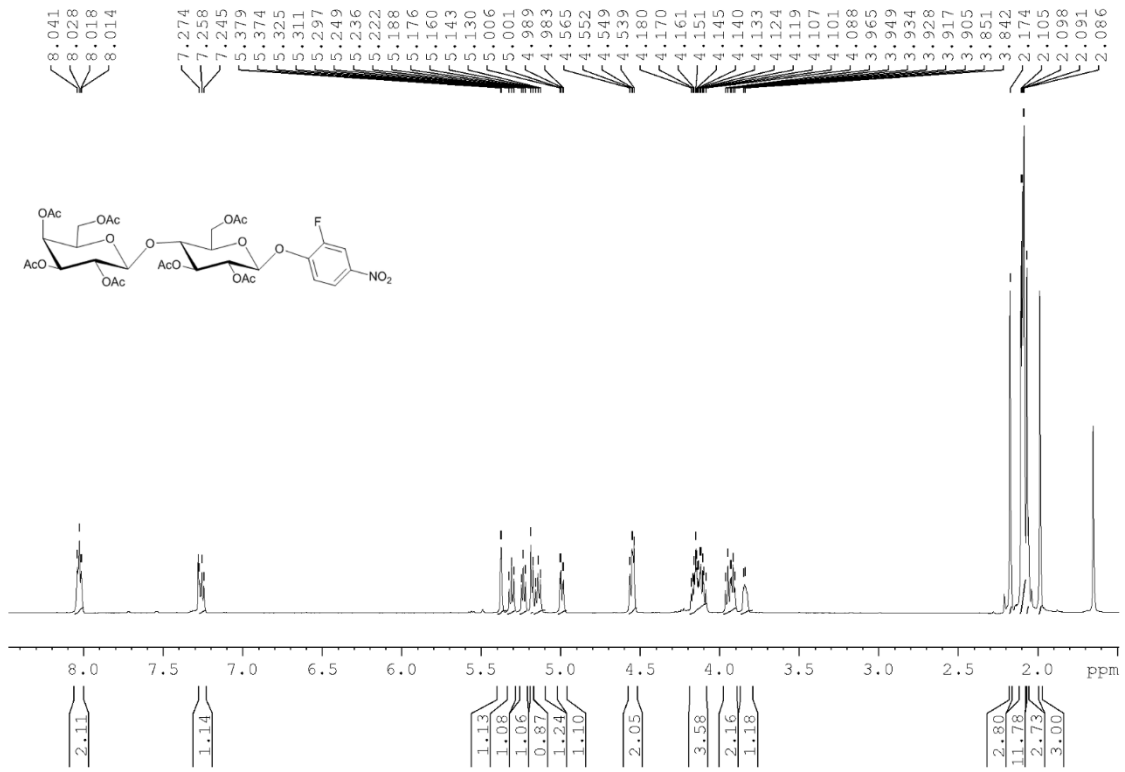

^{13}C NMR (100 MHz, $CDCl_3$) of Compound **7**

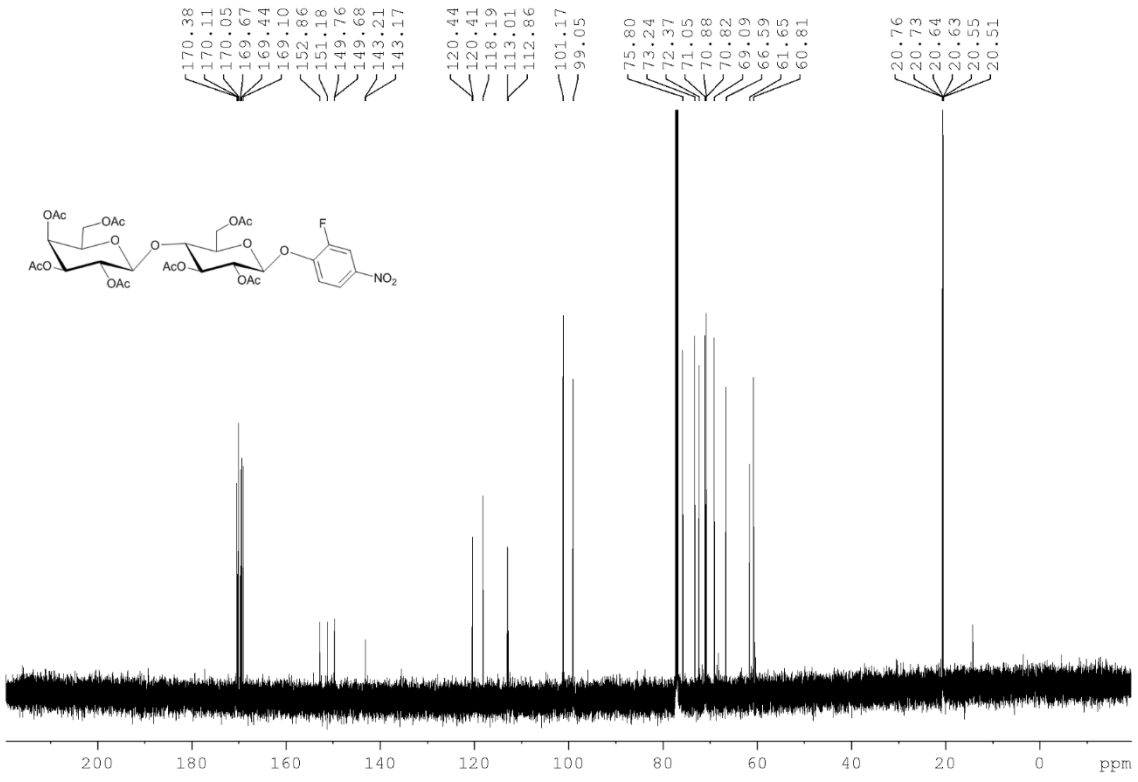

^{19}F NMR (376.4 MHz) of Compound **7**

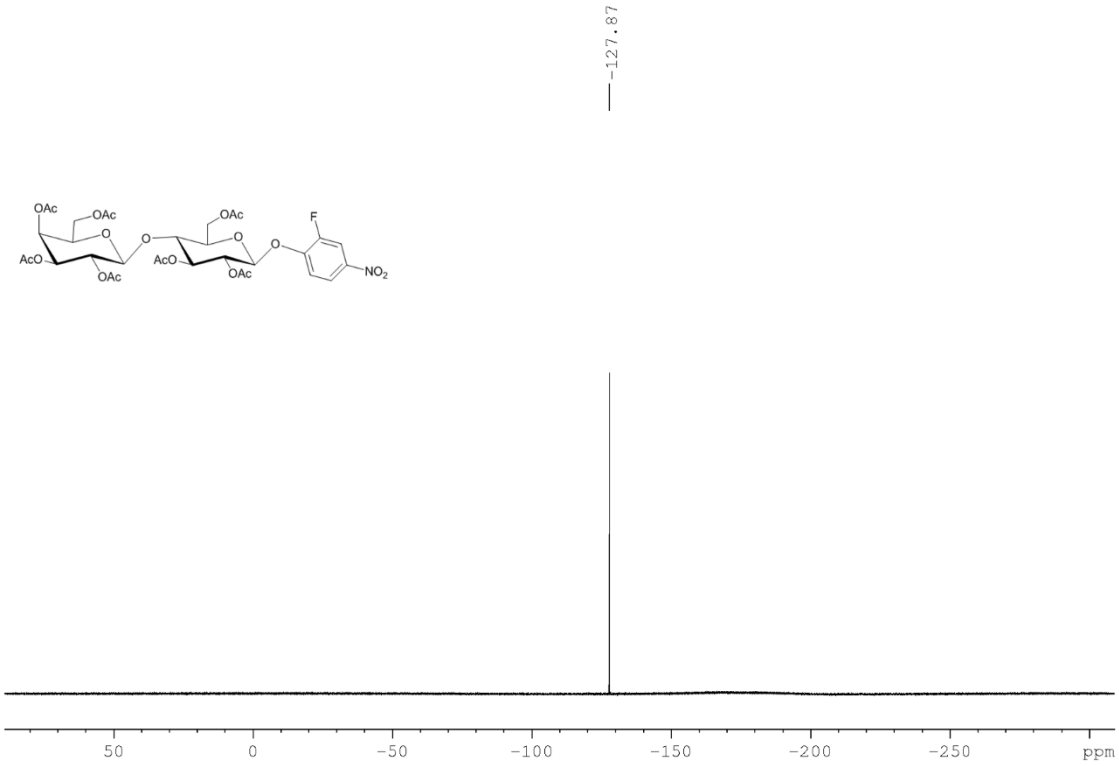

^{1}H NMR (600 MHz, $CDCl_3$) of Compound **8**

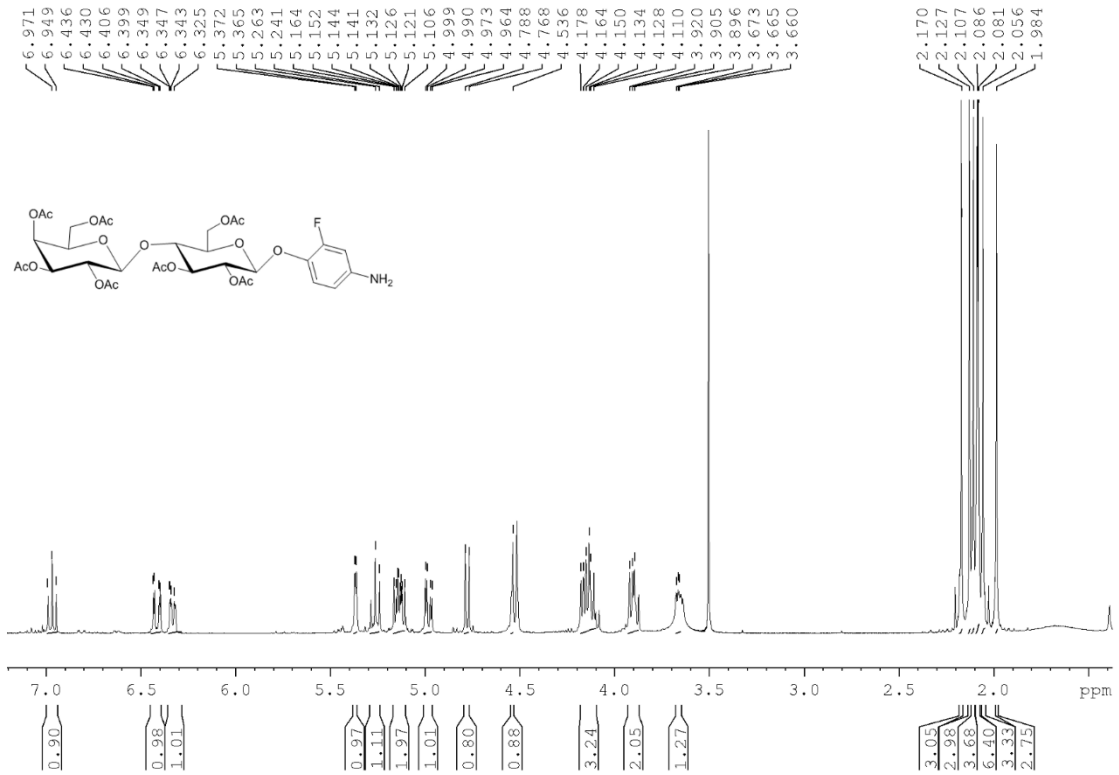

^{13}C NMR (150 MHz, $CDCl_3$) of Compound **8**

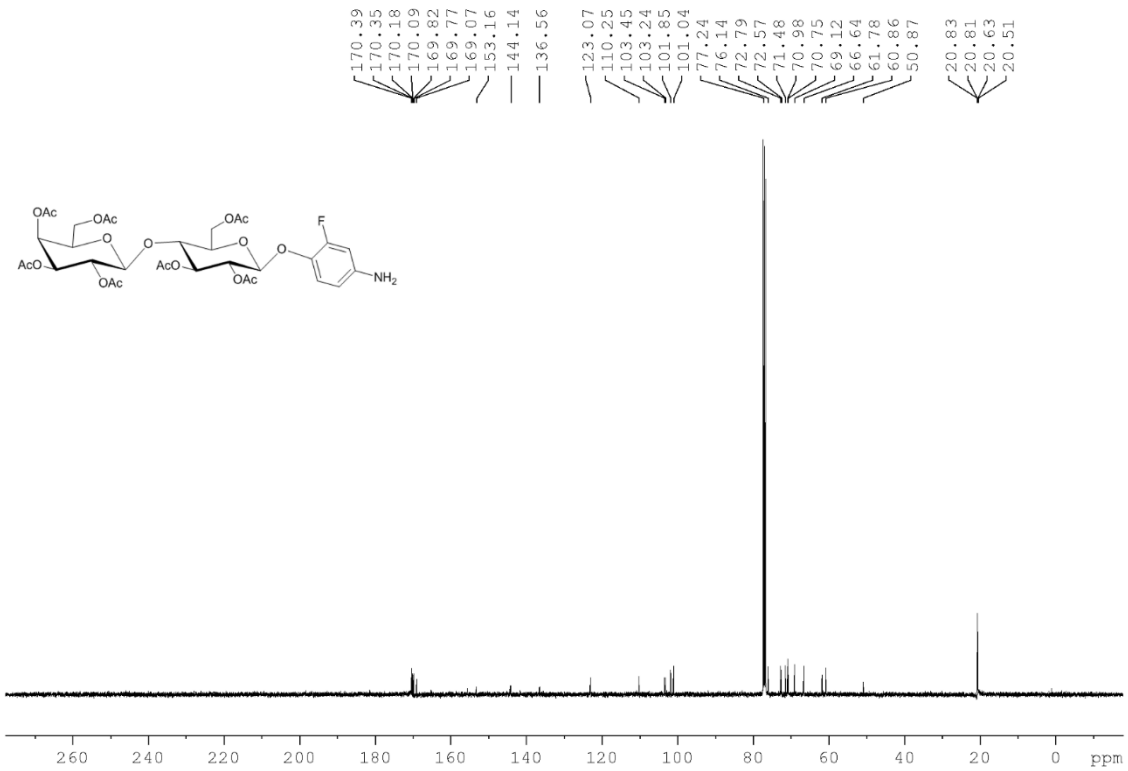

^{19}F NMR (376.4 MHz) of Compound **8**

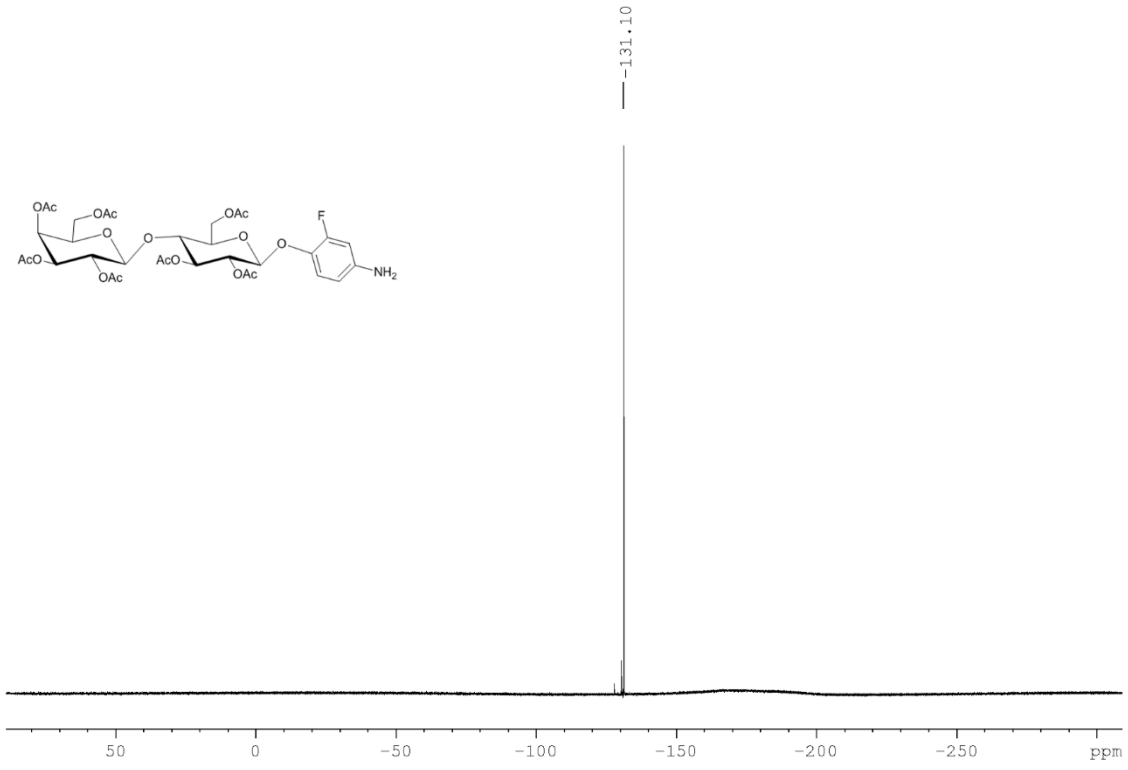

^{1}H NMR (600 MHz, $CDCl_3$) of Compound **9**

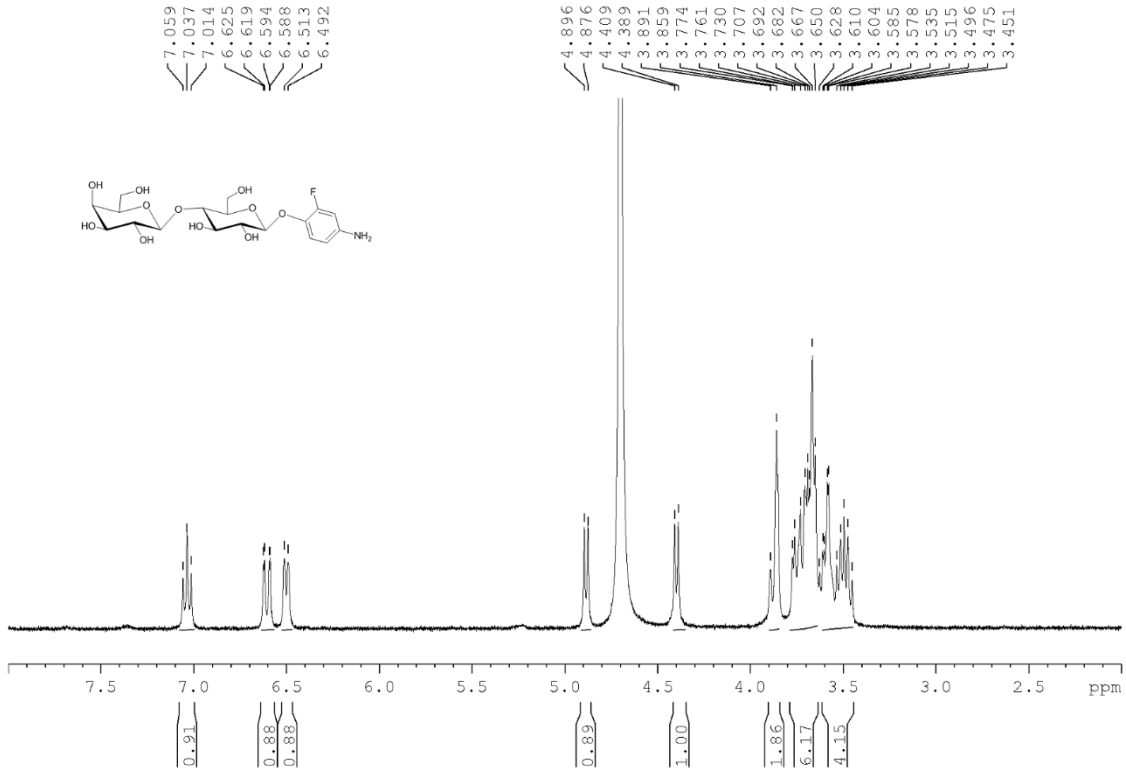

^{13}C NMR (150 MHz, $CDCl_3$) of Compound **9**

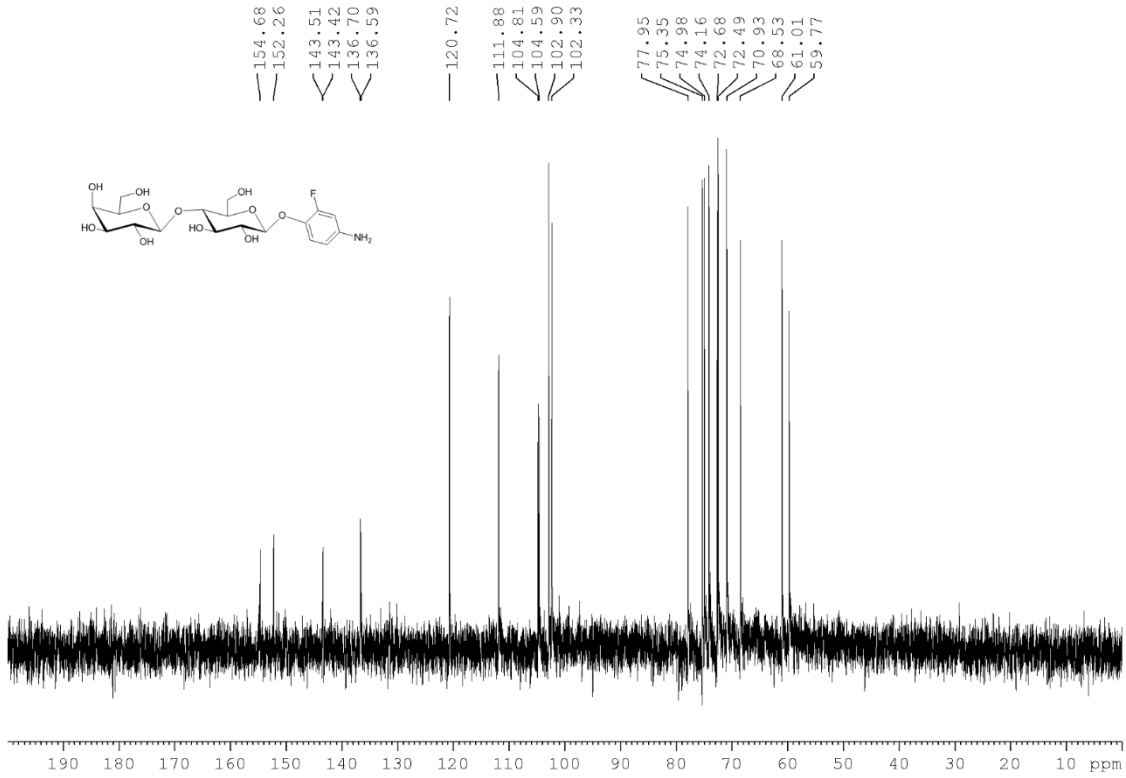

^{19}F NMR (376.4 MHz) of Compound **9**

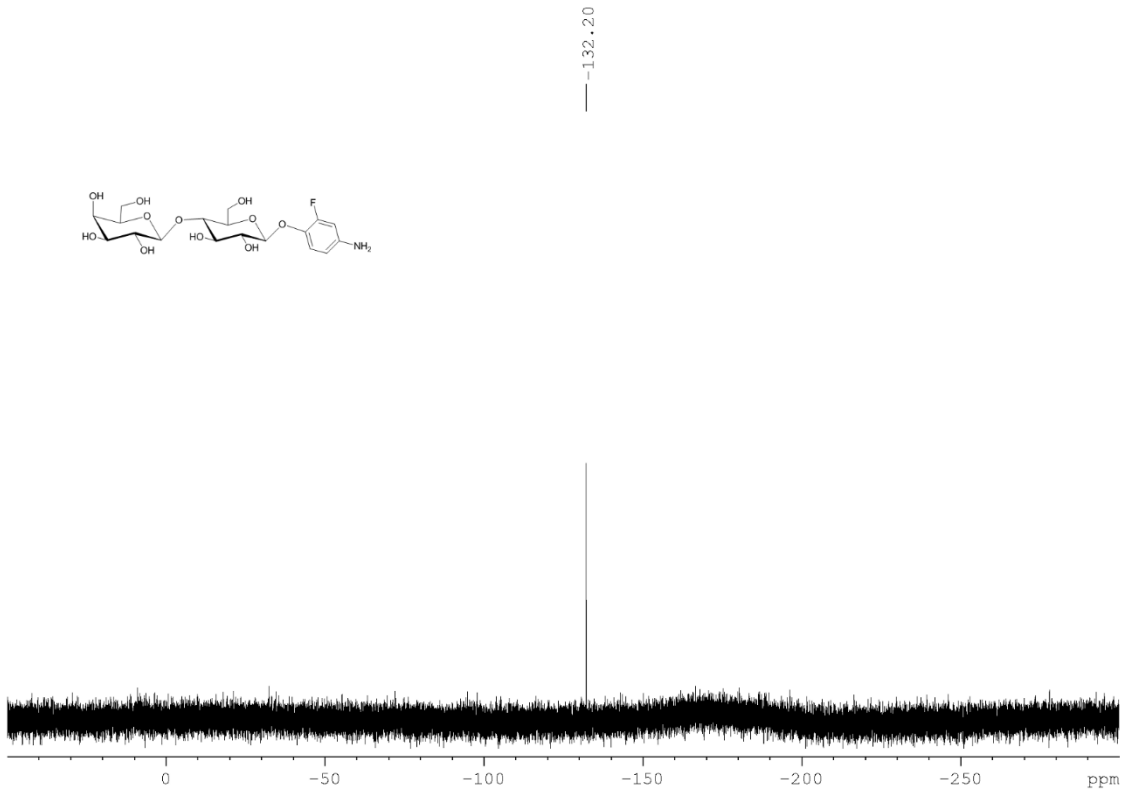

^{1}H NMR (600 MHz, DMSO) of Compound **11**

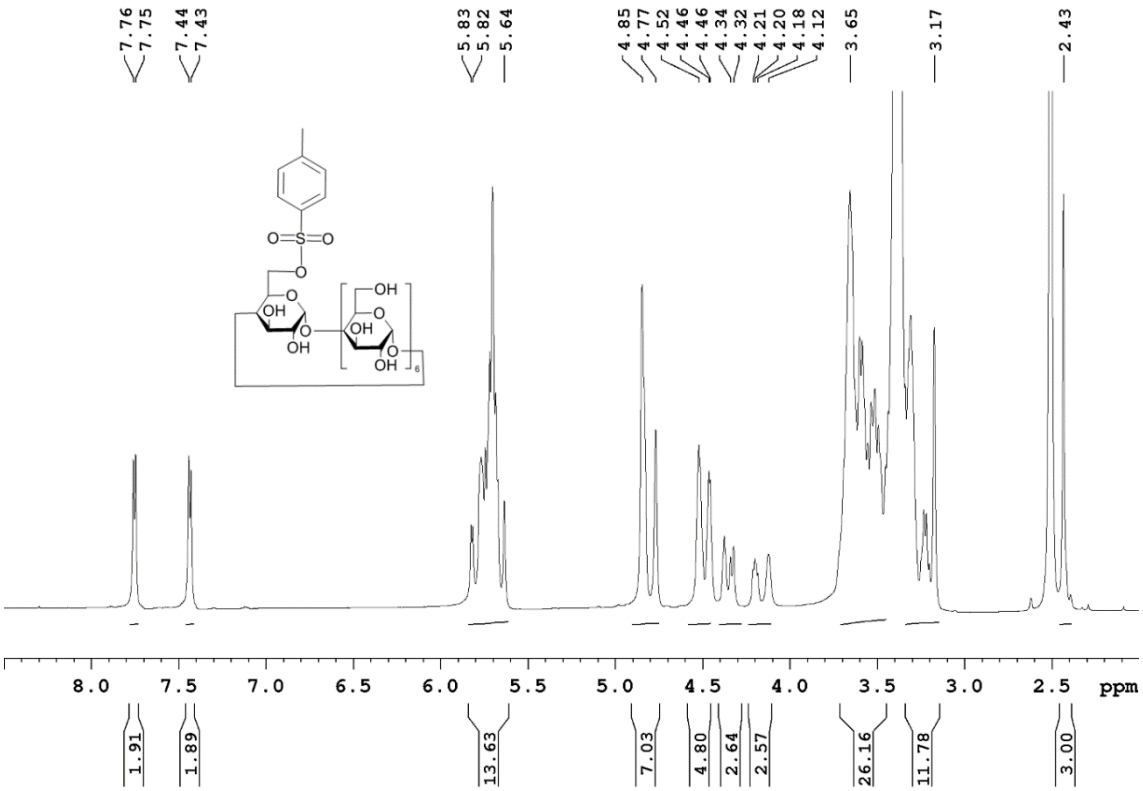

^{13}C NMR (150 MHz, DMSO) of Compound **11**

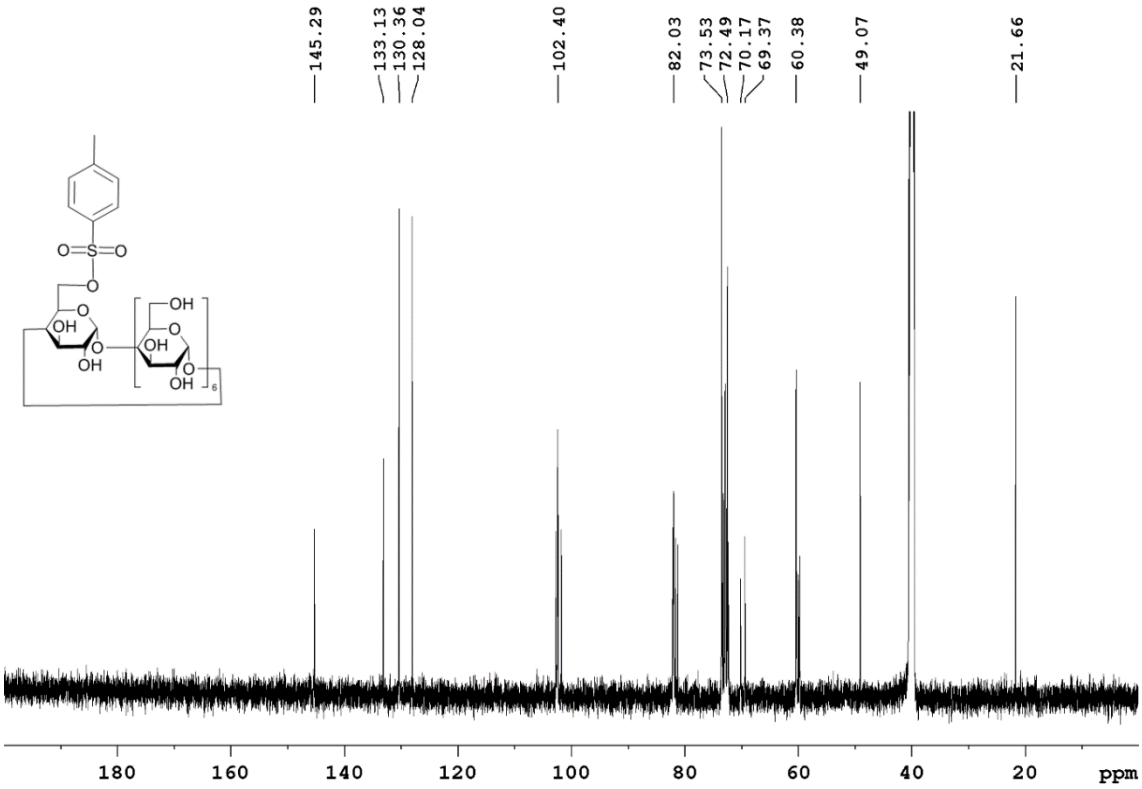

^{1}H NMR (400 MHz, D_2O) of Compound **12**

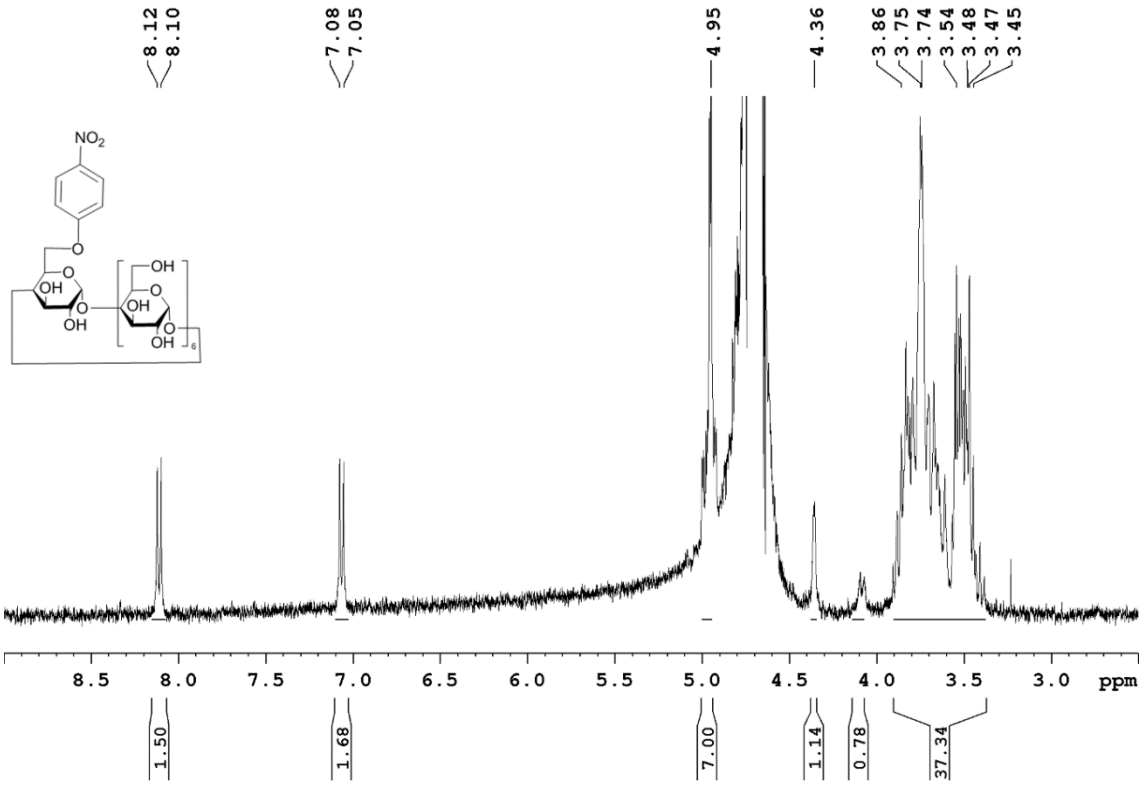

.

^{13}C NMR (100 MHz, D_2O) of Compound **12**

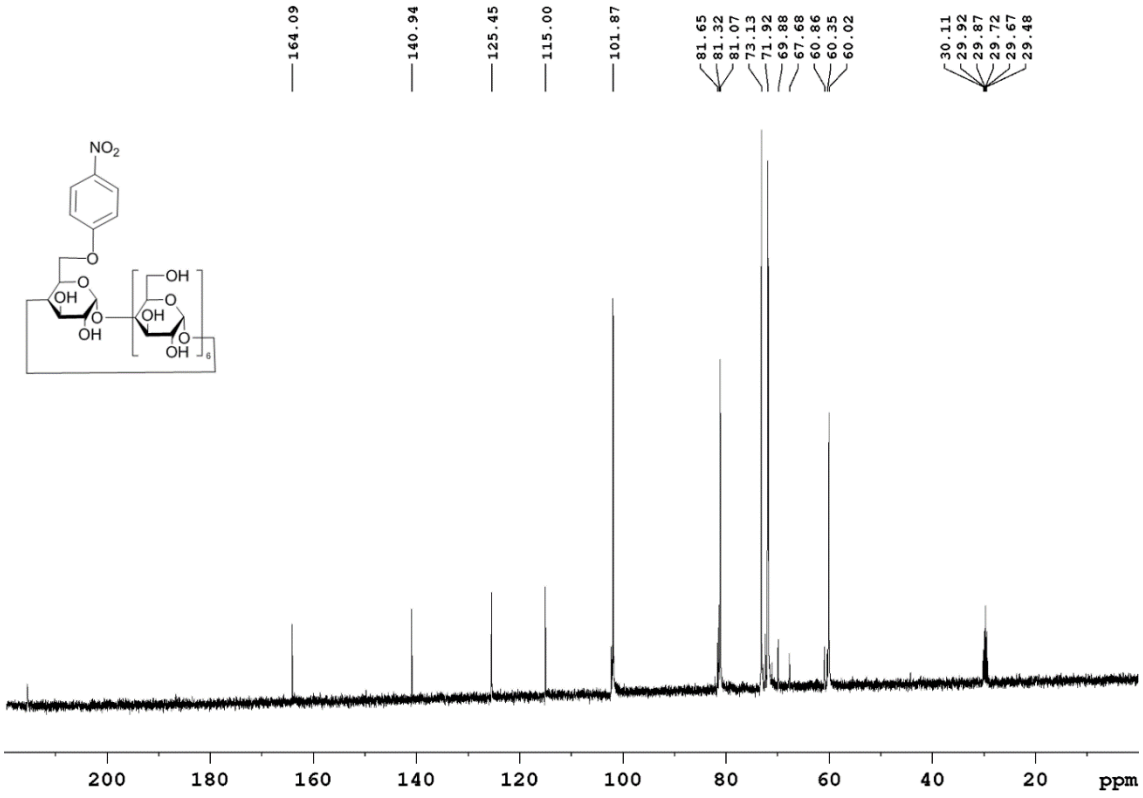

^{1}H NMR (400 MHz, D_2O) of Compound **13**

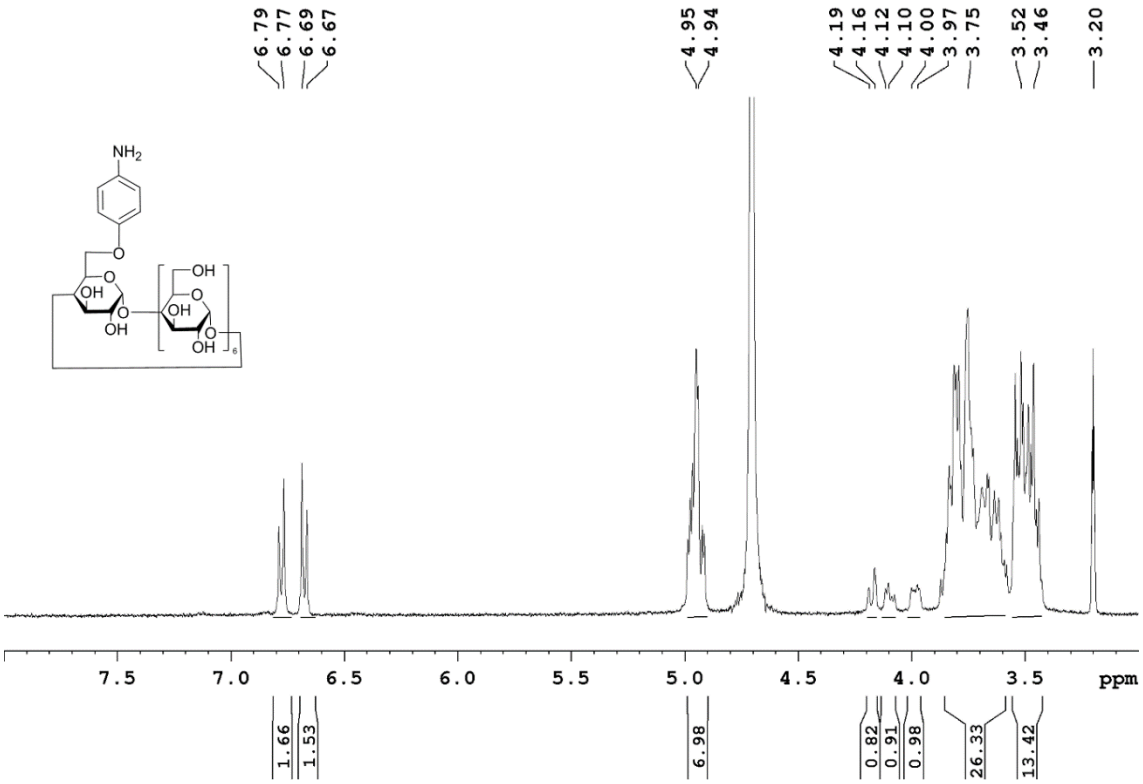

^{13}C NMR (100 MHz, D_2O) of Compound **13**

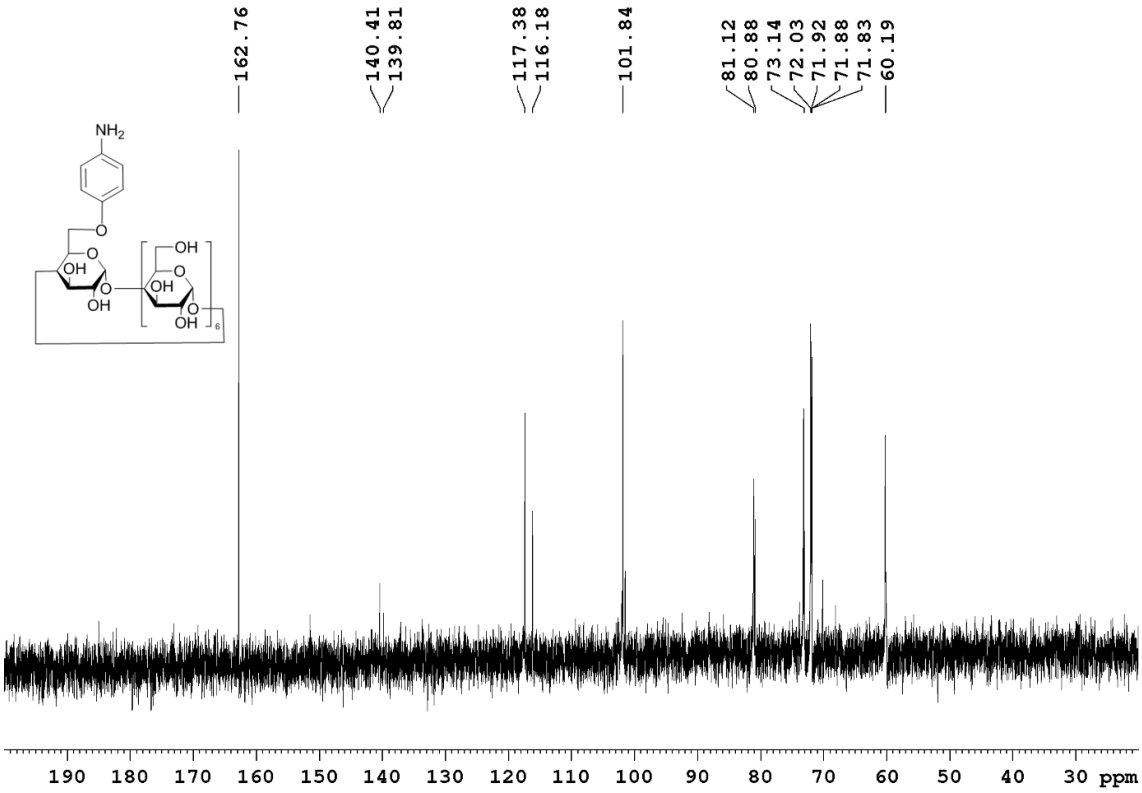

^{1}H NMR (400 MHz, D_2O) of Compound **14**

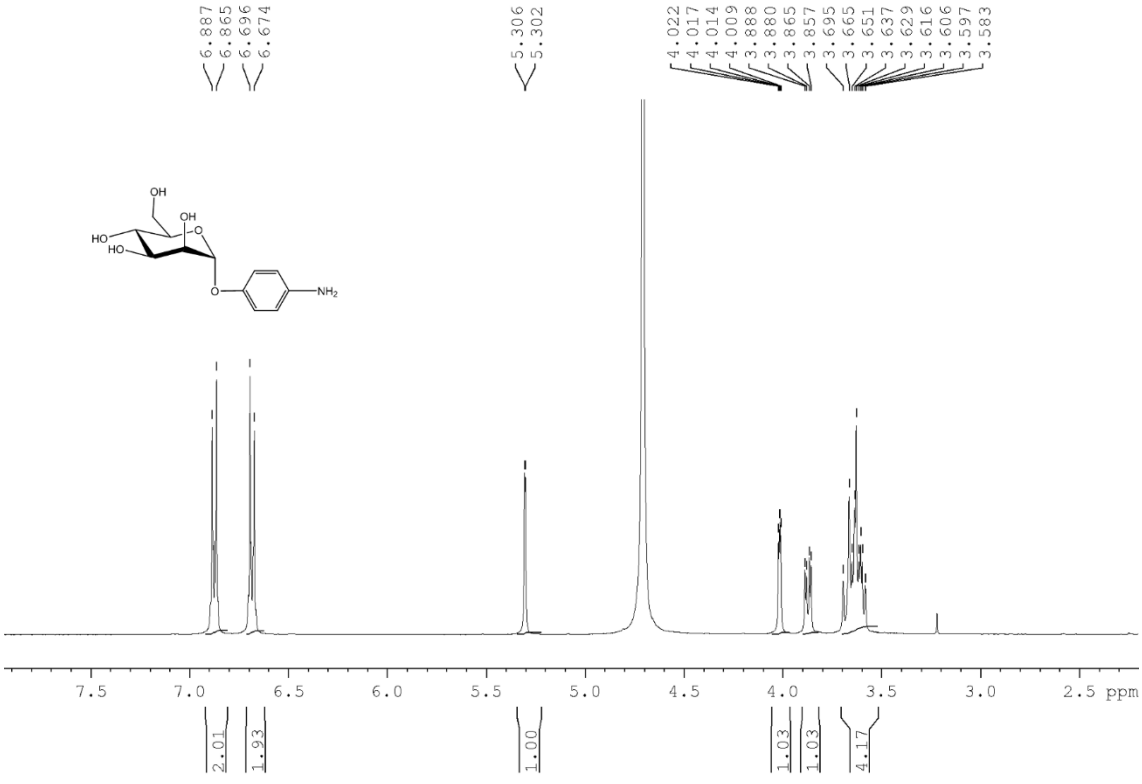

1H NMR (400 MHz, $CDCl_3$) of Compound **17**

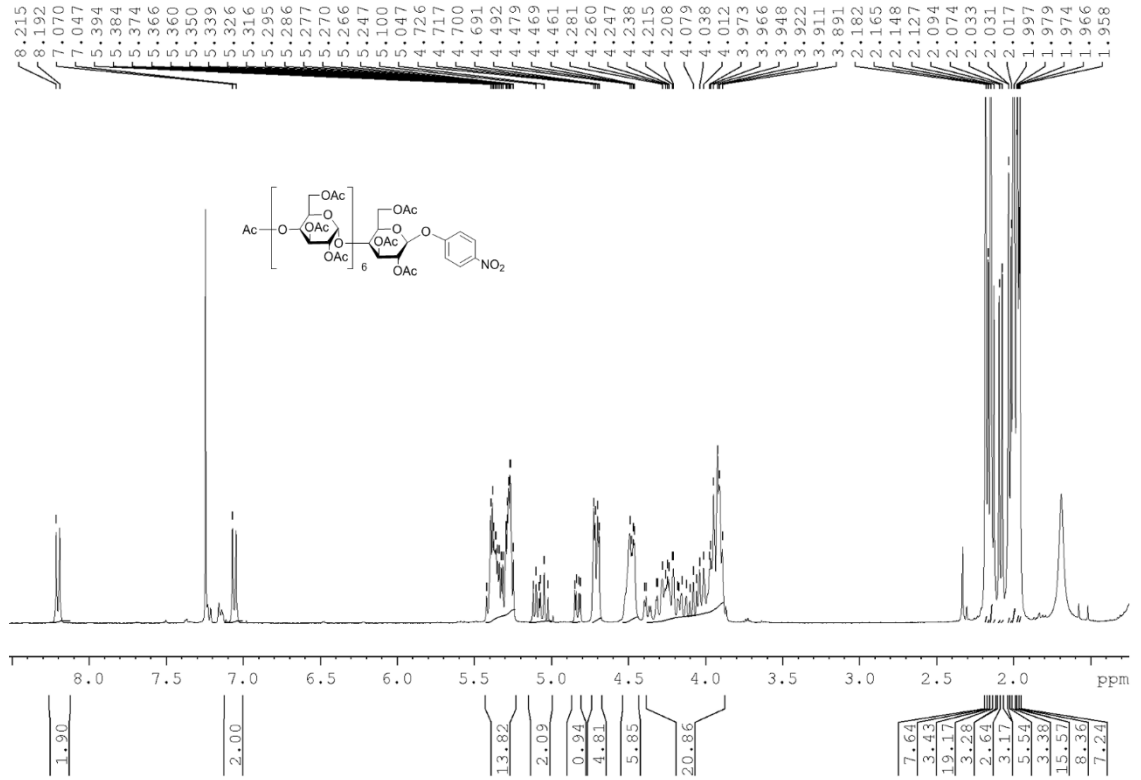

1H NMR (400 MHz, D_2O) of Compound **19**

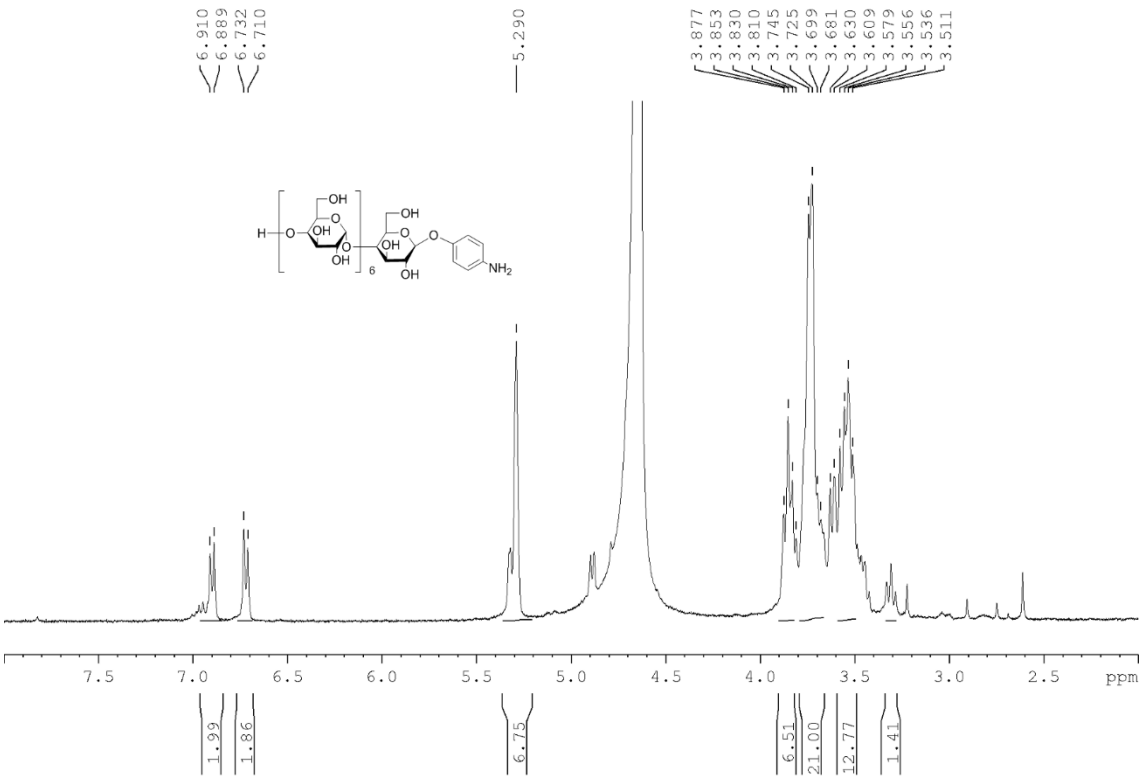

Crystal data and structure refinement for compound 14.

Empirical formula	$C_{48}H_{106}NO_{50.50}$	
Formula weight	1505.33	
Temperature	100(2) K	
Wavelength	1.54178 Å	
Crystal system	Orthorhombic	
Space group	$P2_12_12_1$	
Unit cell dimensions	a = 13.4308(5) Å	α= 90°.
	b = 18.7532(7) Å	β= 90°.
	c = 27.5222(11) Å	γ = 90°.
Volume	6932.0(5) $Å^3$	
Z	4	
Density (calculated)	1.442 Mg/m^3	
Absorption coefficient	1.149 mm^{-1}	
F(000)	3220	
Crystal size	0.3 x 0.29 x 0.2 mm^3	
Theta range for data collection	2.851 to 70.062°.	
Index ranges	$-15\leq h\leq 16$, $-20\leq k\leq 22$, $-33\leq l\leq 33$	
Reflections collected	73460	
Independent reflections	13089 [R(int) = 0.0449]	
Completeness to theta = 67.679°	100.0 %	
Absorption correction	Semi-empirical from equivalents	
Max. and min. transmission	0.7533 and 0.6719	
Refinement method	Full-matrix least-squares on F^2	
Data / restraints / parameters	13089 / 265 / 1042	
Goodness-of-fit on F^2	1.019	
Final R indices [$I>2\sigma(I)$]	R1 = 0.0699, wR2 = 0.2047	
R indices (all data)	R1 = 0.0723, wR2 = 0.2083	
Absolute structure parameter	0.02(3)	
Largest diff. peak and hole	0.861 and -0.649 $e.Å^{-3}$	

X-Ray diffraction experimental:

X-ray structural analyses for crystals of amBCD were performed on a Bruker APEX Duo CCD at 100(2) K with an Oxford Cobra cryostat, with samples mounted on a MiTeGen microloop using Cu Kα radiation (λ = 1.54178 Å). Bruker APEX[5] software was used to collect and reduce data and determine the space group. Absorption corrections were applied using SADABS.[6] Structures were solved with the XT structure solution program[7] using Intrinsic Phasing and refined with the XL refinement package[8] using Least Squares minimisation in Olex2.[9] All non-hydrogen atoms were refined anisotropically. Hydrogen atoms were assigned to calculated positions using a riding model with appropriately fixed isotropic thermal parameters.

The oxyaniline group was disordered over two sites with 72:28% occupancy and refined with restraints (DFIX, SIMU) and constraints (EADP). Several ethoxy groups were also disordered in two positions and were modelled with restraints (DFIX, SADI, SIMU) and constraints (EADP) (C26O27, 75:25%; C37O38, 79; 21% occupied). The D_2O molecules were refined with either full (O4s, O5s, O6s, O7s, O8s, O11s, O14s, O15s, O16s, O17s) three quarters (O3s, O9s) or half occupancy (O1s, O2s, O10s, O12s, O13s, O18s). Hydrogen atoms were added and refined using restraints (DFIX). There are a range of short intermolecular D-H…H-D contacts and large residual density (0.88eÅ-3). Only the highest density peaks were chosen for modelling as D_2O. There are probably many more. Only one conformation for each D_2O chosen. Even with antibumping restraints there are close contacts.

Chirality: C12 = R;C13 = R;C15 = R;C17 = S;C19 = R;C20 = R;C22 = R;C24 = S;C25 = R;C30 = R;C31 = R;C33 = R;C35 = S;C36= R;C41 = R;C42 = R;C44 = R;C46 = S;C47 = R;C52 = R;C53 = R;C55 = R;C57 = S;C58 = R;C64 = R;C66 = R;C68 = S;C69 = R;C75 = R;C77 = R;C79 = S.

Crystallographic data, CCDC 1840053, can be obtained free of charge from the Cambridge Crystallographic Data Centre via www.ccdc.cam.ac.uk/ data_request/cif.

Crystal Data for $C_{48}H_{75}D_{31}NO_{50.5}$ (*M* =1536.52 g/mol): orthorhombic, space group $P2_12_12_1$ (no. 19), *a* = 13.4452(5) Å, *b* = 18.7434(7) Å, *c* = 27.5154(11) Å, *V* = 6934.1(5) Å3, *Z* = 4, *T* = 100(2) K, μ(CuKα) = 1.149 mm-1, *Dcalc* = 1.472 g/cm3, 61478 reflections measured (5.704° ≤ 2Θ ≤ 140.008°), 13049 unique (R_{int} = 0.0346, R_{sigma} = 0.0240) which were used in all calculations. The final R_1 was 0.0683 (I > 2σ(I)) and wR_2 was 0.1978 (all data).

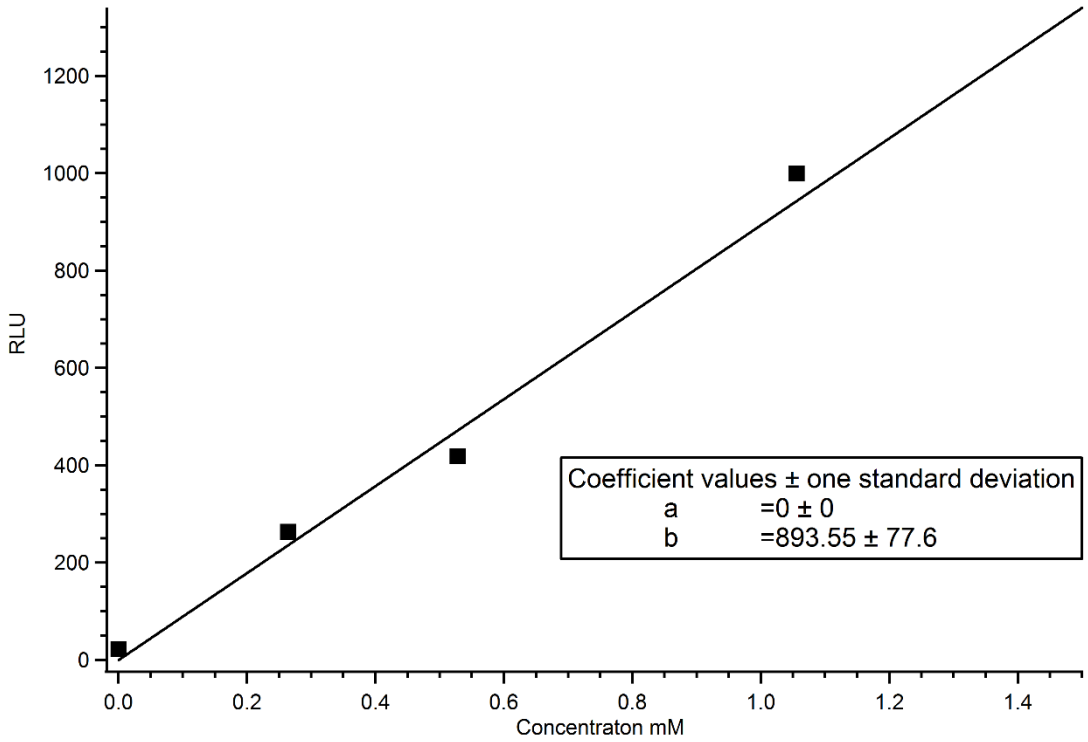

Linear range calibration plot for standard dilutions of ATP tested by Aquasnap TOTAL ATP water test kits and a hydrogima luminometer.

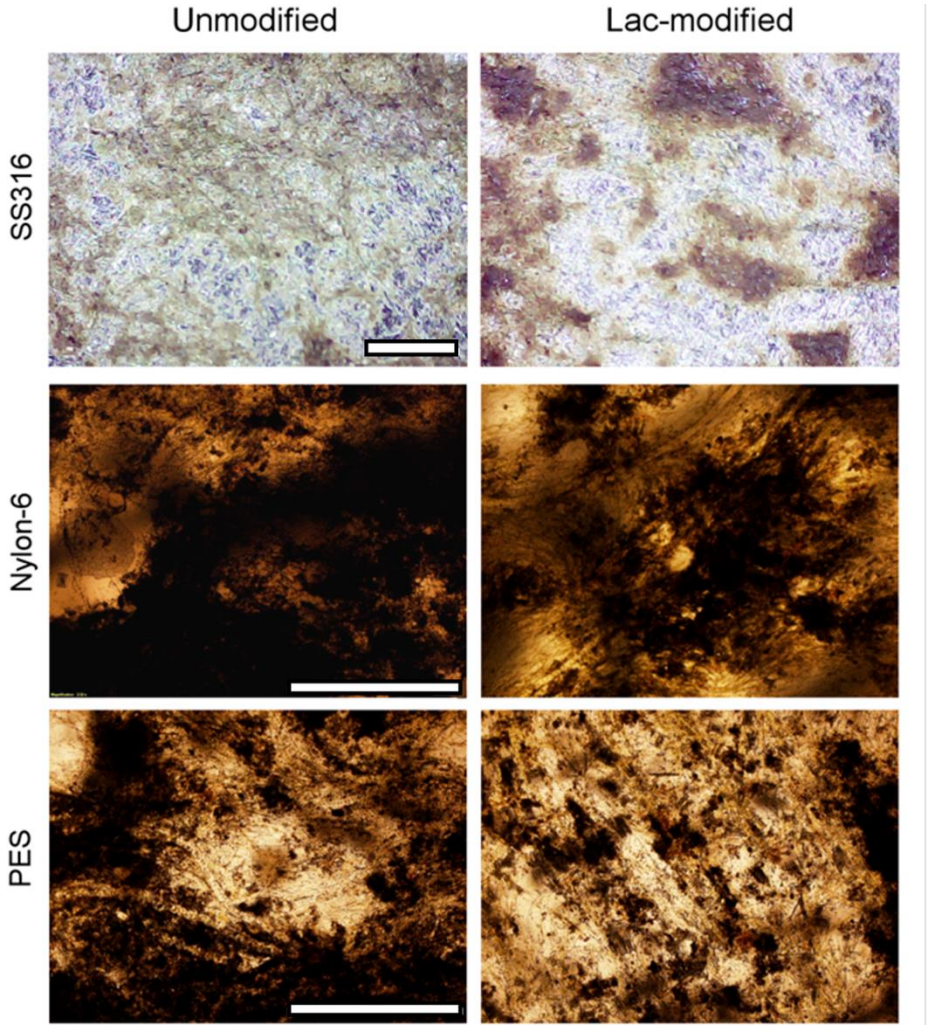

Optical microscope images of SS316, nylon-6 and PES coupons extracted after 20 day immersion in coastal waters prior to rinsing; scalebar = 1 mm. Left column: typical images for coupons that had not undergone coating with lactosides prior to immersion. Right column: typical images for coupons that had undergone coating with lactosides prior to immersion. All samples displayed biomass accumulation and the density of foulants appears to be similar independently of surface coating. Reproduced with permission from *ACS Sustainable Chem. Eng.*, **2018**, *6* (1), pp 1141–1151. Copyright 2017 American Chemical Society.

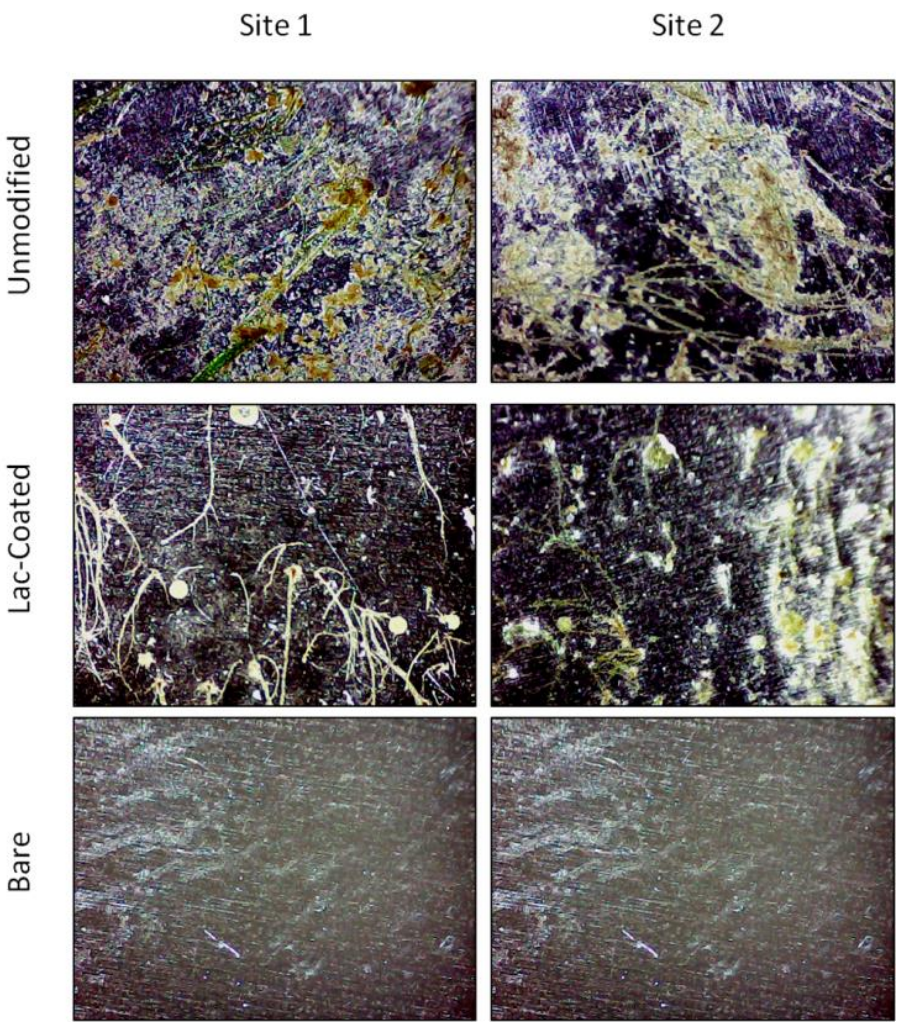

Optical microscope images of SS316 coupons extracted after 20 day immersion in coastal waters at sites 1 and 2; samples were rinsed under the same conditions prior to imaging. Top row: coupons not coated with an aryldiazonium layer of glycosides. Middle row: coupons coated with a layer of lactosides prior to immersion. Bottom row: a coupon sample as supplied by the vendor, without undergoing any immersion tests. All samples displayed biomass accumulation but the density of foulants is higher on unmodified than on lactoside-modified samples. Similar conclusions can be drawn based on images of samples from either site. **All images have a width of 4.5 mm**. Reproduced with permission from *ACS Sustainable Chem. Eng.*, **2018**, *6* (1), pp 1141–1151. Copyright 2017 American Chemical Society.

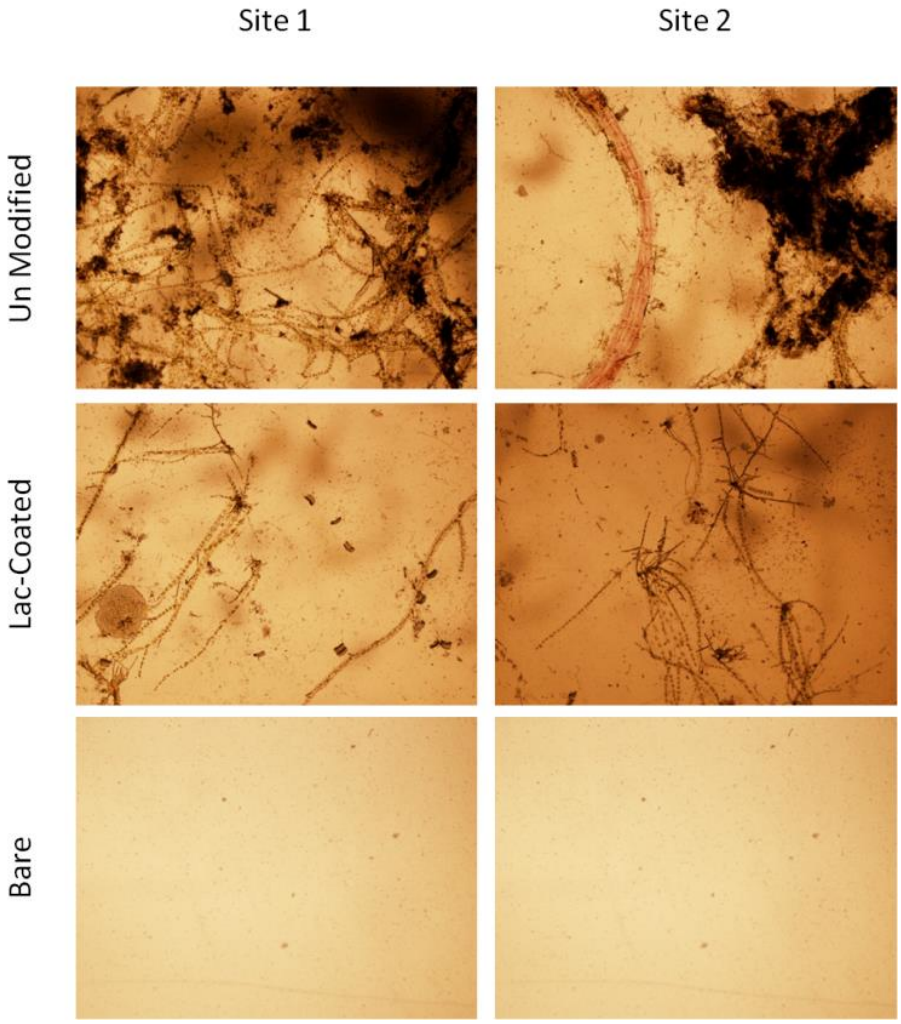

Optical microscope images of Nylon-6 coupons extracted after 20 day immersion in coastal waters at sites 1 and 2; samples were rinsed under the same conditions prior to imaging. Top row: coupons not coated with an aryldiazonium layer of glycosides. Middle row: coupons coated with a layer of lactosides prior to immersion. Bottom row: a coupon sample as supplied by the vendor, without undergoing any immersion tests. All samples displayed biomass accumulation but the density of foulants is higher on unmodified than on lactoside-modified samples. Similar conclusions can be drawn based on images of samples from either site. **All images have a width of 2.6 mm**. Reproduced with permission from *ACS Sustainable Chem. Eng.*, **2018**, *6* (1), pp 1141–1151. Copyright 2017 American Chemical Society.

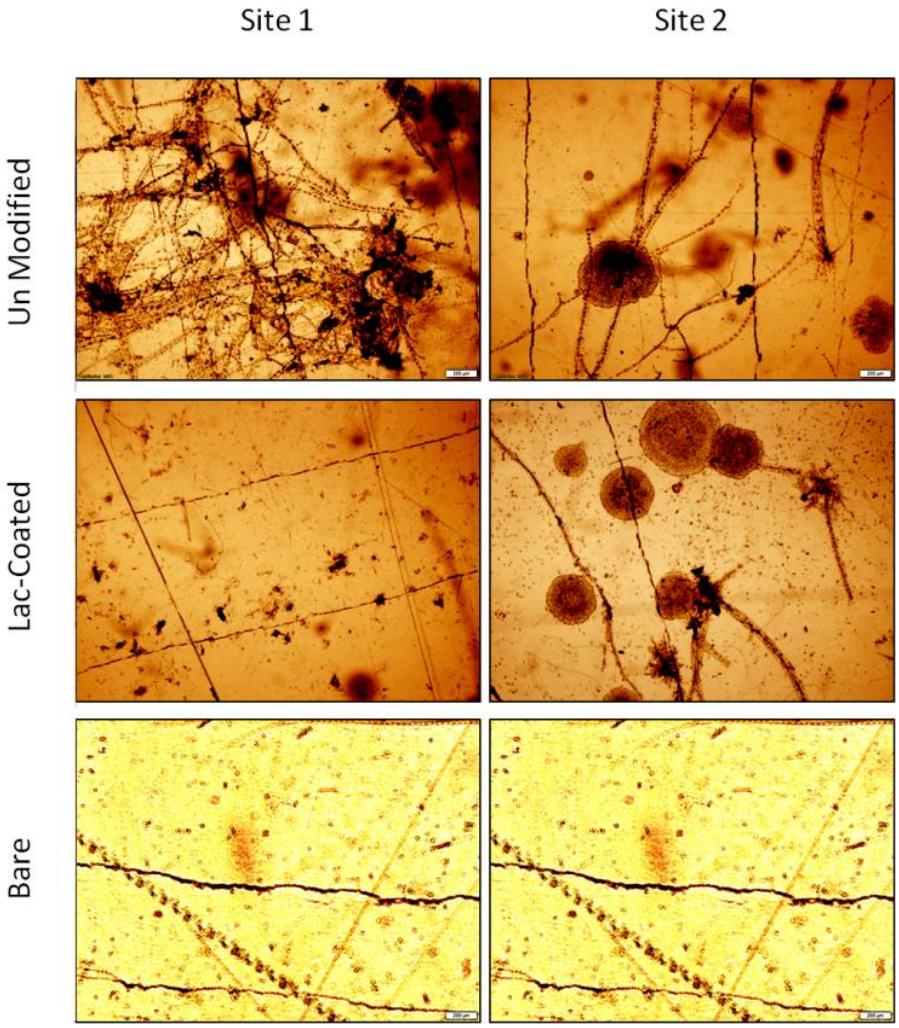

Optical microscope images of PES coupons extracted after 20 day immersion in coastal waters at sites 1 and 2; samples were rinsed under the same conditions prior to imaging. Top row: coupons not coated with an aryldiazonium layer of glycosides. Middle row: coupons coated with a layer of lactosides prior to immersion. Bottom row: a coupon sample as supplied by the vendor, without undergoing any immersion tests. All samples displayed biomass accumulation but the density of foulants is higher on unmodified than on lactoside-modified samples. Similar conclusions can be drawn based on images of samples from either site. **All images have a width of 2.6 mm**. Reproduced with permission from *ACS Sustainable Chem. Eng.*, **2018**, *6* (1), pp 1141–1151. Copyright 2017 American Chemical Society.

ACS Sustainable Chemistry & Engineering

Research Article

Cite This: ACS Sustainable Chem. Eng. 2018, 6, 1141−1151

pubs.acs.org/journal/ascecg

Bioinspired Aryldiazonium Carbohydrate Coatings: Reduced Adhesion of Foulants at Polymer and Stainless Steel Surfaces in a Marine Environment

Adam Myles,[†] Damien Haberlin,[‡] Leticia Esteban-Tejeda,[†] M. Daniela Angione,[†] Michelle P. Browne,[†] Md. Khairul Hoque,[†] Thomas K. Doyle,[§] Eoin M. Scanlan,*[,†] and Paula E. Colavita*[,†]

[†]School of Chemistry, CRANN and AMBER Research Centres, Trinity College Dublin, College Green, Dublin 2, Ireland

[‡]Marine and Renewable Energy Centre, Environmental Research Centre, University College Cork, Beaufort Building, Haulbowline Road, Ringaskiddy, Cork, Ireland

[§]School of Natural Sciences (Zoology), Ryan Institute and Marine and Renewable Energy Centre, National University of Ireland Galway, Galway, Ireland

Supporting Information

ABSTRACT: Surface treatments that minimize biofouling in marine environments are of interest for a variety of applications such as environmental monitoring and aquaculture. We report on the effect of saccharide coatings on biomass accumulation at the surface of three materials that find applications in marine settings: stainless steel 316 (SS316), Nylon-6 (N-6), and poly(ether sulfone) (PES). Saccharides were immobilized via aryldiazonium chemistry; SS316 and N-6 samples were subjected to oxidative surface pretreatments prior to saccharide immobilization, whereas PES was modified via direct reaction of pristine surfaces with the aryldiazonium cations. Functionalization was confirmed by a combination of X-ray photoelectron spectroscopy, contact angle experiments, and fluorescence imaging of lectin−saccharide binding. Saccharide immobilization was found to increase surface hydrophilicity of all materials tested, while laboratory tests demonstrate that the saccharide coating results in reduced protein adsorption in the absence of specific protein−saccharide interactions. The performance of all three materials after modification with aryldiazonium saccharide films was tested in the field via immersion of modified coupons in coastal waters over a 20 day time period. Results from combined infrared spectroscopy, light microscopy, scanning electron and He-ion microscopy, and adenosine-triphosphate content assays show that the density of retained biomass at surfaces is significantly lower on carbohydrate modified samples with respect to unmodified controls. Therefore, functionalization and field test results suggest that carbohydrate aryldiazonium layers could find applications as fouling resistant coatings in marine environments.

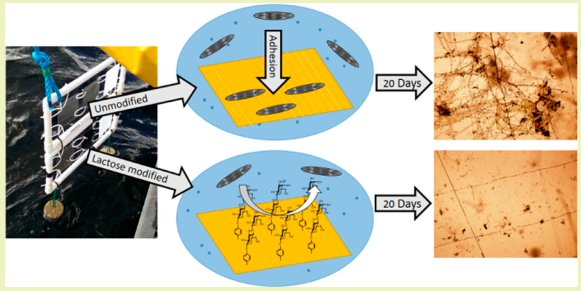

KEYWORDS: *Aryldiazonium, Coatings, Marine, Fouling, Functionalization, Carbohydrates*

INTRODUCTION

Materials immersed in natural waters are typically subject to biofouling, a process that can compromise the integrity of the material or device of interest and result in performance degradation. Structures which are submerged in a marine environment are particularly susceptible to a wide range of opportunistic fouling organisms,[1,2] and material biofouling and colonization can have a negative impact in a wide range of fields, from marine transport to environmental monitoring and aquaculture.[3−6] Marine biofilms result in major economic and environmental problems, from corrosion and loss of functionality of marine structures and vessels[7,8] to the spread of invasive species[9] and increased farmed fish mortality.[10−12] Therefore, there is great interest in developing new strategies for preventing and mitigating biofouling in the marine environment, particularly nontoxic or nonbiocidal strategies that are environmentally sustainable, commercially scalable, and compatible with the modern regulatory landscape.[1,3,4,13]

Biofouling occurs through a complex mechanism that involves multiple processes over a range of time and length scales.[13] It is proposed that, in the initial stages, the surface rapidly becomes conditioned by the adsorption of small molecules and organic matter such as small organics, biopolymers, and proteinaceous material. Microorganisms then adhere onto this primed surface, eventually forming a biofilm onto which larger organisms can attach and subsequently proliferate.[5] Accumulation of undesired biomass can be minimized by interfering at one or more of these stages

Received: September 26, 2017
Revised: November 16, 2017
Published: December 4, 2017

DOI: 10.1021/acssuschemeng.7b03443
ACS Sustainable Chem. Eng. 2018, 6, 1141−1151

of the biofouling cascade. Historic methods of biofilm mitigation involve the use of toxic coatings such as lead-based and organotin paints,[14] which interfere at the micro- and macrofouling stages. However, due to adverse effects on marine ecosystems, these methods have been phased out, and even use of alternative paints and coatings based on copper release is under regulatory scrutiny. The disruption of quorum sensing signals to inhibit/regulate biofilm formation potentially offers a more targeted approach than metal-based biocides; however, this technology is in its infancy, and its environmental impact on ecosystems remains to be assessed.[15]

The most promising nonbiocidal strategies, on the contrary, rely on modifying the physicochemical properties of submerged materials to minimize adsorption and adhesion mainly at early fouling stages. Regulation of surface roughness, electrostatic charge distribution, and wetting behavior have all been investigated as nonbiocidal methods.[13,16] Bioinspired engineered nanotopographies are effective for regulating cell/spore settling; however, complex hierarchical patterns are required to repel settling from heterogeneous populations,[17] thus posing significant problems for cost-effective scalability. Regulation of wetting and spatial control of hydrophobicity at the nanoscale level have also been explored as antifouling mechanisms. Low surface free energy and hydrophobic materials and coatings have a long history in antifouling technologies, and some well-known examples are polysiloxanes, fluoropolymers, and superhydrophobic coatings.[1,6,13,18,19] At the other end of the spectrum, hydrophilic coatings such as those based on polyethylene glycols (PEGs)[20] and bioinspired superhydrophilic zwitterionic polymers[21,22] have similarly demonstrated good performance in laboratory tests.

Surface-immobilized carbohydrates have previously been investigated for the fabrication of hydrophilic coatings for biofouling prevention. Carbohydrates represent an interesting family of biomolecules because they are environmentally benign and highly stable toward oxidation compared to other chemical species such as ethylene glycols.[18,20,23] Previous work has shown that self-assembled monolayers (SAMs) of monosaccharides and disaccharides on gold surfaces can greatly reduce fouling from protein solutions.[24−27] More recently, Ederth et al.[25] demonstrated that galactose-bearing SAMs were successful at reducing *Ulva linza* spore settling, thus showing promise for marine fouling control. Polysaccharides have also been investigated; however, the efficient calcium binding affinity displayed by many of these, e.g. hyaluronic and pectinic acids, has been identified as detrimental for fouling control in the marine environment.[28,29] Nonetheless, relative to other functional coatings, carbohydrates are underexplored in marine applications, and results from field tests are rare in the literature.

We recently showed that aryldiazonium chemistry offers a viable route for the immobilization of saccharides at carbon, metal, and selected polymer surfaces.[30] This immobilization strategy can be carried out from solution via spontaneous reaction, resulting in thin conformal functional films that can be applied via flow, spray, or dip coating methods using aqueous solutions, thus making it attractive and feasible for large scale applications. Covalent grafting of mono- and disaccharide-bearing aryldiazonium cations to carbon, polydimethylsiloxane (PDMS), and poly(ether sulfone) (PES) was found to significantly reduce protein adsorption in laboratory tests.[31−33] Interestingly, in the case of PES surfaces, the ability to prevent protein adsorption translated well to field tests, whereby aryldiazonium glycoside coatings were found to reduce biomass accumulation after prolonged exposure to wastewater effluents.[33] These prior results strongly suggest that aryldiazonium carbohydrate coatings could be effective at minimizing biofouling in the complex environment of natural waters; however, to the best of our knowledge, these coatings have not been tested in marine settings.

In this work, we report a study of the performance of carbohydrates immobilized via aryldiazonium grafting as fouling resistant coatings on coupons of three different materials of technological importance: stainless steel, nylon, and PES. Polyamide materials and metal alloys are used regularly in the marine environment and are particularly susceptible to marine fouling, while PES is a common membrane material used in aquatic sensors. Lactosides were chosen for immobilization via spontaneous aryldiazonium grafting because of their lack of calcium-binding carboxylic acid residues[28] and on the basis of previously published comparative tests on the performance of simple glycosides.[24,32,33] First, we report on the effectiveness of spontaneous functionalization reactions on the above substrates; second, we report the results of immersion tests in a coastal environment for 20 days over the summer period. Results from field tests indicate that carbohydrate coatings show promise as a sustainable and environmentally benign approach for reducing adhesion and retention of marine foulants.

EXPERIMENTAL METHODS

Chemicals and Materials. Polyamide-Nylon-6 (N6) sheets, marine grade stainless steel 316 foil (SS316), and poly(ether sulfone) sheets (PES) were purchased from Goodfellow; formaldehyde solution for molecular biology ≥36.0% in H_2O, hypophosphorous acid solution 50 wt % in H_2O, sodium hypochlorite (bleach), sodium hydroxide, potassium hydroxide, phosphate buffered saline buffer (0.010 M PBS, pH 7.4), sodium nitrite, hydrochloric acid, and fluoroboric acid were purchased from Sigma-Aldrich. Aquasnap ATP Total Water testing strips were purchased from Water Technology Ltd. Bovine serum albumin (BSA) conjugates with Alexa Fluor 647 were purchased from Biosciences. BSA and peanut agglutinin from *Arachis hypogaea* (PNA) conjugates with fluorescein isothiocyanate (FITC) were purchased from Sigma-Aldrich. 4-Aminophenol-β-D-lactopyranose and its fluorinated analogue 2-fluoro-4-aminophenol-β-D-lactopyranose (Scheme 1) were synthesized as previously described.[30,33] The peracetylated lactoside 2-fluoro-4-aminophenyl-2,3,4,6-tetra-*O*-acetyl-β-D-galactopyranosyl-(1 → 4)-2,3,6-tri-*O*-acetyl-β-D-glucopyranoside (Scheme 1) was used for infrared experiments; synthesis and characterization of this compound are reported in the Supporting Information.

Surface Modification. Prior to modification with aryldiazonium cations, both polyamide and stainless steel surfaces were preactivated, while PES surfaces did not require preactivation[33] and were used after light cleaning in methanol only. N6 samples were preactivated by overnight immersion at 30 °C in a 36% aqueous formaldehyde solution with a catalytic amount of hypophosphorous acid. Stainless steel samples (SS316) were pretreated with 0.5% NaClO in basic aqueous solution (KOH 1% and NaOH 1%);[32] surfaces were immersed 3 times in fresh solution for 10 min at room temperature. Samples were rinsed thoroughly with deionized water and functionalized via immersion in freshly prepared 1.0 mM solutions of aryldiazonium cations generated in situ from the corresponding amine, 4-aminophenol-β-D-lactopyranose (Scheme 1), following previously published protocols.[30] Briefly, a 1.25 mM solution of the 4-aminophenol in 0.00150 M HBF_4 was prepared and cooled to 4 °C or less in an ice bath for 1 h. The cold precursor solution was diluted via addition of a 0.010 M $NaNO_2$ to a final concentration of 0.0010 M in 4-aminophenol precursor, acid, and nitrite. Samples were immersed immediately into the precursor solution, kept in the dark for 1 h, and then rinsed with deionized water and kept under wet storage in

DOI: 10.1021/acssuschemeng.7b03443
ACS Sustainable Chem. Eng. 2018, 6, 1141−1151

Scheme 1. 4-Aminophenol-β-D-lactopyranose Compounds Used for All Functionalized Samples and Reaction Protocol Used for Diazotization and Functionalization with Aryldiazonium Cations in Situ

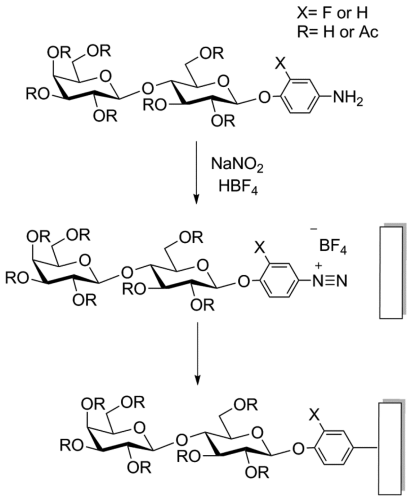

deionized water prior to further testing. For field studies, a typical batch size for material modification was 3 L, while laboratory experiments involved the preparation of 25 mL solutions. Functionalization using peracetylated precursors followed the same protocol except for the use of acetonitrile as a solvent; samples were rinsed using sonication in acetonitrile/methanol, a protocol that had been shown to be effective at removing physisorbed acetylated aryldiazonium glycosides.[30]

Surface Characterization. Water contact angles (WCAs) were determined for all samples using the sessile drop method (FTA1000), using 20 μL droplets. Infrared reflectance absorption spectroscopy (IRRAS) characterization was carried out on a Bruker Tensor 27 infrared spectrometer equipped with a mercury cadmium telluride detector and a VeeMax II specular reflectance accessory with a wire grid polarizer. All spectra were collected using p-polarized light; 100 scans at 4 cm^{-1} were collected for all samples, and an unmodified sample was used as background. X-ray photoelectron spectroscopy (XPS) was carried out on a VG Scientific ESCAlab MK II system with an Al Kα source at 90° takeoff angle. Wide surveys and core level spectra were collected at 50 and 20 eV pass energy, respectively. All spectra were calibrated to the Cr $2p_{3/2}$ peak of Cr_2O_3 present in the stainless steel substrate at 576.7 eV (Figure S1).[34,35] Fits were carried out using commercial software (CasaXPS) using Voigt line shapes and background correction; atomic ratios were calculated from peak areas after correction for relative sensitivity factors (RSF_{C1s} = 1; RSF_{F1s} = 4.43; RSF_{Cr2p} = 11.7; RSF_{Fe2p} = 16.4). Optical depths were calculated from UV−vis transmittance measurements (Lambda 35 PerkinElmer). Scanning electron microscopy (SEM) images were obtained on a Karl Zeiss Ultra Field Emission SEM at accelerating voltages between 2 and 3 kV in secondary electron mode. Helium ion microscopy (HIM) was obtained on a Karl Zeiss NanoFab HIM at 0.2−0.6 pA beam currents and 30 kV accelerating voltage, while sample charging was minimized using a flood gun.

Affinity Binding and Protein Adsorption Studies via Fluorescence Imaging. To determine protein rejection ability, samples of N6 and SS316 were incubated in 0.2 mg mL^{-1} solutions of BSA fluorescent conjugates in PBS at pH 7.4 for 1 h; Alexa-647 and FITC were the dyes used for N6 and SS316, respectively. To determine lectin binding affinity, samples of SS316 were incubated for 1 h in a 0.2 mg mL^{-1} solution of PNA-FITC conjugate in pH 7.4 PBS buffer with 0.1 mM $CaCl_2$ and $MgCl_2$. All samples were washed with PBS solution prior to imaging to remove excess unbound protein. Fluorescence images were acquired using an Olympus BX51 inverted microscope with cellSense digital image processing software. Emission intensities were analyzed in triplicate using ImageJ software.[32]

ATP Determinations. Adenosine triphosphate (ATP) concentrations per square centimeter of substrate material were determined using the luciferase assay as implemented in a commercial kit (Aquasnap Total Water).[36] The assay was first calibrated using standard solutions and the luminometer (Hygiena) to obtain a conversion from relative luminescence units (RLU) to ATP concentration (in nM range). Samples of approximately 1 cm^2 were cut from each coupon in triplicate; the cutting was suspended in a known volume of deionized water (10 or 5 mL, depending on level of fouling) in sterile centrifuge tubes and then sonicated for 10 min. The value of RLU was determined for each water sample and converted to ATP concentration; water samples were diluted if needed to bring the ATP concentration within the linear range of the assay. Postsonication, the cuttings were dried under argon, and their masses were determined; the relative exposed area was estimated from the mass of the cleaned sample cutting, and this value was used to surface-normalize ATP determinations on individual cutting. Values were compared using ANOVA at 5% significance level (α = 0.05).

Coastal Immersion Study. Immersion studies were carried out on August 24, 2016 in Bertraghboy Bay, County Galway, at the site of an unused salmon farming platform (Lehanagh pool). Following functionalization, 6 control and 6 functionalized coupons, 100 × 100 mm^2 in size, were transported within 24 h under wet storage to the testing site located at 150 m from the shore (53.402267°N, 9.820329°W). Polyethylene frames on which N6, SS316, and PES coupons had been mounted were set up as shown in Figure 1a. Frames

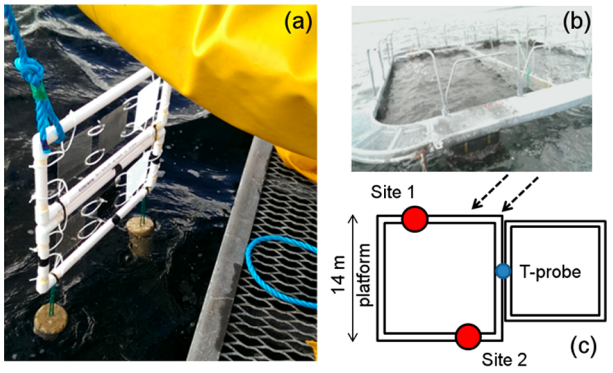

Figure 1. (a) Assembled frame with coupons, arranged from left to right, PES, SS316, and N6, immediately prior to immersion in seawater. (b) Salmon farm platform from which frames with coupons were suspended. (c) Scheme showing the two adjacent platforms and the location of frames at sites 1 and 2 relative to the tide (dashed arrows); a temperature probe measured surface water temperature at the position indicated in blue.

were transported by power boat to the testing site and suspended from the edge of the test site (Figure 1b) at a depth of approximately 1 m, considered to be optimal for rapid biofouling.[37] The frames were weighted to ensure that all samples would remain in a vertical position throughout the duration of the trial which lasted 20 days over the summer months (August 24 to September 13). The mean water temperature during the 20 day trial was 16.84 ± 0.31 °C (maximum 18.20 °C, minimum 16.23 °C), measured from readings at 1 m depth (StowAway TidbiT). Two positions were chosen for suspending the frames: these are denoted as site 1 and site 2 and are mapped to the platform configuration in Figure 1c. Three samples of each control and functionalized coupon were mounted at each site, i.e. a total of 12 coupons, 4 of each material distributed over the 2 sites. After the 20 day test, all samples were transported to the laboratory immersed in seawater prior to testing. Samples were rinsed under a stream of deionized water delivered 10 cm above the sample by gravity for 30 s on each side. This procedure was used across all samples to remove loosely attached biomass. Samples were analyzed immediately or stored frozen for further characterization.

DOI: 10.1021/acssuschemeng.7b03443
ACS Sustainable Chem. Eng. 2018, 6, 1141−1151

RESULTS

Aryldiazonium Modification of Stainless Steel and Nylon Coupons. Coupons of PES, SS316, and N6 were first modified using lactoside groups via spontaneous reaction of aryldiazonium cations to yield surfaces denoted as Lac-PES, Lac-SS, and Lac-N6. Aryldiazonium cation solutions were freshly prepared immediately prior to functionalization following standard diazotization protocols; briefly, the arylamine compound was reacted with sodium nitrite in acid aqueous solution at 4 °C (Scheme 1), yielding the corresponding aryldiazonium cation, a highly reactive species.

Work from our group demonstrated that PES undergoes functionalization by spontaneous reaction after immersion of pristine substrates in these solutions, and we refer to our previous publication for a full characterization of Lac-PES surfaces thus obtained.[33] In the case of SS316 and N6, surfaces were preactivated prior to functionalization. SS316 surfaces were preactivated in caustic hypochlorite (bleach) solutions; this treatment is known to have cleaning and oxidizing effects on SS316 surfaces.[38−40] N6 surfaces were pretreated by immersion in formaldehyde solutions, which are known to activate amide groups in polyamides via formation of *N*-methylol groups.[36,41,42] Preactivation treatments were found to increase surface hydrophilicity, as evident from a marked change in water contact angle (Figure 2). The WCA of SS316

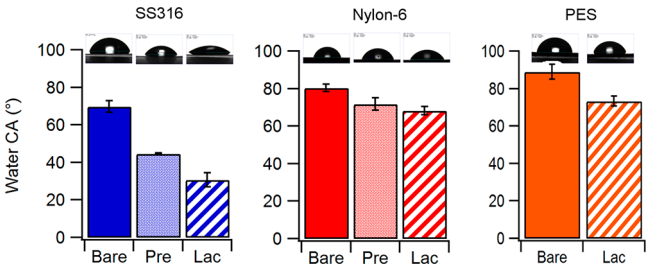

Figure 2. Water contact angle values obtained on bare, pretreated (except for PES), and lactose-modified (Lac) surfaces of SS316, Nylon-6, and PES. Samples were preactivated in caustic bleach and formaldehyde solutions in the cases of SS316 and Nylon-6, respectively.

decreases from 69.8 to 44.5°, as expected from oxidative cleaning of adventitious organics and exposure of a hydrophilic oxide film.[43] The WCA of nylon also decreases from a value of 80.4°, in agreement with literature values for pristine N6, to 71.7°; this is consistent with an increase in the surface density of hydroxyl groups resulting from formaldehyde treatment. Coupons of all three materials tested displayed a significant change in WCA after immersion in the aryldiazonium cation solution. Figure 2 shows that all surfaces decreased their WCA, as expected from the immobilization of hydrophilic saccharide groups and in agreement with previous reports on the effect of lactoside immobilization.[31]

Lactoside immobilization was further confirmed using binding studies using PNA lectin. PNA is known to display binding affinity toward galactose[44] and can be used to confirm the presence of surface-bound lactosides as these display an available galactose unit at the solid−liquid interface. Lac-SS and Lac-N6 coupons were incubated for 1 h in a solution of fluorescently labeled PNA and rinsed with PBS prior to imaging; Figure 3 shows fluorescence microscopy images of pretreated and Lac-modified surfaces after PNA incubation and

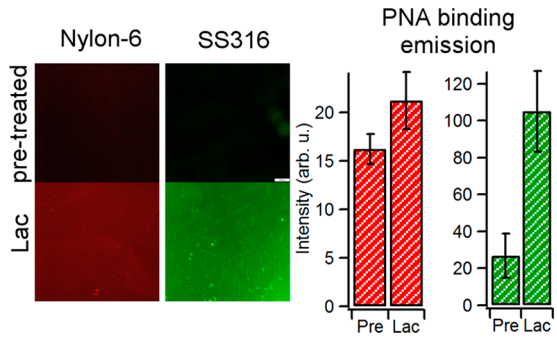

Figure 3. Fluorescence images obtained after lectin binding experiments using dye-conjugated PNA on Nylon-6 and SS316 after pretreatment and after aryldiazonium modification with lactosides (Lac). The images show that the emission intensity is higher on lactose-modified surfaces. Bar plots represent average emission intensities of Alexa-PNA on Nylon-6 (red bars) and of FITC-PNA on SS316 (green bars) obtained at pretreated (Pre) and lactose-modified coupons (Lac).

a comparison of average emission intensities. The stronger emission observed for surfaces after reaction with aryldiazonium cations indicates preferential specific binding with respect to the corresponding bare pretreated surface and is therefore supporting of functionalization. No evidence of modification was found in the absence of pretreatment for either SS316 or N6 surfaces.

Protein adsorption experiments were also carried out using fluorescently labeled BSA, a protein that does not display specific binding with glycosides. Figure 4 shows images of

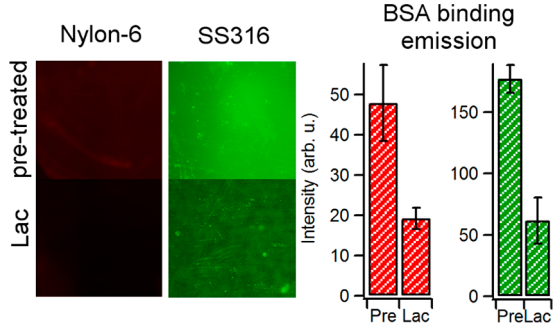

Figure 4. Fluorescence images obtained after protein adsorption experiments using dye-conjugated BSA on Nylon-6 and SS316 after pretreatment and after aryldiazonium modification with lactosides (Lac). The images show that the emission intensity is lower on lactose-modified surfaces. Bar plots represent average emission intensities of Alexa-BSA on Nylon-6 (red bars) and of FITC-BSA on SS316 (green bars) obtained at pretreated (Pre) and lactose-modified coupons (Lac).

pretreated and Lac-modified SS316 and N6 with a summary of average emission intensity values obtained using BSA on pretreated and modified coupons. After functionalization with lactosides, a decrease in emission is observed compared to the pretreated surface, thus indicating that less BSA adsorbs at Lac-SS and Lac-N6 surfaces. This indicates, first, that the increase in fluorescence observed for Lac-SS and Lac-N6 after incubation in PNA solutions is the result of specific Gal-PNA interactions. Second, that immobilization of small saccharides leads to a decrease in unspecific protein binding, in agreement with

DOI: 10.1021/acssuschemeng.7b03443
ACS Sustainable Chem. Eng. 2018, 6, 1141−1151

observations on the effect of glycoside coatings on carbon and other polymer surfaces.[31,33]

In the case of SS316, functionalization was also confirmed using the fluoro-substituted derivative of the lactoside precursor shown in Scheme 1, as the presence of fluorine substituents provides good elemental contrast between the functional layer and the bare substrate. Survey spectra of pretreated and modified SS316 in Figure 5a show the characteristic peaks of

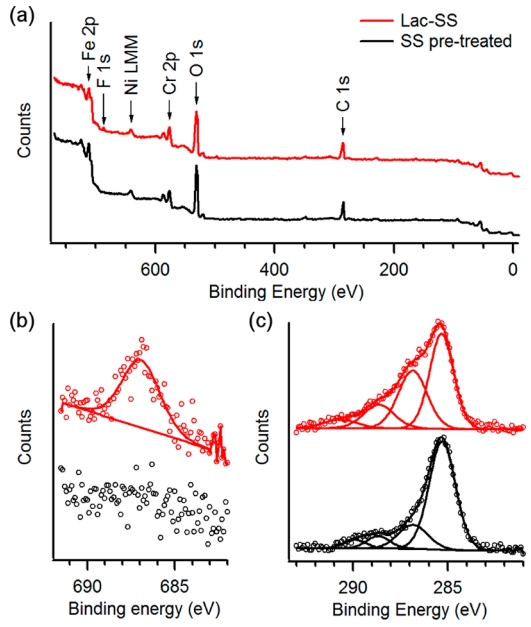

Figure 5. (a) Survey XPS spectra of SS316 after pretreatment (black) and after modification with F-substituted aryl-lactoside (red). (b) F 1s and (c) C 1s high resolution spectra; these spectra show that upon reaction with aryldiazonium lactosides, peak contributions appear at 687 and 286−289 eV that can be attributed to F atoms and C−O groups, respectively.

stainless steel associated with Fe 2p, Cr 2p, Ni LMM, O 1s, and C 1s lines.[45,46] Figures 5b and c show the spectra of SS316 in the F 1s and C 1s regions, respectively, after pretreatment and after surface modification in solutions of the fluorinated aryldiazonium lactoside.

Analysis of peak area ratios and fitting of the C 1s line yielded results summarized in Table 1. The pretreated SS316 surface shows C/Cr and Cr/Fe atomic ratios that are consistent with those observed for plasma cleaned SS316 by Williams et al.;[46] the surface was found to be C- and Cr-rich with respect to the bulk composition, in agreement with previous compositional studies.[34] Deconvolution of the C 1s line shows the presence of 4 main peaks at 285.3 eV (C−C and C−H), at 286.8 and 288.7 eV (C−O), and at 289.9 eV (C═O), in agreement with previous reports for stainless steel surfaces.[47] After functionalization, a clear peak is evident at 687.0 eV consistent with the F 1s binding energy of fluorinated organics, where F atoms are in a low F/C content environment.[48,49] Identical changes were obtained in the F 1s region after functionalization using chloride as a counterion (Figure S2), thus confirming that the F 1s peak does not arise from tetrafluoroborate contamination. Therefore, this result suggests that after functionalization the aryl group is bound to the SS316 surface. The conclusion is further supported by an increase of the C 1s peak intensity relative to the Cr 2p signal, which arises from the substrate alloy. The fit of the C 1s line of Lac-SS (Figure 5c) shows (a) the appearance of a contribution at 290.5 eV, consistent with the binding energy expected for a C−F group;[48,50,51] and (b) increased emission in the region 286−289 eV, consistent with greater surface density of C−O containing groups and with the presence of surface bound glycosides. The RSF corrected peak area ratio $(A_{286} + A_{288})$: A_{687} = 12.2 is in good agreement with the 12:1 ratio of C−O to C−F expected from the molecular stoichiometry of the fluorinated precursor, thus confirming the assignment of peaks in the region 286−289 eV to, predominantly, C−O groups from the lactoside with likely minor contributions from substrate carbon. These results therefore indicate that the functionalization protocol resulted in surface modification of SS316 with aryl-lactosides.

An estimate of the molecular density can be obtained by assuming that the SS316 substrate surface consists of Cr_2O_3/Fe_2O_3 with 40% Cr_2O_3 content (Cr/Fe = 0.67), as calculated from XPS and in agreement with Williams et al.[46] Considering that both Cr_2O_3 and Fe_2O_3 have a density of 5.2 g cm^{-3}, the photoelectron attenuation depth of Cr 2p photoelectrons can be predicted to be λ = 1.5 nm using Gries' G-1 predictive formula.[52] Under the assumption that no photoelectrons escape from depths >3λ, the average experimental F/Cr 0.17 ± 0.10 atomic ratio measured over 5 samples yields an estimated mean density of 1.9 × 10^{-9} mol cm^{-2}.[53] For a perfectly smooth surface, this coverage is equivalent to <5 monolayers of lactosides.[30,54] Given that the microscopic roughness factor of unpolished SS316 is >1, the estimated coverage value suggests the presence of a relatively sparse lactoside layer, as expected from a spontaneous reaction of the oxide surface with these bulky aryldiazonium cations and consistent with thin molecular layers formed on carbon substrates via similar protocols.[31]

Finally, functionalization of SS316 surfaces was confirmed using a peracetylated analogue of the aminophenol lactoside precursor (see Scheme 1): acetyl moieties serve as infrared labels thanks to their intense infrared absorbances.[30] Figure 6 shows the IRRAS spectrum of a SS316 sample after functionalization (surface, bottom trace), compared to the transmittance spectrum of the peracetylated phenyl-glycoside precursor compound (bulk, top trace).[30] The IRRAS spectrum displays the characteristic peaks of acetyl groups at 1760 cm^{-1} (C═O stretching), 1373 cm^{-1} (CH_3 bending), and 1246 cm^{-1} (C−O−C asymmetric stretching).[55] The peak centered at 1080 cm^{-1} is associated with C−O stretching modes of the carbohydrate ring, while the peak at 1510 cm^{-1} arises from C−C skeletal vibrations of phenyl rings.[33,55]

In summary, the functionalization protocol outlined in Scheme 2 was found to be successful at grafting lactoside

Table 1. Summary of Results from XPS Analysis of Spectra in Figure 5[a]

	SS pretreated	Lac-SS
C 1s (eV)	285.3 (70%)	285.1 (46%)
	286.8 (18%)	286.7 (33%)
	288.7 (7%)	288.4 (15%)
	289.9 (5%)	290.5 (6%)
F 1s (eV)		687.0
C/Cr at.	6.9	7.6
F/Cr at.		0.30
Cr/Fe at.	0.67	0.68

[a]Values in parentheses indicate percent contribution to the total peak intensity; elemental ratios are calculated as atomic ratios.

DOI: 10.1021/acssuschemeng.7b03443
ACS Sustainable Chem. Eng. 2018, 6, 1141−1151

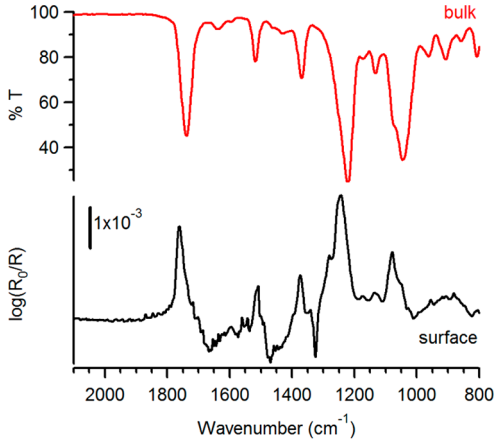

Figure 6. Infrared transmittance spectrum of a peracetylated aminophenol lactoside precursor (red, top) and IRRAS spectrum at 80° incidence of the organic layer obtained after modification of a SS316 sample (black, bottom) with the same aryldiazonium precursor. The IRRAS spectrum displays the characteristic peaks of the precursor compound; peak assignments are discussed in the main text.

Scheme 2. Protocol Used for the Modification of SS316, N6, and PES

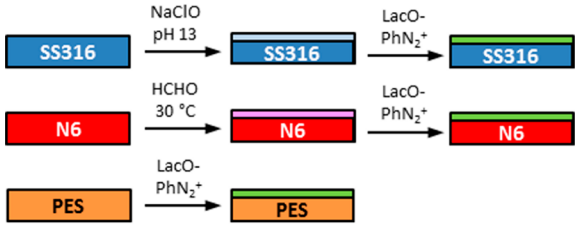

groups via spontaneous reactions of aryldiazonium cations onto SS316 and N6 surfaces. To the best of our knowledge, this is the first reported protocol for the modification of nylon using aryldiazonium cations. It is interesting to note that the pretreatment protocol results in the formation of −OH groups, and it is therefore likely that the functionalization mechanism involves nucleophilic attack of the hydroxyl onto the electron deficient para position of the aryl ring, in analogy to the S_N1 hydrolysis mechanism of aryldiazonium cations (see Scheme S1).[56] As regards stainless steel functionalization, most previous reports make use of cathodic electrografting reactions that can be driven even in the presence of a continuous passive oxide.[57−59] Small et al.[60] recently reported on the spontaneous attachment of fluorinated aryldiazonium salts on stainless steel from solution, achieved by polishing samples immediately prior to modification. Mechanical polishing breaks down the steel passive oxide, exposing the iron-rich underlayer which can act as an effective spontaneous reductant in aryldiazonium grafting, in agreement with findings on various oxide-free metals.[61] In our case, we carried out an oxidizing pretreatment which is expected to yield instead a homogeneous hydrophilic passive oxide that cannot directly reduce the aryldiazonium cation; nonetheless, this oxide surface offers a high density of functional M−OH and/or M-OOH sites[60,62] available to chemical reaction. There are few reports of spontaneous aryldiazonium reactions on oxides;[63,64] however, the spontaneous formation of M−O−Ar bonds has been demonstrated experimentally.[64] On the basis of our results, spontaneous grafting can take place on passivated stainless steel surfaces via aryl group cross-linking. It is likely that, as in the case of reactions with primary alcohols, functionalization proceeds via nucleophilic substitution involving oxide hydroxyl groups (see Scheme S1).[56]

Field Tests of Bare and Lactose-Modified Surfaces. Control and lactose-modified coupons remained immersed in

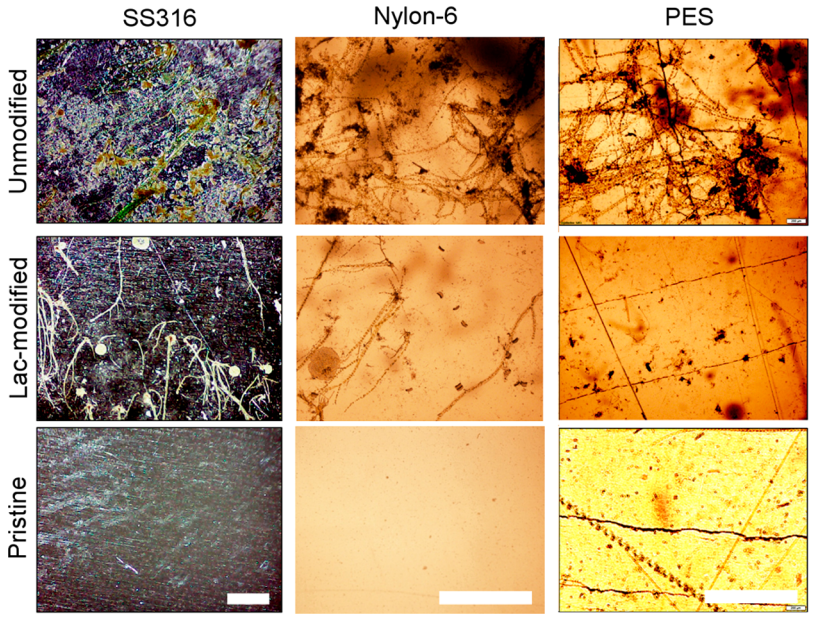

Figure 7. Optical microscope images of coupons of SS316, Nylon-6, and PES (scale bar = 1 mm) extracted after 20 day immersion in coastal waters at site 1 (see Figure 1); samples were rinsed under the same conditions prior to imaging. The top row shows images of coupons that had not been coated with an aryldiazonium layer of glycosides; the middle row shows coupons that had been coated with a layer of lactosides prior to immersion, and the bottom row shows samples as supplied by the vendor without undergoing any immersion tests. All immersed samples display biomass accumulation; however, the density of adhered organic matter appears to be higher on unmodified when compared to lactoside-modified samples.

DOI: 10.1021/acssuschemeng.7b03443
ACS Sustainable Chem. Eng. 2018, 6, 1141−1151

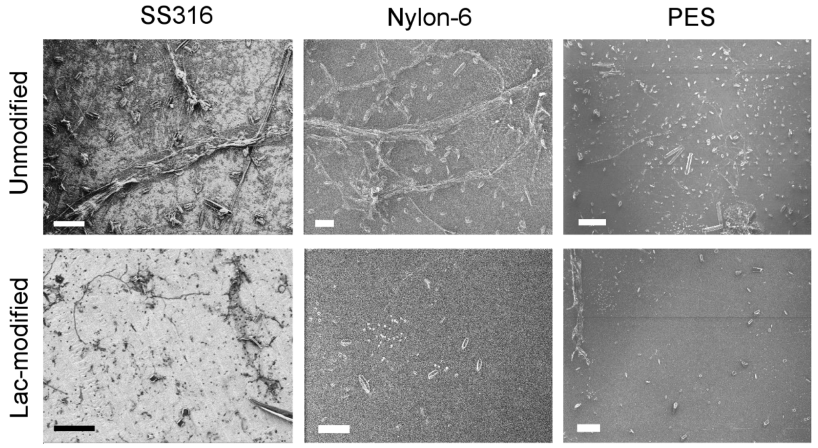

Figure 8. Microscopy images of coupons of SS316 (SEM, scale bar = 40 μm), Nylon-6 (HIM, scale bar = 40 μm), and PES (HIM, scale bar = 100 μm). The figures show details of surfaces after 20 day immersion in coastal waters followed by rinsing under identical conditions prior to imaging. The top row shows images of coupons that had not been coated with an aryldiazonium layer of glycosides; the bottom row shows coupons that had been coated with a layer of lactosides prior to immersion.

coastal waters for 20 days, at the end of which samples were taken out of the water, and the amount of biomass accumulated on the coupons was compared using a combination of optical and scanning microscopies, ATP content analysis, IRRAS in the case of SS316, and optical transmission in the case of PES. After immersion, minimal differences were observed among different coupon materials and between lactose-modified samples and unmodified controls of the same material upon visual inspection (Figure S3). However, after controlled light rinsing, it was possible to observe clear and significant differences between coated and uncoated samples, as discussed below.

Figure 7 shows representative optical microscopy images of SS316, N6, and PES coupons positioned at site 1 with images of a corresponding pristine surface that had not undergone immersion; images of coupons at site 2 showed a similar trend (Figures S4–S6). Samples that had been coated with the aryldiazonium layer of lactoside units were found to display a visibly lower density of foulants. Unmodified samples in Figure 7 (top row) appear to show the evidence of secondary adhesive structures (algae pads or stalks),[65] which are mostly absent in Lac-modified samples (middle row) and are important for the development of microbial slimes. Figure 8 shows images at higher resolution obtained by SEM and HIM microscopies on SS316 and polymer coupons, respectively. It is possible to observe the presence of diatoms and mucilaginous trails; visual inspection suggests that pennate diatoms dominate the retained deposits, in agreement with typical findings in marine fouling experiments.[65] Scanning microscopy images also confirmed that a higher density of foulants remained adhered to the unmodified coupons compared to the modified ones for all tested materials.

Total ATP is an indicator of microbial biomass content and can be used to assess biomass accumulation at surfaces.[66] Samples of known size taken from coupons were immersed into identical volumes of deionized water and sonicated to extract adsorbed biomass; a commercial bioluminescence assay was used to compare the ATP content extracted from control and lactose-modified samples. All RLU values were determined in deionized water, and dilution factors were chosen which ensured that measurements fell within the linear dynamic range of the assay;[67] this procedure allowed for a conversion of RLU values to ATP concentrations in the extract and subsequent conversion to ATP mass released per unit area. Figure 9a shows a summary of ATP determinations obtained for SS316, Nylon-6, and PES surfaces after immersion tests and prior to any rinsing. A comparison of ATP values indicates that biofilm accumulation was unaffected by the nature of the substrate

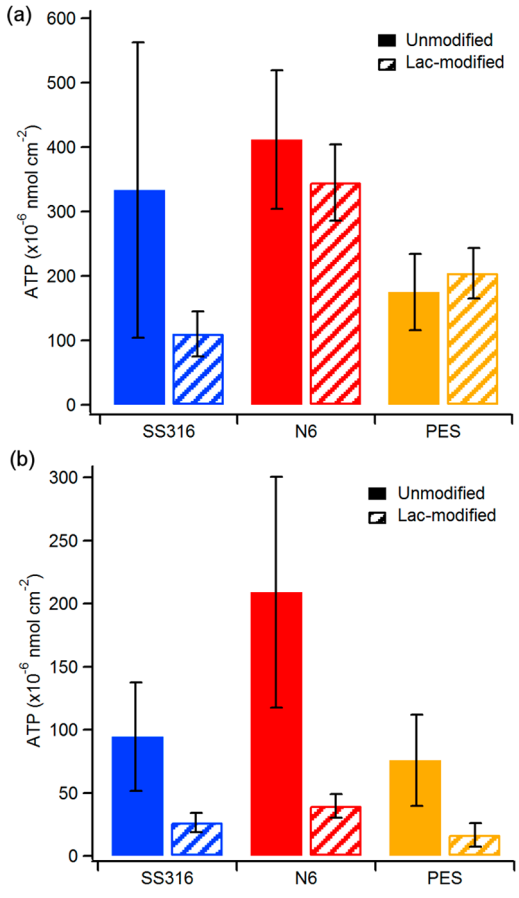

Figure 9. Average ATP released per unit area from unmodified (solid) and lactose-modified (striped) SS316, Nylon-6, and PES coupons after 20 day immersion tests in coastal waters prior to any rinsing (a) and after controlled rinsing (b). Error bars indicate 90% confidence interval (C.I.).

DOI: 10.1021/acssuschemeng.7b03443
ACS Sustainable Chem. Eng. 2018, 6, 1141−1151

material with similar values obtained for SS316, N6, and PES coupons (P = 0.18). ATP values were found to be similar for control and modified coupons; in the case of SS316, results suggest a beneficial effect from the coating (P = 0.08) at a slightly higher significance level that might be clarified by further studies with a larger sample size.

Figure 9b shows a comparison of ATP values obtained at the three surfaces after controlled rinsing. The level of ATP measured at unmodified (control) surfaces was found to vary depending on the material, with results indicating that Nylon-6 retains the highest levels of biomass. A comparison between control and lactose-modified samples clearly shows that surfaces coated by carbohydrate layers have significantly lower amounts of retained biomass; this was confirmed in the case of SS316 (P = 0.04), N6 (P = 0.03), and PES (P = 0.04).

The controlled rinsing process resulted in a reduction of ATP for all samples; however, the effect is noticeably greater in the case of lactose-modified surfaces yielding reductions of 75, 89, and 92% for SS316, Nylon-6, and PES, respectively. These results therefore indicate that the lactoside layer has a strong impact on the ability of foulants to adhere to the material surface, thus improving resistance to biomass retention; this effect is particularly evident in the case of the two polymers tested.

IRRAS analysis was carried out to compare biomass accumulation at control and modified SS316; this was not possible in the case of N6 and PES due to the poor reflectance of these substrates. Figure 10 shows representative IRRAS

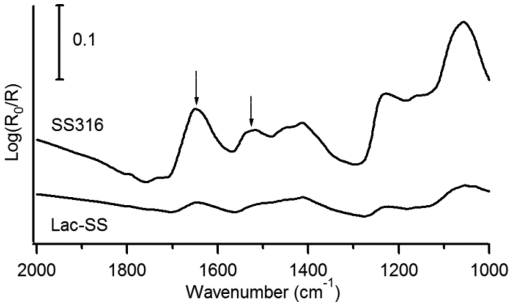

Figure 10. IRRAS spectra at 45° incidence of SS316 unmodified sample and lactose-modified SS316 after 20 day immersion tests; this specific sample was located at site 2; however, in all cases, unmodified samples show more intense absorption peaks. Arrows indicate peaks at 1645 and 1525 cm^{-1} corresponding to amide I and amide II modes, respectively.

spectra in the amide region of both a control and a lactose-modified SS316 sample after rinsing. The spectra show peaks at 1640 and 1530 cm^{-1}, which are assigned to the amide I and amide II modes, respectively, of polypeptides.[55] These peaks display higher intensity for unmodified SS316, thus indicating that the surface density of proteinaceous material accumulated on control surfaces is higher than on lactose-modified surfaces.

PES coupons used in our studies were optically transparent; therefore, a quantitative assessment of biomass accumulation could also be obtained through measurements of optical depth ($-ln(T)$). Figure 11 shows a comparison of the optical depth at 600 nm measured through PES coupons using a pristine PES sample as background: lactose-modified samples were more transparent than unmodified ones and independently of the site tested displayed significantly lower optical depth than the

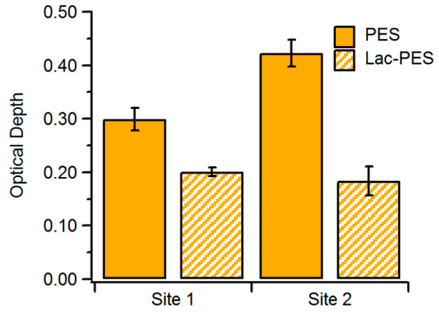

Figure 11. Optical depth of PES coupons at 600 nm measured after 20 day immersion test followed by controlled rinsing. Lac-modified samples are more transparent than unmodified ones.

corresponding control sample. These results are in agreement with ATP determinations and with microscopy observations.

Carbohydrate layers prepared via aryldiazonium chemistry are molecular coatings in the 1−2 nm thickness range that preserve the topography of the original substrate[31,33] so that their main effect is expected to be on surface chemistry and free energy. Results from field experiments show that in the absence of rinsing these coatings do not significantly impact fouling resistance, and little difference is observed with controls. Coupons extracted after the 20 day immersion were significantly fouled by a mixture of organisms, and the presence of the coating did not affect marine biofilm formation. However, the accumulated biomass was dramatically reduced at carbohydrate-modified surfaces after only light rinsing by gravity driven streams. SEM and HIM imaging of samples showed that rinsing leaves a relatively clean surface, indicating effective detachment of the biofilm under very mild treatment. Therefore, these carbohydrate coatings were found to be effective at reducing adhesion of foulants on all three materials tested.

Recent field tests of coatings based on zwitterionic polymers by Hibbs et al.[68] resulted in similar findings: zwitterionic coatings were found to affect foulant retention after jet rinsing, rather than to alter the amount of biomass accumulated on the coupons over the testing period. The striking agreement with our trends suggests analogies in the mode of action of carbohydrate thin films: these are thought to control fouling by regulating surface hydration, which is a similar mechanism to that proposed for zwitterionic polymers,[1] albeit in the absence of a change in surface electrostatic charge. It has been proposed that the exact distribution of charged regions in zwitterionic coatings might play a role in modulating settlement behavior;[68] it would be therefore relevant to carry out experiments similar to those by Aldred et al.[22] on settlement behavior to investigate whether glycoside structure and presentation could be similarly leveraged in carbohydrate coatings.

CONCLUSIONS

Functionalization and field test results suggest that carbohydrate aryldiazonium layers could find applications as fouling resistant coatings. For all materials tested, the density of retained biomass at surfaces was found to be significantly lower on carbohydrate modified samples with respect to unmodified controls. The mode of action of these layers appears to affect biofilm adhesion rather than biofilm formation, operating via fouling release rather than via antifouling mechanisms. It is recognized that fouling minimization in natural seawaters is extremely challenging due to the presence of multiple organism

DOI: 10.1021/acssuschemeng.7b03443
ACS Sustainable Chem. Eng. 2018, 6, 1141−1151

populations with a wide range of adhesion mechanisms. ATP tests suggest that fouling resistance observed for lactoside−aryldiazonium layers is comparable to that observed for more chemically complex coating systems in laboratory assays, which use populations containing a single organism. It is therefore significant that the promising results herein reported were obtained in coastal waters over prolonged times of exposure and during the summer months, when fouling activity is maximized.

Given the marked differences in physicochemical properties among SS316 and the two polymers, it is also encouraging to observe similar trends independent of material, as it suggests potential applicability on a variety of devices, including devices consisting of mixed materials. Although comprehensive fouling control remains elusive, our experiments indicate that thin carbohydrate layers could enhance the effectiveness of other fouling control methods. For instance, they could be easily combined/integrated with topography-based antifouling strategies as they coat surfaces conformally with few molecular layers, or they could be combined with mechanical methods to reduce power consumption associated with foulant removal. The observed performance together with the complete absence of toxicity and environmental impact of glycan-based coatings make them attractive as a sustainable fouling mitigation strategy.

■ ASSOCIATED CONTENT

Supporting Information

The Supporting Information is available free of charge on the ACS Publications website at DOI: 10.1021/acssuschemeng.7b03443.

Additional XPS spectra, details of compound synthesis, proposed functionalization mechanism, and comparison of coupons in the absence of rinsing and immersed at the two different sites (PDF)

■ AUTHOR INFORMATION

Corresponding Authors

*E-mail: colavitp@tcd.ie.

*E-mail: eoin.scanlan@tcd.ie.

ORCID

Eoin M. Scanlan: 0000-0001-5176-2310

Paula E. Colavita: 0000-0003-1008-2874

Funding

This publication emanated from research conducted with the financial support of Science Foundation Ireland (SFI) Grants 12/RC/2278 and 12/RC/2302; A.M. acknowledges support from the School of Chemistry.

Notes

The authors declare the following competing financial interest(s): Some of the authors are co-inventors of patent filings covering selected aspects in this article.

■ ACKNOWLEDGMENTS

The authors are grateful to T. McDermott, D. Jackson, and F. Kane of the Marine Institute Ireland and Majbritt Bolton-Warberg of Carna Research Station (NUIG) for access to boating equipment and coastal testing facilities. The authors are also grateful to J. Headlam and A. Long (NUIG) for their assistance during the sampling periods. The authors also thank Dr. J. O'Brien, Dr. M. Ruether, Dr. M. Feeney, Dr. G. Hessman, and Dr. S. N. Stamatin for assistance with NMR, MS, and XPS characterization. The authors acknowledge Advanced Microscopic Laboratory (AML) and D. Daly of Trinity College Dublin for providing access to SEM and HIM.

■ REFERENCES

(1) Callow, J. A.; Callow, M. E. Trends in the development of environmentally friendly fouling-resistant marine coatings. *Nat. Commun.* **2011**, *2*, 244.

(2) Fitridge, I.; Dempster, T.; Guenther, J.; de Nys, R. The impact and control of biofouling in marine aquaculture: a review. *Biofouling* **2012**, *28* (7), 649−669.

(3) Cao, S.; Wang, J.; Chen, H.; Chen, D. Progress of marine biofouling and antifouling technologies. *Chin. Sci. Bull.* **2011**, *56* (7), 598−612.

(4) Chambers, L. D.; Stokes, K. R.; Walsh, F. C.; Wood, R. J. K. Modern approaches to marine antifouling coatings. *Surf. Coat. Technol.* **2006**, *201* (6), 3642−3652.

(5) Yebra, D. M.; Kiil, S.; Dam-Johansen, K. Antifouling technology—past, present and future steps towards efficient and environmentally friendly antifouling coatings. *Prog. Org. Coat.* **2004**, *50* (2), 75−104.

(6) Whelan, A.; Regan, F. Antifouling strategies for marine and riverine sensors. *J. Environ. Monit.* **2006**, *8* (9), 880−886.

(7) Videla, H. A.; Characklis, W. G. Biofouling and microbially influenced corrosion. *Int. Biodeterior. Biodegrad.* **1992**, *29* (3), 195−212.

(8) Schultz, M. P.; Bendick, J. A.; Holm, E. R.; Hertel, W. M. Economic impact of biofouling on a naval surface ship. *Biofouling* **2011**, *27* (1), 87−98.

(9) Minchin, D.; Gollasch, S. Fouling and Ships' Hulls: How Changing Circumstances and Spawning Events may Result in the Spread of Exotic Species. *Biofouling* **2003**, *19* (sup1), 111−122.

(10) Ruane, N. M.; Rodger, H.; Mitchell, S.; Doyle, T.; Baxter, E.; Fringuelli, E. *GILPAT: An Investigation into Gill Pathologies in Marine Reared Finfish*; Marine Institute: 2013.

(11) Carl, C.; Guenther, J.; Sunde, L. M. Larval release and attachment modes of the hydroid Ectopleura larynx on aquaculture nets in Norway. *Aquacult. Res.* **2011**, *42* (7), 1056−1060.

(12) Baxter, E. J.; Sturt, M. M.; Ruane, N. M.; Doyle, T. K.; McAllen, R.; Rodger, H. D. Biofouling of the hydroid Ectopleura larynx on aquaculture nets in Ireland: Implications for finfish health. *Fish Vet. J.* **2012**, *13*, 17−29.

(13) Magin, C. M.; Cooper, S. P.; Brennan, A. B. Non-toxic antifouling strategies. *Mater. Today* **2010**, *13* (4), 36−44.

(14) Senda, T.; Miyata, O.; Kihara, T.; Yamada, Y. Inspection Method for the Identification of TBT-containing Antifouling Paints. *Biofouling* **2003**, *19* (sup1), 231−237.

(15) Dobretsov, S.; Teplitski, M.; Paul, V. Mini-review: quorum sensing in the marine environment and its relationship to biofouling. *Biofouling* **2009**, *25* (5), 413−427.

(16) Bixler, G. D.; Bhushan, B. Biofouling: lessons from nature. *Philos. Trans. R. Soc., A* **2012**, *370* (1967), 2381−2417.

(17) Schumacher, J. F.; Aldred, N.; Callow, M. E.; Finlay, J. A.; Callow, J. A.; Clare, A. S.; Brennan, A. B. Species-specific engineered antifouling topographies: correlations between the settlement of algal zoospores and barnacle cyprids. *Biofouling* **2007**, *23* (5), 307−317.

(18) Banerjee, I.; Pangule, R. C.; Kane, R. S. Antifouling Coatings: Recent Developments in the Design of Surfaces That Prevent Fouling by Proteins, Bacteria, and Marine Organisms. *Adv. Mater. (Weinheim, Ger.)* **2011**, *23* (6), 690−718.

(19) Lejars, M.; Margaillan, A.; Bressy, C. Fouling Release Coatings: A Nontoxic Alternative to Biocidal Antifouling Coatings. *Chem. Rev.* **2012**, *112* (8), 4347−4390.

(20) Rosenhahn, A.; Schilp, S.; Kreuzer, H. J.; Grunze, M. The role of "inert" surface chemistry in marine biofouling prevention. *Phys. Chem. Chem. Phys.* **2010**, *12* (17), 4275−4286.

(21) Kirschner, C. M.; Brennan, A. B. Bio-Inspired Antifouling Strategies. *Annu. Rev. Mater. Res.* **2012**, *42* (1), 211−229.
(22) Aldred, N.; Li, G.; Gao, Y.; Clare, A. S.; Jiang, S. Modulation of barnacle (Balanus amphitrite Darwin) cyprid settlement behavior by sulfobetaine and carboxybetaine methacrylate polymer coatings. *Biofouling* **2010**, *26* (6), 673−683.
(23) Perrino, C.; Lee, S.; Choi, S. W.; Maruyama, A.; Spencer, N. D. A Biomimetic Alternative to Poly(ethylene glycol) as an Antifouling Coating: Resistance to Nonspecific Protein Adsorption of Poly(l-lysine)-graft-dextran. *Langmuir* **2008**, *24* (16), 8850−8856.
(24) Ostuni, E.; Chapman, R. G.; Holmlin, R. E.; Takayama, S.; Whitesides, G. M. A Survey of Structure−Property Relationships of Surfaces that Resist the Adsorption of Protein. *Langmuir* **2001**, *17* (18), 5605−5620.
(25) Ederth, T.; Ekblad, T.; Pettitt, M. E.; Conlan, S. L.; Du, C.-X.; Callow, M. E.; Callow, J. A.; Mutton, R.; Clare, A. S.; D'Souza, F.; Donnelly, G.; Bruin, A.; Willemsen, P. R.; Su, X. J.; Wang, S.; Zhao, Q.; Hederos, M.; Konradsson, P.; Liedberg, B. Resistance of Galactoside-Terminated Alkanethiol Self-Assembled Monolayers to Marine Fouling Organisms. *ACS Appl. Mater. Interfaces* **2011**, *3* (10), 3890−3901.
(26) Luk, Y.-Y.; Kato, M.; Mrksich, M. Self-Assembled Monolayers of Alkanethiolates Presenting Mannitol Groups Are Inert to Protein Adsorption and Cell Attachment. *Langmuir* **2000**, *16* (24), 9604−9608.
(27) Hederos, M.; Konradsson, P.; Liedberg, B. Synthesis and Self-Assembly of Galactose-Terminated Alkanethiols and Their Ability to Resist Proteins. *Langmuir* **2005**, *21* (7), 2971−2980.
(28) Cao, X.; Pettit, M. E.; Conlan, S. L.; Wagner, W.; Ho, A. D.; Clare, A. S.; Callow, J. A.; Callow, M. E.; Grunze, M.; Rosenhahn, A. Resistance of Polysaccharide Coatings to Proteins, Hematopoietic Cells, and Marine Organisms. *Biomacromolecules* **2009**, *10* (4), 907−915.
(29) Nurioglu, A. G.; Esteves, A. C. C.; de With, G. Non-toxic, non-biocide-release antifouling coatings based on molecular structure design for marine applications. *J. Mater. Chem. B* **2015**, *3* (32), 6547−6570.
(30) Jayasundara, D. R.; Duff, T.; Angione, M. D.; Bourke, J.; Murphy, D. M.; Scanlan, E. M.; Colavita, P. E. Carbohydrate Coatings via Aryldiazonium Chemistry for Surface Biomimicry. *Chem. Mater.* **2013**, *25* (20), 4122−4128.
(31) Zen, F.; Angione, M. D.; Behan, J. A.; Cullen, R. J.; Duff, T.; Vasconcelos, J. M.; Scanlan, E. M.; Colavita, P. E. Modulation of Protein Fouling and Interfacial Properties at Carbon Surfaces via Immobilization of Glycans Using Aryldiazonium Chemistry. *Sci. Rep.* **2016**, *6*, 24840.
(32) Esteban-Tejeda, L.; Duff, T.; Ciapetti, G.; Daniela Angione, M.; Myles, A.; Vasconcelos, J. M.; Scanlan, E. M.; Colavita, P. E. Stable hydrophilic poly(dimethylsiloxane) via glycan surface functionalization. *Polymer* **2016**, *106*, 1−7.
(33) Angione, M. D.; Duff, T.; Bell, A. P.; Stamatin, S. N.; Fay, C.; Diamond, D.; Scanlan, E. M.; Colavita, P. E. Enhanced Antifouling Properties of Carbohydrate Coated Poly(ether sulfone) Membranes. *ACS Appl. Mater. Interfaces* **2015**, *7* (31), 17238−17246.
(34) Mandrino, D.; Godec, M.; Torkar, M.; Jenko, M. Study of oxide protective layers on stainless steel by AES, EDS and XPS. *Surf. Interface Anal.* **2008**, *40* (3−4), 285−289.
(35) Hassel, M.; Hemmerich, I.; Kuhlenbeck, H.; Freund, H.-J. High Resolution XPS Study of a Thin Cr_2O_3(111) Film Grown on Cr(110). *Surf. Sci. Spectra* **1996**, *4* (3), 246−252.
(36) Beeskow, T.; Kroner, K. H.; Anspach, F. B. Nylon-Based Affinity Membranes: Impacts of Surface Modification on Protein Adsorption. *J. Colloid Interface Sci.* **1997**, *196* (2), 278−291.
(37) Railkin, A. I. *Marine Biofouling: Colonization Processes and Defenses*. CRC Press: Boca Raton, FL, 2003.
(38) Tanane, O.; Abboud, Y.; Aitenneite, H.; El Bouari, A. Corrosion inhibition of the 316L stainless steel in sodium hypochlorite media by sodium silicate. *J. Mater. Environ. Sci.* **2016**, *7* (1), 131.
(39) Lins, V. d. F. C.; Gonçalves, G. A. d. S.; Leão, T. P.; Soares, R. B.; Costa, C. G. F.; Viana, A. K. d. N. Corrosion resistance of AISI 304 and 444 stainless steel pipes in sanitizing solutions of clean-in-place process. *Mater. Res.* **2016**, *19*, 333−338.
(40) Pierozynski, B.; Kowalski, I. The Influence of Hypochlorite-Based Disinfectants on the Pitting Corrosion of Welded Joints of 316L Stainless Steel Dairy Reactor. *Int. J. Electrochem. Sci.* **2011**, *6*, 3913.
(41) Cairns, T. L.; Foster, H. D.; Larchar, A. W.; Schneider, A. K.; Schreiber, R. S. Preparation and Properties of N-Methylol, N-Alkoxymethyl and N-Alkylthiomethyl Polyamides. *J. Am. Chem. Soc.* **1949**, *71* (2), 651−655.
(42) Lin, J.; Winkelman, C.; Worley, S. D.; Broughton, R. M.; Williams, J. F. Antimicrobial treatment of nylon. *J. Appl. Polym. Sci.* **2001**, *81* (4), 943−947.
(43) Tang, S.; Lu, N.; Myung, S.-W.; Choi, H.-S. Enhancement of adhesion strength between two AISI 316 L stainless steel plates through atmospheric pressure plasma treatment. *Surf. Coat. Technol.* **2006**, *200* (18−19), 5220−5228.
(44) Maupin, K. A.; Liden, D.; Haab, B. B. The fine specificity of mannose-binding and galactose-binding lectins revealed using outlier motif analysis of glycan array data. *Glycobiology* **2012**, *22* (1), 160−169.
(45) Hryniewicz, T.; Rokosz, K.; Rokicki, R. Electrochemical and XPS studies of AISI 316L stainless steel after electropolishing in a magnetic field. *Corros. Sci.* **2008**, *50* (9), 2676−2681.
(46) Williams, D. F.; Kellar, E. J. C.; Jesson, D. A.; Watts, J. F. Surface analysis of 316 stainless steel treated with cold atmospheric plasma. *Appl. Surf. Sci.* **2017**, *403* (Supplement C), 240−247.
(47) Saulou, C.; Despax, B.; Raynaud, P.; Zanna, S.; Marcus, P.; Mercier-Bonin, M. Plasma-Mediated Modification of Austenitic Stainless Steel: Application to the Prevention of Yeast Adhesion. *Plasma Processes Polym.* **2009**, *6* (12), 813−824.
(48) Dilks, A.; Kay, E. Plasma polymerization of ethylene and the series of fluoroethylenes: plasma effluent mass spectrometry and ESCA studies. *Macromolecules* **1981**, *14* (3), 855−862.
(49) Ferraria, A. M.; Lopes da Silva, J. D.; Botelho do Rego, A. M. XPS studies of directly fluorinated HDPE: problems and solutions. *Polymer* **2003**, *44* (23), 7241−7249.
(50) Golub, M. A.; Wydeven, T.; Johnson, A. L. Similarity of Plasma-Polymerized Tetrafluoroethylene and Fluoropolymer Films Deposited by rf Sputtering of Poly(tetrafluoroethylene). *Langmuir* **1998**, *14* (8), 2217−2220.
(51) Gu, X.; Nemoto, T.; Teramoto, A.; Ito, T.; Ohmi, T. Effect of Additives in Organic Acid Solutions for Post-CMP Cleaning on Polymer Low-k Fluorocarbon. *J. Electrochem. Soc.* **2009**, *156* (6), H409−H415.
(52) Powell, C. J.; Jablonski, A. NIST Electron Inelastic-Mean-Free-Path Database, Version 1.2. In *NIST Standard Reference Database*, National Institute of Standards and Technology: Gaithersburgh, MD, 2010; Vol. *71*.
(53) Nichols, B. M.; Butler, J. E.; Russell, J. N.; Hamers, R. J. Photochemical Functionalization of Hydrogen-Terminated Diamond Surfaces: A Structural and Mechanistic Study. *J. Phys. Chem. B* **2005**, *109* (44), 20938−20947.
(54) Hinz, H. J.; Kuttenreich, H.; Meyer, R.; Renner, M.; Fruend, R.; Koynova, R.; Boyanov, A.; Tenchov, B. Stereochemistry and size of sugar head groups determine structure and phase behavior of glycolipid membranes: densitometric, calorimetric, and x-ray studies. *Biochemistry* **1991**, *30* (21), 5125−5138.
(55) Socrates, G. *Infrared and Raman Characteristic Group Frequencies: Tables and Charts*; John Wiley & Sons: Hoboken, NJ, 2001.
(56) García Martínez, A.; de la Moya Cerero, S.; Osío Barcina, J.; Moreno Jiménez, F.; Lora Maroto, B. The Mechanism of Hydrolysis of Aryldiazonium Ions Revisited: Marcus Theory vs. Canonical Variational Transition State Theory. *Eur. J. Org. Chem.* **2013**, *2013* (27), 6098−6107.
(57) Hinge, M.; Gonçalves, E. S.; Pedersen, S. U.; Daasbjerg, K. On the electrografting of stainless steel from para-substituted aryldiazo-

DOI: 10.1021/acssuschemeng.7b03443
ACS Sustainable Chem. Eng. 2018, 6, 1141−1151

nium salts and the thermal stability of the grafted layer. *Surf. Coat. Technol.* **2010**, *205* (3), 820−827.
(58) Hinge, M.; Ceccato, M.; Kingshott, P.; Besenbacher, F.; Pedersen, S. U.; Daasbjerg, K. Electrochemical modification of chromium surfaces using 4-nitro- and 4-fluorobenzenediazonium salts. *New J. Chem.* **2009**, *33* (12), 2405−2408.
(59) Le, X. T.; Zeb, G.; Jégou, P.; Berthelot, T. Electrografting of stainless steel by the diazonium salt of 4-aminobenzylphosphonic acid. *Electrochim. Acta* **2012**, *71*, 66−72.
(60) Small, L. J.; Hibbs, M. R.; Wheeler, D. R. Spontaneous Aryldiazonium Film Formation on 440C Stainless Steel in Non-aqueous Environments. *Langmuir* **2014**, *30* (47), 14212−14218.
(61) Adenier, A.; Barré, N.; Cabet-Deliry, E.; Chaussé, A.; Griveau, S.; Mercier, F.; Pinson, J.; Vautrin-Ul, C. Study of the spontaneous formation of organic layers on carbon and metal surfaces from diazonium salts. *Surf. Sci.* **2006**, *600* (21), 4801−4812.
(62) Maurice, V.; Cadot, S.; Marcus, P. Hydroxylation of ultra-thin films of α-Cr_2O_3(0001) formed on Cr(110). *Surf. Sci.* **2001**, *471* (1−3), 43−58.
(63) Dechézelles, J.-F.; Griffete, N.; Dietsch, H.; Scheffold, F. A General Method to Label Metal Oxide Particles with Fluorescent Dyes Using Aryldiazonium Salts. *Part. Part. Syst. Charact.* **2013**, *30* (7), 579−583.
(64) Hurley, B. L.; McCreery, R. L. Covalent Bonding of Organic Molecules to Cu and Al Alloy 2024 T3 Surfaces via Diazonium Ion Reduction. *J. Electrochem. Soc.* **2004**, *151* (5), B252−B259.
(65) Molino, P. J.; Wetherbee, R. The biology of biofouling diatoms and their role in the development of microbial slimes. *Biofouling* **2008**, *24* (5), 365−379.
(66) Karl, D. M. Total microbial biomass estimation derived from the measurement of particulate adenosine-5′-triphosphate. In *Handbook of Methods in Aquatic Microbial Ecology*; Kemp, P. F., Cole, J. J., Sherr, B. F., Sherr, E. B., Eds.; Lewis Publishers: Boca Raton, FL, 1993; pp 359−368.
(67) Omidbakhsh, N.; Ahmadpour, F.; Kenny, N. How Reliable Are ATP Bioluminescence Meters in Assessing Decontamination of Environmental Surfaces in Healthcare Settings? *PLoS One* **2014**, *9* (6), e99951.
(68) Hibbs, M. R.; Hernandez-Sanchez, B. A.; Daniels, J.; Stafslien, S. J. Polysulfone and polyacrylate-based zwitterionic coatings for the prevention and easy removal of marine biofouling. *Biofouling* **2015**, *31* (7), 613−624.

DOI: 10.1021/acssuschemeng.7b03443
ACS Sustainable Chem. Eng. 2018, 6, 1141−1151

ACS APPLIED BIO MATERIALS
Cite This: ACS Appl. Bio Mater. 2018, 1, 825−832
Article
www.acsabm.org

Spontaneous Aryldiazonium Grafting for the Preparation of Functional Cyclodextrin-Modified Materials

Adam Myles,[†] James A. Behan,[†] Brendan Twamley,[†] Paula E. Colavita,*[,†,‡] and Eoin M. Scanlan*[,†]

[†]School of Chemistry, Trinity College Dublin, College Green, Dublin 2, Ireland
[‡]CRANN and AMBER Research Centres, Trinity College Dublin, College Green, Dublin 2, Ireland

Supporting Information

ABSTRACT: A mild and efficient surface modification protocol for the preparation of β-cyclodextrin (βCD) modified surfaces through aryldiazonium-mediated grafting is reported. Monosubstituted 6-*O*-aminophenol-β-cyclodextrin (amβCD) was synthesized through a three-step protocol. This compound was found to form supramolecular aggregates in aqueous solutions at relatively low concentrations via cavity-directed self-assembly. Disruption of these supramolecular structures through judicious choice of solvent was found to be essential for the formation of the reactive aryldiazonium species from the amino-phenolic precursor and for spontaneous surface grafting from aqueous solutions. Cyclodextrin thin films were prepared on carbon macroscopic substrates and electrodes and were characterized via infrared reflectance absorption spectroscopy (IRRAS), cyclic voltammetry, and water contact angle measurements. Protein adsorption studies demonstrated that βCD adlayers reduced nonspecific protein adsorption. βCD moieties in adlayers can be used nonetheless for specific host−guest complexation and are grafted at the surface with monolayer coverage (1.2×10^{-10} mol cm^{-2}) as demonstrated via experiments using ferrocene, a redox probe. Finally, cyclodextrin covalent immobilization was demonstrated also on stainless steel and polyamide samples, two substrates with wide ranging technological applications.

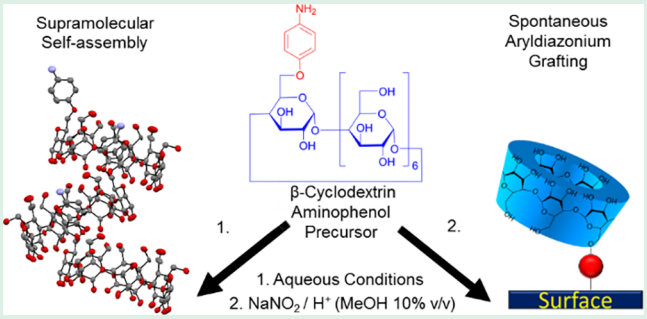

KEYWORDS: *β-cyclodextrin, aryldiazonium, surface coating, host−guest, supramolecular*

INTRODUCTION

Cyclodextrins (CDs) are cyclic oligosaccharides most commonly consisting of 6 (α), 7 (β), or 8 (γ) glucose units linked together by a (1, 4) glycosidic bond. They possess a torus structure with a hydrophilic exterior and a relatively hydrophobic cavity capable of forming host−guest inclusion complexes with a wide range of hydrophobic compounds.[1,2] The unique properties of cyclodextrins, coupled with their relative abundance and low cost, render them extremely versatile and useful substrates with diverse applications in supramolecular chemistry, drug delivery, separation science, solubility enhancement, and sensor technology.[3−5] In order to impart the desirable features of cyclodextrin onto surfaces, there exists a range of surface modification techniques including physisorption, chemisorption, and covalent modification approaches; importantly, several of these approaches maintain the functionality of the cyclodextrin cavity on the surface and enable the design of functional materials with broad application. Surface modification can be achieved via physisorption methods such as hydrogen bonding or through host−guest activity with surface expressed binding groups.[6] Physisorbed coatings generally display low stability and can typically be removed by physical displacement through sonication. More stable cyclodextrin surfaces can be achieved either by production of a polymeric deposition incorporating cyclodextrins[1,2,7,8] or through chemisorption, i.e., specific chemical modification to produce covalently bound cyclodextrins at the surface. Examples of this include grafting to cellulose via acid cross-linking,[9] production of gold surfaces modified via thiolene chemistry,[10] and electrochemical grafting of cyclodextrins onto conductive surfaces.[6,11] Covalent immobilization of cyclodextrins has several benefits over physisorption and polymeric layer deposition, including coating stability and the potential to retain surface properties and morphology. Spontaneous diazonium grafting is an attractive strategy for the production of a covalently modified cyclodextrin surface as it involves mild conditions, is easily scalable, and is applicable to a wide variety of materials including carbon, polymer, and metal alloy surfaces.[12−17] However, to the best of our knowledge there are no reports on the application of these spontaneous reactions to cyclodextrin immobilization. We have demonstrated previously that modification of surfaces through aryldiazonium chemistry with mono- and disaccharides is possible on a wide variety of materials including carbon and polymers.[13,14,16,18] The aryl ring is required for formation of a reasonably stable diazonium

Received: June 25, 2018
Accepted: August 14, 2018
Published: August 14, 2018

DOI: 10.1021/acsabm.8b00266
ACS Appl. Bio Mater. 2018, 1, 825−832

cation, as alkyl diazonium species are typically highly unstable and unsuitable for surface functionalization. The monotosylation of the primary face (i.e., the 6′ alcohol of the saccharide) opens up many avenues for cyclodextrin modification,[8,19] including a potential pathway for producing a cyclodextrin diazonium salt-based grafting agent. Modification of the primary face to include an aromatic tail can however result in βCD in aqueous solution to readily form supramolecular host−guest complexes.[20−22] Complex formation can compromise the reactivity of aromatic tail groups via inclusion in the cavity of neighboring βCD units and thus potentially prevent further reactions such as those leading to surface covalent grafting.

In this work, we report the synthesis and characterization of a βCD-based aryldiazonium precursor molecule. We demonstrate that prevention of supramolecular host−guest assembly is essential for successful spontaneous surface grafting.[23−25] Disruption was achieved via cavity binding of a high affinity substrate such as adamantane or through modulation of the solvent polarity, with the latter method resulting in surfaces that display βCD sites available for binding of organic substrates. Carbon materials were modified using aryldiazonium salts from these CD glycosides in aqueous solutions and under mild conditions, resulting in glycosylated surfaces that display protein rejection behavior in the absence of specific host−guest interactions.[13,16,26] Cavity binding of surface-bound cyclodextrin was confirmed using a ferrocene/ferrocenium redox probe.[11] The functionalization method was then applied to two insulating surfaces of industrial interest: a metal alloy, stainless steel 316, and a polyamide, nylon-6, thus expanding the range of applications of this functionalization methodology.[26]

RESULTS AND DISCUSSION

Aryldiazonium Precursor Synthesis and Characterization. Monosubstituted 6-*O*-aminophenol-β-cyclodextrin (amβCD) was synthesized through a three-step protocol outlined in Scheme 1. β-Cyclodextrin (βCD) 1 was

Scheme 1. Synthesis of the amβCD Precursor Sample in Three Steps

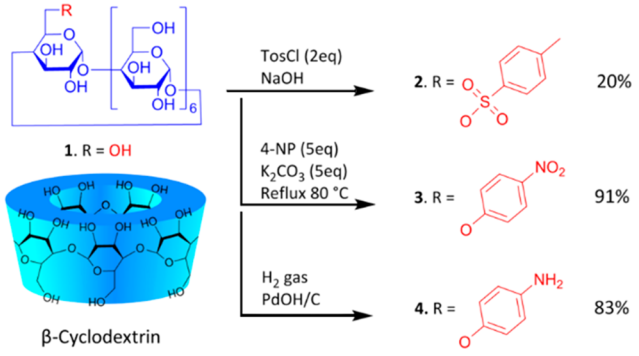

monotosylated upon reaction with *p*-toluenesulfonyl chloride in alkaline solution.[19] The reaction mixture was neutralized through addition of 6 M hydrochloric acid, and the resulting precipitate was filtered and repeatedly recrystallized from a 1:1 MeOH/H_2O mixture until a degree of tosylation (DT %) greater than 90% as determined by ^{1}H NMR was obtained.[27] The monotosyl-βCD 2 was subsequently refluxed at 80 °C in the presence of excess *p*-nitrophenol in DMF to furnish the nitrophenolic derivative 3.[21] The desired aminophenol derivative 4 was prepared by hydrogenoloysis of 3 in the presence of Pd on charcoal.[13]

Functionalization of carbon surfaces was first attempted via diazotization of amβCD under standard activating conditions (1 mM, aqueous $NaNO_2/H^+$), as indicated in Scheme 2, that

Scheme 2. Aryl Diazonium Salt Formation

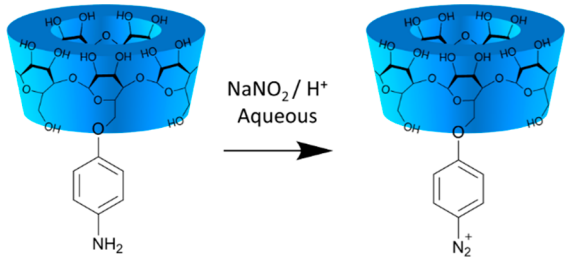

are known to result in covalent grafting on carbon. However, these reactions were unsuccessful as no evidence of surface modification was observed. It was therefore hypothesized that self-assembly may lead to inactivation of the amino-phenolic tail, thus preventing diazotization and/or covalent grafting of aryldiazonium cations.[13,14,16,18,26]

This might occur if a neighboring cyclodextrin moiety complexes the amino-phenolic tail within the cavity, leading to the formation of supramolecular aggregates. In order to confirm that aggregation amβCD occurs in aqueous conditions at 1.0 mM, a solution of amβCD was prepared in ultrapure water with sonication, filtered through a 0.45 μm PES membrane filter, and analyzed via dynamic light scattering (DLS) after a 1 h period of incubation at room temperature. DLS results are shown in the Supporting Information (Figure S1) and reveal scattering intensity equivalent to spherical particles with hydrodynamic radius >100 nm for amβCD at 1.0 mM. This indicates that aggregates of amβCD develop over 1 h at relatively low concentrations, and identical experiments using unmodified βCD units do not yield scattering intensity at hydrodynamic sizes >2 nm (Figure S1) in agreement with prior reports,[28] strongly indicating that aggregate formation is due to the presence of the amino-phenolic tails in amβCD. DLS experiments carried out under the same conditions but with addition of adamantane in 1:1 ratio with amβCD resulted in nearly identical stability to that of unmodified βCD, therefore indicating that the cavity binding of the amino-phenolic tail is crucial to aggregate formation. Further evidence of involvement of amino-phenolic tails in the aggregation process was obtained from the ^{1}H NMR of aromatic protons of freshly prepared solutions of amβCD in D_2O, as shown for 1.2 and 3.0 mM concentrations in Figure 1a.

Spectra show a clear change in chemical shift, indicating differences in the local environment of these protons at the two concentrations. This confirms that cavity-directed self-assembly via host−guest interactions of the phenyl rings is important for the aggregation process. NMR titration experiments were carried out over the concentration range 0.5−3.0 mM (Figure S2) and show a progressive change in the observed chemical shift (δobs) of aromatic protons. The δ_{obs} can be expressed as a function of the total concentration (C_{tot}), the relative chemical shift of the aromatic protons in monomeric βCD (δ_{mon}), and that of aromatic protons in the cavity of host−guest aggregates (δ_{agg}). Equation 1 shows the

DOI: 10.1021/acsabm.8b00266
ACS Appl. Bio Mater. 2018, 1, 825−832

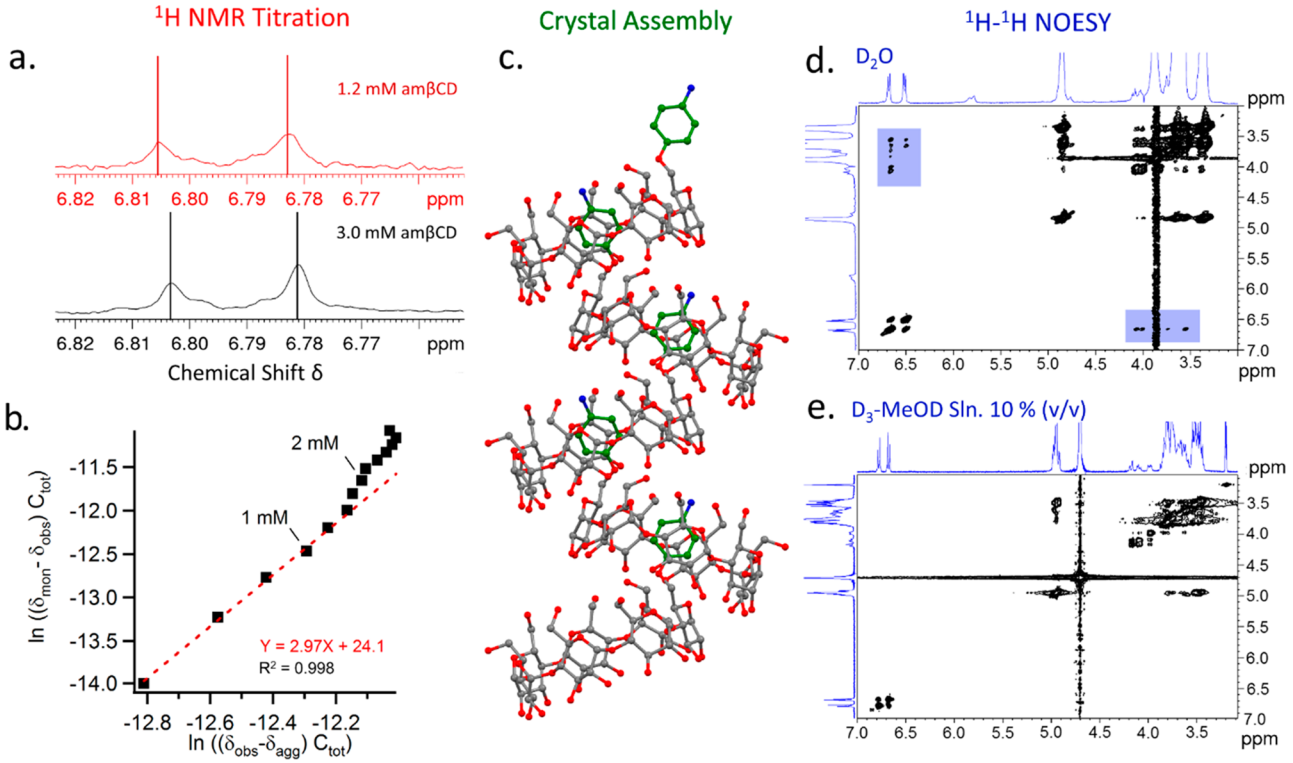

Figure 1. (a) ^{1}H NMR (400 MHz) of amβCD in D_2O at 1.2 and 3.0 mM showing differing observed chemical shift of aromatic doublet, due to host−guest interactions. (b) Plot of concentration components from eq 1 for determining the aggregation number n from the slope; points represent measured data, and the dashed line is the best fit trend line. (c) Illustration of the one-dimensional helical self-assembly of amβCD obtained by X-ray crystallography. Aromatic carbons have been highlighted (green), and water of crystallization and hydrogen atoms have been omitted for clarity. (d) ^{1}H−^{1}H NOESY spectrum of amβCD in D_2O; through-space interactions between aromatic (tail) and saccharide (cavity) protons are highlighted in blue. (e) ^{1}H−^{1}H NOESY spectrum of amβCD in D_3-MeOD 10% v/v in D_2O. No interaction peaks are observed between aromatic (tail) and saccharide (cavity) implying negligible host−guest interactions under these conditions.

relationship between the association constant for the monomer−aggregate equilibrium of amβCD, K_a, the aggregation number n, and the relative chemical shifts, where δ_{mon} and δ_{agg} are determined by extrapolation (Figure S3).[20] For a detailed description of eq 1 see Supporting Information.

$$\ln(C_{tot}(\delta_{mon} - \delta_{obs})) = n \ln(C_{tot}(\delta_{obs} - \delta_{agg})) + \ln n - (n - 1) \ln(\delta_{mon} - \delta_{agg}) + \ln K_a \quad (1)$$

A linear fit of the concentration expressions from eq 1 (Figure 1b) yielded the aggregation number n = 2.97, confirming that this species forms trimeric structures at concentrations <1.5 mM. At higher concentrations it is possible to observe a second regime that suggests formation of larger aggregates (n > 3). These findings are consistent with reports that show that dimerization results in further host−guest self-assembly in other phenyl-modified βCD species.[20−22] From the intercept of the best fit to eq 1, a pK_{tri} = −5.66 is obtained for the trimer equilibrium constant. Assuming a noncooperative self-assembly process (pK_n = (n − 1) pK_2, $n \geq 2$), the dimer formation constant is estimated at pK_{dim} = 2.83 or $K_{dim} \approx 680$, in excellent agreement with phenyl−CD host−guest K_a values reported by Liu et al.[21]

Cyclodextrins displaying modifications with aromatic groups have been reported to form crystals via one of three pathways, cavity-tail self-inclusion, packed layers, and one-dimensional self-assembly.[20−22] Crystals of amβCD were grown from solutions in both D_2O and H_2O over 15 days at >3 mM concentration. X-ray crystallographic data analysis revealed that the compound crystallizes by aromatic tail penetration into the cyclodextrin cavity along a screw axis to form a linear head-to-tail supramolecular structure (Figure 1c).[21]These data confirm that self-assembly occurs via the insertion of the amino-phenol tail into the βCD cavity.

Results indicate that aggregate disruption is essential for the amino-phenolic tails to be available for further reactions. As shown by DLS, it is possible to achieve this via cavity blocking with a high-affinity substrate such as adamantane. However, binding of such substrates effectively blocks the cavity, while it is more advantageous for further applications to achieve disruption by modulating solvent conditions while retaining an empty cavity. Nuclear Overhauser effect (NOE) NMR spectroscopy was used to investigate the role solvent plays in supramolecular assembly. ^{1}H−^{1}H NOESY was performed on amβCD under various conditions. In D_2O (Figure 1d) strong interactions were seen between the aromatic protons at 6.8 and 6.6 ppm and the saccharide protons of the cavity, particularly the glycan H-5 and H-3 protons at peak positions 3.6 and 3.7 ppm, thus confirming host−guest interactions.[21] These peaks disappear upon selective cavity binding to adamantane (Figure S4) or when exposing the supramolecular assembly to a solvent system which contains a significant organic component, i.e., 10% v/v MeOH in water (Figure 1e). It was thus concluded that self-assembly behavior of compound **4** can be minimized either through pre-emptive host−guest binding or through careful modulation of solvent conditions.[23,24]

DOI: 10.1021/acsabm.8b00266
ACS Appl. Bio Mater. 2018, 1, 825−832

Carbon Functionalization with βCD Moieties. Surface functionalization was carried out under conditions that promote disaggregation of **4** in solution while retaining a free cavity available for binding. Diazotization and surface grafting reactions were therefore carried out in 10% MeOH in aqueous solutions (Figure 2a): a 1.25 mM solution of amβCD

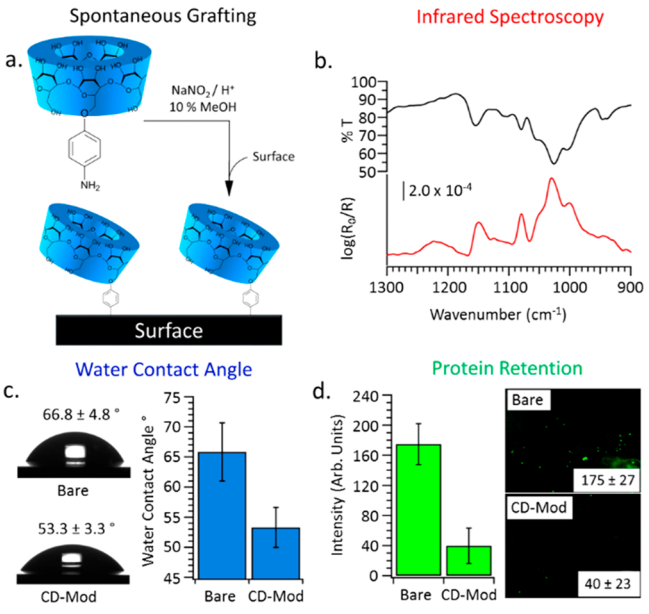

Figure 2. (a) Schematic representation of surface modification. (b) Infrared spectra showing transmittance spectrum of bulk amβCD diazonium precursor (top trace, black) and an IRRAS spectrum of a carbon surface after spontaneous grafting with βCD (bottom trace, red). (c) Water contact angle (WCA) results for polished glassy carbon plates before (bare) and after (CD-Mod) functionalization with βCD; a significant decrease in WCA is observed after modification reactions. (d) Protein adsorption studies on polished glassy carbon (bare) and on βCD-functionalized carbon (CD-Mod) using FITC-BSA; values are average emission intensity after incubation in FITC-BSA solutions, while error bars represent 95% CI.

was prepared in 1.25 mM HBF_4. This solution was then chilled to <4 °C for 1 h, then diluted by addition of 0.010 M $NaNO_2$ to a final concentration of 1.0 mM βCD. Immediately after diazotization, the aryldiazonium cation solution was placed in contact with the substrate material, by either immersion or drop casting; the surface was kept in the dark for 1 h and subsequently rinsed and sonicated in methanol and water prior to characterization.[13,14,18,26]

Confirmation of spontaneous βCD grafting to amorphous carbon was obtained by ex situ infrared reflectance absorption spectroscopy (IRRAS). Figure 2b shows the IRRAS of a carbon surface[29] modified via the process above. The transmittance spectrum of amβCD precursor compound in bulk form is also shown for comparison. Both spectra display characteristic peaks at 1145, 1080, 1024, and 993 cm^{-1} corresponding to C−O stretching modes and O−H deformations of the carbohydrate rings.[30] The presence of these peaks is diagnostic for the presence of carbohydrate moieties at the carbon surface and is consistent with formation of a βCD adlayer. These peaks were not observed in the IRRAS of samples which had been immersed in a 10% MeOH solution of amβCD alone, without $NaNO_2$. Importantly, the peaks were also absent from samples immersed in an aqueous solution of amβCD and $NaNO_2/H^+$ but prepared without addition of 10% MeOH. The above control experiments indicate that both diazotization conditions and disruption of host−guest complex aggregates are essential to observe evidence of surface functionalization. Furthermore, they strongly indicate that βCD immobilization occurs via covalent bond formation by the reaction of the aryldiazonium cation with the carbon substrate.[13,18,26,29]

Reaction of carbon with aryldiazonium cations of amβCD was also found to result in a significant change in surface wetting properties, consistent with the presence of a saccharide adlayer. Figure 2c shows the water contact angle (WCA) of glassy carbon (GC) before and after functionalization. Results indicate that there is a significant decrease in WCA from (65.8 ± 4.8)° (95% CI) to (53.3 ± 3.3)° (95% CI). The increased hydrophilicity is attributed to increased surface density of hydroxyl groups resulting from grafting of βCD, and it is in agreement with reported changes after modification with simpler mono- and disaccharide moieties.[13,14,18,26] To investigate whether changes in wetting properties also affect interfacial interactions with biomolecules such as proteins,[13,18,26,31,32] GC plates were incubated in buffered solutions of fluorescently labeled bovine serum albumin (BSA-FITC) at room temperature for 2 h. GC plates were rinsed and subsequently examined under microscopy with fluorescence excitation at 470 nm. The βCD-modified GC displayed lower FITC emission, thus indicating reduced protein retention when compared to unmodified samples (Figure 2d). These findings correlate well with WCA data and are consistent with previous findings on saccharide-modified surfaces.[13,14]

Surface Host−Guest Binding. βCD is known to form 1:1 inclusion complexes with ferrocene in solution;[11,33] therefore ferrocene was used as a redox probe to investigate the surface density of βCD sites and confirm availability of the surface-bound cavity to host−guest complexation. Two GC electrodes, one modified with βCD via the spontaneous reaction and one freshly polished, were immersed in a 5.0 mM solution of ferrocene in MeOH, rinsed, and then tested via cyclic voltammetry (CV). Figures 3a and 3b show CVs obtained at 200 mV s^{-1} in 0.5 M KCl aqueous supporting electrolyte for the βCD-modified and bare GC, respectively.

GC electrodes modified with βCD (Figure 3a) display the characteristic oxidation and reduction peaks of ferrocene/ferrocenium (Fc/Fc^+) with a formal potential at 0.26 V vs Ag/AgCl.[11] In contrast, in the absence of modification, the bare GC surface shows no evidence of faradaic peaks, thus indicating that no significant amounts of ferrocene physisorb at bare GC. These results strongly suggest that the peaks observed in Figure 3a arise from specific CD−ferrocene binding interactions at the electrode interface. The first anodic sweep in Figure 3a is markedly different from that of subsequent cycles, and its greater asymmetry suggests the presence of contributions from nonsurface-bound redox species. This behavior is likely to arise from small amounts of weakly bound Fc^+ that is free to diffuse into solution. Peaks in subsequent cycles display instead symmetric peaks, whose intensity decreases slightly over multiple cycles. This is consistent with progressive partitioning of the more soluble Fc^+ species into the aqueous phase after each anodic sweep.[11] The total integrated charge associated with the anodic peak of the second cycle (0.2−0.5 V) was used to provide an estimate of surface coverage, Γ, for βCD−Fc complexes. Using eq 2 for a 1-electron transfer ($n = 1$), a scan rate $\nu = 0.2$ V s^{-1}, and an

DOI: 10.1021/acsabm.8b00266
ACS Appl. Bio Mater. 2018, 1, 825−832

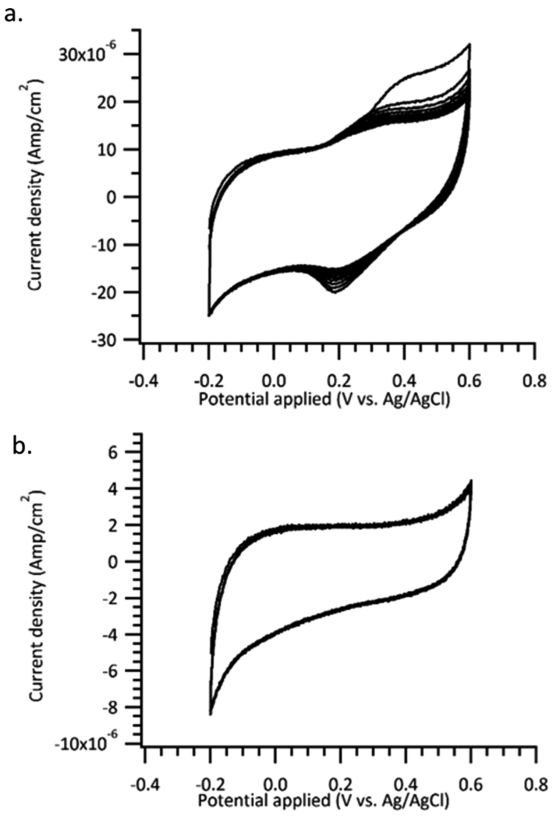

Figure 3. Cyclic voltammograms of CD-modified (a) and bare (b) glassy carbon electrodes after incubation in a 5 mM ferrocene solution in methanol, followed by rinsing. Voltammograms were obtained in 0.5 M KCl solutions at 200 mV s^{-1}.

experimentally determined electrode geometric area[34] A = 0.196 cm^2:

$$\Gamma = \frac{Q}{nFA} = \frac{\int_{V_1}^{V_2} i\,dV}{nFA\nu} \quad (2)$$

The value of Γ obtained was 1.2×10^{-10} mol cm^{-2}. This value is in excellent agreement with $\Gamma = 1.4 \times 10^{-10}$ mol cm^{-2} calculated from crystallographic data for a hexagonal closed-packed layer of amβCD with its phenyl ring oriented normal to the carbon surface (see Supporting Information). This indicates that spontaneous aryldiazonium grafting of amβCD results in monolayer coverage. Further evidence for monolayer coverage was provided by atomic force microscopy measurements of the thickness of βCD adlayers, which yielded values consistent with the presence of a monolayer[35] (see Supporting Information). Monolayer control of aryldiazonium functionalization reactions is notoriously difficult to achieve, due to the tendency of these cations to cross-link yielding multilayers, particularly under electrografting conditions. The steric hindrance of the CD moiety is therefore likely to provide an intrinsic control mechanism for suppressing multilayer formation, as observed in previous studies on applications of bulky substitutents for monolayer control.[18,36−40]

Functionalization of Insulating Surfaces. One of the major advantages of spontaneous aryldiazonium reactions is the ability to impart surface functionality onto materials without the requirement of an electrical contact. This makes the spontaneous reaction a versatile method which was recently extended from the modification of conductors, e.g., carbon, Ni, Fe, Zn,[12] to the modification of polymeric insulators[13,14,26] and oxide-passivated alloy surfaces such as stainless steel.[17,26] Therefore, we investigated the applicability

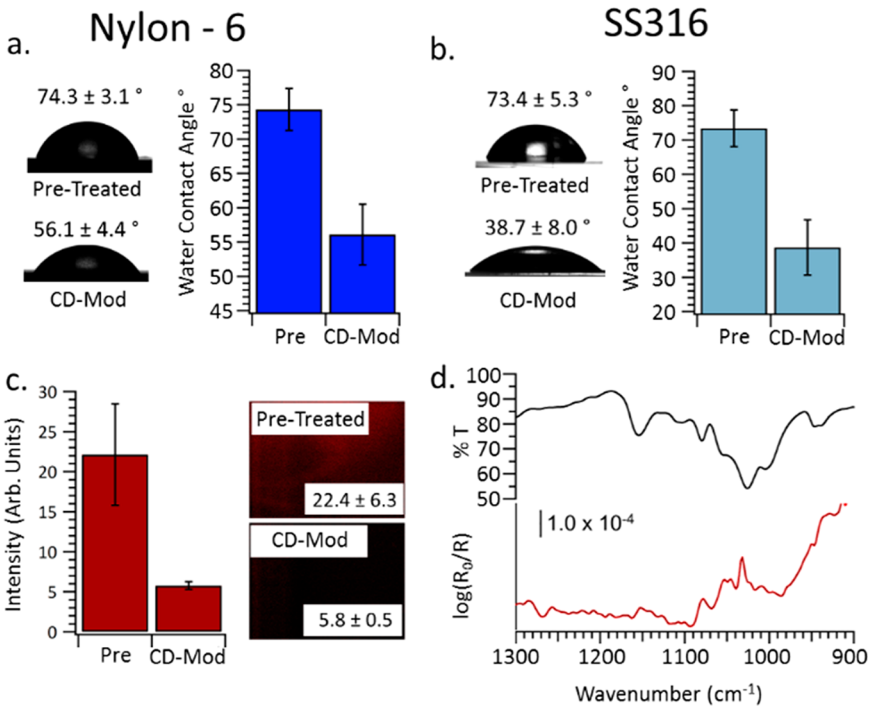

Figure 4. Water contact angles for nylon-6 (a) and SS316 (b) before and after spontaneous reactions with aryldiazonium cations from amβCD. (c) Protein adsorption tests on nylon-6 using fluorescently labeled BSA (Alexa-BSA); the bar chart shows average emission intensity measured after incubation in Alex-BSA solutions on surfaces before and after modifications. (d) IRRAS spectrum obtained on SS316 after functionalization reactions with βCD; the transmittance spectrum of amβCD is shown in the graph for comparison.

DOI: 10.1021/acsabm.8b00266
ACS Appl. Bio Mater. 2018, 1, 825−832

of spontaneous grafting for the immobilization of βCD on nylon-6 and stainless steel 316 (SS316), a polymeric and an alloy material of importance for a wide range of applications. Nylon-6 samples were pretreated via formaldehyde activation, while SS316 coupons were subject to an oxidative activation treatment.[26] Samples were subsequently immersed in solutions of the aryldiazonium cation from amβCD, as in Figure 2a. Figure 4a and 4b shows the resulting WCA values obtained on nylon-6 and SS316 both prior to and post immersion in the aryldiazonium grafting solution.

In all cases, hydrophilicity increased, as expected after modification with βCD adlayers. The effect on protein adsorption resulting from βCD grafting on nylon-6 was also characterized using buffered solutions of BSA labeled with Alexa Fluor-647. After incubation in such solutions the total emission arising from adsorbed protein is lower in the case of nylon-6 modified with βCD (Figure 4c). The IRRAS spectrum obtained from SS316 surfaces after modification with βCD is shown in Figure 4d. The spectrum compares well with the one obtained in transmittance from the precursor amβCD. These experiments therefore confirm that the spontaneous reaction results in grafting of βCD functional moieties on materials with a wide range of properties.

METHODS AND MATERIALS

Chemicals and Materials. β-Cyclodextrin 98%, *p*-nitrophenol reagent-plus ≥99%, and adamantane 99+% were purchased from Fisher Scientific; *p*-toluenesulfonyl chloride 99%, palladium hydroxide on activated charcoal, *N*,*N*-dimethylformamide anhydrous 99.8%, sodium hypochlorite (bleach), sodium hydroxide, potassium hydroxide, phosphate-buffered saline buffer (0.010 M PBS, pH 7.4), sodium nitrite, hydrochloric acid, fluoroboric acid, ferrocene 98%, and bovine serum albumin (BSA) conjugates with fluorescein isothiocyanate (FITC) were purchased from Sigma-Aldrich; BSA conjugates with Alexa Fluor 647 were purchased from Biosciences; Marine grade stainless steel 316 foil (SS316) and polyamide sheets nylon-6 (N-6) were purchased from Goodfellow; Sigradur K glassy carbon plates and Sigradur G glassy carbon discs were purchased from HTW.

Diazonium Precursor Molecule Characterization. High-resolution mass spectra were obtained using a MADLDI-Q-ToF Premier instrument. Nuclear magnetic resonance experiments were carried out using a Bruker Avance III 400 NMR and a Bruker Avance II 600 NMR. NMR titration experiments were performed on an Agilent 400-MR equipped with a 5 mm OneNMR probe for proton and multinuclear detection and an automatic sample changer. Infrared spectra of bulk precursor samples were measured on a PerkinElmir Spectrum100 FTIR with an ATR sampling accessory. Hydrodynamic diameters of modified β-cyclodextrin compounds in solution were determined via dynamic light-scattering (DLS) measurements on a Malvern Zeta Sizer Nano ZS; curves are obtained using refractive indices of n = 1.56 and n = 1.33 for the cyclodextrin aggregates and liquid phase, respectively.

Substrate Surface Preparation. Carbon substrates for infrared reflectance absorption spectroscopy experiments (IRRAS) were prepared via DC magnetron sputtering (Torr International Inc.) in Ar; deposition was carried out on an optically thick Ti underlayer (Grade 2) on which carbon was subsequently sputtered from a graphite target (99.999%). Glassy carbon substrates were polished with alumina slurries (Buehler) with decreasing particle size of 1 (on nylon cloth), 0.3, and 0.05 μm (on nylon microcloth); each polishing step was followed by 3 min sonication in each of *n*-hexane, methanol (semiconductor grade), and ultrapure H_2O.

General Functionalization Procedure. Initially surfaces were cleaned using semiconductor grade methanol and ultrapure H_2O and were modified with aryldiazonium cyclodextrin cations through spontaneous grafting protocols similar to those reported previously for other diazonium-based carbohydrate surface coatings. A 1.5 mM solution of HBF_4 was prepared in a 10% MeOH:DI H_2O solution which was used to make a solution of 1.25 M amβCD which was subsequently chilled to <4 °C in ice for 1 h. This solution was then diluted to a final concentration of 0.0010 M using a 0.010 M solution of $NaNO_2$. The sample surface was then placed in contact with this solution, kept in the dark for 1 h at RT, rinsed with deionized water, sonicated in MeOH and H_2O for 1 min in each solvent, dried under argon flow, and stored under argon prior to analysis. This procedure was followed for all nonpolymeric surfaces, which are easily damaged by sonication and which were instead subjected to a light rinsing step. Nylon-6 samples were preactivated by overnight immersion at 30 °C in a 36% aqueous formaldehyde solution with a catalytic amount of hypophosphorous acid. Stainless steel samples (SS316) were pretreated with 0.5% NaClO in basic aqueous solution (KOH 1% and NaOH 1%) for 1 h.

Surface Characterization. A Bruker Tensor 27 infrared spectrometer was used to perform infrared reflectance absorption spectroscopy (IRRAS) characterization. The spectrometer was equipped with a mercury cadmium telluride detector and a VeeMax II specular reflectance accessory with a wire grid polarizer. All spectra were collected using p-polarized light at an angle of incidence of 80° using an unmodified sample as a background; 100 scans at 4 cm^{-1} were collected for all samples. Water contact angles (WCAs) were determined for all samples using the sessile drop method (FTA1000), using 20 μL droplets. Thickness and surface roughness measurements were carried out via atomic force microscopy (AFM, Asylum Research) using silicon cantilevers, following previously published procedures.

Fluorescence Microscopy. To determine protein rejection ability, Sigradur K Glassy carbon plates treated with the above functionalization procedure and unmodified control plates were immersed in 0.2 mg mL^{-1} solutions of BSA-FITC or BSA-Alexa Fluor 647 conjugates in PBS at pH 7.4 for 1 h. All samples were washed with PBS solution prior to imaging to remove excess unbound protein. Fluorescence images were acquired using an Olympus BX51 inverted microscope with cellSense digital image processing software. Emission intensities were analyzed in triplicate using ImageJ software.

Electrochemistry. Cyclic voltammetry was performed in aqueous 0.5 M KCl at a scan rate of 200 mV s^{-1} with a potential window between −0.2 and 0.6 V. Electrochemical measurements were carried out using a Metrohm Autolab AUT50324 potentiostat with a frequency response analyzer (FRA) module using a three-electrode setup. A static disc holder (Pine Instruments) enclosing the GC disc was used as working electrode, and a saturated Ag/AgCl electrode and a graphite rod were used as reference and counter electrodes, respectively. The electrochemical cell consisted of a beaker with a custom-made Teflon cap, and all solutions were degassed with argon gas prior to measurement. Ferrocene binding experiments were performed by immersion of GC electrodes in a 5.0 mM solution of ferrocene in MeOH for 45 min. Samples were rinsed gently with DI water to remove unbound ferrocene prior to cyclic voltammetry measurements.

CONCLUSIONS

We have demonstrated that a synthetic *p*-nitrophenol cyclodextrin substrate, prepared from native β-cyclodextrin via a three-step synthesis, is suitable for aryldiazonium grafting onto a range of materials. The synthesized CD-derivative aggregates in solution, at relatively low concentrations, via cavity-directed self-assembly. We demonstrate that disruption of these aggregates is essential for successful functionalization and that this can be achieved via cavity binding with high-affinity substrates or via modulation of solvent properties. The latter method was leveraged to achieve spontaneous grafting of βCD groups. The resulting adlayers were found to be hydrophilic and to reduce protein retention, while the binding properties of βCD moieties were preserved once covalently linked to the surface. This suggests that these βCD adlayers can potentially

DOI: 10.1021/acsabm.8b00266
ACS Appl. Bio Mater. 2018, 1, 825−832

play a dual role in reducing nonspecific binding to biomolecules, while presenting a binding cavity available for leveraging specific host−guest interactions. Importantly, the specific route to surface immobilization reported in this work yielded closed-packed monolayers of βCD, a feature that is important, e.g., for effective control of assay sensitivity in βCD sensing applications. It is anticipated that this approach will find widespread application in the preparation of cyclodextrin surfaces as the process is readily scalable and applicable to a wide range of polymeric, alloy, and carbon surfaces.

■ ASSOCIATED CONTENT

Supporting Information

The Supporting Information is available free of charge on the ACS Publications website at DOI: 10.1021/acsabm.8b00266.

Experimental procedures for cyclodextrin modification, DLS, NMR, and X-ray data for aggregation studies, monolayer thickness and coverage estimates, and ^{1}H and ^{13}C NMR spectra of modified cyclodextrins (PDF)

■ AUTHOR INFORMATION

Corresponding Authors

*E-mail: colavitp@tcd.ie.
*E-mail: eoin.scanlan@tcd.ie.

ORCID

Paula E. Colavita: 0000-0003-1008-2874
Eoin M. Scanlan: 0000-0001-5176-2310

Notes

The authors declare no competing financial interest.

■ ACKNOWLEDGMENTS

This publication has emanated from research conducted with the financial support of Science Foundation Ireland (SFI) Grant Nos. 12/RC/2278 and 13/CDA/2213. The authors also thank Dr. J. O'Brien, Dr. M. Ruether, Dr. M. Feeney, and Dr. G. Hessman for assistance with NMR and MS characterization. A.M. and J.A.B. gratefully acknowledge support from the School of Chemistry and the Irish Research Council Grant No. GOIPG/2014/399, respectively.

■ REFERENCES

(1) Gong, T.; Zhou, Y.; Sun, L.; Liang, W.; Yang, J.; Shuang, S.; Dong, C. Effective Adsorption of Phenolic Pollutants from Water Using β-Cyclodextrin Polymer Functionalized Fe_3O_4 Magnetic Nanoparticles. *RSC Adv.* **2016**, *6*, 80955−80963.

(2) Zhao, F.; Repo, E.; Yin, D.; Meng, Y.; Jafari, S.; Sillanpää, M. EDTA-Cross-Linked β-Cyclodextrin: An Environmentally Friendly Bifunctional Adsorbent for Simultaneous Adsorption of Metals and Cationic Dyes. *Environ. Sci. Technol.* **2015**, *49*, 10570−10580.

(3) Gharbi, A.; Humblot, V.; Turpin, F.; Pradier, C.-M.; Imbert, C.; Berjeaud, J.-M. Elaboration of Antibiofilm Surfaces Functionalized with Antifungal-Cyclodextrin Inclusion Complexes. *FEMS Immunol. Med. Microbiol.* **2012**, *65*, 257−269.

(4) Hu, Q.-D.; Tang, G.-P.; Chu, P. K. Cyclodextrin-Based Host−Guest Supramolecular Nanoparticles for Delivery: From Design to Applications. *Acc. Chem. Res.* **2014**, *47*, 2017−2025.

(5) Zhang, Y.; Xu, H.; Ma, X.; Shi, Z.; Yin, J.; Jiang, X. Self-Assembly of Amphiphilic Anthracene-Functionalized β-Cyclodextrin (CD-AN) through Multi-Micelle Aggregation. *Macromol. Rapid Commun.* **2016**, *37*, 998−1004.

(6) Park, I.-K.; von Recum, H. A.; Jiang, S.; Pun, S. H. Supramolecular Assembly of Cyclodextrin-Based Nanoparticles on Solid Surfaces for Gene Delivery. *Langmuir* **2006**, *22*, 8478−8484.

(7) Li, H.; Meng, B.; Chai, S.-H.; Liu, H.; Dai, S. Hyper-Crosslinked β-Cyclodextrin Porous Polymer: An Adsorption-Facilitated Molecular Catalyst Support for Transformation of Water-Soluble Aromatic Molecules. *Chem. Sci.* **2016**, *7*, 905−909.

(8) Raoov, M.; Mohamad, S.; Abas, M. R. Synthesis and Characterization of β-Cyclodextrin Functionalized Ionic Liquid Polymer as a Macroporous Material for the Removal of Phenols and As(V). *Int. J. Mol. Sci.* **2014**, *15*, 100−119.

(9) Voncina, B.; Le Marechal, A. M. Grafting of Cotton with β-Cyclodextrin via Poly(carboxylic acid). *J. Appl. Polym. Sci.* **2005**, *96*, 1323−1328.

(10) Shi, Y.; Goodisman, J.; Dabrowiak, J. C. Cyclodextrin Capped Gold Nanoparticles as a Delivery Vehicle for a Prodrug of Cisplatin. *Inorg. Chem.* **2013**, *52*, 9418−9426.

(11) Diget, J. S.; Petersen, H. N.; Schaarup-Jensen, H.; Sørensen, A. U.; Nielsen, T. T.; Pedersen, S. U.; Daasbjerg, K.; Larsen, K. L.; Hinge, M. Synthesis of β-Cyclodextrin Diazonium Salts and Electrochemical Immobilization onto Glassy Carbon and Gold Surfaces. *Langmuir* **2012**, *28*, 16828−16833.

(12) Adenier, A.; Barré, N.; Cabet-Deliry, E.; Chaussé, A.; Griveau, S.; Mercier, F.; Pinson, J.; Vautrin-Ul, C. Study of the Spontaneous Formation of Organic Layers on Carbon and Metal Surfaces from Diazonium Salts. *Surf. Sci.* **2006**, *600* (21), 4801−4812.

(13) Angione, M. D.; Duff, T.; Bell, A. P.; Stamatin, S. N.; Fay, C.; Diamond, D.; Scanlan, E. M.; Colavita, P. E. Enhanced Antifouling Properties of Carbohydrate Coated Poly(ether sulfone) Membranes. *ACS Appl. Mater. Interfaces* **2015**, *7*, 17238−17246.

(14) Esteban-Tejeda, L.; Duff, T.; Ciapetti, G.; Daniela Angione, M.; Myles, A.; Vasconcelos, J. M.; Scanlan, E. M.; Colavita, P. E. Stable Hydrophilic Poly(dimethylsiloxane) via Glycan Surface Functionalization. *Polymer* **2016**, *106*, 1−7.

(15) Hicks, J. M.; Wong, Z. Y.; Scurr, D. J.; Silman, N.; Jackson, S. K.; Mendes, P. M.; Aylott, J. W.; Rawson, F. J. Tailoring the Electrochemical Properties of Carbon Nanotube Modified Indium Tin Oxide via in Situ Grafting of Aryl Diazonium. *Langmuir* **2017**, *33*, 4924−4933.

(16) Jayasundara, D. R.; Cullen, R. J.; Colavita, P. E. In Situ and Real Time Characterization of Spontaneous Grafting of Aryldiazonium Salts at Carbon Surfaces. *Chem. Mater.* **2013**, *25*, 1144−1152.

(17) Small, L. J.; Hibbs, M. R.; Wheeler, D. R. Spontaneous Aryldiazonium Film Formation on 440C Stainless Steel in Non-aqueous Environments. *Langmuir* **2014**, *30*, 14212−14218.

(18) Zen, F.; Angione, M. D.; Behan, J. A.; Cullen, R. J.; Duff, T.; Vasconcelos, J. M.; Scanlan, E. M.; Colavita, P. E. Modulation of Protein Fouling and Interfacial Properties at Carbon Surfaces via Immobilization of Glycans Using Aryldiazonium Chemistry. *Sci. Rep.* **2016**, *6*, 24840.

(19) Tripodo, G.; Wischke, C.; Neffe, A. T.; Lendlein, A. Efficient synthesis of pure monotosylated beta-cyclodextrin and its dimers. *Carbohydr. Res.* **2013**, *381*, 59−63.

(20) Liu, Y.; Fan, Z.; Zhang, H.-Y.; Diao, C.-H. Binding Ability and Self-Assembly Behavior of Linear Polymeric Supramolecules Formed by Modified β-Cyclodextrin. *Org. Lett.* **2003**, *5*, 251−254.

(21) Liu, Y.; Fan, Z.; Zhang, H.-Y.; Yang, Y.-W.; Ding, F.; Liu, S.-X.; Wu, X.; Wada, T.; Inoue, Y. Supramolecular Self-Assemblies of β-Cyclodextrins with Aromatic Tethers: Factors Governing the Helical Columnar versus Linear Channel Superstructures. *J. Org. Chem.* **2003**, *68*, 8345−8352.

(22) Liu, Y.; You, C.-C.; Zhang, M.; Weng, L.-H.; Wada, T.; Inoue, Y. Molecular Interpenetration within the Columnar Structure of Crystalline Anilino-β-cyclodextrin. *Org. Lett.* **2000**, *2*, 2761−2763.

(23) Eftink, M. R.; Andy, M. L.; Bystrom, K.; Perlmutter, H. D.; Kristol, D. S. Cyclodextrin Inclusion Complexes: Studies of the Variation in the Size of Alicyclic Guests. *J. Am. Chem. Soc.* **1989**, *111*, 6765−6772.

(24) Harries, D.; Rau, D. C.; Parsegian, V. A. Solutes Probe Hydration in Specific Association of Cyclodextrin and Adamantane. *J. Am. Chem. Soc.* **2005**, *127*, 2184−2190.

(25) Soto Tellini, V. H.; Jover, A.; García, J. C.; Galantini, L.; Meijide, F.; Tato, J. V. Thermodynamics of Formation of Host−Guest Supramolecular Polymers. *J. Am. Chem. Soc.* **2006**, *128*, 5728−5734.
(26) Myles, A.; Haberlin, D.; Esteban-Tejeda, L.; Angione, M. D.; Browne, M. P.; Hoque, M. K.; Doyle, T. K.; Scanlan, E. M.; Colavita, P. E. Bioinspired Aryldiazonium Carbohydrate Coatings: Reduced Adhesion of Foulants at Polymer and Stainless Steel Surfaces in a Marine Environment. *ACS Sustainable Chem. Eng.* **2018**, *6*, 1141−1151.
(27) Tan, T.; Ng, S.-c.; Wang, Y.; Xiao, Y. Synthesis of Mono-6-tosyl-β-cyclodextrin, a Key Intermediate for the Functional Cyclodextrin Derivatives. *Protocol Exchange* **2011**, DOI: 10.1038/protex.2011.214.
(28) Bonini, M.; Rossi, S.; Karlsson, G.; Almgren, M.; Lo Nostro, P.; Baglioni, P. Self-Assembly of β-Cyclodextrin in Water. Part 1: Cryo-TEM and Dynamic and Static Light Scattering. *Langmuir* **2006**, *22*, 1478−1484.
(29) Cullen, R. J.; Jayasundara, D. R.; Soldi, L.; Cheng, J. J.; Dufaure, G.; Colavita, P. E. Spontaneous Grafting of Nitrophenyl Groups on Amorphous Carbon Thin Films: A Structure−Reactivity Investigation. *Chem. Mater.* **2012**, *24*, 1031−1040.
(30) Socrates, G. *Infrared and Raman Characteristic Group Frequencies: Tables and Charts*; Wiley: 2001.
(31) Mbuli, B. S.; Nxumalo, E. N.; Mhlanga, S. D.; Krause, R. W.; Pillay, V. L.; Oren, Y.; Linder, C.; Mamba, B. B. Development of Antifouling Polyamide Thin-Film Composite Membranes Modified with Amino-Cyclodextrins and Diethylamino-Cyclodextrins for water treatment. *J. Appl. Polym. Sci.* **2014**, x DOI: 10.1002/app.40109.
(32) Yu, Z.; Pan, Y.; He, Y.; Zeng, G.; Shi, H.; Di, H. Preparation of a Novel Anti-Fouling β-Cyclodextrin-PVDF Membrane. *RSC Adv.* **2015**, *5*, 51364−51370.
(33) Nietzold, C.; Dietrich, P. M.; Lippitz, A.; Panne, U.; Unger, W. E. S. Cyclodextrin & Ferrocene Host & Guest Complexes on Silicon Oxide Surfaces. *Surf. Interface Anal.* **2016**, *48*, 606−610.
(34) Behan, J. A.; Stamatin, S. N.; Hoque, M. K.; Ciapetti, G.; Zen, F.; Esteban-Tejeda, L.; Colavita, P. E. Combined Optoelectronic and Electrochemical Study of Nitrogenated Carbon Electrodes. *J. Phys. Chem. C* **2017**, *121*, 6596−6604.
(35) Zen, F.; Angione, M. D.; Behan, J. A.; Cullen, R. J.; Duff, T.; Vasconcelos, J. M.; Scanlan, E. M.; Colavita, P. E. Modulation of Protein Fouling and Interfacial Properties at Carbon Surfaces via Immobilization of Glycans Using Aryldiazonium Chemistry. *Sci. Rep.* **2016**, *6*, 24840.
(36) Combellas, C.; Jiang, D.-e.; Kanoufi, F.; Pinson, J.; Podvorica, F. I. Steric Effects in the Reaction of Aryl Radicals on Surfaces. *Langmuir* **2009**, *25*, 286−293.
(37) Combellas, C.; Kanoufi, F.; Pinson, J.; Podvorica, F. I. Sterically Hindered Diazonium Salts for the Grafting of a Monolayer on Metals. *J. Am. Chem. Soc.* **2008**, *130*, 8576−8577.
(38) Greenwood, J.; Phan, T. H.; Fujita, Y.; Li, Z.; Ivasenko, O.; Vanderlinden, W.; Van Gorp, H.; Frederickx, W.; Lu, G.; Tahara, K.; Tobe, Y.; Uji-i, H.; Mertens, S. F. L.; De Feyter, S. Covalent Modification of Graphene and Graphite Using Diazonium Chemistry: Tunable Grafting and Nanomanipulation. *ACS Nano* **2015**, *9*, 5520−5535.
(39) Zhao, H.; Li, D.; Dong, G.; Duan, L.; Liu, X.; Wang, L. Volatilize-Controlled Oriented Growth of the Single-Crystal Layer for Organic Field-Effect Transistors. *Langmuir* **2014**, *30*, 12082−12088.
(40) Chretien, J.-M.; Ghanem, M. A.; Bartlett, P. N.; Kilburn, J. D. Covalent Tethering of Organic Functionality to the Surface of Glassy Carbon Electrodes by Using Electrochemical and Solid-Phase Synthesis Methodologies. *Chem. - Eur. J.* **2008**, *14*, 2548−2556.

DOI: 10.1021/acsabm.8b00266
ACS Appl. Bio Mater. 2018, 1, 825−832